

Abstract

Common marmosets (*Callithrix jacchus*) are small-bodied New World primates that are increasingly popular as model animals for neuroscience research. Their lissencephalic cortex provides substantial advantages for the application of high-density electrophysiological techniques to enhance our understanding of local cortical circuits and their cognitive and motor functions. The oculomotor circuitry underlying saccadic eye movements has been a popular system to study cognitive control. Most of what we know about this system, comes from electrophysiological studies on macaques, but most of their cortical oculomotor areas are buried within sulci and harder to access for high-density recordings. In contrast, marmosets provide greater advantages for studies of the oculomotor system, since critical areas of this network such as the frontal eye fields (FEF) and lateral intraparietal area (LIP) are easily accessible at the cortical surface. In contrast to the well-established macaques, little is known about functional connectivity patterns of common marmosets. In this thesis, we used resting-state ultra-high-field fMRI on anesthetized marmosets and macaques along with awake human subjects, to examine and compare the functional organization of the brain, with emphasis on the saccade system. Independent component analysis revealed homologous resting-state networks in marmoset to those in macaques and humans, including a distributed frontoparietal network. Seed-region analyses of the marmoset superior colliculus (SC) revealed the strongest frontal functional connectivity with area 8aD bordering area 6DR. This frontal region exhibited a similar functional connectivity pattern to the FEF in macaques and humans. The results supported an evolutionarily preserved frontoparietal system and provided a starting point for invasive neurophysiological studies in the marmoset saccade system. We started by investigating the function of the marmoset posterior parietal cortex with electrical

microstimulation. We implanted 32-channel Utah arrays at the location of area LIP as identified from our resting-state fMRI study and applied microstimulation while animals watched videos. Similar to macaque studies, stimulation evoked fixed-vector and goal-directed saccades, staircase saccades, and eyeblinks in marmosets. These findings demonstrated that the marmoset area LIP plays a role in the regulation of eye movements and is potentially homologous to that of the macaque. Next, we recorded the neuronal activity in marmoset areas LIP and 8aD using linear electrode arrays while animals performed a pro/antisaccade task. The antisaccade task is a popular paradigm to probe executive control. In this task, participants suppress a prepotent stimulus-driven response in favor of a less potent response away from the stimulus. Our behavioral findings indicated that area 8aD neurons were significantly more active for correct than erroneous antisaccades in contralateral directions, with respect to the recording site. We found neurons with significant stimulus-related activity in area LIP and significant saccade-related neurons in both areas 8aD and LIP. These findings provided further evidence on the role of marmoset frontal and parietal oculomotor areas in oculomotor control, supporting marmosets as alternative primate models of the oculomotor system.

Keywords: Common marmosets, oculomotor system, resting-state fMRI, functional connectivity, frontal eye fields, lateral intraparietal area, intracortical microstimulation, Utah arrays, linear arrays, pro/antisaccade task.

Summary for Lay Audience

The oculomotor system is a brain circuitry that underlies saccades, which are rapid eye movements that we naturally do to visually observe our environment. Most of what we know about this system, comes from electrophysiological studies on macaque monkeys. However, when it comes to more advanced electrophysiological techniques, macaque's brain with its extensive cortical folding makes it hard to access cortical oculomotor areas that are buried deep within the folds. On the other hand, common marmoset monkeys are small-bodied primates with a smooth cortex that allows easier access to oculomotor areas right at the surface of the brain, providing substantial advantages for higher density recording techniques. To consider marmosets as alternative primate models of the oculomotor system, it is necessary to investigate the functional organization of this system in these species and identify homologous oculomotor areas that serve a similar function to that of the macaque. My PhD project aimed to investigate that through a range of experimental techniques. We used the resting-state fMRI technique to explore the functional organization of marmoset brain and identified a frontoparietal network that potentially represented the oculomotor system. We identified brain areas such as area 8aD and the lateral intraparietal area (LIP) within this network that had a similar pattern of functional connectivity to the corresponding oculomotor areas in the macaque. Our findings supported a preserved frontoparietal network in these species and allowed for more invasive investigation of the identified oculomotor areas with electrophysiology. We chose to investigate area LIP as identified from our fMRI findings, using electrical microstimulation techniques. The goal was to examine whether the stimulation of area LIP in marmoset will evoke saccadic eye movements. Similar to macaque studies, we found that microstimulating area LIP in marmosets elicited both fixed-vector and goal-directed saccades. Our findings demonstrated that area LIP

in marmosets has a similar role in regulating eye movements to that of the macaque and is potentially homologous to it. Next, we recorded neuronal activity in areas LIP and 8aD of marmosets while the animal was performing a saccadic eye movement task called the pro/antisaccade task. We found neurons within each area that demonstrated significant saccade related activity in specific epochs of the task. These findings provided further evidence on the role of marmoset oculomotor areas in saccadic eye movements and supported common marmosets as alternative primate models of the oculomotor system.

Co-Authorship Statement

Maryam Ghahremani, Kevin D. Johnston, Liya Ma, R. Matthew Hutchison, Lauren K. Hayrynen, Ravi S. Menon, Stefan Everling.

As the primary author of this thesis, Maryam Ghahremani was responsible for animal training, data collection, data analysis, interpretation of findings, and composition of manuscripts. Dr. Ravi Menon and his team kindly assisted in designing experimental setups and monitoring data acquisition for fMRI scans in chapter 2. Dr. Matthew Hutchison assisted in parts of the data analysis for chapter 2. Dr. Kevin Johnston provided invaluable support in experimental design, animal training, data collection and surgical procedures involved in chapters 3 and 4. Dr. Liya Ma was instrumental in the data analysis of chapter 4. Lauren Hayrynen was a great help in surgical procedures, animal training and data collection in chapters 3 and 4. Dr. Stefan Everling was the principal investigator who supervised every step of all projects, performed all surgical operations, designed experiments, and oversaw data analysis, interpretations, and manuscript revisions for all the experimental chapters involved in this thesis.

Dedication

To my beloved family
for their endless support, patience and encouragement
to make this academic journey possible

Acknowledgements

First and foremost, I would like to thank my supervisor Dr. Stefan Everling, for giving me the opportunity to work in his pioneering lab, and for his continuous advice and support throughout the term of my PhD studies. He has been an inspiring mentor, especially in challenging phases of my PhD, and a remarkable role model of strength, persistence and enthusiasm for discovery. Under his admirable supervision, I could earn the necessary skills toward becoming a dedicated scientist.

I'd like to thank Dr. Kevin Johnston for his advice and assistance in animal training and electrophysiological recording sessions. He has certainly been a great source of knowledge when I was in doubt, and his great sense of humor is always refreshing.

Thank you to Dr. Sahand Babapoor for his sincere help when I moved to London from South Korea and didn't know anyone. I greatly appreciate his mentorship and support, both before and after moving to London, to adapt to my new academic life and lab family.

Thank you to Dr. Liya Ma for being a wonderful mentor especially throughout my last project, sharing her extensive knowledge and expertise to help me achieve more than I could ever achieve, considering the limited time I had. She has always been an inspiring colleague and friend to talk to and seek advice from.

I also would like to thank my academic advisors, Dr. Ravi Menon, Dr. Julio Martinez-Trujillo and Dr. Susanne Schmid for their constructive feedback and guidance throughout my PhD

studies. They certainly played an important role in making improvements in my analyses, interpretations and communication skills.

Thank you to Nicole Hague, Ashley Kirley, Lauren Schaeffer and Cheryl Vander Tuin for their invaluable support to run animal trainings and experiments. Thank you to Alex Li, Joseph Gati, Kyle Gilbert and Miranda Bellyou for helping me collect the fMRI data for my first project. Without their instrumental help, I could not finish my PhD projects.

Many thanks to Susan Simpson for being an amazing person and a great source of counselling within the Neuroscience program. I also want to thank Sandra Pehilj, Fabiana Tepedino, and Francesca Mancuso from the International and Exchange Students Centre (IESC) for their endless care and support all along the time I spent at Western University.

A special thank you goes to my dear friends in London community and around the world, as well as the rest of the neuroscience community, including Justine, Alex, Ramina, Susheel, Darren, Janahan, Raymond, Yuki, Borna, Nasim, Milad, Sebastian, Maryams (Nouri and Mozaffari), Jason, Brandon and Nikoo. It was wonderful having them around and thanks to their warm presence, Robarts was a fun place to work at.

The last but certainly not the least, I want to extend my greatest appreciation to my parents, my brother, and my fiancé for being the greatest sources of mental support, encouragement and love. Without them, I would certainly not have seen a day like today. Thank you for being in my life!

Table of Contents

Abstract	ii
Summary for Lay Audience	iv
Co-Authorship Statement	vi
Dedication	vii
Acknowledgements	viii
List of Figures	xiii
List of Abbreviations	xxi
CHAPTER 1	1
1 Introduction	1
1.1 Saccades	1
1.1.1 Saccade Characteristics	3
1.1.2 Reflexive versus Voluntary Saccades	4
1.1.3 Saccade and Attention	6
1.2 Oculomotor Circuitry	7
1.2.1 Superior Colliculus (SC)	8
1.2.2 Frontal Eye Field (FEF)	16
1.2.3 Posterior Parietal Cortex (PPC)	21
1.3 Common Marmoset Monkeys	27
1.3.1 Oculomotor Network in Common Marmosets	30
1.3.2 Resting-state fMRI	32
1.3.3 Intracortical Electrical Microstimulation	37
1.3.4 Laminar Electrodes	42
1.3.5 Pro/Antisaccade Task	43
1.4 Research Objectives	49
1.4.1 Extracting resting-state functional connectivity maps in common marmosets with further emphasis on the frontoparietal network	49
1.4.2 Examining oculomotor effects of systemic microstimulation in marmoset putative area LIP50	50
1.4.3 Investigating the post-stimulus neuronal activity of marmoset cortical oculomotor areas 8aD and LIP during the pro/antisaccade task	51
1.5 References	52
CHAPTER 2	73
2 Frontoparietal Functional Connectivity in the Common Marmoset	73
2.1 Abstract	73
2.2 Introduction	74
2.3 Materials and Methods	77
2.3.1 Marmoset data acquisition	77
2.3.2 Macaque data acquisition	78
2.3.3 Human data acquisition	80

2.3.4	Image preprocessing	80
2.3.5	Independent component analysis	81
2.3.6	Region of interest analysis	82
2.3.7	Surface-based registrations	84
2.3.8	Assessing functional hubs in the marmoset	85
2.4	Results	86
2.4.1	Resting-state networks	86
2.4.2	Seed-based connectivity patterns	92
2.4.3	Functional hubs	102
2.5	Discussion	104
2.5.1	Exploratory analysis of RSN homologies	105
2.5.2	Functional connectivity of the superior colliculus	108
2.5.3	Locations of the frontal eye fields in marmosets	110
2.5.4	Functional connectivity of the frontal eye fields	112
2.5.5	Hubs	112
2.6	Conclusion	114
2.7	Acknowledgements	114
2.8	Supplementary Material	115
2.9	References	116
CHAPTER 3		125
3	Electrical microstimulation evokes saccades in posterior parietal cortex of common marmosets	125
3.1	Abstract	125
3.2	Introduction	126
3.3	Methods	128
3.3.1	Subjects	128
3.3.2	Microstimulation Protocol	130
3.3.3	Eye Movement Recording	131
3.3.4	Confirming Array Location	132
3.3.5	Ex vivo MRI scan	132
3.3.6	In vivo micro-CT scan	134
3.3.7	Data Analysis	134
3.4	Results	136
3.4.1	Confirming the location of the array	136
3.4.2	Oculomotor Effects of LIP Microstimulation	138
3.4.3	Saccade Latency and Duration	140
3.4.4	Staircase saccades	143
3.4.5	Effects of initial eye position	144
3.4.6	Saccade Direction and Amplitude	148
3.5	Discussion	150
3.6	Acknowledgements	158
3.7	References	158
CHAPTER 4		163
4	Post-stimulus neuronal activity in marmoset frontal and parietal oculomotor areas during the pro/antisaccade task	163

4.1	Abstract	163
4.2	Introduction	164
4.3	Materials and Methods	167
4.3.1	Subjects	167
4.3.2	Surgical procedures	168
4.3.3	Behavioral task	169
4.3.4	Electrophysiological recording	171
4.3.5	Data analysis	173
4.3.6	Behavioral analysis	173
4.3.7	Neuronal classification analysis	174
4.3.8	Spike Density Function	175
4.4	Results	176
4.4.1	Saccade behavior	176
4.4.2	Single unit activity	180
4.5	Discussion	191
4.5.1	Behavior	192
4.5.2	Stimulus related neuronal activity	194
4.5.3	Saccade related neuronal activity	196
4.6	References	200
CHAPTER 5		201
5	General Discussion	201
5.1	The frontoparietal pattern of functional connectivity underlying saccade circuitry is preserved across Old World (macaques and humans) and New World (marmosets) species	202
5.1.1	Summary of the main findings	202
5.1.2	Caveats and future directions	203
5.2	Microstimulation of the LIP in marmosets evokes both fixed-vector and convergent saccades, supporting its homologous role to the macaque LIP.	206
5.2.1	Summary of the main findings	206
5.2.2	Caveats and future directions	207
5.3	Marmoset oculomotor areas LIP and 8aD contain neurons with significant stimulus-related and saccade related activity after the onset of peripheral stimulus in the pro/antisaccade task	210
5.3.1	Summary of the main findings	210
5.3.2	Caveats and future directions	211
5.4	References	214
Appendix: Documentation of Ethics Approval		218
CURRICULUM VITAE		219

List of Figures

Figure 1-1. Brain circuitry underlying saccadic eye movements in primates, demonstrating afferent and efferent projections of the superior colliculus (SC). Lines represent connection between brain areas involved in the oculomotor circuitry, with triangles referring to excitatory connections and bars representing inhibitory connections. DLPFC: dorsolateral prefrontal cortex, FEF: frontal eye fields, SEF: supplementary eye fields, LIP: lateral intraparietal area, LGN: lateral geniculate nucleus, SCi: superior colliculus intermediate layers, SCs: superior colliculus superficial layers, MD: mediodorsal nucleus, Pul: pulvinar, SNr: substantia nigra pars reticulata, SNc: substantia nigra pars compacta, OPN: omnipause neurons. Based on the figure in Box 1(a) from Munoz and Everling (2004)..... 12

Figure 2-1. Homologous core resting-state networks of primate species. Note that the z-statistic maps are thresholded according to the z-score color bars provided for each species. The resulting z-statistic maps of the networks were projected onto each species respective surface model. These networks correspond to the following human RSNs: (A) visual network (VIS), (B) dorsal somatomotor network (SMd), (C) ventral somatomotor network (SMv), (D) cingulo-operculum network (SG), (E) dorsal attention network (DAN)/cognitive control network (CON), (F) salience network (SAL), and (G) default mode network (DMN). Human connectivity maps were taken from Hutchison and Everling (2012). 90

Figure 2-2. Basal ganglia network in the common marmoset (left), macaque (middle), and human (right). The z-statistic map of each species was overlaid onto the respective high-resolution template. Note that the z-statistic maps are thresholded according to the z-score color bars provided. 90

Figure 2-3. Flat map representation of RSN 5 (from Fig. 1E) in marmosets (left) and macaques (right) displaying a frontoparietal pattern of functional connectivity. z-statistic maps are thresholded according to the z-score color bars provided. The obtained maps were projected onto the cortical flat-map models of macaques and marmosets with borders of the cortical areas superimposed. White lines marked on the map refer to the location of LIP, VIP, MIP, and AIP macaques (from Felleman and Van Essen 1991). 91

Figure 2-4. Lateral (left) and medial (right) views of the brain showing the functional connectivity patterns of the SC (first row), area 8aD (second row) and area 8aV (third row) in common marmosets projected onto marmoset cortical surface model with cortical borders superimposed. z-Statistic maps are thresholded according to the z-score color bar provided, displaying only the positive functional connectivity. Asterisk indicates the location of the seed. The figures at the bottom left and right corners of 8aD and 8aV maps represent the lateral (left) and medial (right) views of principal projections to area 8aD and 8aV, respectively, reported by Reser et al. (2013) based on fluorescent tracer injections from more than 0.5% of the labeled neurons (light yellow) to more than 16% (dark red) (Reser et al. 2013)..... 94

Figure 2-5. Functional connectivity patterns in the right hemisphere of macaques and common marmosets. Group averaged connectivity patterns of the SC (left column) and FEF (right column) are shown on flattened cortical representations of the macaque (top) and marmoset (bottom). Asterisks indicate the location of the FEF seed. The SC is not visualized in a cortical representation. Note that the z-statistic maps are thresholded according to the z-score color bars provided and they differ for each map. The z-statistic maps were averaged across each group with multiple-comparison corrections achieved at cluster level with $z > 2.3$ and cluster significance: $p < 0.05$ and were projected onto the cortical flat-map models of macaques and marmosets. Areas marked in green represent cortical face patches in macaques (Schwiedrzik et al. 2015). White lines marked on the map refer to the location of LIP, VIP, MIP, and AIP macaques (from Felleman and Van Essen 1991). 96

Figure 2-6. Coronal view of the functional connectivity patterns in frontal, parietal, temporal and subcortical areas in the common marmoset, obtained from ICA (first row), SC-based (second row), and FEF-based (third row) analysis. The numbers at the bottom of the figure represent the distance from the anterior commissure. The z-statistic maps were averaged across the group with multiple-comparison corrections achieved at cluster level with $z > 2.3$ and cluster significance: $p < 0.05$. SC: superior colliculus, Amy: amygdala, CD: caudate nucleus, LIP: lateral intraparietal, PG: postcentral gyrus, MT: medial temporal, FST: fundal area of the superior temporal sulcus, Pul: pulvinar, 3N: oculomotor nucleus, 4N: trochlear nucleus, 6N: abducens nucleus, TPO: temporo-parietooccipital, 8aV: anterior ventral area 8, 6DR: rostral dorsal area 6, TE3: temporal area TE2, S2E: secondary somatosensory cortex-external part, V6A: visual area V6. 97

Figure 2-7. Inter-species surface-based registration of the SC functional connectivity maps between common marmosets and macaques. The top left panel displays the marmoset SC-connectivity map projected onto the marmoset brain surface while the top right panel shows the marmoset SC-connectivity map projected onto the macaque brain surface. The bottom left panel displays the macaque SC-connectivity map projected onto the marmoset brain surface while the bottom right panel shows the macaque SC-connectivity map projected onto the macaque brain surface. The black circles marked in marmoset SC-connectivity map projected onto marmoset brain surface (top left panel) indicates the locations at which Blum et al. (1982) were able to evoke saccadic eye movements in anesthetized marmosets using microstimulation. Note that the z-statistic maps are thresholded according to the z-score color bars provided and they differ for each map. The z-statistic maps were averaged across each group with multiple-comparison corrections achieved at cluster level with $z > 2.3$ and cluster significance: $p < 0.05$ and were projected on to the cortical surface models of macaques and marmosets (Chaplin et al. 2013; Van Essen 2005)..... 100

Figure 2-8. Inter-species surface-based registration of the FEF functional connectivity maps between common marmosets, macaques and humans. The first row displays the marmoset FEF-connectivity map projected onto the marmoset brain surface (left), macaque brain surface (middle) and human brain surface (right), respectively. The second row displays the macaque FEF-connectivity map projected onto the marmoset (left), macaque (middle), and human (right) brain surface, respectively. The third row displays the human FEF-connectivity map projected onto the marmoset (left), macaque (middle) and human (right) brain surface, respectively. The asterisks mark the location of the FEF seed in each species. Note that the z-statistic maps are thresholded according to the zscore color bars provided and they differ for each map. The z-statistic maps were averaged across each group with multiple-comparison corrections achieved at cluster level with $z > 2.3$ and cluster significance: $p < 0.05$ for marmosets and macaques and $z > 3.7$, cluster significance: $p < 0.05$ for humans, and were projected onto the cortical surface models of humans, macaques and marmosets (Chaplin et al. 2013; Van Essen 2005)..... 101

Figure 2-9. Hub identification in the common marmoset. The BC was evaluated for 115 cortical regions of the right hemisphere (Paxinos et al. 2012) calculated from the group-averaged and binarized functional connectivity matrix. The values for the highest 45 regions are rank ordered

with significant regions are indicated with asterisks. The inset image displays the lateral and medial views with regions color-coded according to the BC value. 103

Supplementary figure 2-1. Direct comparison of the functional connectivity maps of areas 8aD and 8aV at cortical (A) and subcortical (B) levels. Warm z-score colors refer to regions where area 8aD had significantly higher functional connectivity than 8aV, while cold z-score colors reflect areas where area 8aV had significantly higher functional connectivity than 8aD. The z-statistic maps were corrected for multiple-comparison at a cluster level of $z > 2.3$ with cluster significance $p < 0.05$ 115

Figure 3-1. Identification of the positioning of the array with ex vivo MRI for *marmoset B* and in vivo micro-CT scan for *marmoset W*. *Left*: the location of the array for both *marmoset B* and *marmoset W* registered on the surface space of the left hemisphere of the marmoset brain, with cortical boundaries overlaid in white. *Right*: the location of the arrays is displayed in more detail by zooming into the area enclosed within the blue box at *left*, with all the overlapping and neighboring areas labeled according to the NIH brain parcellation map (Liu et al. 2018). The purple patches demonstrate the overlapping area between the arrays from both animals. LIP, lateral intraparietal area; MIP, medial intraparietal area; VIP, ventral intraparietal area; AIP, anterior intraparietal area; PE, parietal area PE; PEC, caudal part of parietal area PE; PG, parietal area PG; OPt, occipito-parietal transitional area; V6A, visual area 6A; V3A, visual area 3A; M, medial; L, lateral; P, posterior; A, anterior. 137

Figure 3-2. *A*: mapping the results of electrical microstimulation on individual sites of the array implanted in left area LIP for *marmosets B* (*left*) and *W* (*right*). Each circle corresponds to an electrode channel within the array. Red circles indicate sites that elicited saccades upon microstimulation. Blue circles designate sites that elicited blinks, and open circles indicate sites in which no specific response was observed as a result of microstimulation. Circles with a cross sign refer to sites in which no spike activity was recorded. Dashed line marks the approximate border line of area MIP based on the location of the shallow intraparietal sulcus from the NIH atlas, as depicted in Fig. 1. *B*: mapping the distribution of saccade onset thresholds with gradients of red. Circles with a cross sign refer to sites whose microstimulation did not evoke saccades. Dark red circles are sites with the highest saccade onset thresholds of $>200 \mu\text{A}$. Light red marks sites with thresholds in the range of $150\text{--}200 \mu\text{A}$. Orange marks sites with thresholds

of 100–150 μA . Light yellow marks sites with the lowest saccade thresholds in the range of 40–to 100 μA . A, anterior; P, posterior; M, medial; L, lateral. 139

Figure 3-3. A: examples of saccades from a representative site (marked on the array grid at top right) of the array that was microstimulated at 3 different current amplitudes: 75 μA (left), 100 μA (center), and 200 μA (right). For each plot, the dashed line marks the onset of microstimulation, and the x-axis represents time in milliseconds with a calibration bar of 40 ms. The traces at top refer to the horizontal eye movements (Eh), and the traces at bottom refer to the vertical eye movements (Ev). The calibration bar for the amplitude of these traces is given at 5° for all plots. B: bar plots representing % of elicited saccades (left) and their amplitude (right) at each microstimulation current amplitude (x-axis) from the same representative site. 141

Figure 3-4. A: saccade onset latency from all saccadic sites of the array for both marmosets as a function of the amplitude of the microstimulation current. B: the duration of all saccades for both animals as a function of the amplitude of the microstimulation current. Error bars were calculated based on the standard error from the mean. 142

Figure 3-5. Representative examples of staircase saccades from 2 individual sites of the array stimulated at 150 μA (left) and 225 μA (right), respectively. Dashed line refers to the onset of stimulation, and the solid horizontal bar shows the duration of stimulation. x-Axis refers to time with a calibration bar of 40 ms. The traces at top display horizontal eye movements (Eh) and the traces at bottom vertical eye movements (Ev) with an amplitude calibration bar of 5°... 143

Figure 3-6. Effect of initial eye position on stimulation-evoked saccades. A: examples of the effect of initial eye position on evoked saccades from 2 representative sites of the array as marked on the array grids at top. Left: fixed-vector saccades. Right: goal-directed saccades. Circles indicate the starting position of saccades. Vertical and horizontal axes illustrate the distribution of starting position of saccades across the display. L, left; R, right; U, up; D, down. Saccade amplitude calibration bar is given for 2°. B: corresponding regression plots for the representative sites displayed in A. Each panel displays 2 scatterplots for each of the horizontal (Kh) and vertical (Kv) saccade components, with the y-axis being the size of saccades defined as the difference of saccade offset and onset (ΔEh , horizontal; ΔEv , vertical), vs. different initial

eye positions (Eh, horizontal; Ev, vertical). Dots represent saccade trials from that representative site, and the line represents the regression line of best fit..... 146

Figure 3-7. The results of regression analysis from all 10 sites of the array in which the effect of initial eye position was examined. These specific sites are marked on the array grid as shown at top right. A: slopes of horizontal saccade components (Kh). B: slopes of vertical saccade components (Kv). x-Axis represents individual sites, and y-axis represents slopes..... 147

Figure 3-8. A: mapping the average saccade vectors across all saccadic sites of the array for marmosets B (left) and W (right). Each square corresponds to an array electrode. Gray squares refer to sites that did not elicit saccades upon microstimulation. Each arrow represents the average saccade vector evoked across all saccade trials, with its associated amplitude and direction. The amplitude of the saccades is measured by the calibration bar given for 2°. Each arrow is plotted based on vertical and horizontal axes that represent vertical (Ev) and horizontal (Eh) eye movements, respectively. B: examples of individual saccades constituting an average saccade vector from 4 representative array sites per animal, marked by 1, 2, 3, and 4 in A. Saccade amplitude calibration bar is given for 2°. Circles indicate the starting position of saccades. For each site, vertical and horizontal axes refer to vertical (Ev) and horizontal (Eh) eye movements, respectively. A, anterior; P, posterior; M, medial; L, lateral. 149

Figure 4-1. Task and the location of recording electrodes. (A) Blocked prosaccade and antisaccade task adapted for marmosets. Animals were presented with a central instruction cue (top: dot for Pro, bottom: cross for Anti) and had to generate a saccade toward a highly salient (top, Pro) or a small dim stimulus (bottom, Anti) to receive reward. (B) Recording locations. Top: coronal sections of parietal and frontal cortices depicting locations of electrode penetrations with respect to cytoarchitecturally defined regions of marmoset cortex. Bottom: lateral view of marmoset brain with parietal and frontal sections marked. *This figure was modified from Johnston et al (2019), J of Neurosci. 39(10):1855–1866.* 172

Figure 4-2. (A) Distribution of saccadic reaction times for correct (blue bars) and error (red bars) responses on prosaccade (left) and antisaccade (right) trials. (B) Examples of saccadic eye movement traces for prosaccades (left) and antisaccades (right). (C) Bar plots of the percent accuracy in prosaccade (left) and antisaccade (right) blocks, across three time periods within a

block: the beginning, the middle and the end of the block. Error bars were calculated based on the standard error from the mean..... 179

Figure 4-3. Average and single cell activity in area LIP of common marmosets based on stimulus period (30 to 80 ms after the stimulus onset) in the pro/antisaccade task. (A) Stimulus-aligned (left) and saccade-aligned (right) spike activity of representative single cells in area LIP significant activity during the stimulus period defined. (A) Stimulus-aligned (left) and saccade-aligned (right) average firing rate of LIP neurons with significant activity during the stimulus period. Dashed line in all plots on the left panel marks the onset of the salient stimulus while in the right panel it marks the onset of saccade. Pro ipsi: ipsilateral prosaccade, Pro contra: contralateral prosaccade, Anti ipsi: ipsilateral antisaccade, Anti contra: contralateral antisaccade..... 184

Figure 4-4. Average and single cell activity in area LIP of common marmosets based on perisaccadic period (from -70 to 100 ms around the saccade onset) in the pro/antisaccade task. (A) Stimulus aligned (left) and saccade-aligned (right) spike activity of representative single cells in area LIP with significant activity during the perisaccadic period. (B) Stimulus-aligned (left) and saccade-aligned (right) average firing rate of area LIP neurons with significant activity during the perisaccadic period. Dashed line in all plots on the left panel marks the onset of the salient stimulus while in the right panel it marks the onset of saccade. Pro ipsi: ipsilateral prosaccade, Pro contra: contralateral prosaccade, Anti ipsi: ipsilateral antisaccade, Anti contra: contralateral antisaccade..... 187

Figure 4-5. Average and single cell activity in area 8aD of common marmosets based on perisaccadic period (from -70 to 100 ms around the saccade onset) in the pro/antisaccade task. (A) Stimulus-aligned (left) and saccade-aligned (right) spike activity of representative single cells in area 8aD with significant activity during the perisaccadic period. (B) Stimulus-aligned (left) and saccade-aligned (right) average firing rate of area 8aD neurons with significant activity during the perisaccadic period. Dashed line in all plots on the left panel marks the onset of the salient stimulus while in the right panel it marks the onset of saccade. Pro ipsi: ipsilateral prosaccade, Pro contra: contralateral prosaccade, Anti ipsi: ipsilateral antisaccade, Anti contra: contralateral antisaccade..... 188

Figure 4-6. Discharge rate of single neurons in marmoset areas 8aD and LIP for ipsilateral versus contralateral prosaccades and antisaccades. (A) Scatter plots depicting relative discharge rates of area 8aD neurons in pro (left) and anti (right) trials on ipsilateral versus contralateral saccades. (B) Scatter plots depicting relative discharge rates of area LIP neurons in pro (left) and anti (right) trials on ipsilateral versus contralateral saccades. 190

Figure 4-7. Scatter plots depicting the relative discharge rate of single neurons in marmoset areas 8aD (left) and LIP (right) for correct versus error contralateral antisaccade trials. 191

List of Abbreviations

ACC	Anterior Cingulate Cortex
AIP	Anterior IntraParietal
BC	Betweenness Centrality
BOLD	Blood Oxygenation Level Dependent
CBF	Cerebral Blood Flow
CBV	Cerebral Blood Volume
CSF	CerebroSpinal Fluid
CN	Caudate Nucleus
CON	Cognitive Control Network
DAN	Dorsal Attention Network
DLPFC	Dorsolateral PreFrontal Cortex
DMN	Default Mode Network
EEG	ElectroEncephalography
EMG	ElectroMyography
EPI	Echo-Planar Imaging
FEF	Frontal Eye Field
fMRI	functional Magnetic Resonance Imaging
FOV	Field Of View
FST	Fundal of the Superior Temporal sulcus
GPe	Globus Pallidus external
IC	Independent Component
ICA	Independent Component Analysis
IPS	IntraParietal Sulcus
LGN	Lateral Geniculate Nucleus
LIP	Lateral IntraParietal
MDN	MedioDorsal Nucleus
MIP	Medial IntraParietal
MST	Medial Superior Temporal
ms	Millisecond

MT	Medial Temporal
NHP	Non-Human Primate
OPN	OmniPause Neuron
PFC	PreFrontal Cortex
PPC	Posterior Parietal Cortex
RSN	Resting State Network
SAL	Saliience Network
SCs	Superior Colliculus superficial
SCi	Superior Colliculus intermediate
SEF	Supplementary Eye Field
SNC	Substantia Nigra pars compacta
SNr	Substantia Nigra pars reticulata
SNR	Signal to Noise Ratio
SRT	Saccade Reaction Time
SC	Superior Colliculus
SMd	dorsal SomatoMotor
SMv	ventral SomatoMotor
TE	Echo Time
TMS	Transcranial Magnetic Stimulation
TPO	Temporo-ParietoOccipital
TR	Repetition Time
TSE	Turbo Spin Echo
UIEA	Utah Intracortical Electrode Array
VIP	Ventral IntraPatietal

CHAPTER 1

1 Introduction

1.1 Saccades

Over the past century, there has been a rapid expansion in the field of eye movement research owing to the realization that multiple aspects of cognitive and psychological processes of the human brain are tightly related to eye movements. The primary purposes of eye movements are to bring the highest resolution part of the eye, the fovea, towards the object of interest in our surrounding, and to stabilize the observed retinal image (Walls, 1962; Gilchrist, 2011). The vestibulo-ocular reflex is an example of eye movements that stabilize a retinal image by moving the eye relative to the head movements (Hess and Angelaki, 1997). Smooth pursuit eye movements occur when we are tracking a moving visual target, keeping its retinal image stable, while its background is moving in the opposite direction (Barnes, 2008). Vergence eye movements happen when the two eyes simultaneously move in opposite directions while trying to track a target that moves towards or away from us (Hung et al., 1994). Saccades are rapid movements of the eyes that point the fovea to an object of interest, followed by a fixation period during which the eyes are nearly stationary. When looking at a relatively static object with our heads still, we mainly perform saccadic eye movements and when the situation becomes more dynamic with either us moving or the object moving, other eye movements mentioned before are triggered to keep the fovea aligned with the object of interest. All movements except the vergence eye movement are conjugate movements, meaning that both of our eyes move in the same direction throughout the movement (Land, 2011). Saccadic eye movements have a significant diagnostic value and have been used in identifying cognitive and motor impairments

in patients suffering from psychiatric and neurologic disorders (Fukushima et al., 1990; Crevits and De Ridder, 1997; Broerse et al., 2001; Li et al., 2003). Saccades bring a portion of the visual field onto the high-resolution fovea and then the foveated object is analyzed in detail during the subsequent fixation period. The sequence of fixations and saccades involved in this kind of eye movement, are often referred to as scanpaths (Gilchrist, 2011). This “saccade and fixate” strategy helps us gather information during fixation periods and then shift our gaze by means of saccades, to fixate on the next object of interest while viewing the visual world. Aside from processing visual information at the current location of interest, during the fixation period information is also being processed from the periphery of the current fixated location in order to identify potential locations for the next fixation, which defines when and to where the next saccade is directed (Gilchrist, 2011). It is important to point out here, that despite the absence of saccades, the eyes are not completely stationary during fixation periods. The three miniature eye movements that occur during fixation are drift, tremor, and microsaccades (Carpenter, 1988) and their purpose is to prevent the visual image from fading due to neural adaptation (Otero-Millan et al., 2008).

Saccades are generated by six extraocular muscles that are attached to the eyeball and the socket, organized in three agonist/antagonist pairs which allow rotations in all three dimensions. These muscles are innervated by motoneurons within three cranial nerves: oculomotor, trochlear and abducens (Büttner-Ennever and Horn, 2002). The neural command for an eye movement must consider the mechanical restraints of the tissues that support the eyeball. These supporting tissues impose viscous drag and elastic restoring forces that need to be overcome in order to move the eyes. In saccadic eye movements, the motoneurons discharge includes a phasic component consisting of a burst in activity that is to overcome the viscous drag forces.

Once a saccade is made to a target location, to hold the eye fixated requires opposing the elastic restoring forces that tend to bring the eyeball back to its central position and the tonic component of motoneurons firing rate is meant to overcome these restoring forces (Robinson, 1970; Angelaki, 2011). In spite of the forces involved, the eyeball is a relatively light and mobile structure and therefore does not have a high metabolic cost compared to the great advantages it provides in quickly gathering visual information.

1.1.1 Saccade Characteristics

Saccades can have different amplitudes and direction, but for a given size and direction they have a general characteristic temporal profile with the eye initially stable and then rapidly accelerating up to a certain peak velocity, then rapidly decelerating and returning to the stable state (Gilchrist, 2011). To make smaller amplitude saccades, we mostly rely on our eye movements, but when making larger amplitude saccades, our gaze shifts involve a coordination of both eye and head movements, with the head helping to redirect the eye to its selected target location (Corneil et al., 2002a, 2002b). In species with a more limited oculomotor range however, jerky saccade-like movements of the head are commonly observed even for smaller amplitude saccades, compensating for the lack of a wider oculomotor range (Land, 2011).

Latency of saccades is defined as the amount of time taken to initiate a saccade from the onset of stimulation (target appearance). It is a task dependent parameter that generally varies within a very wide interval from as low as 100 ms to as high as 1000 ms, but a typical saccade latency is around 200 ms (Carpenter, 1988). The wide variability in saccade latency has been explained through considering a saccade as the outcome of a decision-making process. In order to generate

a saccade, a decision signal has to accumulate over time until it reaches a required threshold and this accumulation rate varies across trials (Carpenter and Williams, 1995). Features of the stimulus presented can impact saccade latency since, saccades are generally slower if the target has a low intensity, low contrast or high spatial frequency (Kalesnykas and Hallett, 1994; Ludwig et al., 2004). Other factors affecting saccade latency include fixation disengagement by introducing a gap period between currently fixated target and the appearance of the next target (Saslow, 1967; Forbes and Klein, 1996), and the remote distractor effect where the saccade target is presented simultaneously with a distractor (Walker et al., 1997). The former effect is known to decrease saccade latency, while the latter generally increases saccade latency.

Just before the onset of the saccade, the oculomotor system is known to enter a state of no return known as the dead-time during which, it has decided on a given movement and even changing or moving the saccade target at this point does not affect the outcome movement. Studies have shown the duration of the dead-time period to be about 70 ms, though it also depends on the distance between the location of the previous target and that of the present target (Becker and Jürgens, 1979).

1.1.2 Reflexive versus Voluntary Saccades

Reflexive saccades are the kind of saccadic eye movements that occur naturally in response to the appearance of a stimulus in our visual field. Visually guided saccades are an example of reflexive saccades that are exogenously driven by a stimulus presented on the display (Luna and Velanova, 2011). The presence of a new stimulus helps drive the motor accumulation to the necessary threshold to issue motor commands resulting in a reflexive saccade (Carpenter and Williams, 1995). Express saccades are known as the most reflexive kind of eye movements

towards a visual stimulus. Express saccades have an extremely short latency (70-100ms) and were first noted by Fischer and Boch (1983) who observed a bimodal pattern in the SRT distribution with an early peak that they corresponded to express saccades and a second peak with longer latency (120-200ms) corresponding to regular saccades (Fischer and Boch, 1983). Gap paradigm (Saslow, 1967) is an example of an experimental paradigm to observe express saccades. In this task, a short delay (150-250ms for macaques) is introduced between disappearance of the central fixation point and the appearance of the target to which a saccade is to be made. The early offset of the fixation point in this task helps to reduce activity of SC fixation neurons (Dorris and Munoz, 1995) and the disinhibition of SC saccade neurons, thus increasing the build-up activity and getting the system closer to a response threshold (Dorris and Munoz, 1998). This together with stimulus-evoked responses triggers an express saccade.

Aside from being elicited by a target of interest presented in the visual field, saccades can also be generated internally into what's known as voluntary saccades. Voluntary saccades are guided by voluntary control, generated in the absence of a stimulus onset at saccade destination and are therefore cognitively driven or endogenous eye movements (Luna and Velanova, 2011). Due to the absence of a stimulus and the higher order processes involved, these endogenous saccades are generally slower on average compared to the exogenous reflexive saccades (Walker et al., 2000). There are several saccade paradigms that have been designed for laboratory use to study voluntary saccades. These include the memory-guided saccade paradigm which identifies voluntary saccades that are elicited by memory processes (Hikosaka and Wurtz, 1983a), and the antisaccade paradigm which examines voluntary antisaccades that are made following the inhibition of a reflexive saccade to the opposite direction (Hallett, 1978; Munoz and Everling, 2004). We will go over such saccade paradigms in more details in part 3

of the current chapter. When the time and location of a target becomes predictable through training and practice, a new category of voluntary saccades emerges, known as anticipatory saccades that occur before the target appears. Since the target location is anticipated beforehand, the attention is disengaged from that and rather focused on initiating processes to make a saccade to the location of the new target that is learned and anticipated through practice (Coe et al., 2002).

1.1.3 Saccade and Attention

Visual scenes that we are exposed to in our daily life, can contain far too much information to be grasped in just a single glance. Attention is the brain mechanism that helps us have an effective vision and be able to focus on our object or location of interest in an optimal manner. Attention is a filtering mechanism by which the brain chooses certain objects or locations over others in a pool of incoming sensory information. To allow selection of that object or location, attention has to work in a coordinated fashion with saccadic eye movements and in this sense saccade processing and attention are associated with one another (Zhao et al., 2012). Attention can occur either voluntarily by selecting objects or locations that are in line with the goals of the observer (top-down attention), or involuntarily by salient properties of the stimulus on its own (bottom-up attention) (Klein, 1994). In this sense, reflexive saccades are related to bottom-up attention and voluntary saccade related to top-down attention. In top-down attention for voluntary saccades, the location of the next saccade is being processed by higher order cortical areas and thus a covert shift of attention to a spatial location helps in processing a saccade to that location. On the other hand, in bottom-up attention for reflexive saccades, the sudden

appearance of a stimulus at a spatial location reflexively brings the attention towards the stimulus at that location which is followed by a reflexive saccade towards that stimulus. Such overt shift of attention to that location via making a saccade towards it, aids in processes involved in perception of the object at that location (Moore and Armstrong, 2003). In either case, reflexive or voluntary saccade, attention occurs first. Considering that we can attend to a location without moving our eyes, perceptual attention can operate independent of saccades, but saccades cannot be issued without attention. Attention is shifted to the target of a saccade while saccade planning is under way (Zhao et al., 2012). Thus, saccade related findings often have implications with regard to attention mechanisms in the brain. In what follows we will go over several brain areas involved in the oculomotor system that contribute to the attention network.

1.2 Oculomotor Circuitry

The cortical and subcortical circuitry controlling saccadic eye movements is perhaps the most thoroughly understood sensorimotor system in the primate brain (Munoz et al., 2000; Schiller and Tehovnik, 2001). Most of what we know about the oculomotor circuitry comes from the Old-World macaque monkeys. Closer proximity of their brain structure and function to that of human brain and their remarkable ability to learn saccade tasks similar to those implemented in human, has been the greatest inspiration to investigate this circuitry on this primate species. What follows is a summary of what we know about the network subserving saccadic eye movements and its constituent components based on the large body of literature on macaques. The network subserving saccadic eye movements encompasses areas in posterior parietal,

superior temporal, and frontal cortices, as well as subcortical brain regions (Donaldson, 1990; Johnston and Everling, 2008). Prominent oculomotor areas in the macaque include the frontal eye fields (FEFs) (Bruce et al., 1985), lateral intraparietal area (LIP) (Shibutani et al., 1984) and supplementary eye fields (SEFs) (Schlag and Schlag-Rey, 1987; Huerta and Kaas, 1990), all of which send direct projections to the midbrain superior colliculus (SC) (Goldman and Nauta, 1976; Selemon and Goldman-Rakic, 1988), an area critical for saccade generation. The dorsolateral prefrontal cortex (DLPFC) is another cortical area known to be involved in saccade circuitry, containing neurons with direct projections to the SC (Johnston and Everling, 2006). Anatomical tracing studies have also found that the anterior cingulate cortex (ACC) has direct projections to the FEF and is potentially involved in cognitive and sensorimotor integration involved in saccade processing (Naito et al., 2000; Wang et al., 2004). However, microstimulation of areas DLPFC and ACC at physiologically relevant current levels has not evoked saccades (Funahashi et al., 1991) and thus, they are thought to have a more modulatory function.

Depending on the objectives of a research project and the kinds of questions being asked, different aspects and components of the oculomotor network have been explored in the past. My research projects mostly involved areas SC, FEF and LIP. In what follows, we will go over these pivotal saccade-related areas of interest to this work in further details.

1.2.1 Superior Colliculus (SC)

Superior colliculus (SC) is a subcortical brain area located at the roof of the brainstem that plays a crucial role in guidance and coordination of orienting response. It integrates motor, cognitive

and multisensory information and in turn sends motor commands directly to the brainstem, thereby invoking the eyes, neck and shoulder to implement the orienting response (Corneil et al., 2002a; Boehnke and Munoz, 2008; Rezvani and Corneil, 2008). SC neurons are organized into topographic maps that contain representations of the contralateral space, that is essential in spatially guided behavior (White and Munoz, 2011). Functionally, the SC consists of two parts: a superficial layer that is exclusively involved in visual processing (Goldberg and Wurtz, 1972), and an intermediate to deep layer that is involved in motor (Wurtz and Goldberg, 1971), multisensory (Meredith and Stein, 1983, 1985), and higher cognitive processes (Basso and May, 2017).

1.2.1.1 SC Afferent and Efferent Projections

The superficial SC mostly receives visual inputs, coming mainly from the retina (Hubel et al., 1975) and primary visual cortex (Fries, 1984; Lock et al., 2003). In comparison, the deeper parts of the SC receive much more corticotectal projections. Cortical brain areas contribute to the saccadic eye movement mostly through their projections to the deeper SC and they include prominently the frontal eye field (FEF) (Bruce et al., 1985; Stanton et al., 1988a), dorsolateral prefrontal cortex (DLPFC) (Goldman and Nauta, 1976), lateral intraparietal area (LIP) (Lynch et al., 1985), and supplementary eye field (SEF) (Huerta and Kaas, 1990) (Fig. 1). Projections from frontal areas are thought to represent the higher-level top-down control of the deeper SC and play a significant role in flexible control of oculomotor behavior (Everling and Munoz, 2000). Aside from corticotectal projections, there are also subcortical projections from the basal ganglia (Künzle and Akert, 1977) to the deeper SC. Basal ganglia sends direct inhibitory

projections from the substantia nigra pars reticulata (SNr) to the deeper SC to regulate saccadic burst initiation (Sakamoto and Hikosaka, 1989; Hikosaka et al., 2000) (Fig. 1).

In terms of outputs, the superficial SC in primates mainly projects to the pulvinar nuclei within the thalamus (Berman and Wurtz, 2010), the lateral geniculate nucleus (LGN) (Harting et al., 1978), and deeper parts of the SC (Helms et al., 2004). The deeper SC sends projections to the substantia nigra pars compacta (SNc) (Comoli et al., 2003), paramedian pontine reticular formation (PPRF) and rostral interstitial nucleus of the medial longitudinal fasciculus (rMLF) which are where the horizontal and vertical saccade premotor circuitry is located (Rodgers et al., 2006). SCi projections to the SNc contains information about the transient visual activity to the dopaminergic system within the basal ganglia, reinforcing the context right before relevant visual events (Comoli et al., 2003; Redgrave and Gurney, 2006). Neurons within the PPRF and mesencephalic reticular formation (MRF) produce the necessary burst signal for driving horizontal (Sasaki and Shimazu, 1981) and vertical saccades (Moschovakis et al., 1991a, 1991b), respectively. Omnipause neurons (OPNs) are another class of brainstem neurons that play an important role in saccade generation, acting as an inhibitory gate for saccades (Keller, 1974). The SCi also has projections to the cerebellum. The cerebellum is involved in all types of mammalian eye movements (Albus, 1971; Thier, 2011). One of its most prominent roles is to prevent large field images from slipping on the retina as might be the case in saccadic, smooth pursuit or the VOR eye movements. The region of the cerebellum in charge of that is known as the floccular region (FR) that aids in stabilizing the visual image on the retina by moving the eyes in the direction of the expected image movement (Lisberger and Fuchs, 1978a, 1978b). The oculomotor vermis of the cerebellum is more specifically involved in saccades, subserving the need to control an initial movement (Aschoff and Cohen, 1971; Barash et al., 1999). There

are also indirect projections from deeper SC to the FEF via the mediodorsal thalamus (MDN) (Lynch et al., 1994) and to the LIP via the pulvinar (Clower et al., 2001). SC outputs to the FEF are believed to carry an internal copy of the saccade motor command, known as the corollary discharge, to the cortex immediately before the onset of movement to warn the cortex of an upcoming eye movement and a potential need to update the visual representations (Sommer and Wurtz, 2004, 2006). It is through this projection that our view is maintained stable during the rapid shifts of the visual axis caused by saccades (Sommer and Wurtz, 2006, 2008). Aside from these projections, anatomical studies have also reported on the existence of a lateral inhibitory network across the deeper SC (Munoz and Istvan, 1998), which plays a key role in the winner-take-all mechanism of visual attention by which only one spatial location gets to reach threshold, in order to guide the allocation of attention (Itti and Koch, 2001; Wolfe and Horowitz, 2004).

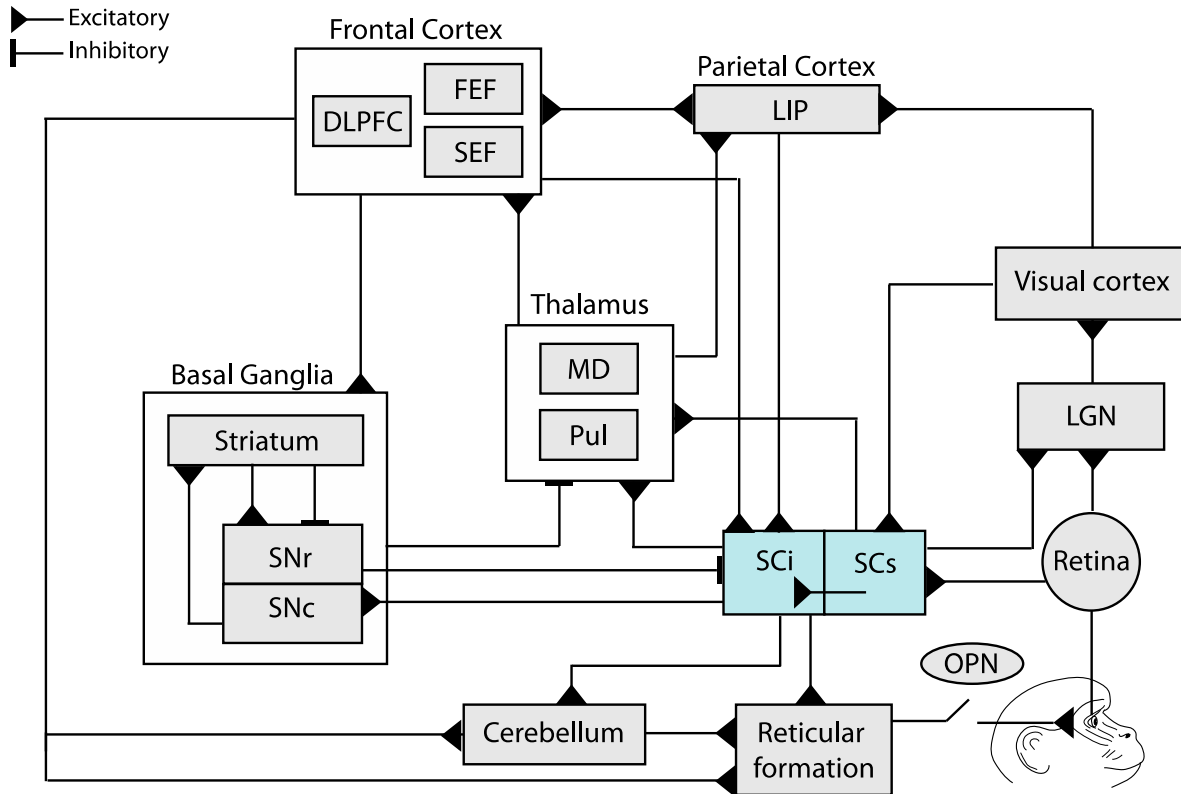


Figure 1-1. Brain circuitry underlying saccadic eye movements in primates, demonstrating afferent and efferent projections of the superior colliculus (SC). Lines represent connection between brain areas involved in the oculomotor circuitry, with triangles referring to excitatory connections and bars representing inhibitory connections. DLPFC: dorsolateral prefrontal cortex, FEF: frontal eye fields, SEF: supplementary eye fields, LIP: lateral intraparietal area, LGN: lateral geniculate nucleus, SCi: superior colliculus intermediate layers, SCs: superior colliculus superficial layers, MD: mediodorsal nucleus, Pul: pulvinar, SNr: substantia nigra pars reticulata, SNc: substantia nigra pars compacta, OPN: omnipause neurons. Based on the figure in Box 1(a) from Munoz and Everling (2004).

1.2.1.2 Response Properties of SC Neurons

The superficial layers of the SC (SCs) mostly contain neurons that have an exclusively visual response demonstrated by short, high-frequency bursts of action potential shortly after a visual stimulus appears in their response field (Goldberg and Wurtz, 1972). Similar to other visual neurons, SCs neurons show high sensitivity for stimulus intensity (Li and Basso, 2008) but have low preference for specific visual features such as color (Schiller and Malpeli, 1977).

In comparison, neurons in intermediate to deep layers of the SC (SCi) cover a much broader range of response properties matching their integrative role towards the multisensory, motor and cognitive projections they receive. A large portion of SCi neurons are the visuomotor neurons that have a burst of action potential 50 ms after a visual stimulus appears in their response field and then a separate burst of action potential related to the generation of saccades (Mohler and Wurtz, 1976). Saccade-related SCi neurons have a movement field, firing in response to a range of saccade amplitudes and directions directed to that field. Many SCi neurons have closed movement fields the borders of which are clearly defined, as opposed to some with an open-ended field that respond for all saccades that are equal or greater in amplitude than their optimal (Munoz and Wurtz, 1995). The visual and motor response fields of SCi neurons have a close spatial correspondence to make sure that a visual response to a visual stimulus is directly mapped onto the SCi output neurons in charge of eliciting an orienting response to the visual stimulus (Marino et al., 2008). Most SCi neurons have a build-up pattern of activity prior to saccades, in the form of a low-frequency activity that seems to be associated with shift of attention (Kustov and Robinson, 1996), target selection (Basso and Wurtz, 1997) and motor preparation (Corneil et al., 2007). The build-up pattern of activity implies that saccades are initiated when the variable growth of presaccadic activity reaches a

fixed threshold (Stuphorn and Schall, 2002). Electrophysiological recording of the SCi neurons has demonstrated that their pre-target neuronal activity increases as the likelihood of a saccade being generated into the neuron response field increases. Saccade reaction times (SRTs) are also reduced when the location of the upcoming target is more predictable (Dorris and Munoz, 1998). These findings indicate a role of SCi build-up neurons in the initiation of saccades and motor preparation processes.

At the rostral part of the SCi, there are fixation neurons that exhibit a tonic firing rate during fixation and minimal activity during most saccades (Dorris and Munoz, 1995). Studies involving excitation or inhibition of these rostral SCi neurons have demonstrated their importance for saccade initiation and suppression (Munoz and Wurtz, 1993). Everling et al (1999) also observed an increase in the tonic activity of fixation neurons in an antisaccade task, which involves suppressing a saccade prior to the appearance of the stimulus, indicating the role of these neurons in saccade suppression (Everling et al., 1999a).

In 2003, Paré and Hanes used the countermanding task to explore whether the SC contains neurons whose activity patterns are sufficient to control both the cancellation and production of saccades (Paré and Hanes, 2003). The countermanding paradigm tests the ability to inhibit response initiation whenever a less frequent stop signal follows the more frequent go signal. This paradigm has been adapted for saccadic eye movements in monkeys to study the role of a brain area in saccade production (Hanes and Schall, 1995). The hypothesis is that if a neuron is involved in saccade production, it should change its activity just before when a saccade is cancelled instead of executed. This hypothesis was strongly supported in the SC where both saccade and fixation neurons discharged differently when saccades were counter-manded instead of executed, with saccade-related neurons having a significantly reduced firing rate and

fixation neurons with increased firing rate (Paré and Hanes, 2003). These results provided solid evidence that the SC contains the necessary neural signal to be directly involved in regulating whether and when a saccade is produced.

1.2.1.3 SCi and Top-down Control

Neurons in the SCi are functionally known to hold a so-called priority map, a combined representation of sensory salience and behavioral relevance, indicating to the integration of bottom-up sensory information and top-down signals for flexible control of behavior (Fecteau and Munoz, 2006). Target selection is a good example of such integration that has been observed within the activity of SCi visuomotor neurons. Inactivation of SCi has been shown to impair target selection (McPeck and Keller, 2004), while its stimulation can bias selection in favor of the contralateral stimuli with respect to the site of stimulation (Carello and Krauzlis, 2004).

Studies have shown that SCi neurons have discharge rates that correspond to internally and externally driven shifts of visuospatial attention (Dorris et al., 2002, 2007). As mentioned in the previous section, attention is a filtering mechanism by which the brain chooses certain objects or locations over others in a pool of incoming sensory information. It can happen either voluntarily by selecting objects or locations in line with the goals of the observer (top-down attention), or involuntarily by salient properties of the stimulus on its own (bottom-up attention) (Klein, 1994). SCi neurons show increased activity during internally driven shift of attention into their response field, even if there is no visual stimulus presented (Ignashchenkova et al., 2004). SC inactivation studies have reported ignorance of spatial cues that appeared in the

affected region of the visual space, demonstrating the role of SC in covert attention (Lovejoy and Krauzlis, 2010).

SCi neurons also seem to modulate their activity in relation to the expectation of a reward. Both visual and preparatory activity of these neurons is enhanced when a visual stimulus signals an upcoming reward (Ikeda and Hikosaka, 2003). This is potentially due to the SCi receiving direct projections from areas encoding reward related information, such as prefrontal cortex and basal ganglia (Ikeda and Hikosaka, 2007). Reward expectation is an important factor in decision making and thus plays a role in top-down processes.

1.2.2 Frontal Eye Field (FEF)

There is a large body of research over the past decades that has proven the existence of an eye movement area within the prefrontal cortex of primates, known as the frontal eye fields (FEF) (Schall, 1997), microstimulation of which elicited contralateral eye and head movements. Its anatomical location in monkeys was found to be in the anterior bank and fundus of the arcuate sulcus where saccades could be elicited with very low current thresholds ($< 50 \mu\text{A}$) and is now the commonly accepted anatomical location of FEF in monkeys (Robinson and Fuchs, 1969). Systemic microstimulation of FEF in monkeys revealed that the evoked eye movements were indeed saccades whose amplitude varied systemically with the site of stimulation (Robinson and Fuchs, 1969). In what follows we will go over FEF inputs and outputs and its neuronal properties.

1.2.2.1 FEF Afferent and Efferent Projections

FEF is considered the main cortical eye field in primates that has reciprocal connections with occipital, temporal, parietal and other prefrontal cortical areas (Huerta et al., 1987). It has been identified as part of the prefrontal cortex by the presence of a granular layer and incoming projections from the mediodorsal (MD) nucleus of the thalamus (Stanton et al., 1988a, 1989). The medial FEF has been demonstrated to be structurally connected with areas within the parietal cortex and dorsal visual stream whereas the lateral FEF is connected with temporal areas and ventral visual stream (Schall et al., 1995a). The dorsal visual stream is involved in spatial vision and visually-guided motor responses, while the ventral stream is more involved in object perception and identification (Goodale and Milner, 1992).

The FEF receives inputs from both superficial and intermediate layers of the SC, substantia nigra pars compacta and thalamus (Lynch et al., 1994). FEF sends heavy projections to the SC with most of them on the ipsilateral side (Huerta et al., 1986; Stanton et al., 1988b). Other subcortical projections of the FEF include those towards caudate and putamen (Stanton et al., 1988b) as well as pontine and mesencephalic brainstem areas (Büttner-Ennever and Horn, 1997). Through its projections to the SC and brainstem, FEF contributes to controlling whether and when saccades are initiated (Bruce and Goldberg, 1985). Unilateral deactivation of the FEF generally results in a strong contralateral neglect, short-term deficits on visually guided saccades (Crowne et al., 1981; Gregory Keating and Gooley, 1988) but lasting impairments of memory-guided saccades (Dias and Segraves, 1999). The mild impairment of the visually guided saccades has also been observed following SC inactivation, but the deactivation of both regions FEF and SC at once has had much stronger and lasting deficits in saccadic eye movements (Schiller et al., 1979, 1980).

The FEF maintains an organized map of mostly the contralateral visual space in eye-center coordinates (Bruce and Goldberg, 1985). Electrical microstimulation of FEF in macaques elicits short-latency, fixed vector saccades at low currents ($< 50\mu\text{A}$) (Bruce and Goldberg, 1985), with amplitudes that are tuned based on the stimulation site: larger saccades in the dorsomedial parts and smaller ones towards ventrolateral parts (Robinson and Fuchs, 1969). Dorsal and ventral visual streams of the extrastriate cortex send topographical projections to dorsomedial and dorsolateral FEF, respectively that are used to orient and explore objects near the fovea (Schall et al., 1995a). For this reason, the FEF is considered part of the visual system as much as it's thought of as a motor area and numerous FEF neurons have responses to visual stimuli about 50 ms after it appears (Bruce and Goldberg, 1985; Schmolesky et al., 1998).

Contralateral head movements have also been observed following FEF microstimulation in head-unrestrained monkeys that indicate to the involvement of FEF in orienting response in general, which also includes eye movements (Tu and Keating, 2000; Elsley et al., 2007).

1.2.2.2 Response Properties of FEF Neurons

Traditionally, neurons in area FEF have been thought to play a prominent role in the transformation of visual information into saccade commands (Bruce and Goldberg, 1985). Single-unit recordings of FEF neurons have demonstrated several types of neurons within the FEF: saccade or motor neurons that respond before and during saccade generation; fixation neurons that are active during fixation and pause during saccades; visual neurons that respond to presentation of a behaviorally relevant stimuli in their receptive field, and the most common visuomotor neurons that are active in response to both visual stimulation and motor plans

(Bruce and Goldberg, 1985; Schall, 2002). An interesting feature of most of FEF motor and visuomotor neurons was the presence of an anticipatory activity that preceded the cue for saccade initiation whenever the monkey could predict the next saccade, indicating the important role of FEF in saccade initiation (Hanes and Schall, 1996). FEF fixation neurons are activated when monkeys are actively fixating their gaze on a stationary position and electrical microstimulation of these neurons during saccadic eye movement has immediately stopped oculomotor activity (Burman and Bruce, 1997). This is due to the fact that in both SC and FEF, in order to produce saccades, the activity of saccade neurons should increase while the activity of fixation neurons should decrease (Everling and Munoz, 2000).

The countermanding paradigm that was mentioned in the previous section as a tool to explore the role of the SC in saccade production, was also applied by Hanes and colleagues in (1998) to explore the direct involvement of the FEF in saccade production. Electrophysiological recordings of the macaque FEF during the task, demonstrated that saccade-related neurons of the FEF had reduced activity in response to the stop signal while FEF fixation neurons had elevated activity (Hanes et al., 1998). This finding provided evidence that the FEF neurons generate signals that are sufficient to control saccade cancellation and production.

Electrophysiological recordings from corticotectal FEF neurons of macaques performing delayed and gap saccade tasks have shown that these neurons send visual and cognitive signals to the SC and continue affecting it during oculomotor tasks based on their tonic delay activity and increased activity during the gap period (Sommer and Wurtz, 2000). Everling and Munoz (2000) recorded from these corticotectal FEF neurons while monkeys were performing pro and antisaccade tasks and found that they responded to both pro and antisaccade into their response field, with relatively lower presaccadic activity for antisaccade trials. The level of activity

before the presentation of peripheral stimulus was also higher on pro trials than anti trials (Everling and Munoz, 2000). A prosaccade trial requires the monkey to make a saccade towards the peripheral stimulus while an antisaccade trial requires to make a saccade to the opposite direction of where the peripheral stimulus is presented (Munoz and Everling, 2004). This lowered preparatory activity and stimulus related response of saccade related FEF neurons on antisaccade trials was proposed to reduce the excitation of saccade neurons of the SC (Everling and Fischer, 1998; Everling and Munoz, 2000), thereby reducing the risk of generating incorrect response in these trials (saccade towards stimulus). This indicates that correct performance on the antisaccade task is dependent on top-down control of the SC via frontal cortical areas such as the FEF.

1.2.2.3 FEF and Top-down Control

Aside from its pivotal role in saccade generation, the FEF is also involved in a multitude of actions such as target selection, visual search, attention and transformation of visual signals to saccade commands. Studies using visual search paradigms have revealed the role of FEF in top-down control of visual processing. In a visual search paradigm, the subject has to discriminate a visual target among several distractors (Zhou and Desimone, 2011; Schall, 2015). Most FEF neurons in this task initially had visual responses in a non-selective manner to the array of visual stimuli in their receptive field but then had increased activity before the onset of saccade towards the target stimulus, when the target (and not the distractors) fell into their response field (Thompson et al., 1996). In another words, throughout the target selection process, most visually responsive FEF neurons signaled the location of the target stimulus by suppressing the

response to nontarget stimuli. This enhancement of activity was independent of saccade execution, reflecting the distinct role of FEF in spatial attention. This finding was also evident from the fact that only visual and visuomotor and not motor neurons had modulated activity in the absence of saccades, potentially relating to spatial attention (Thompson et al., 2005b; Gregoriou et al., 2012). Therefore, the FEF appears to have a role in highlighting the location of behaviorally relevant targets which might be related to computation of a saliency map for programming a saccade. This attention-related activity of FEF neurons can also induce attention-related modulations of activity in extrastriate areas such as V4. Moore and colleagues microstimulated the FEF with currents lower than those needed to produce saccades, and observed increased response in V4 neurons at response fields matching the locations of FEF response fields and suppressed response in neurons with response fields at other locations (Moore and Armstrong, 2003). This finding indicates to the role of area FEF in top-down control of visual information.

1.2.3 Posterior Parietal Cortex (PPC)

The posterior parietal cortex (PPC) sits at the interface of somatosensory and visual cortices in primates. Its location provides a great interface between frontal motor fields and occipital and temporal visual fields, suggesting a potential role in visually guided behavior. From an evolutionary perspective, PPC came relatively later in the eye movement circuitry, suggesting that it does not directly contribute in saccade generation, but is rather involved in enhancing the sensory guidance of visual behavior by providing regulatory signals in the form of representations (Fang et al., 2005; Paré and Dorris, 2011). Anatomically, the PPC has strong

connections with the prefrontal cortex, dorsal pulvinar and the SC and is therefore considered a node within a higher-order network that only exists in primates (Preuss, 2007).

1.2.3.1 Lateral Intraparietal Area (LIP) and Its Projections

Lateral intraparietal area (LIP) is an area within the lateral bank of the intraparietal sulcus within the PPC that has been implicated to exhibit the strongest connections to the saccade circuitry (Lynch et al., 1985; Blatt et al., 1990). Neurons from this specific subdivision of the PPC have demonstrated both visual and saccade related activity (Andersen et al., 1987) and together they form a coarse representation of the contralateral visual field (Ben Hamed et al., 2001). Area LIP integrates sensory and goal-directed signals into a map in which it holds a representation of spatial locations that can be selected as saccade targets through decision making processes (Paré and Dorris, 2011). Anatomically, the LIP receives input from many visual areas and projects to two prominent oculomotor areas heavily involved in saccade production, the FEF and intermediate SC (Andersen et al., 1990). Reciprocal connections have also been found from FEF to LIP (Ferraina et al., 2002) directly, and from superficial SC to LIP indirectly via the inferior pulvinar (Clower et al., 2001). The LIP can further be subdivided into an antero-dorsal (LIPd) and postero-ventral (LIPv) portion, with the latter having stronger connections with SC and FEF and thus considered as the main interface between visual and saccade systems (Schall et al., 1995a). LIPd is more exclusively connected to the visual areas of the temporal cortex and may have a more prominent role in visual processing (Lewis and Van Essen, 2000).

1.2.3.2 LIP and Saccade Production Processes

Despite the strong connections of area LIP with areas FEF (Schall et al., 1995b) and SC (Lynch et al., 1985), it is not directly involved in the production of saccades. While removing areas FEF and SC severely impairs saccade production in monkeys, removal of area LIP does not impair saccade production (Lynch and McLaren, 1989). Microstimulation studies have demonstrated that in comparison to the FEF and SC, a larger amplitude of electrical current is needed to elicit a saccade when stimulating the LIP (Shibutani et al., 1984). Behavioral studies have found that the magnitude of pre-saccadic activity in LIP is significantly decreased when saccades are made in the absence of a visual stimulus, indicating its rather visual dependency (Ferraina et al., 2002) in comparison to areas FEF and SC with higher presaccadic activity that is correlated with saccade occurrence (Bruce and Goldberg, 1985). If a brain area is involved in saccade production, its neural activity should closely correlate with saccade occurrence. The countermanding paradigm that tests the ability to inhibit response initiation whenever a stop signal follows the frequent go signal (Hanes and Schall, 1995), has been previously applied to both SC (Paré and Hanes, 2003) and FEF (Hanes et al., 1998) to know if they contain neuron involved in saccade production, with activity changes just before saccade cancellation instead of execution. Most movement neurons of the SC (Paré and Hanes, 2003) and FEF (Hanes et al., 1998) have followed this expected behavior recognizing their role in saccade production, but a later study on LIP reported that neurons in this area only rarely changed their activity when saccades were canceled and this change almost always happened later than when the saccade was canceled (Paré and Dorris, 2011). This mere change of presaccadic activity therefore indicates that the area LIP does not contain the necessary signals to produce saccades but is rather involved in more covert processes guiding the saccades.

1.2.3.3 LIP and Saccade Preparation Processes

Rather than saccade production process, area LIP might be more involved in covert processes such as saccade preparation by which the response goal and execution are specified. If a neuron is involved in saccade preparation, its activity will change before an upcoming saccade and is predictive of the timing of the saccade. Anderson and colleagues (1987) imposed a delay period between visual stimulation and the onset of saccade and observed that LIP neurons discharged long before specific saccades corresponding to their response field, and this activity was maintained during the delay period and reduced when saccade was made within the response field without a recent visual stimulation (Andersen et al., 1987). However, there is very weak evidence about whether the sustained activity of LIP neurons is predictive of saccade latency. Studies in SC (Dorris and Munoz, 1998) and FEF (Hanes and Schall, 1996) have demonstrated that saccades are initiated when the variable growth of presaccadic activity reaches a fixed threshold, which usually happens quite late, about 10 to 12 ms before saccade initiation (Paré and Hanes, 2003), consistent with the physiology of saccade circuitry (Hanes and Schall, 1996). This variable growth in presaccadic activity is also observed in LIP neurons but it reaches threshold about 70 ms before saccade initiation (Roitman and Shadlen, 2002) which is far from that of SC and FEF. It is rather closer to the timing of the threshold for saccade target selection in both SC and FEF (Thompson et al., 2005a) and therefore implies that maybe LIP is more involved in guiding saccade target selection, rather than its production.

1.2.3.4 LIP and Top-down Control

The sustained activity of LIP neurons during the delay period may not be associated to movement processes, but rather reflect visual working memory processes related to the presented visual stimulus in the task. Based on the large body of literature on working memory in the prefrontal cortex (PFC), PFC neurons have a similar persistent activity associated with working memory in the delayed response task (Fuster and Alexander, 1971; Bruce and Goldberg, 1985; Funahashi et al., 1989). LIP neurons have also demonstrated a very similar persistent activity during the memory delayed saccade task to that of PFC neurons (Chafee and Goldman-Rakic, 1998). The temporal characteristics of the LIP neuronal activity during the delay period in this task involves broadband oscillations within the Gamma frequency range (Pesaran et al., 2002) that resemble those observed in human EEG data during short term memory (Tallon-Baudry et al., 1998). This might suggest that area LIP neurons contain information about temporarily maintaining the goal of saccade in the absence of visual stimulus. Despite these few findings, the exact relationship of the persistent activity in area LIP to working memory is not as well understood as it is in PFC and further studies looking at deactivation of LIP and the impact on performance in working memory related tasks can help clarify its role.

PPC neuronal activity has also demonstrated some level of attention-related modulations. Saccade processing can be both related to covert and overt shifts of visuospatial attention. Covert shifts of attention to a spatial location helps in processing of saccades directed to that location, while overt shifts of attention to that location by planning a saccade towards it, helps in perceptual processing of objects at that location (Moore et al, 2003). Voluntary shifts of visual attention have been shown to correspond with increased activity in areas FEF and SC

(Moore et al., 2003; Awh et al., 2006) in addition to visual cortical areas. LIP neurons have increased visually evoked responses when the presented stimulus specifies the goal of saccade (Robinson et al., 1978) or during active fixation (Lynch et al., 1977), indicating its role in providing regulatory guiding signals for the action and therefore reflecting a more covert form of attention. The visual search paradigm which involves finding a target within a multi-stimulus display (McPeck and Keller, 2002; Wolfe and Horowitz, 2004), has often been used in studies of visual attention and identification of activity related to saccade target selection. Neuroimaging studies of human subjects performing this task has demonstrated an increased blood flow in PPC when the task gets difficult (Corbetta et al., 1993; Donner et al., 2000, 2002), in line with monkey findings demonstrating deficits in performing the task following LIP inactivation (Wardak et al., 2004). Based on all these observations, area LIP seems to contain neurons that carry information for regulating and guiding a saccade.

The saccade target selection process that occurs in the visual search paradigm is also indicative of a perceptual decision-making process in terms of choosing the next target. Area LIP has been implicated to be involved in visual decision-making, by providing a map that contains supporting evidence about the saliency of competing stimuli. It might then be this decision that then contributes to visual attention, working memory and saccade preparation (Liversedge et al., 2011; Paré and Dorris, 2011). LIP neuronal activity is also affected by the probability of a saccade target resulting in rewards and the amount of reward associated with that location (Churchland et al., 2008). In areas FEF and SC, such economic information is represented in baseline activity (Basso and Wurtz, 1998; Yang and Shadlen, 2007), but in LIP it only shows up immediately after target presentation. This finding implies that LIP does not hold such economic information but instead it modifies the representations that it holds, based on their

economic impact. As part of the decision-making process, LIP neurons seem to predict the ultimate choices made by the subject based on neuronal recordings of area LIP in monkeys performing the motion discrimination task (Shadlen and Newsome, 1996, 2001). Electrical microstimulation of LIP has resulted in decreased latency and increased proportion of choices towards the targets that were associated with the stimulation site, indicating a modulation of perceptual decision making (Hanks et al., 2006).

Overall, area LIP neuronal activity is not directly associated with saccade production as is the case with areas FEF and SC. It rather holds representations about potential saccade targets and therefore helps the saccade system with guidance signals to allow a more flexible control of behavior.

1.3 Common Marmoset Monkeys

Based on all that was discussed in previous sections, it is certainly clear by now that most of our knowledge of the oculomotor system at cortical and subcortical levels comes mainly from neurophysiological studies in macaque monkeys. These studies have provided the foundation for our understanding of saccade control and have revealed fundamental insights into the neural basis of decision making, attention, and other higher executive functions in primates. Despite their fundamental role as a nonhuman primate (NHP) model for saccade control and cognition, macaque monkeys have several shortcomings that have emerged following technological advances in recording devices, urging the neuroscientific research community to seek for alternative NHP models. One of the main disadvantages of using macaques as animal models of oculomotor system is that some of the key frontoparietal areas involved in the system such as the FEF, are deeply buried in sulci, making them difficult to access using high-density

electrophysiological recording techniques such as Utah multielectrode arrays. From a broader point of view, macaques' low birth rate and long sexual maturation makes it difficult to utilize them for transgenic approaches that are popular these days. Due to the animals' large body size, pharmacological studies tend to be very expensive to implement in macaques, requiring higher doses to observe effects. These disadvantages have brought the attention of the biomedical research community to a New World NHP species known as the common marmoset monkey. The common marmoset (*Callithrix jacchus*) is a small-bodied New World primate that has recently gained considerable attention as a model for biomedical research in general (Mansfield, 2003) and neuroscience research in particular (Izpisua Belmonte et al., 2015; Mitchell and Leopold, 2015; Miller et al., 2016; French, 2019). It belongs to South American monkeys of *Callitrichidae* family that are characterized by their small body size and presence of claw-like nails on both hands and feet (Solomon and Rosa, 2014). Their body size excluding their long tail, rarely exceeds 20 cm and they weight around 300 gr on average (Solomon and Rosa, 2014). They are day-active animals that naturally live in family groups of 10-15 members and remain in their social group until adulthood. They reach sexual maturity in about 18 months. With a gestation period of about 5 months, female marmosets generally give birth twice a year, most often to non-identical twins. With their fast sexual maturation, low inter-birth interval, and routinely observed chimeric twinning, marmoset monkeys are becoming an ideal candidate for transgenic primate models of human neurodegenerative disorders (Sasaki et al., 2009; Okano et al., 2012; Kishi et al., 2014; Izpisua Belmonte et al., 2015; Mitchell and Leopold, 2015). In terms of the size of the brain, marmosets have a brain that is more comparable in size to a rat brain. It is almost 12 times smaller in volume than that of the macaque and 180 times smaller than that of human (Stephan et al., 1981; Mitchell and Leopold, 2015). Despite its superficial

resemblance to the rat's brain, the functional organization and anatomical structure of the marmoset brain is still that of a primate, thus more closely resembling that of macaques and humans (Rosa and Tweedale, 2005; McDonald et al., 2014; Mitchell and Leopold, 2015). At the same time in comparison to these larger primates, marmosets possess a lissencephalic (smooth) cortex that offers a great opportunity for high-density electrophysiological recordings and optical imaging in key frontoparietal areas which is particularly interesting for researchers investigating the oculomotor system. Most of the key frontoparietal areas are located right at the surface of the cortex making them easily accessible and well-suited for laminar and high-density recordings (Mitchell and Leopold, 2015).

Marmosets are highly visual, foveate animals that exhibit both saccadic and smooth pursuit eye movements (Mitchell et al., 2014; Mitchell and Leopold, 2015). Recent studies have demonstrated that head-fixed marmosets, like head-fixed macaques, can be trained to perform visual tasks (Mitchell et al., 2014). Thus, the marmoset model holds substantial promise for the study of oculomotor control while providing the opportunity to take advantage of more advanced electrophysiological techniques that can probe the structure and function of the key oculomotor areas in finer details and advance our understanding of local and laminar cortical circuits and their roles in cognitive and motor functions. However, in comparison to the macaque model, our knowledge of marmoset oculomotor areas is currently at an emergent stage and little is known about the functional organization of the saccade network in this species. The anatomical and physiological correspondences between prominent oculomotor hubs in the two species remains to be established. The purpose of my research projects was to investigate the functional organization of the oculomotor network in common marmosets and identify potential homologues of the well-established macaque oculomotor hubs in these New World species.

Establishment of such homologies will be an essential step towards utilizing these species as alternative primate models of the oculomotor system. Upon identifying potential homologues of cortical eye fields in marmosets, I aimed to probe neuronal properties and function of these areas with regards to saccadic eye movements. In what follows, I will go over the details of my approach from resting-state fMRI in lightly anesthetized marmosets to electrophysiological recording in awake behaving marmosets performing the pro/anti saccade task.

1.3.1 Oculomotor Network in Common Marmosets

Common marmoset monkeys are highly visual animals with a well-defined fovea and like other primates, they use saccadic eye movements to direct their high-resolution fovea to an object or location of interest in their visual scene (Mitchell et al., 2014; Mitchell and Leopold, 2015). The marmoset eye is about 11 mm in diameter (Troilo et al., 2009) which is smaller than that of the macaque at 18 mm (Lapuerta and Schein, 1995), and this might explain the difference in visual acuity between the two species, with marmoset visual acuity estimated to be about 30 cycles/deg compared to the macaque at about 50 cycles/deg (Kirk, 2004).

Compared to humans and macaques, marmosets have a much smaller head size and rely more on head movements to redirect their gaze. Head-restrained macaques can make larger saccadic eye movements, while head-restrained marmosets rarely make saccades larger than 10 degrees from the central position (Mitchell and Leopold, 2015).

While macaques are usually reluctant to look at faces, marmoset on the other hand are more interested to gaze directly on faces (Mitchell and Leopold, 2015). Researchers have proposed that this difference might be related to differences in social rules between these two species. In macaques, direct gaze can be interpreted as a threat towards social dominance (Mitchell and

Leopold, 2015) and as a result, macaques rather rely on covert visual attention to observe dominant animals. Marmosets are very social primates on the other hand and may not follow the same social rules as macaques and covert observation and attention may not even be a prominent feature of their social behavior. Aside from this obvious difference in scan paths between the two species, most of gaze characteristics of marmosets and their active exploratory viewing of natural scenes resemble those of macaques (Mitchell et al., 2014; Mitchell and Leopold, 2015). Features such as the relationship between peak velocity of saccades and their amplitude, fixation duration and mean inter-saccade interval were quite similar across both species.

Cortical and subcortical brain areas implicated in controlling eye movements have also been identified in marmosets and are largely homologous to those of macaques. SC is present in marmosets and is known to initiate goal directed eye movements (Bourne and Rosa, 2003; Tailby et al., 2012). Similar to the macaques, marmoset SC receives projections from visual areas V1, V2 and MT as well as regions within the frontal and parietal cortices that potentially represent putative areas FEF and LIP (Collins et al., 2005; Mitchell and Leopold, 2015). Earlier studies that used electrical microstimulation on several frontal cortical areas in marmosets, reported both eye and head movements (Mott et al., 1910). Blum et al (1982) further expanded on these results and found that microstimulation of areas 8aD, 6DC, 6DR and 46 of marmoset frontal cortex evoked ipsilateral and contralateral saccades or slow eye movements of varying speeds (Blum et al., 1982). More recent anatomical studies suggested that it may be located within areas 8aV and 45 (Reser et al., 2013) and task-fMRI studies reported BOLD activation in these areas in response to visual stimuli (Hung et al., 2015). In my first PhD research project we aimed to further identify prominent components of the oculomotor network using resting-

state fMRI on lightly anesthetized marmosets (Ghahremani et al., 2017). Details of the findings of our study will be discussed in chapter 2. In what follows, I will provide further details on the resting-state fMRI technique applied in my first research project and the common approaches to analyze resting-state data.

1.3.2 Resting-state fMRI

Functional Magnetic Resonance Imaging (fMRI) is a class of magnetic resonance imaging (MRI) technique that can demonstrate regional time-varying changes in brain metabolism that can result from task-induced activations or underlying resting-state correlations. fMRI detects local increases in relative blood oxygenation as an indirect measure of neuronal activity, which is commonly known as the blood oxygenation level dependent (BOLD) signal (Huettel et al., 2009). In the early days of functional magnetic resonance imaging (fMRI), researchers were mostly interested in exploring how different brain areas responded to a stimulus presented in a behavioral paradigm to a subject placed inside the MRI scanner. A significant aspect of the brain activity was not taken into consideration this way, since any spontaneous fluctuations in the BOLD signal outside of the stimulus-associated behavioral response were regarded as background “noise”. However, Bharat Biswal who was a graduate student at Wisconsin, decided to do an unusual fMRI experiment in which he asked his test subjects to go inside the scanner and do nothing! He found out that different brain areas had synchronous low frequency fluctuations that correlated together even in the absence of any explicit task and this became the seminal study that established the concept of “functional connectivity” through exploring the low frequency (0.01–0.1 Hz) fluctuations of the BOLD signal at rest (Biswal et al., 1995). Further studies applied exploratory techniques such as independent component analysis (ICA)

on resting-state fMRI functional connectivity maps and identified what's known as brain resting-state networks (RSN) that persist even during light anesthesia (Beckmann et al., 2005; Damoiseaux et al., 2006; Vincent et al., 2007; Smith et al., 2009). Some studies demonstrated that the identified functional connectivity maps had substantial similarities to task-based fMRI maps in which a subject performed behavioral tasks. Moreover, the anatomical connectivity maps that resulted from tracer injections, substantially overlapped with the discovered functional connectivity maps (Vincent et al., 2007). These studies demonstrated that the coherent spontaneous BOLD signal fluctuations not only represent the processing of ongoing cognitive tasks but may also reflect functional brain organizations that persist regardless of different levels of consciousness. Within the past decades, the study of resting-state functional connectivity has been a remarkable non-invasive approach in examining the functional organization of the human brain in patients with brain disorders versus healthy subjects that has enhanced our understanding of larger scale changes of brain networks. Unlike task-based fMRI that typically highlights only a single brain network associated with a behavioral task, resting-state fMRI allows the observation of multiple networks at once. Its relatively shorter duration (5-10 min) compared to task-based fMRI (30 min or more) and simplicity of the procedure has also made resting-state fMRI an easier tool to replicate experiments and compare results across the researchers community (Shen, 2015).

fMRI studies have also been conducted on Old World monkeys such as macaques, performing saccade tasks while inside the scanner and their findings have provided strong evidence that fMRI was able to identify prominent cortical oculomotor areas such as FEF and LIP in anatomical locations that corresponded very closely to what was found through electrophysiological approaches (Koyama et al., 2004; Vincent et al., 2007; Ford et al., 2009).

Saccade generation appeared to evoke BOLD activation in regions along the arcuate sulcus and intraparietal sulcus that matched the anatomical location of areas FEF and LIP, respectively.

Furthermore, researchers have tried applying the same exploratory techniques such as ICA on resting-state fMRI data from lightly anesthetized macaque monkeys, revealing potential homologs across many of human resting-state networks (RSNs) in the macaque. One of these networks is a lateralized fronto-parietal network present in both human and macaque that has been implicated in attentional and oculomotor processes that is of interest to oculomotor research (Beckmann et al., 2005; Jafri et al., 2008; Smith et al., 2009). Hutchison et al. (2012) further explored this network using the seed-based analysis in both species and reported on a consistent functional connectivity between the oculomotor cortical area FEF and several other regions involved in the ICA-driven fronto-parietal network. These regions included the LIP, dorsolateral PFC, ACC, and SEF, all of which are implicated to be part of the oculomotor system based on electrophysiological findings on monkeys. These findings indicated that the fronto-parietal network underlies the saccadic eye movement circuitry and is evolutionarily preserved across macaques and humans.

Over the last few years, considerable amount of effort has also been directed toward mapping the marmoset brain (Okano & Mitra, 2015) and establishing homologies between cortical areas in this species and the macaque (Solomon and Rosa, 2014; Bakola et al., 2015).

A study led by Belcher et al (2013) was the first comprehensive resting-state fMRI investigation of awake common marmosets that was able to identify a set of twelve resting-state brain networks that were functionally relevant and spatially consistent with those found in humans (Belcher et al., 2013). In an effort to identify a homologous fronto-parietal network in common marmosets to what was found in macaques and humans, my first project aimed to apply similar

analytic approaches of ICA and seed-based correlation to extract all marmoset RSNs and narrow down the constituent components of such putative front-parietal network that may underly the oculomotor circuitry in these species. In what follows, I will go over the details of these conventional approaches of analyzing resting-state fMRI data.

1.3.2.1 Methods to Analyze Resting-state fMRI Data

There are different analytical approaches that have been developed for analyzing resting-state fMRI data, but the two most commonly applied approaches are the independent component analysis (ICA) and seed-based analysis. ICA a data-driven approach without any previous assumption about the functional connectivity patterns in the brain. It assumes that fMRI data consist of a set of spatially or temporally overlapping components along with other artifactual components related to head motion, respiratory, and pulsation movements (Hyvärinen and Oja, 2000). Each component is assumed to have an independent spatial pattern and an associated time course. The spatial ICA algorithm aims to minimize the spatial overlap between these components based on the independence of the signals. Once the analysis is done and the independent components are identified, the investigator will have to identify which components are RSNs and which ones are artifacts based on prior knowledge of RSNs and artifactual patterns of activity. Also, the investigator has to determine the optimal number of components in the ICA prior to running the analysis and controversy exists as to what the optimal number of independent components is that can best delineate RSNs. Some studies have tried to determine an optimal number through developing a template-matching algorithm (Demertzi et al., 2014), but standardized approaches are lacking, particularly for NHPs. Based on previous reports that have applied ICA on NHPs, the optimal number of independent components for

NHPs falls in the range of 20–30 components, allowing for optimal detection of RSNs (Hutchison and Everling, 2012; Belcher et al., 2013; Mantini et al., 2013).

Being a “model-free” algorithm, ICA attempts to identify cortical activation patterns common to a group of voxels, rather than comparing the activation of individual voxels with a hypothesized time course, as is the case in the seed-based analysis (Hyvärinen and Oja, 2000).

The seed-based analysis is probably among the first approaches applied to analyze resting-state fMRI data (Biswal et al., 1995). As opposed to ICA, seed-based analysis is not a data-driven approach and relies on prior knowledge of the seed area (Lee et al., 2013). A brain region of interest is selected as the seed, whose BOLD signal time course is extracted and averaged across all its voxels. The extracted average time course is then correlated with every other voxel in the brain resulting in functional connectivity maps of the region of interest with the rest of the brain as defined by the strength of the correlation coefficient.

Both ICA and seed-based analyses have been used in my first research paper towards identifying the network underlying the oculomotor system in common marmosets and I will provide further details about it in Chapter 2.

Despite the considerable advantages that fMRI techniques have provided in understanding the functional organization of the oculomotor system in common marmoset monkeys, microstimulation and electrophysiological recording techniques are still necessary to characterize the properties of cortical oculomotor areas in marmosets. Aside from putative area FEF, area LIP was another prominent oculomotor area that I identified in my resting-state investigations, with the strongest SC functional connectivity within the posterior parietal cortex (PPC). The parcellation and homology of marmoset PPC is far less clear compared to what is known in macaques and electrophysiological techniques in awake animals are required to

confirm the identification of a marmoset area LIP and establishment of common functional properties. Up until recently, no studies had investigated the oculomotor properties of the cytoarchitectonically defined region LIP in the common marmoset. In my second research project, we applied for the first time electrical microstimulation to the PPC of awake behaving marmosets and monitored eye position while the animals were allowed to make unrestricted eye movements. We implanted a 32 channel Utah arrays in area LIP of marmosets and applied stimulation trains of varying currents while observing movements. In what follows, I will explain the details of the intracortical electrical microstimulation technique and Utah arrays that were used in this project.

1.3.3 Intracortical Electrical Microstimulation

Electrical microstimulation has long been used as a tool to characterize the function and properties of brain areas by activating neuronal populations within them and observing the response (Tehovnik et al., 2006; Clark et al., 2011). It was first discovered by Fritsch & Hitzig in 1870 who applied a pulse of direct current to electrodes on the surface of the cortex in dogs via a battery and observed contralateral body movements (Fritsch G., Hitzig E. 1870). Microstimulation protocols developed drastically since then, to produce a more reliable activation while minimizing damage to neural tissue (Tehovnik, 1996; Tehovnik et al., 2006). There are two main parameters that determine the spatial extent of neural activation induced by electrical microstimulation: the physical spread of current which is related to the distance from the electrode tip, and the excitability of the neural elements within the region of microstimulation, with myelinated axons and the initial segment being the most excitable parts (Ranck, 1975; Clark et al., 2011). There are several other parameters controlled by the

experimenter that can change how microstimulation affects neural activity. These parameters include the duration and polarity of the applied pulse, inter-pulse frequency, amplitude of the current applied as well as the temporal characteristics of the pulse train (Clark et al., 2011). Pulse waveforms usually involve square pulses and can be monophasic or biphasic. Monophasic waveforms have only one pulse polarity across all single pulses involved and are known to produce a charge buildup at the electrode-tissue interface which can result in electrode corrosion and tissue damage (Merrill et al., 2005; Hanson et al., 2008). These effects can be avoided by using biphasic waveforms that are composed of cathodal and anodal phases of equal duration. Biphasic pulses reduce the electrolytic damage to brain tissue by minimizing the net charge that is delivered to the cortex (Tehovnik, 1996; Reilly and Diamant, 2011). Biphasic pulses may be anodal leading or cathodal leading, but the most effective biphasic waveforms tend to use cathodal leading pulses, since the initial pulse is depolarizing. When negative current is injected into the tissue, the internal negative charge of the neuron becomes positive with respect to its surroundings leading to depolarization and subsequent induction of action potentials. Since cathodal pulses have significantly lower thresholds for nerve excitation (Reilly and Diamant, 2011), the leading cathodal pulse of a biphasic waveform evokes the desired excitation effect with lower amplitude stimulations followed by the anodal pulse that then implements charge reversal to avoid tissue damages (Lilly et al., 1955; Merrill et al., 2005). The frequency that is typically applied falls in the range of 30 to 333 Hz, with current amplitudes varying between 5 to 500 μ A (Clark et al., 2011).

Intracortical electrical microstimulation has been used in the context of saccadic eye movement studies since long time ago. Robinson and colleagues conducted the first study in which they evoked saccadic eye movements by microstimulation of oculomotor areas FEF and SC in

macaque monkeys (Robinson and Fuchs, 1969; Robinson, 1972). The elicited eye movements had similar characteristics to endogenous saccades in terms of the relationship between saccade and duration (Fuchs, 1967). Freedman and colleagues (1996) replicated this study in head-unrestrained monkeys and observed that SC microstimulation resulted in combined eye and head movements with velocity and amplitudes similar to visually guided saccades (Freedman et al., 1996). Microstimulation has also been applied to other known oculomotor areas in monkeys such as the SEF (Tehovnik et al., 2000) and LIP (Thier and Andersen, 1998) and saccadic eye movements have been elicited as a result, though the stimulation currents have been typically higher for these areas. In general, microstimulation of PPC in the awake behaving macaque has been shown to evoke body movements, eye blinks, and both saccadic and smooth eye movements (Fleming and Crosby, 1955; Shibutani et al., 1984; Kurylo and Skavenski, 1991; Thier and Andersen, 1998). Thier and Andersen (1998) found that the region within the PPC from which saccades could be evoked was restricted to area LIP, from which they observed both fixed-vector saccades, for which amplitude and direction were invariant with respect to initial eye position, and convergent or goal-directed saccades which tended to drive the eyes to a fixed goal location in space. Until very recently, no studies had investigated the oculomotor properties of the putative area LIP in the common marmoset and there was no report of microstimulation applied to LIP in this species. Consequently, in my second project, for the first time we probed the oculomotor function of area LIP in alert marmosets by means of intracortical electrical microstimulation. The goal was to provide further evidence on top of my resting-state fMRI findings, that a macaque homologue area LIP does exist within marmoset PPC with strong SC functional connectivity, the microstimulation of which can evoke saccades. To apply the microstimulation with maximal coverage of the area of interest, we implanted a

32 channel Utah array at the location of area LIP as defined from resting-state fMRI (Ghahremani et al., 2017) and the Paxinos atlas (Paxinos et al., 2012) and applied stimulation trains of varying currents to each channel. In what follows, I will briefly talk about Utah electrode arrays.

1.3.3.1 Utah Intracortical Electrode Arrays (UIEA)

Utah Intracortical Electrode Array (UIEA) is a silicon-micromachined structure that allows the simultaneous implantation of multiple microelectrodes in a small brain area to record or stimulate a population of neurons at close proximity to its tip (Maynard et al., 1997).

The first versions of recording electrodes to use for cortical tissues were made of glass and platinum wires (Renshaw et al., 1940; Woldring and Dirken, 1950; Patil and Thakor, 2016). Since then, different kinds of cortical electrodes were developed that uses a variety of biocompatible metals such as iridium (Dowben and Rose, 1953), stainless steel (Green, 1958), tungsten (Hubel and Wiesel, 1959), and platinum (Wolbarsht et al., 1960). Single movable electrodes were introduced by Evarts in 1960 which became a very productive recording technique in neurophysiology for recording neuronal activity in macaque monkeys (Evarts, 1960). However, the use of single electrodes limited data collection to one or two neurons at a time and there was a need to have simultaneous multielectrode recordings. Marg and Adams in 1967 were the first to use multielectrode arrays to obtain activity from multiple neurons at the same time (Marg and Adams, 1967). Since then with advancement in semiconductor electronics industry, lots of improvements were made to electrode arrays. Electrodes reduced in size allowing the array to become denser and electrode contacts became multiplexed to decrease the number of readout lines from the interface (Escabí et al., 2014; Kang et al., 2014). Utah

electrode arrays (UEA), also known as UIEAs, were introduced in the late 1990s and have been successfully used to record from the cortex of cats and monkeys (Rousche and Normann, 1998; Fraser and Schwartz, 2011). The UIEA is built from a thin silicon substrate on top of which a grid of electrically isolated electrode needles is arranged. Each electrode is coated with polyimide with its tip exposed to provide the desired impedance. There are gold contact pads at the back of the array that provide electrical access to each electrode (Maynard et al., 1997). UIEAs have been great tools to obtain stable high-density recordings from larger populations of neurons, providing high spatial resolution within a small area of the brain. The application of UIEAs however, is limited when it comes to regions of the brain that are buried deep within sulci in more complex NHP species such as the macaque. This is especially the case for some of prominent oculomotor cortical areas in the macaque such as the FEF and LIP. On the other hand, the smooth cortex of common marmoset monkeys provides a great opportunity to apply such high-density techniques on cortical oculomotor areas that sit at the surface of the marmoset brain. In my second project, we used a 32 channel Utah array (Blackrock systems) to electrically microstimulate sites within the marmoset PPC in an attempt to characterize a putative area LIP, the microstimulation of which would elicit saccades. I will introduce the findings of this work in more details in chapter 3. This project was the first study that used microstimulation to identify a saccade-related area in marmoset parietal cortex, area LIP. All microstimulation sessions were carried out in the absence of any explicit saccadic eye movement task. Marmosets were head fixed and just viewed video clips displayed to them on the screen. As a follow-up to the findings of this study, we decided to investigate the role of neurons within marmoset area LIP in more details, by recording from neurons while animals were engaged in a pro/antisaccade task. Simultaneous recordings were also obtained from 8aD

neurons using two laminar electrodes inserted to each region while the animal was performing the pro/anti saccade task. This investigation shaped the last chapter of my PhD research that I will go over in details in chapter 4. In what follows, I will talk about laminar electrodes that were used in my last project to record from neurons in putative areas FEF and LIP in common marmosets.

1.3.4 Laminar Electrodes

Another class of multielectrode recording systems is the laminar electrode probe that allows simultaneous recording of cortical layers by using multiple closely spaced array of electrodes along its shaft (Michon et al., 2016). The cerebral cortex of the mammalian brain has certain degree of laminar organization across all cortical areas, with different layers having neurons with distinct origins and connectivity patterns (Nandy et al., 2017; Miller et al., 2018). There are canonical circuits composed of excitatory and inhibitory interneurons within these laminar cortical layers that have distinct patterns of projection within and between themselves as well as with other cortical and subcortical areas (Mountcastle, 1997; Callaway, 1998; Douglas and Martin, 2004, 2007). Laminar electrodes provide the opportunity to simultaneously record the neuronal activity from different cortical layers using multiple contacts that are in a linear configuration along the shaft. There can be typically 8 to 64 electrodes per shaft. The electrode material is generally platinum, iridium oxide or gold (Atlas website). Some shafts feature a pointy tip instead of the standard chisel-shaped tip that allows the probe to be inserted into the brain without the need to puncture or cut the dura and reduces any dimpling effect during insertion. The probe can be driven into the brain using screw-driven microdrives that provide a convenient way to position the probe in the region of interest (Kloosterman et al., 2009; Michon

et al., 2016). The neuronal recordings can be in the form of local field potentials of populations of neurons, multi-unit activity or single-unit spike activity.

Laminar recording techniques applied on macaques have been mainly focused on visual cortical areas such as V1, V2 (Ziemba et al., 2019), and V4, (Nandy et al., 2017; Pettine et al., 2019). Being a more complex NHP species, macaques' brain has more cortical folding and thus more regions that are buried deep within sulci, which in turn limits the application of laminar probes in such areas. Marmoset's lissencephalic cortex on the other hand, provides a great advantage to apply laminar recording techniques since most areas are readily accessible at the surface of the cortex with minimal folding that allow to unveil their laminar characteristics. In my last project, we aimed to obtain extracellular laminar recordings from area 8aD (putative FEF) and LIP of marmosets using silicon-based 16 contact microelectrodes with 150 um interelectrode spacing (ATLAS Neuroengineering) that were inserted into the cortex with electrode micromanipulators (Kopf Instruments) attached to a stereotaxic frame. The details of this work will be provided in chapter 4. Throughout our laminar recording sessions, marmosets were performing the pro/antisaccade task while neuronal responses from areas 8aD and LIP were being recorded. In the next section, I will introduce the pro/anti saccade task in more details.

1.3.5 Pro/Antisaccade Task

Prosaccades are the natural automatic eye movements to the sudden appearance of a visual stimuli, moving the fovea towards the stimulus location. Prosaccade is also known as a visually guided saccade, since the appearance of a visual cue guides the direction of the saccade. In a prosaccade task, a central fixation point appears for a period of time and then the target stimulus is presented in a peripheral location. The subject is then required to make a saccade towards the

stimulus (Hutton, 2008). The prosaccade task itself has several variations based on the timing of events. For example, in the step task, the peripheral stimulus appears at the same time that the central fixation point disappears, whereas in the gap task, the central fixation point disappears before the target stimulus is presented (Hutton, 2008). It has been found that saccade reaction time significantly decreases in the gap task, generally referred to as the “gap effect” (Saslow, 1967). By introducing a delay between the disappearance of the central fixation point and appearance of the peripheral stimulus in gap trials, the attention seems to disengage from the central fixation point before the stimulus appears and therefore less time is needed to reallocate the attention towards the stimulus (Jin and Reeves, 2009). Since the prosaccade task elicits an automatic response, it does not involve a great deal of cognitive engagements. On the other hand, the antisaccade task is meant to investigate top-down voluntary control of eye movements and emphasizes mostly on inhibitory control with minimal working memory demands (Hallett, 1978; Munoz and Everling, 2004). In the antisaccade task, subjects are instructed to suppress a reflexive saccade in response to the sudden appearance of a visual target (prosaccade) and instead, generate a saccade of the same amplitude in the opposite direction (antisaccade) (Hallett, 1978; Munoz and Everling, 2004). Even though it sounds simple to do, many human participants have direction errors in performing the antisaccade task. Two main processes are required for correct performance on the antisaccade task: suppression of the reflexive prosaccade, and inversion of the stimulus-driven vector into the correct voluntary antisaccade vector that points to the mirror location (Munoz and Everling, 2004). The observed direction errors are thought to reflect a failure in inhibiting the reflexive saccade and not an inability to generate the voluntary antisaccade, since a corrective antisaccade is almost always generated after short intersaccadic intervals, showing awareness of the task demands. It is

common to have prosaccade trials randomly intermixed or as separate blocks with antisaccade trials to make comparisons of neuronal response characteristics between these two trial types throughout a recording session. In this case, there is an instruction cue that informs the subject about which trial type to perform, prosaccade or antisaccade. This instruction cue is usually conveyed through either the color of the central fixation point, green for prosaccade and red for antisaccade trials, or its shape, a dot for prosaccade and a cross for antisaccade trials (Munoz and Everling, 2004).

Compared to prosaccades, antisaccades tend to have longer latency associated with the need to inhibit a reflexive saccade and the endogenous planning to make a saccade in the opposite direction of the stimulus location. The inhibition of an automatic involuntary response in favor of a voluntary goal-directed response in the antisaccade task demonstrates cognitive functions that can be linked to the prefrontal cortex (PFC) (Asaad et al., 2000; Miller and Cohen, 2001). Patients with lesions to the frontal cortex often have difficulty in correctly performing the anti-saccade task (Guitton et al., 1985; Pierrot-Deseilligny et al., 1991; Everling and Fischer, 1998). Single neuron recordings and fMRI studies in macaque monkeys have reported that there is a difference in preparatory activity (just before the visual stimulus onset) of PFC neurons between prosaccade and antisaccade trials (Everling and DeSouza, 2005; Ford et al., 2009). The dorsolateral PFC has extensive projections to the SC (Leichnetz et al., 1981) and FEF (Selemon and Goldman-Rakic, 1988). Studies have revealed that the activity of PFC-SC projection neurons is increased around the time of stimulus onset on antisaccade trials with higher activity levels associated with lower saccade reaction time in these trials. Electrophysiological recordings on the SC and FEF have revealed that saccade neurons in these two areas have lower activity on antisaccade trials than prosaccade trials, while fixation neurons have higher activity

on antisaccade than prosaccade trials (Everling et al., 1999b). This finding implies that there exists a top-down signal that inhibits saccade neurons or excites fixation neurons in SC and FEF to avoid generating the reflexive saccade on antisaccade trials. Since all cortical outputs are excitatory (Creutzfeldt, 2013), such top-down signal coming from the PFC would then act through either exciting the fixation neurons or activating a network of inhibitory interneurons (Munoz and Istvan, 1998; Johnston and Everling, 2008) to achieve the behavioral goals associated with antisaccade trials. More recent studies have supported this claim, reporting that the dorsolateral PFC does not seem to suppress the saccade-related activity of SC neurons (Everling and Johnston, 2013; Johnston et al., 2014). It could also be that the fixation neurons in the FEF, which are more active on antisaccade trials, project to the inhibitory interneurons in the SC to exert inhibition of SC saccade neurons (Munoz and Everling, 2004).

Another possible source of the inhibitory projections to the SC and FEF could be the SEF whose neurons have demonstrated increased visual and saccade-related responses in antisaccade trials (Schlag and Schlag-Rey, 1987; Schlag-Rey et al., 1997; Amador et al., 1998). SEF fixation neurons showed increased activity on antisaccade trials during the instruction period and their activity was lower on trials in which a direction error had occurred (Schlag-Rey et al., 1997; Amador et al., 2004). SEF has direct projections to both the FEF and SC (Huerta et al., 1987; Shook et al., 1990) and thus could potentially excite local inhibitory interneurons to inhibit saccade neurons in these areas. Substantia nigra pars reticulata (SNpr) within the basal ganglia, is another brain area that has been proposed to inhibit FEF and SC saccade neurons (Hikosaka et al., 2000). SNpr contains neurons that tonically discharge during fixation and pause for saccades (Hikosaka and Wurtz, 1983b; Munoz and Everling, 2004), some of which have direct projections to the SC and thalamus which in turn projects to the FEF

(Hikosaka and Wurtz, 1983b). These SNpr neurons could tonically inhibit saccade neurons in SC and FEF and this inhibition might be enhanced for antisaccade trials (Munoz and Everling, 2004). Further work in the future is required in order to address the precise role of the aforementioned sources in the inhibition of FEF and SC saccade neurons in the antisaccade task. Aside from the suppression of the reflexive saccade, the second step of the correct performance on the antisaccade task involves inverting the saccade vector to the mirror location of the stimulus. In the antisaccade task, the visual response to the appearance of the peripheral stimulus is initially mapped onto SC and FEF neurons of the wrong hemisphere (contralateral to the hemifield containing the stimulus). This is the activity that needs to be suppressed and instead, SC and FEF saccade neurons of the opposite hemisphere (ipsilateral to stimulus location) should generate a saccade that is the inverted version of the reflexive response. Some studies have shown that the signal for saccade vector inversion in the antisaccade task might originate in the LIP (Munoz and Everling, 2004; Zhang and Barash, 2004). Recordings obtained from monkey LIP neurons during pro/antisaccade task have demonstrated that most LIP neurons represented the target vector and only few represented the direction of movement with a delayed activity (Gottlieb and Goldberg, 1999). Zhang and Barash (2000) also investigated area LIP neurons using a memory-delayed version of the antisaccade task and found certain neurons in area LIP that became active when the saccade vector but not the visual stimulus was aligned with their response field (Zhang and Barash, 2000). However, the response latency of these neurons was about 50 ms after the stimulus onset which is the common latency for visual neurons in the LIP. The authors argued that the presence of such paradoxical activity in this subset of LIP neurons might indicate to a re-mapped visual response that could contribute to the saccade vector inversion in anti-saccade task (Zhang and Barash, 2000, 2004). Nyffler and

colleagues (2008) also tried to study the dynamics of vector inversion using single-pulse transcranial magnetic stimulation (TMS) of PPC during a delayed antisaccade task. They found out that early application of TMS impaired vector inversion process and late application of TMS impaired the inverted vector signal that was stored to perform the antisaccade trials (Nyffeler et al., 2008).

In common marmosets, there is only one study by our group so far that has looked at the neuronal activity in marmoset areas 8aD and LIP during the instruction period of the pro/antisaccade task using laminar electrodes (Johnston et al., 2019). Their findings demonstrated prominent task-dependent activity in alpha/gamma bands and single neuron activity during the preparatory period in area 8aD in specific (Johnston et al., 2019). They mainly focused on the preparatory period from 500 to 0 ms before the peripheral stimulus onset, ignoring any activity occurring later in the trial. My last PhD project was a continuation of this work that aimed to investigate neuronal activity of marmoset area 8aD and LIP in pro/antisaccade task, with a focus on the activity from the peripheral stimulus onset until around the time of saccade generation (perisaccadic period). This is another important epoch during the antisaccade task that can give us insight about any stimulus-related and saccade-related neuronal activity and cognitive and decision-making processes involved after the peripheral stimulus is presented and the animal has to make a saccade response. The findings of this study will be discussed in chapter 5.

1.4 Research Objectives

1.4.1 Extracting resting-state functional connectivity maps in common marmosets with further emphasis on the frontoparietal network

Over the last few years, lots of effort has been directed toward mapping the marmoset brain (Okano and Mitra, 2015) and establishing cross-species homologies between marmosets and macaques (Solomon and Rosa, 2014; Bakola et al., 2015). A study led by Belcher et al (2013) was the first resting-state fMRI investigation of awake common marmosets that identified twelve resting-state brain networks, consistent with those found in humans (Belcher et al., 2013). My first project replicated this study on a 9.4T MRI scanner at Robarts Research Institute in 4 lightly anesthetized marmosets, aiming to identify a homologous marmoset frontoparietal network to that of macaques and humans. I initially applied the spatial ICA technique to extract all marmoset resting state networks, among which I identified a frontoparietal network that potentially subserved attention and oculomotor system. To narrow down the constituent components of this frontoparietal network, I applied seed-based correlation analysis by placing a seed in area SC which is well defined in marmosets and heavily implicated in saccade system. I found several frontal, parietal and temporal cortical regions that exhibited strong functional connectivity with the SC, potentially representing the oculomotor circuitry in marmosets. Area 8aD bordering 6DR was the region within the frontal cortex that exhibited the strongest SC connectivity in marmoset. I next placed a seed in this area to observe its functional connectivity patterns across the whole brain. These patterns revealed a similarity to FEF functional connectivity in macaques, providing evidence that area 8aD bordering 6DR is the potential homologue of the macaque FEF in common marmosets (Ghahremani et al., 2017).

1.4.2 Examining oculomotor effects of systemic microstimulation in marmoset putative area LIP

In my resting-state investigations, I identified an area within marmoset posterior parietal cortex (PPC) with the strongest SC functional connectivity that potentially represented a homologue of macaque area LIP. Since the parcellation of marmoset PPC is far less clear compared to what is known in macaques, electrophysiological techniques in awake animals are required to confirm the identification of a marmoset area LIP and establishment of common functional properties. Up until recently, no studies had investigated the oculomotor properties of the cytoarchitecturally defined region LIP in the common marmoset. In my second project, we applied for the first time electrical microstimulation to the PPC of awake behaving marmosets and monitored eye position while the animals were allowed to make unrestricted eye movements. We implanted a 32 channel Utah arrays in area LIP of two marmosets, as identified from my resting-state fMRI findings, and applied stimulation trains of varying currents. The goal was to provide further evidence on top of my resting-state fMRI findings (Ghahremani et al., 2017), that a macaque homologue area LIP does exist within marmoset PPC with strong SC functional connectivity, the microstimulation of which can evoke saccades. We found that similar to macaques, microstimulation of the LIP in marmosets could evoke both fixed-vector and convergent saccades, supporting its homologous role to the macaque LIP in modulating eye movements (Ghahremani et al., 2019).

1.4.3 Investigating the post-stimulus neuronal activity of marmoset cortical oculomotor areas 8aD and LIP during the pro/antisaccade task

My second project on microstimulation of area LIP provided evidence for the involvement of area LIP in saccadic eye movements in marmoset. All microstimulation sessions were carried out in the absence of any explicit saccade task. Marmosets were head fixed and just freely viewed video clips displayed to them on the screen. As a follow-up to the findings of this study, we decided to investigate the role of neurons within marmoset area LIP in more details, by recording from neurons while animals were engaged in a pro/antisaccade task. So far, there is only one study by our group that looked at neuronal activity in marmoset areas 8aD and LIP during the instruction period of the pro/antisaccade task using laminar electrodes (Johnston et al., 2019). Their findings demonstrated prominent task-dependent activity in alpha/gamma bands and single neuron activity during the preparatory period in area 8aD (Johnston et al., 2019). Their data analysis was limited to the preparatory period from 500 to 0 ms before the peripheral stimulus onset. My last PhD project was in fact a continuation of this work that aimed to investigate neuronal activity of marmoset area LIP and 8aD during the pro/antisaccade task, with a focus on the activity from the peripheral stimulus onset until the perisaccadic period. We found neurons with significant stimulus-related activity in area LIP and neurons with significant saccade-related activity in both areas 8aD and LIP of common marmosets. These findings demonstrate a potential role of marmoset frontal and parietal oculomotor areas in saccadic eye movements and support the marmoset as a potential alternative primate model for studying the oculomotor system.

1.5 References

- Albus JS (1971) A theory of cerebellar function. *Math Biosci* 10:25–61.
- Amador N, Schlag-Rey M, Schlag J (1998) Primate antisaccades. I. Behavioral characteristics. *J Neurophysiol* 80:1775–1786.
- Amador N, Schlag-Rey M, Schlag J (2004) Primate antisaccade. II. Supplementary eye field neuronal activity predicts correct performance. *J Neurophysiol* 91:1672–1689.
- Andersen RA, Asanuma C, Essick G, Siegel RM (1990) Corticocortical connections of anatomically and physiologically defined subdivisions within the inferior parietal lobule. *J Comp Neurol* 296:65–113.
- Andersen RA, Essick GK, Siegel RM (1987) Neurons of area 7 activated by both visual stimuli and oculomotor behavior. *Exp Brain Res* 67:316–322.
- Andersen RA, Snyder LH, Bradley DC, Xing J (1997) Multimodal representation of space in the posterior parietal cortex and its use in planning movements. *Annu Rev Neurosci* 20:303–330.
- Angelaki DE (2011) The oculomotor plant and its role in three-dimensional eye orientation. *Oxf Handb Eye Mov* Available at: <https://www.oxfordhandbooks.com/view/10.1093/oxfordhb/9780199539789.001.0001/oxfordhb-9780199539789-e-008>.
- Asaad WF, Rainer G, Miller EK (2000) Task-specific neural activity in the primate prefrontal cortex. *J Neurophysiol* 84:451–459.
- Aschoff JC, Cohen B (1971) Changes in saccadic eye movements produced by cerebellar cortical lesions. *Exp Neurol* 32:123–133.
- Awh E, Armstrong KM, Moore T (2006) Visual and oculomotor selection: links, causes and implications for spatial attention. *Trends Cogn Sci* 10:124–130.
- Bakola S, Burman KJ, Rosa MGP (2015) The cortical motor system of the marmoset monkey (*Callithrix jacchus*). *Neurosci Res* 93:72–81.
- Barash S, Melikyan A, Sivakov A, Zhang M, Glickstein M, Thier P (1999) Saccadic dysmetria and adaptation after lesions of the cerebellar cortex. *J Neurosci Off J Soc Neurosci* 19:10931–10939.
- Barnes GR (2008) Cognitive processes involved in smooth pursuit eye movements. *Brain Cogn* 68:309–326.
- Basso MA, May PJ (2017) Circuits for Action and Cognition: A View from the Superior Colliculus. *Annu Rev Vis Sci* 3:197–226.

- Basso MA, Wurtz RH (1997) Modulation of neuronal activity by target uncertainty. *Nature* 389:66–69.
- Basso MA, Wurtz RH (1998) Modulation of Neuronal Activity in Superior Colliculus by Changes in Target Probability. *J Neurosci* 18:7519–7534.
- Becker W, Jürgens R (1979) An analysis of the saccadic system by means of double step stimuli. *Vision Res* 19:967–983.
- Beckmann CF, DeLuca M, Devlin JT, Smith SM (2005) Investigations into resting-state connectivity using independent component analysis. *Philos Trans R Soc Lond B Biol Sci* 360:1001–1013.
- Belcher AM, Yen CC, Stepp H, Gu H, Lu H, Yang Y, Silva AC, Stein EA (2013) Large-Scale Brain Networks in the Awake, Truly Resting Marmoset Monkey. *J Neurosci* 33:16796–16804.
- Ben Hamed S, Duhamel JR, Bremmer F, Graf W (2001) Representation of the visual field in the lateral intraparietal area of macaque monkeys: a quantitative receptive field analysis. *Exp Brain Res* 140:127–144.
- Berman RA, Wurtz RH (2010) Functional identification of a pulvinar path from superior colliculus to cortical area MT. *J Neurosci Off J Soc Neurosci* 30:6342–6354.
- Biswal B, Yetkin FZ, Haughton VM, Hyde JS (1995) Functional connectivity in the motor cortex of resting human brain using echo-planar MRI. *Magn Reson Med* 34:537–541.
- Blatt GJ, Andersen RA, Stoner GR (1990) Visual receptive field organization and cortico-cortical connections of the lateral intraparietal area (area LIP) in the macaque. *J Comp Neurol* 299:421–445.
- Blum B, Kulikowski JJ, Carden D, Harwood D (1982) Eye movements induced by electrical stimulation of the frontal eye fields of marmosets and squirrel monkeys. *Brain Behav Evol* 21:34–41.
- Boehnke SE, Munoz DP (2008) On the importance of the transient visual response in the superior colliculus. *Curr Opin Neurobiol* 18:544–551.
- Bourne JA, Rosa MGP (2003) Laminar expression of neurofilament protein in the superior colliculus of the marmoset monkey (*Callithrix jacchus*). *Brain Res* 973:142–145.
- Broerse A, Crawford TJ, den Boer JA (2001) Parsing cognition in schizophrenia using saccadic eye movements: a selective overview. *Neuropsychologia* 39:742–756.
- Bruce CJ, Goldberg ME (1985) Primate frontal eye fields. I. Single neurons discharging before saccades. *J Neurophysiol* 53:603–635.

- Bruce CJ, Goldberg ME, Bushnell MC, Stanton GB (1985) Primate frontal eye fields. II. Physiological and anatomical correlates of electrically evoked eye movements. *J Neurophysiol* 54:714–734.
- Burman DD, Bruce CJ (1997) Suppression of task-related saccades by electrical stimulation in the primate's frontal eye field. *J Neurophysiol* 77:2252–2267.
- Büttner-Ennever JA, Horn AK (1997) Anatomical substrates of oculomotor control. *Curr Opin Neurobiol* 7:872–879.
- Büttner-Ennever JA, Horn AKE (2002) Oculomotor system: a dual innervation of the eye muscles from the abducens, trochlear, and oculomotor nuclei. *Mov Disord Off J Mov Disord Soc* 17 Suppl 2:S2-3.
- Callaway EM (1998) Local circuits in primary visual cortex of the macaque monkey. *Annu Rev Neurosci* 21:47–74.
- Carello CD, Krauzlis RJ (2004) Manipulating intent: evidence for a causal role of the superior colliculus in target selection. *Neuron* 43:575–583.
- Carpenter RH, Williams ML (1995) Neural computation of log likelihood in control of saccadic eye movements. *Nature* 377:59–62.
- Carpenter RHS (1988) *Movements of the eyes*, 2nd rev. & enlarged ed. London, England: Pion Limited.
- Chafee MV, Goldman-Rakic PS (1998) Matching patterns of activity in primate prefrontal area 8a and parietal area 7ip neurons during a spatial working memory task. *J Neurophysiol* 79:2919–2940.
- Churchland AK, Kiani R, Shadlen MN (2008) Decision-making with multiple alternatives. *Nat Neurosci* 11:693–702.
- Clark KL, Armstrong KM, Moore T (2011) Probing neural circuitry and function with electrical microstimulation. *Proc Biol Sci* 278:1121–1130.
- Clementz BA (1998) Psychophysiological measures of (dis)inhibition as liability indicators for schizophrenia. *Psychophysiology* 35:648–668.
- Clower DM, West RA, Lynch JC, Strick PL (2001) The inferior parietal lobule is the target of output from the superior colliculus, hippocampus, and cerebellum. *J Neurosci Off J Soc Neurosci* 21:6283–6291.
- Coe B, Tomihara K, Matsuzawa M, Hikosaka O (2002) Visual and Anticipatory Bias in Three Cortical Eye Fields of the Monkey during an Adaptive Decision-Making Task. *J Neurosci* 22:5081–5090.

- Collins CE, Lyon DC, Kaas JH (2005) Distribution across cortical areas of neurons projecting to the superior colliculus in new world monkeys. *Anat Rec A Discov Mol Cell Evol Biol* 285:619–627.
- Comoli E, Coizet V, Boyes J, Bolam JP, Canteras NS, Quirk RH, Overton PG, Redgrave P (2003) A direct projection from superior colliculus to substantia nigra for detecting salient visual events. *Nat Neurosci* 6:974–980.
- Corbetta M, Miezin FM, Shulman GL, Petersen SE (1993) A PET study of visuospatial attention. *J Neurosci Off J Soc Neurosci* 13:1202–1226.
- Corneil BD, Munoz DP, Olivier E (2007) Priming of Head Premotor Circuits During Oculomotor Preparation. *J Neurophysiol* 97:701–714.
- Corneil BD, Olivier E, Munoz DP (2002a) Neck Muscle Responses to Stimulation of Monkey Superior Colliculus. I. Topography and Manipulation of Stimulation Parameters. *J Neurophysiol* 88:1980–1999.
- Corneil BD, Olivier E, Munoz DP (2002b) Neck Muscle Responses to Stimulation of Monkey Superior Colliculus. II. Gaze Shift Initiation and Volitional Head Movements. *J Neurophysiol* 88:2000–2018.
- Creutzfeldt OD (2013) *Cortex Cerebri: Leistung, strukturelle und funktionelle Organisation der Hirnrinde*. Springer-Verlag.
- Crevits L, De Ridder K (1997) Disturbed striatoprefrontal mediated visual behaviour in moderate to severe parkinsonian patients. *J Neurol Neurosurg Psychiatry* 63:296–299.
- Crowne DP, Yeo CH, Russell IS (1981) The effects of unilateral frontal eye field lesions in the monkey: Visual-motor guidance and avoidance behaviour. *Behav Brain Res* 2:165–187.
- Currie J, Ramsden B, McArthur C, Maruff P (1991) Validation of a clinical antisaccadic eye movement test in the assessment of dementia. *Arch Neurol* 48:644–648.
- Damoiseaux JS, Rombouts S a. RB, Barkhof F, Scheltens P, Stam CJ, Smith SM, Beckmann CF (2006) Consistent resting-state networks across healthy subjects. *Proc Natl Acad Sci U S A* 103:13848–13853.
- Dash S, Peel TR, Lomber SG, Corneil BD (2018) Frontal Eye Field Inactivation Reduces Saccade Preparation in the Superior Colliculus but Does Not Alter How Preparatory Activity Relates to Saccades of a Given Latency. *eNeuro* 5 Available at: <https://www.ncbi.nlm.nih.gov/pmc/articles/PMC5952303/>.
- Demertzi A, Gómez F, Crone JS, Vanhauzenhuyse A, Tshibanda L, Noirhomme Q, Thonnard M, Charland-Verville V, Kirsch M, Laureys S, Soddu A (2014) Multiple fMRI system-level baseline connectivity is disrupted in patients with consciousness alterations. *Cortex J Devoted Study Nerv Syst Behav* 52:35–46.

- Dias EC, Segraves MA (1999) Muscimol-induced inactivation of monkey frontal eye field: effects on visually and memory-guided saccades. *J Neurophysiol* 81:2191–2214.
- Donaldson IML (1990) *The Neurobiology of Saccadic Eye Movements (Reviews of Oculomotor Research Vol. 3)*: edited by R. H. Wurtz and M. E. Goldberg, Elsevier, 1989. Dfl. 360.00 (xxii + 424 pages) ISBN 0 444 81017 X. *Trends Neurosci* 13:355–357.
- Donner T, Kettermann A, Diesch E, Ostendorf F, Villringer A, Brandt SA (2000) Involvement of the human frontal eye field and multiple parietal areas in covert visual selection during conjunction search. *Eur J Neurosci* 12:3407–3414.
- Donner TH, Kettermann A, Diesch E, Ostendorf F, Villringer A, Brandt SA (2002) Visual feature and conjunction searches of equal difficulty engage only partially overlapping frontoparietal networks. *NeuroImage* 15:16–25.
- Doricchi F, Perani D, Incoccia C, Grassi F, Cappa SF, Bettinardi V, Galati G, Pizzamiglio L, Fazio F (1997) Neural control of fast-regular saccades and antisaccades: an investigation using positron emission tomography. *Exp Brain Res* 116:50–62.
- Dorris MC, Klein RM, Everling S, Munoz DP (2002) Contribution of the primate superior colliculus to inhibition of return. *J Cogn Neurosci* 14:1256–1263.
- Dorris MC, Munoz DP (1995) A neural correlate for the gap effect on saccadic reaction times in monkey. *J Neurophysiol* 73:2558–2562.
- Dorris MC, Munoz DP (1998) Saccadic Probability Influences Motor Preparation Signals and Time to Saccadic Initiation. *J Neurosci* 18:7015–7026.
- Dorris MC, Olivier E, Munoz DP (2007) Competitive Integration of Visual and Preparatory Signals in the Superior Colliculus during Saccadic Programming. *J Neurosci* 27:5053–5062.
- Douglas RJ, Martin KAC (2004) Neuronal circuits of the neocortex. *Annu Rev Neurosci* 27:419–451.
- Douglas RJ, Martin KAC (2007) Mapping the Matrix: The Ways of Neocortex. *Neuron* 56:226–238.
- Dowben RM, Rose JE (1953) A metal-filled microelectrode. *Science* 118:22–24.
- Elsley JK, Nagy B, Cushing SL, Corneil BD (2007) Widespread presaccadic recruitment of neck muscles by stimulation of the primate frontal eye fields. *J Neurophysiol* 98:1333–1354.
- Escabí MA, Read HL, Viventi J, Kim D-H, Higgins NC, Storace DA, Liu ASK, Gifford AM, Burke JF, Campisi M, Kim Y-S, Avrin AE, Spiegel Jan V der, Huang Y, Li M, Wu J,

- Rogers JA, Litt B, Cohen YE (2014) A high-density, high-channel count, multiplexed μ ECoG array for auditory-cortex recordings. *J Neurophysiol* 112:1566–1583.
- Evarts EV (1960) Effects of sleep and waking on spontaneous and evoked discharge of single units in visual cortex. *Fed Proc* 19:828–837.
- Everling S, DeSouza JFX (2005) Rule-dependent activity for prosaccades and antisaccades in the primate prefrontal cortex. *J Cogn Neurosci* 17:1483–1496.
- Everling S, Dorris MC, Klein RM, Munoz DP (1999a) Role of primate superior colliculus in preparation and execution of anti-saccades and pro-saccades. *J Neurosci Off J Soc Neurosci* 19:2740–2754.
- Everling S, Dorris MC, Klein RM, Munoz DP (1999b) Role of Primate Superior Colliculus in Preparation and Execution of Anti-Saccades and Pro-Saccades. *J Neurosci* 19:2740–2754.
- Everling S, Fischer B (1998) The antisaccade: a review of basic research and clinical studies. *Neuropsychologia* 36:885–899.
- Everling S, Johnston K (2013) Control of the superior colliculus by the lateral prefrontal cortex. *Philos Trans R Soc Lond B Biol Sci* 368:20130068.
- Everling S, Munoz DP (2000) Neuronal correlates for preparatory set associated with pro-saccades and anti-saccades in the primate frontal eye field. *J Neurosci Off J Soc Neurosci* 20:387–400.
- Fang P-C, Stepniewska I, Kaas JH (2005) Ipsilateral cortical connections of motor, premotor, frontal eye, and posterior parietal fields in a prosimian primate, *Otolemur garnetti*. *J Comp Neurol* 490:305–333.
- Fecteau JH, Munoz DP (2006) Saliency, relevance, and firing: a priority map for target selection. *Trends Cogn Sci* 10:382–390.
- Ferraina S, Paré M, Wurtz RH (2002) Comparison of cortico-cortical and cortico-collicular signals for the generation of saccadic eye movements. *J Neurophysiol* 87:845–858.
- Fischer B, Boch R (1983) Saccadic eye movements after extremely short reaction times in the monkey. *Brain Res* 260:21–26.
- Fleming JFR, Crosby EC (1955) The parietal lobe as an additional motor area; the motor effects of electrical stimulation and ablation of cortical areas 5 and 7 in monkeys. *J Comp Neurol* 103:485–512.
- Forbes K, Klein RM (1996) The magnitude of the fixation offset effect with endogenously and exogenously controlled saccades. *J Cogn Neurosci* 8:344–352.

- Ford KA, Gati JS, Menon RS, Everling S (2009) BOLD fMRI activation for anti-saccades in nonhuman primates. *NeuroImage* 45:470–476.
- Fraser GW, Schwartz AB (2011) Recording from the same neurons chronically in motor cortex. *J Neurophysiol* 107:1970–1978.
- Freedman EG, Stanford TR, Sparks DL (1996) Combined eye-head gaze shifts produced by electrical stimulation of the superior colliculus in rhesus monkeys. *J Neurophysiol* 76:927–952.
- French JA (2019) The Marmoset as a Model in Behavioral Neuroscience and Psychiatric Research. In: *The Common Marmoset in Captivity and Biomedical Research*, pp 477–491. Elsevier. Available at: <https://linkinghub.elsevier.com/retrieve/pii/B9780128118290000261>.
- Fries W (1984) Cortical projections to the superior colliculus in the macaque monkey: a retrograde study using horseradish peroxidase. *J Comp Neurol* 230:55–76.
- Fuchs AF (1967) Saccadic and smooth pursuit eye movements in the monkey. *J Physiol* 191:609–631.
- Fukushima J, Fukushima K, Morita N, Yamashita I (1990) Further analysis of the control of voluntary saccadic eye movements in schizophrenic patients. *Biol Psychiatry* 28:943–958.
- Funahashi S, Bruce CJ, Goldman-Rakic PS (1989) Mnemonic coding of visual space in the monkey's dorsolateral prefrontal cortex. *J Neurophysiol* 61:331–349.
- Funahashi S, Bruce CJ, Goldman-Rakic PS (1991) Neuronal activity related to saccadic eye movements in the monkey's dorsolateral prefrontal cortex. *J Neurophysiol* 65:1464–1483.
- Fuster JM, Alexander GE (1971) Neuron activity related to short-term memory. *Science* 173:652–654.
- Ghahremani M, Hutchison RM, Menon RS, Everling S (2017) Frontoparietal Functional Connectivity in the Common Marmoset. *Cereb Cortex N Y N 1991* 27:3890–3905.
- Ghahremani M, Johnston KD, Ma L, Hayrynen LK, Everling S (2019) Electrical microstimulation evokes saccades in posterior parietal cortex of common marmosets. *J Neurophysiol* 122:1765–1776.
- Gilchrist I (2011) Saccades. *Oxf Handb Eye Mov* Available at: <https://www.oxfordhandbooks.com/view/10.1093/oxfordhb/9780199539789.001.0001/oxfordhb-9780199539789-e-005>.
- Gnadt JW, Andersen RA (1988) Memory related motor planning activity in posterior parietal cortex of macaque. *Exp Brain Res* 70:216–220.

- Goldberg ME, Wurtz RH (1972) Activity of superior colliculus in behaving monkey. I. Visual receptive fields of single neurons. *J Neurophysiol* 35:542–559.
- Goldman PS, Nauta WJ (1976) Autoradiographic demonstration of a projection from prefrontal association cortex to the superior colliculus in the rhesus monkey. *Brain Res* 116:145–149.
- Goodale MA, Milner AD (1992) Separate visual pathways for perception and action. *Trends Neurosci* 15:20–25.
- Gottlieb J, Goldberg ME (1999) Activity of neurons in the lateral intraparietal area of the monkey during an antisaccade task. *Nat Neurosci* 2:906–912.
- Green JD (1958) A Simple Microelectrode for recording from the Central Nervous System. *Nature* 182:962–962.
- Gregoriou GG, Gotts SJ, Desimone R (2012) Cell-type-specific synchronization of neural activity in FEF with V4 during attention. *Neuron* 73:581–594.
- Gregory Keating E, Gooley SG (1988) Saccadic disorders caused by cooling the superior colliculus or the frontal eye field, or from combined lesions of both structures. *Brain Res* 438:247–255.
- Guitton D, Buchtel HA, Douglas RM (1985) Frontal lobe lesions in man cause difficulties in suppressing reflexive glances and in generating goal-directed saccades. *Exp Brain Res* 58:455–472.
- Hallett PE (1978) Primary and secondary saccades to goals defined by instructions. *Vision Res* 18:1279–1296.
- Hallett PE, Adams BD (1980) The predictability of saccadic latency in a novel voluntary oculomotor task. *Vision Res* 20:329–339.
- Hanes DP, Patterson WF, Schall JD (1998) Role of frontal eye fields in countermanding saccades: visual, movement, and fixation activity. *J Neurophysiol* 79:817–834.
- Hanes DP, Schall JD (1995) Countermanding saccades in macaque. *Vis Neurosci* 12:929–937.
- Hanes DP, Schall JD (1996) Neural control of voluntary movement initiation. *Science* 274:427–430.
- Hanks TD, Ditterich J, Shadlen MN (2006) Microstimulation of macaque area LIP affects decision-making in a motion discrimination task. *Nat Neurosci* 9:682–689.
- Hanson T, Fitzsimmons N, O’Doherty JE (2008) Technology for Multielectrode MicroStimulation of Brain Tissue. In: *Methods for Neural Ensemble Recordings*, 2nd

ed. (Nicollelis MA, ed) *Frontiers in Neuroscience*. Boca Raton (FL): CRC Press/Taylor & Francis. Available at: <http://www.ncbi.nlm.nih.gov/books/NBK3896/>.

- Harting JK, Casagrande VA, Weber JT (1978) The projection of the primate superior colliculus upon the dorsal lateral geniculate nucleus: autoradiographic demonstration of interlaminar distribution of tectogeniculate axons. *Brain Res* 150:593–599.
- Helms MC, Ozen G, Hall WC (2004) Organization of the intermediate gray layer of the superior colliculus. I. Intrinsic vertical connections. *J Neurophysiol* 91:1706–1715.
- Hess BJM, Angelaki DE (1997) Kinematic Principles of Primate Rotational Vestibulo-Ocular Reflex II. Gravity-Dependent Modulation of Primary Eye Position. *J Neurophysiol* 78:2203–2216.
- Hikosaka O, Takikawa Y, Kawagoe R (2000) Role of the basal ganglia in the control of purposive saccadic eye movements. *Physiol Rev* 80:953–978.
- Hikosaka O, Wurtz RH (1983a) Visual and oculomotor functions of monkey substantia nigra pars reticulata. III. Memory-contingent visual and saccade responses. *J Neurophysiol* 49:1268–1284.
- Hikosaka O, Wurtz RH (1983b) Visual and oculomotor functions of monkey substantia nigra pars reticulata. IV. Relation of substantia nigra to superior colliculus. *J Neurophysiol* 49:1285–1301.
- Hubel DH, LeVay S, Wiesel TN (1975) Mode of termination of retinotectal fibers in macaque monkey: An autoradiographic study. *Brain Res* 96:25–40.
- Hubel DH, Wiesel TN (1959) Receptive fields of single neurones in the cat's striate cortex. *J Physiol* 148:574–591.
- Huerta MF, Kaas JH (1990) Supplementary eye field as defined by intracortical microstimulation: connections in macaques. *J Comp Neurol* 293:299–330.
- Huerta MF, Krubitzer LA, Kaas JH (1986) Frontal eye field as defined by intracortical microstimulation in squirrel monkeys, owl monkeys, and macaque monkeys: I. Subcortical connections. *J Comp Neurol* 253:415–439.
- Huerta MF, Krubitzer LA, Kaas JH (1987) Frontal eye field as defined by intracortical microstimulation in squirrel monkeys, owl monkeys, and macaque monkeys. II. Cortical connections. *J Comp Neurol* 265:332–361.
- Huettel SA, Song AW, McCarthy G (2009) *Functional Magnetic Resonance Imaging*. Oxford University Press, Incorporated.
- Hung C-C, Yen CC, Ciuchta JL, Papoti D, Bock NA, Leopold DA, Silva AC (2015) Functional Mapping of Face-Selective Regions in the Extrastriate Visual Cortex of the Marmoset. *J Neurosci* 35:1160–1172.

- Hung GK, Ciuffreda KJ, Semmlow JL, Horng JL (1994) Vergence eye movements under natural viewing conditions. *Invest Ophthalmol Vis Sci* 35:3486–3492.
- Hutchison RM, Everling S (2012) Monkey in the middle: why non-human primates are needed to bridge the gap in resting-state investigations. *Front Neuroanat* 6 Available at: <https://www.ncbi.nlm.nih.gov/pmc/articles/PMC3405297/>.
- Hutton SB (2008) Cognitive control of saccadic eye movements. *Brain Cogn* 68:327–340.
- Hyvärinen A, Oja E (2000) Independent component analysis: algorithms and applications. *Neural Netw* 13:411–430.
- Ignashchenkova A, Dicke PW, Haarmeier T, Thier P (2004) Neuron-specific contribution of the superior colliculus to overt and covert shifts of attention. *Nat Neurosci* 7:56–64.
- Ikeda T, Hikosaka O (2003) Reward-dependent gain and bias of visual responses in primate superior colliculus. *Neuron* 39:693–700.
- Ikeda T, Hikosaka O (2007) Positive and negative modulation of motor response in primate superior colliculus by reward expectation. *J Neurophysiol* 98:3163–3170.
- Itti L, Koch C (2001) Computational modelling of visual attention. *Nat Rev Neurosci* 2:194–203.
- Izpisua Belmonte JC et al. (2015) Brains, genes, and primates. *Neuron* 86:617–631.
- Jafri MJ, Pearlson GD, Stevens M, Calhoun VD (2008) A Method for Functional Network Connectivity Among Spatially Independent Resting-State Components in Schizophrenia. *NeuroImage* 39:1666–1681.
- Jin Z, Reeves A (2009) Attentional release in the saccadic gap effect. *Vision Res* 49:2045–2055.
- Johnston K, Everling S (2006) Monkey Dorsolateral Prefrontal Cortex Sends Task-Selective Signals Directly to the Superior Colliculus. *J Neurosci* 26:12471–12478.
- Johnston K, Everling S (2008) Neurophysiology and neuroanatomy of reflexive and voluntary saccades in non-human primates. *Brain Cogn* 68:271–283.
- Johnston K, Everling S (2011) An Approach to Understanding the Neural Circuitry of Saccade Control in the Cerebral Cortex Using Antidromic Identification in the Awake Behaving Macaque Monkey Model. In: *Animal Models of Movement Disorders: Volume II* (Lane EL, Dunnett SB, eds), pp 161–181 *NeuroMethods*. Totowa, NJ: Humana Press. Available at: https://doi.org/10.1007/978-1-61779-301-1_9.
- Johnston K, Koval MJ, Lomber SG, Everling S (2014) Macaque dorsolateral prefrontal cortex does not suppress saccade-related activity in the superior colliculus. *Cereb Cortex N Y N* 1991 24:1373–1388.

- Johnston K, Ma L, Schaeffer L, Everling S (2019) Alpha Oscillations Modulate Preparatory Activity in Marmoset Area 8Ad. *J Neurosci Off J Soc Neurosci* 39:1855–1866.
- Jun JJ et al. (2017) Fully integrated silicon probes for high-density recording of neural activity. *Nature* 551:232–236.
- Kalesnykas RP, Hallett PE (1994) Retinal eccentricity and the latency of eye saccades. *Vision Res* 34:517–531.
- Kang J, Wen J, Jayaram SH, Yu A, Wang X (2014) Development of an equivalent circuit model for electrochemical double layer capacitors (EDLCs) with distinct electrolytes. *Electrochimica Acta* 115:587–598.
- Keller EL (1974) Participation of medial pontine reticular formation in eye movement generation in monkey. *J Neurophysiol* 37:316–332.
- Kirk EC (2004) Comparative morphology of the eye in primates. *Anat Rec A Discov Mol Cell Evol Biol* 281A:1095–1103.
- Kishi N, Sato K, Sasaki E, Okano H (2014) Common marmoset as a new model animal for neuroscience research and genome editing technology. *Dev Growth Differ* 56:53–62.
- Klein RM (1994) Perceptual-motor expectancies interact with covert visual orienting under conditions of endogenous but not exogenous control. *Can J Exp Psychol Rev Can Psychol Exp* 48:167–181.
- Kloosterman F, Davidson TJ, Gomperts SN, Layton SP, Hale G, Nguyen DP, Wilson MA (2009) Micro-drive Array for Chronic in vivo Recording: Drive Fabrication. *J Vis Exp JoVE* Available at: <https://www.ncbi.nlm.nih.gov/pmc/articles/PMC2793172/>.
- Koyama M, Hasegawa I, Osada T, Adachi Y, Nakahara K, Miyashita Y (2004) Functional magnetic resonance imaging of macaque monkeys performing visually guided saccade tasks: comparison of cortical eye fields with humans. *Neuron* 41:795–807.
- Künzle H, Akert K (1977) Efferent connections of cortical, area 8 (frontal eye field) in *Macaca fascicularis*. A reinvestigation using the autoradiographic technique. *J Comp Neurol* 173:147–163.
- Kurylo DD, Skavenski AA (1991) Eye movements elicited by electrical stimulation of area PG in the monkey. *J Neurophysiol* 65:1243–1253.
- Kustov AA, Robinson DL (1996) Shared neural control of attentional shifts and eye movements. *Nature* 384:74–77.
- Land MF (2011) Oculomotor behaviour in vertebrates and invertebrates. *Oxf Handb Eye Mov* Available at: <https://www.oxfordhandbooks.com/view/10.1093/oxfordhb/9780199539789.001.0001/oxfordhb-9780199539789-e-001> [Accessed March 9, 2020].

- Lapuerta P, Schein SJ (1995) A four-surface schematic eye of macaque monkey obtained by an optical method. *Vision Res* 35:2245–2254.
- Lee MH, Smyser CD, Shimony JS (2013) Resting-State fMRI: A Review of Methods and Clinical Applications. *Am J Neuroradiol* 34:1866–1872.
- Leichnetz GR, Spencer RF, Hardy SG, Astruc J (1981) The prefrontal corticotectal projection in the monkey; an anterograde and retrograde horseradish peroxidase study. *Neuroscience* 6:1023–1041.
- Lewis JW, Van Essen DC (2000) Corticocortical connections of visual, sensorimotor, and multimodal processing areas in the parietal lobe of the macaque monkey. *J Comp Neurol* 428:112–137.
- Li C-SR, Chang H-L, Lin S-C (2003) Inhibition of return in children with attention deficit hyperactivity disorder. *Exp Brain Res* 149:125–130.
- Li X, Basso MA (2008) Preparing to move increases the sensitivity of superior colliculus neurons. *J Neurosci Off J Soc Neurosci* 28:4561–4577.
- Lilly JC, Hughes JR, Alvord EC, Galkin TW (1955) Brief, noninjurious electric waveform for stimulation of the brain. *Science* 121:468–469.
- Lisberger SG, Fuchs AF (1978a) Role of primate flocculus during rapid behavioral modification of vestibuloocular reflex. I. Purkinje cell activity during visually guided horizontal smooth-pursuit eye movements and passive head rotation. *J Neurophysiol* 41:733–763.
- Lisberger SG, Fuchs AF (1978b) Role of primate flocculus during rapid behavioral modification of vestibuloocular reflex. II. Mossy fiber firing patterns during horizontal head rotation and eye movement. *J Neurophysiol* 41:764–777.
- Liversedge S, Gilchrist I, Everling S (2011) *The Oxford Handbook of Eye Movements*. OUP Oxford.
- Lock TM, Baizer JS, Bender DB (2003) Distribution of corticotectal cells in macaque. *Exp Brain Res* 151:455–470.
- Lovejoy LP, Krauzlis RJ (2010) Inactivation of primate superior colliculus impairs covert selection of signals for perceptual judgments. *Nat Neurosci* 13:261–266.
- Ludwig CJH, Gilchrist ID, McSorley E (2004) The influence of spatial frequency and contrast on saccade latencies. *Vision Res* 44:2597–2604.
- Luna B, Velanova K (2011) Development from reflexive to controlled eye movements. *Oxf Handb Eye Mov* Available at: <https://www.oxfordhandbooks.com/view/10.1093/oxfordhb/9780199539789.001.0001/oxfordhb-9780199539789-e-035>.

- Lynch JC, Graybiel AM, Lobeck LJ (1985) The differential projection of two cytoarchitectonic subregions of the inferior parietal lobule of macaque upon the deep layers of the superior colliculus. *J Comp Neurol* 235:241–254.
- Lynch JC, Hoover JE, Strick PL (1994) Input to the primate frontal eye field from the substantia nigra, superior colliculus, and dentate nucleus demonstrated by transneuronal transport. *Exp Brain Res* 100:181–186.
- Lynch JC, McLaren JW (1989) Deficits of visual attention and saccadic eye movements after lesions of parietooccipital cortex in monkeys. *J Neurophysiol* 61:74–90.
- Lynch JC, Mountcastle VB, Talbot WH, Yin TC (1977) Parietal lobe mechanisms for directed visual attention. *J Neurophysiol* 40:362–389.
- Ma L, Selvanayagam J, Ghahremani M, Hayrynen LK, Johnston KD, Everling S (2020) Single unit activity in marmoset posterior parietal cortex in a gap saccade task. *J Neurophysiol* Available at: <https://journals.physiology.org/doi/abs/10.1152/jn.00614.2019>.
- Mansfield K (2003) Marmoset models commonly used in biomedical research. *Comp Med* 53:383–392.
- Mantini D, Corbetta M, Romani GL, Orban GA, Vanduffel W (2013) Evolutionarily novel functional networks in the human brain? *J Neurosci Off J Soc Neurosci* 33:3259–3275.
- Marg E, Adams JE (1967) Indwelling multiple micro-electrodes in the brain. *Electroencephalogr Clin Neurophysiol* 23:277–280.
- Marino RA, Rodgers CK, Levy R, Munoz DP (2008) Spatial relationships of visuomotor transformations in the superior colliculus map. *J Neurophysiol* 100:2564–2576.
- Maynard EM, Nordhausen CT, Normann RA (1997) The Utah intracortical Electrode Array: a recording structure for potential brain-computer interfaces. *Electroencephalogr Clin Neurophysiol* 102:228–239.
- McDonald JS, Clifford CWG, Solomon SS, Chen SC, Solomon SG (2014) Integration and segregation of multiple motion signals by neurons in area MT of primate. *J Neurophysiol* 111:369–378.
- McPeck RM, Keller EL (2002) Saccade Target Selection in the Superior Colliculus During a Visual Search Task. *J Neurophysiol* 88:2019–2034.
- McPeck RM, Keller EL (2004) Deficits in saccade target selection after inactivation of superior colliculus. *Nat Neurosci* 7:757–763.
- Meredith MA, Stein BE (1983) Interactions among converging sensory inputs in the superior colliculus. *Science* 221:389–391.

- Meredith MA, Stein BE (1985) Descending efferents from the superior colliculus relay integrated multisensory information. *Science* 227:657–659.
- Merrill DR, Bikson M, Jefferys JGR (2005) Electrical stimulation of excitable tissue: design of efficacious and safe protocols. *J Neurosci Methods* 141:171–198.
- Michon F, Aarts A, Holzhammer T, Ruther P, Borghs G, McNaughton B, Kloosterman F (2016) Integration of silicon-based neural probes and micro-drive arrays for chronic recording of large populations of neurons in behaving animals. *J Neural Eng* 13:046018.
- Miller CT, Freiwald WA, Leopold DA, Mitchell JF, Silva AC, Wang X (2016) Marmosets: A Neuroscientific Model of Human Social Behavior. *Neuron* 90:219–233.
- Miller EK, Cohen JD (2001) An integrative theory of prefrontal cortex function. *Annu Rev Neurosci* 24:167–202.
- Miller EK, Lundqvist M, Bastos AM (2018) Working Memory 2.0. *Neuron* 100:463–475.
- Mitchell JF, Leopold DA (2015) The marmoset monkey as a model for visual neuroscience. *Neurosci Res* 93:20–46.
- Mitchell JF, Reynolds JH, Miller CT (2014) Active vision in marmosets: a model system for visual neuroscience. *J Neurosci Off J Soc Neurosci* 34:1183–1194.
- Mohler CW, Wurtz RH (1976) Organization of monkey superior colliculus: intermediate layer cells discharging before eye movements. *J Neurophysiol* 39:722–744.
- Moore T, Armstrong KM (2003) Selective gating of visual signals by microstimulation of frontal cortex. *Nature* 421:370–373.
- Moore T, Armstrong KM, Fallah M (2003) Visuomotor origins of covert spatial attention. *Neuron* 40:671–683.
- Moschovakis AK, Scudder CA, Highstein SM (1991a) Structure of the primate oculomotor burst generator. I. Medium-lead burst neurons with upward on-directions. *J Neurophysiol* 65:203–217.
- Moschovakis AK, Scudder CA, Highstein SM, Warren JD (1991b) Structure of the primate oculomotor burst generator. II. Medium-lead burst neurons with downward on-directions. *J Neurophysiol* 65:218–229.
- Mott FW, Schuster E, Halliburton WD (1910) Cortical lamination and localisation in the brain of the marmoset. *Proc R Soc Lond Ser B Contain Pap Biol Character* 82:124–134.
- Mountcastle VB (1997) The columnar organization of the neocortex. *Brain J Neurol* 120 (Pt 4):701–722.

- Munoz DP, Armstrong IT, Hampton KA, Moore KD (2003) Altered Control of Visual Fixation and Saccadic Eye Movements in Attention-Deficit Hyperactivity Disorder. *J Neurophysiol* 90:503–514.
- Munoz DP, Dorris MC, Paré M, Everling S (2000) On your mark, get set: brainstem circuitry underlying saccadic initiation. *Can J Physiol Pharmacol* 78:934–944.
- Munoz DP, Everling S (2004) Look away: the anti-saccade task and the voluntary control of eye movement. *Nat Rev Neurosci* 5:218–228.
- Munoz DP, Istvan PJ (1998) Lateral inhibitory interactions in the intermediate layers of the monkey superior colliculus. *J Neurophysiol* 79:1193–1209.
- Munoz DP, Wurtz RH (1993) Fixation cells in monkey superior colliculus. II. Reversible activation and deactivation. *J Neurophysiol* 70:576–589.
- Munoz DP, Wurtz RH (1995) Saccade-related activity in monkey superior colliculus. I. Characteristics of burst and buildup cells. *J Neurophysiol* 73:2313–2333.
- Naito E, Kinomura S, Geyer S, Kawashima R, Roland PE, Zilles K (2000) Fast reaction to different sensory modalities activates common fields in the motor areas, but the anterior cingulate cortex is involved in the speed of reaction. *J Neurophysiol* 83:1701–1709.
- Nandy AS, Nassi JJ, Reynolds JH (2017) Laminar Organization of Attentional Modulation in Macaque Visual Area V4. *Neuron* 93:235–246.
- Nyffeler T, Hartmann M, Hess CW, Müri RM (2008) Visual vector inversion during memory antisaccades--a TMS study. *Prog Brain Res* 171:429–432.
- O'Driscoll GA, Alpert NM, Matthyse SW, Levy DL, Rauch SL, Holzman PS (1995) Functional neuroanatomy of antisaccade eye movements investigated with positron emission tomography. *Proc Natl Acad Sci* 92:925–929.
- Okano H, Hikishima K, Iriki A, Sasaki E (2012) The common marmoset as a novel animal model system for biomedical and neuroscience research applications. *Semin Fetal Neonatal Med* 17:336–340.
- Okano H, Mitra P (2015) Brain-mapping projects using the common marmoset. *Neurosci Res* 93:3–7.
- Otero-Millan J, Troncoso XG, Macknik SL, Serrano-Pedraza I, Martinez-Conde S (2008) Saccades and microsaccades during visual fixation, exploration, and search: Foundations for a common saccadic generator. *J Vis* 8:21–21.
- Paré M, Dorris MC (2011) The role of posterior parietal cortex in the regulation of saccadic eye movements. *Oxf Handb Eye Mov* Available at:

<https://www.oxfordhandbooks.com/view/10.1093/oxfordhb/9780199539789.001.0001/oxfordhb-9780199539789-e-014>.

- Paré M, Hanes DP (2003) Controlled movement processing: superior colliculus activity associated with countermanded saccades. *J Neurosci Off J Soc Neurosci* 23:6480–6489.
- Patil AC, Thakor NV (2016) Implantable neurotechnologies: a review of micro- and nanoelectrodes for neural recording. *Med Biol Eng Comput* 54:23–44.
- Pesaran B, Pezaris JS, Sahani M, Mitra PP, Andersen RA (2002) Temporal structure in neuronal activity during working memory in macaque parietal cortex. *Nat Neurosci* 5:805–811.
- Pettine WW, Steinmetz NA, Moore T (2019) Laminar segregation of sensory coding and behavioral readout in macaque V4. *Proc Natl Acad Sci* 116:14749–14754.
- Pierrot-Deseilligny C, Rivaud S, Gaymard B, Agid Y (1991) Cortical control of reflexive visually-guided saccades. *Brain J Neurol* 114 (Pt 3):1473–1485.
- Preuss TM (2007) Evolutionary Specializations of Primate Brain Systems. In: *PRIMATE ORIGINS: Adaptations and Evolution* (Ravosa MJ, Dagosto M, eds), pp 625–675. Boston, MA: Springer US. Available at: http://link.springer.com/10.1007/978-0-387-33507-0_18.
- Ranck JB (1975) Which elements are excited in electrical stimulation of mammalian central nervous system: A review. *Brain Res* 98:417–440.
- Redgrave P, Gurney K (2006) The short-latency dopamine signal: a role in discovering novel actions? *Nat Rev Neurosci* 7:967–975.
- Reilly JP, Diamant AM (2011) *Electrostimulation: Theory, Applications, and Computational Model*. Artech House.
- Renshaw B, Forbes A, Morison BR (1940) Activity of isocortex and hippocampus: electrical studies with micro-electrodes. *J Neurophysiol* 3:74–105.
- Reser DH, Burman KJ, Yu H-H, Chaplin TA, Richardson KE, Worthy KH, Rosa MGP (2013) Contrasting patterns of cortical input to architectural subdivisions of the area 8 complex: a retrograde tracing study in marmoset monkeys. *Cereb Cortex N Y N* 1991 23:1901–1922.
- Rezvani S, Corneil BD (2008) Recruitment of a Head-Turning Synergy by Low-Frequency Activity in the Primate Superior Colliculus. *J Neurophysiol* 100:397–411.
- Richmond BJ, Optican LM (1987) Temporal encoding of two-dimensional patterns by single units in primate inferior temporal cortex. II. Quantification of response waveform. *J Neurophysiol* 57:147–161.

- Robinson DA (1970) Oculomotor unit behavior in the monkey. *J Neurophysiol* 33:393–403.
- Robinson DA (1972) Eye movements evoked by collicular stimulation in the alert monkey. *Vision Res* 12:1795–1808.
- Robinson DA, Fuchs AF (1969) Eye movements evoked by stimulation of frontal eye fields. *J Neurophysiol* 32:637–648.
- Robinson DL, Goldberg ME, Stanton GB (1978) Parietal association cortex in the primate: sensory mechanisms and behavioral modulations. *J Neurophysiol* 41:910–932.
- Rodgers CK, Munoz DP, Scott SH, Paré M (2006) Discharge properties of monkey tectoreticular neurons. *J Neurophysiol* 95:3502–3511.
- Roitman JD, Shadlen MN (2002) Response of neurons in the lateral intraparietal area during a combined visual discrimination reaction time task. *J Neurosci Off J Soc Neurosci* 22:9475–9489.
- Rosa MGP, Tweeddale R (2005) Brain maps, great and small: lessons from comparative studies of primate visual cortical organization. *Philos Trans R Soc Lond B Biol Sci* 360:665–691.
- Rousche PJ, Normann RA (1998) Chronic recording capability of the Utah Intracortical Electrode Array in cat sensory cortex. *J Neurosci Methods* 82:1–15.
- Sakamoto M, Hikosaka O (1989) Eye movements induced by microinjection of GABA agonist in the rat substantia nigra pars reticulata. *Neurosci Res* 6:216–233.
- Sasaki E et al. (2009) Generation of transgenic non-human primates with germline transmission. *Nature* 459:523–527.
- Sasaki S, Shimazu H (1981) Reticulovestibular organization participating in generation of horizontal fast eye movement. *Ann N Y Acad Sci* 374:130–143.
- Saslow MG (1967) Latency for Saccadic Eye Movement*. *JOSA* 57:1030–1033.
- Schall JD (1997) Visuomotor Areas of the Frontal Lobe. In: *Extrastriate Cortex in Primates* (Rockland KS, Kaas JH, Peters A, eds), pp 527–638 *Cerebral Cortex*. Boston, MA: Springer US. Available at: https://doi.org/10.1007/978-1-4757-9625-4_13.
- Schall JD (2002) The neural selection and control of saccades by the frontal eye field. *Philos Trans R Soc B Biol Sci* 357:1073–1082.
- Schall JD (2015) Visuomotor Functions in the Frontal Lobe. *Annu Rev Vis Sci* 1:469–498.
- Schall JD, Hanes DP, Thompson KG, King DJ (1995a) Saccade target selection in frontal eye field of macaque. I. Visual and premovement activation. *J Neurosci* 15:6905–6918.

- Schall JD, Morel A, King DJ, Bullier J (1995b) Topography of visual cortex connections with frontal eye field in macaque: convergence and segregation of processing streams. *J Neurosci Off J Soc Neurosci* 15:4464–4487.
- Schiller PH, Malpeli JG (1977) Properties and tectal projections of monkey retinal ganglion cells. *J Neurophysiol* 40:428–445.
- Schiller PH, Malpeli JG, Schein SJ (1979) Composition of geniculostriate input of superior colliculus of the rhesus monkey. *J Neurophysiol* 42:1124–1133.
- Schiller PH, Tehovnik EJ (2001) Look and see: how the brain moves your eyes about. *Prog Brain Res* 134:127–142.
- Schiller PH, True SD, Conway JL (1980) Deficits in eye movements following frontal eye-field and superior colliculus ablations. *J Neurophysiol* 44:1175–1189.
- Schlag J, Schlag-Rey M (1987) Evidence for a supplementary eye field. *J Neurophysiol* 57:179–200.
- Schlag-Rey M, Amador N, Sanchez H, Schlag J (1997) Antisaccade performance predicted by neuronal activity in the supplementary eye field. *Nature* 390:398–401.
- Schmolesky MT, Wang Y, Hanes DP, Thompson KG, Leutgeb S, Schall JD, Leventhal AG (1998) Signal timing across the macaque visual system. *J Neurophysiol* 79:3272–3278.
- Selemon LD, Goldman-Rakic PS (1988) Common cortical and subcortical targets of the dorsolateral prefrontal and posterior parietal cortices in the rhesus monkey: evidence for a distributed neural network subserving spatially guided behavior. *J Neurosci* 8:4049–4068.
- Selvanayagam J, Johnston KD, Schaeffer DJ, Hayrynen LK, Everling S (2019) Functional Localization of the Frontal Eye Fields in the Common Marmoset Using Microstimulation. *J Neurosci Off J Soc Neurosci* 39:9197–9206.
- Shadlen MN, Newsome WT (1996) Motion perception: seeing and deciding. *Proc Natl Acad Sci U S A* 93:628–633.
- Shadlen MN, Newsome WT (2001) Neural basis of a perceptual decision in the parietal cortex (area LIP) of the rhesus monkey. *J Neurophysiol* 86:1916–1936.
- Shen HH (2015) Core Concept: Resting-state connectivity. *Proc Natl Acad Sci U S A* 112:14115–14116.
- Shibutani H, Sakata H, Hyvärinen J (1984) Saccade and blinking evoked by microstimulation of the posterior parietal association cortex of the monkey. *Exp Brain Res* 55:1–8.

- Shook BL, Schlag-Rey M, Schlag J (1990) Primate supplementary eye field: I. Comparative aspects of mesencephalic and pontine connections. *J Comp Neurol* 301:618–642.
- Smith SM, Fox PT, Miller KL, Glahn DC, Fox PM, Mackay CE, Filippini N, Watkins KE, Toro R, Laird AR, Beckmann CF (2009) Correspondence of the brain's functional architecture during activation and rest. *Proc Natl Acad Sci U S A* 106:13040–13045.
- Solomon SG, Rosa MGP (2014) A simpler primate brain: the visual system of the marmoset monkey. *Front Neural Circuits* 8:96.
- Sommer MA, Wurtz RH (2000) Composition and topographic organization of signals sent from the frontal eye field to the superior colliculus. *J Neurophysiol* 83:1979–2001.
- Sommer MA, Wurtz RH (2004) What the brain stem tells the frontal cortex. II. Role of the SC-MD-FEF pathway in corollary discharge. *J Neurophysiol* 91:1403–1423.
- Sommer MA, Wurtz RH (2006) Influence of the thalamus on spatial visual processing in frontal cortex. *Nature* 444:374–377.
- Sommer MA, Wurtz RH (2008) Brain circuits for the internal monitoring of movements. *Annu Rev Neurosci* 31:317–338.
- Stanton GB, Deng S-Y, Goldberg EM, McMullen NT (1989) Cytoarchitectural characteristic of the frontal eye fields in macaque monkeys. *J Comp Neurol* 282:415–427.
- Stanton GB, Goldberg ME, Bruce CJ (1988a) Frontal eye field efferents in the macaque monkey: I. Subcortical pathways and topography of striatal and thalamic terminal fields. *J Comp Neurol* 271:473–492.
- Stanton GB, Goldberg ME, Bruce CJ (1988b) Frontal eye field efferents in the macaque monkey: II. Topography of terminal fields in midbrain and pons. *J Comp Neurol* 271:493–506.
- Stephan H, Frahm H, Baron G (1981) New and revised data on volumes of brain structures in insectivores and primates. *Folia Primatol Int J Primatol* 35:1–29.
- Stuphorn V, Schall JD (2002) Neuronal control and monitoring of initiation of movements. *Muscle Nerve* 26:326–339.
- Tailby C, Cheong SK, Pietersen AN, Solomon SG, Martin PR (2012) Colour and pattern selectivity of receptive fields in superior colliculus of marmoset monkeys. *J Physiol* 590:4061–4077.
- Tallon-Baudry C, Bertrand O, Peronnet F, Pernier J (1998) Induced gamma-band activity during the delay of a visual short-term memory task in humans. *J Neurosci Off J Soc Neurosci* 18:4244–4254.

- Tehovnik EJ (1996) Electrical stimulation of neural tissue to evoke behavioral responses. *J Neurosci Methods* 65:1–17.
- Tehovnik EJ, Sommer MA, Chou IH, Slocum WM, Schiller PH (2000) Eye fields in the frontal lobes of primates. *Brain Res Brain Res Rev* 32:413–448.
- Tehovnik EJ, Tolias AS, Sultan F, Slocum WM, Logothetis NK (2006) Direct and indirect activation of cortical neurons by electrical microstimulation. *J Neurophysiol* 96:512–521.
- Thier P (2011) The oculomotor cerebellum. *Oxf Handb Eye Mov* Available at: <https://www.oxfordhandbooks.com/view/10.1093/oxfordhb/9780199539789.001.0001/oxfordhb-9780199539789-e-010>.
- Thier P, Andersen RA (1998) Electrical microstimulation distinguishes distinct saccade-related areas in the posterior parietal cortex. *J Neurophysiol* 80:1713–1735.
- Thompson KG, Bichot NP, Sato TR (2005a) Frontal eye field activity before visual search errors reveals the integration of bottom-up and top-down salience. *J Neurophysiol* 93:337–351.
- Thompson KG, Biscoe KL, Sato TR (2005b) Neuronal basis of covert spatial attention in the frontal eye field. *J Neurosci Off J Soc Neurosci* 25:9479–9487.
- Thompson KG, Hanes DP, Bichot NP, Schall JD (1996) Perceptual and motor processing stages identified in the activity of macaque frontal eye field neurons during visual search. *J Neurophysiol* 76:4040–4055.
- Troilo D, Totonelly K, Harb E (2009) Imposed anisometropia, accommodation, and regulation of refractive state. *Optom Vis Sci Off Publ Am Acad Optom* 86:E31–39.
- Tu TA, Keating EG (2000) Electrical Stimulation of the Frontal Eye Field in a Monkey Produces Combined Eye and Head Movements. *J Neurophysiol* 84:1103–1106.
- Vincent JL, Patel GH, Fox MD, Snyder AZ, Baker JT, Van Essen DC, Zempel JM, Snyder LH, Corbetta M, Raichle ME (2007) Intrinsic functional architecture in the anaesthetized monkey brain. *Nature* 447:83–86.
- Walker R, Deubel H, Schneider WX, Findlay JM (1997) Effect of remote distractors on saccade programming: evidence for an extended fixation zone. *J Neurophysiol* 78:1108–1119.
- Walker R, Walker DG, Husain M, Kennard C (2000) Control of voluntary and reflexive saccades. *Exp Brain Res* 130:540–544.
- Walls GL (1962) The evolutionary history of eye movements. *Vision Res* 2:69–80.

- Wang Y, Matsuzaka Y, Shima K, Tanji J (2004) Cingulate cortical cells projecting to monkey frontal eye field and primary motor cortex. *Neuroreport* 15:1559–1563.
- Wardak C, Olivier E, Duhamel J-R (2004) A deficit in covert attention after parietal cortex inactivation in the monkey. *Neuron* 42:501–508.
- White BJ, Munoz DP (2011) The superior colliculus. In: *The Oxford handbook of eye movements*, pp 195–213 Oxford library of psychology. New York, NY, US: Oxford University Press.
- Wolbarsht ML, Macnichel EF, Wagner HG (1960) Glass Insulated Platinum Microelectrode. *Science* 132:1309–1310.
- Woldring S, Dirken MNJ (1950) Spontaneous unit-activity in the superficial cortical layers. *Acta Physiol Pharmacol Neerl* 1:369–379.
- Wolfe JM, Horowitz TS (2004) What attributes guide the deployment of visual attention and how do they do it? *Nat Rev Neurosci* 5:495–501.
- Wurtz RH, Goldberg ME (1971) Superior colliculus cell responses related to eye movements in awake monkeys. *Science* 171:82–84.
- Yang T, Shadlen MN (2007) Probabilistic reasoning by neurons. *Nature* 447:1075–1080.
- Zhang M, Barash S (2000) Neuronal switching of sensorimotor transformations for antisaccades. *Nature* 408:971–975.
- Zhang M, Barash S (2004) Persistent LIP Activity in Memory Antisaccades: Working Memory For a Sensorimotor Transformation. *J Neurophysiol* 91:1424–1441.
- Zhao M, Gersch TM, Schnitzer BS, Doshier BA, Kowler E (2012) Eye movements and attention: The role of pre-saccadic shifts of attention in perception, memory and the control of saccades. *Vision Res* 74:40–60.
- Zhou H, Desimone R (2011) Feature-based attention in the frontal eye field and area V4 during visual search. *Neuron* 70:1205–1217.
- Ziamba CM, Perez RK, Pai J, Kelly JG, Hallum LE, Shooner C, Movshon JA (2019) Laminar Differences in Responses to Naturalistic Texture in Macaque V1 and V2. *J Neurosci* 39:9748–9756.

CHAPTER 2

2 Frontoparietal Functional Connectivity in the Common Marmoset¹

2.1 Abstract

In contrast to the well-established macaque monkey, little is known about functional connectivity patterns of common marmoset monkey (*Callithrix jacchus*) that is poised to become the leading transgenic primate model. Here, we used resting-state ultra-high-field fMRI data collected from anesthetized marmosets and macaques along with awake human subjects, to examine and compare the brain's functional organization, with emphasis on the saccade system. Exploratory independent component analysis revealed eight resting-state networks in marmosets that greatly overlapped with corresponding macaque and human networks including a distributed frontoparietal network. Seed-region analyses of the superior colliculus (SC) showed homolog areas in macaques and marmosets. The marmoset SC displayed the strongest frontal functional connectivity with area 8aD at the border to area 6DR. Functional connectivity of this frontal region revealed a similar functional connectivity pattern as the frontal eye fields in macaques and humans. Furthermore, areas 8aD, 8aV, PG, TPO, TE2, and TE3 were identified as major hubs based on region-wise evaluation of betweenness centrality, suggesting that these cortical regions make up the functional core of the marmoset brain. The results support an evolutionarily preserved frontoparietal system and provide a starting point for invasive neurophysiological studies in the marmoset saccade and visual systems.

¹ A version of Chapter 2 is published as: Frontoparietal functional connectivity in the common marmoset, Maryam Ghahremani, R. Mathew Hutchison, Ravi S. Menon, Stefan Everling, *Cerebral Cortex*. 27(8), 3890-3905.

2.2 Introduction

The neural circuitry controlling saccadic eye movements is the best understood sensory-motor system in the primate brain. The network subserving saccadic eye movements encompasses areas in posterior parietal, superior temporal, and frontal cortices, as well as subcortical brain regions (Wurtz and Goldberg 1989; Johnston and Everling 2008). Detailed mechanistic knowledge of this system at the cortical and subcortical level comes mainly from neurophysiological studies in awake behaving macaque monkeys. These studies have not only provided the foundation for our understanding of saccade control, but have revealed, and continue to reveal, fundamental insights into the neural basis of decision making, attention, and other higher executive functions in primates. More recently, task-based and resting-state functional MRI has shown homologous frontoparietal network patterns in macaque monkeys and humans (Koyama et al. 2004; Baker et al. 2006; Ford et al. 2009; Kagan et al. 2010; Hutchison et al. 2011; Hutchison et al. 2012; Mantini et al. 2013).

Despite their fundamental role as a nonhuman primate model for saccade control and cognition, macaque monkeys have also several shortcomings: (1) many of the key frontoparietal areas are deeply buried in sulci, making them difficult or even impossible to access for laminar neural recordings and manipulations; (2) their low birth rate and long sexual maturation make it difficult to utilize transgenic approaches; (3) pharmacological studies are very expensive due to the animals' large body size. These disadvantages are not present in the small New World common marmoset monkey (*Callithrix jacchus*). The marmoset's fast sexual maturation, low inter-birth interval, and routinely observed chimeric twinning make it the leading candidate for transgenic primate models (Sasaki et al. 2009; Okano et al. 2012; Kishi et al. 2014; Izpisua Belmonte et al. 2015; Mitchell and Leopold 2015; Sasaki 2015). The lissencephalic (smooth)

marmoset cortex also offers the opportunity for laminar electrophysiological recordings and optical imaging in key frontoparietal areas. Further, it has been recently demonstrated that head-fixed marmosets, like head-fixed macaques, can be trained to perform visual tasks (Mitchell et al. 2014). Thus, the common marmoset holds tremendous promise as a nonhuman primate model for neuroscientific discovery (Thart et al. 2012; Hashikawa et al. 2015; Mitchell and Leopold 2015; Miller et al. 2016). In contrast to the macaque monkey, little is known about the functional organization of the saccade network in this species.

Here, we used ultra-high-field resting-state (RS) fMRI at 9.4 T to explore frontoparietal brain networks in lightly anesthetized marmosets through correlations of blood-oxygen-level-dependent (BOLD) signals. In the absence of explicit task demands, the correlation structure of spontaneously fluctuating BOLD signals in the low frequency range (0.01–0.1 Hz) resemble both task-evoked (Toro et al. 2008; Smith et al. 2009; Laird et al. 2011) and anatomical (Vincent et al. 2007; Damoiseaux and Greicius 2009; Greicius et al. 2009; Van Den Heuvel et al. 2009; Honey et al. 2009) connectivity patterns. Resting-state fMRI has been extensively applied to human subjects and has made important contributions to identifying normal and abnormal network patterns (Menon 2011; Raichle 2011; Buckner et al. 2013). Resting-state fMRI studies have also demonstrated that macaque monkeys (awake and anesthetized) exhibit a functional architecture largely homologous to humans (Vincent et al. 2007; Margulies et al. 2009; Hutchison et al. 2011; Hutchison and Everling 2012; Mantini et al. 2012; Mantini et al. 2013; Sallet et al. 2013; Miranda-Dominguez et al. 2014; Neubert et al. 2014). In common marmosets, the first exploratory independent component analysis (ICA) of resting-state data in awake animals identified several networks, some of which were homologous with those found in humans, including the visual network, somatomotor network, and orbitofrontal network

(Belcher et al. 2013). In the present study, ICA revealed similar network patterns as those observed in awake animals (Belcher et al. 2013) and extracted a distributed frontoparietal network component. To directly identify the putative frontoparietal saccade network, a seed-based analysis approach was used to examine the functional connectivity profiles of the superior colliculus and frontal eye fields – critical subcortical and cortical components of the primate saccade system, respectively (Johnston and Everling 2008; Johnston and Everling 2011). The focus of this study is the marmoset FEF, as this area and its patterns of functional connectivity are well established in both macaques and humans (Hutchison et al. 2012). The FEF not only plays a significant role in the control of saccades but it is also involved in the covert attention (Corbetta and Shulman 2002; Moore and Armstrong 2003; Schall 2004). However, the exact location of a putative FEF in marmosets is currently unknown since the area has not yet been investigated by electrophysiological approaches. Therefore, we initially investigated the connectivity of the SC which can easily be located on the roof of the midbrain. As a fundamental brain area of the saccadic eye movement circuitry, the SC receives extensive projections from the FEF (Leichnetz et al. 1981; Fries 1984) and thus the area with the strongest functional connectivity in frontal cortex with the SC can be designated as the putative FEF. The resulting functional connectivity pattern revealed frontoparietal network patterns that likely corresponds to the saccade network, providing a starting point for future invasive studies. For comparative purposes, we performed similar analyses on data collected from lightly anaesthetized macaques at 7T, and awake human subjects at 3T, to evaluate the inter-species correspondence among the identified networks. The results demonstrate overlapping network patterns between marmosets, macaques, and humans, supporting the common marmoset as an alternative primate model to

the macaque for studying neural processes in the frontoparietal saccade network (Mitchell et al. 2014).

2.3 Materials and Methods

Experimental procedures on nonhuman primates were in accordance with the Canadian Council of Animal Care policy and protocols approved by the Animal Use Subcommittee of the University of Western Ontario Council on Animal Care. Human subjects provided written informed consent for their participation in accordance with the University of Western Ontario Health Sciences Research Ethics Board. Imaging was performed at the Centre for Functional and Metabolic Mapping at the Robarts Research Institute of the University of Western Ontario.

2.3.1 Marmoset data acquisition

We performed resting-state fMRI scans on four lightly anesthetized male common marmoset monkeys (*Callithrix jacchus*), aged 2-3 years and weighing 350-500g. Resting-state data was acquired using a 9.4T small animal MRI scanner equipped with a 12-cm gradient coil set of 400mT/m strength (Agilent, Palo Alto, CA, USA). A 15-channel phased array receive coil with a 2-channel transmit coil was designed in-house for marmoset fMRI on this scanner. Positioning of the animal in the custom-built MRI bed was implemented similar to the setup presented by Belcher et al. (2013). Each animal underwent 3 fMRI sessions. Six functional scans were acquired in each session using a 2-dimensional echo-planar imaging sequence (EPI2D) with parameters: TR = 1500 ms, volumes = 400, TE = 15 ms, and flip angle = 35°. Each functional volume comprised of 40 slices with an in-plane resolution of 0.5 × 0.5 mm and slice thickness

of 0.5 mm. The field of view (FOV) was 40×40 mm, and the matrix size was 80×80 . A standard whole-brain T1-weighted structural scan with 0.5-mm resolution along with a T2-weighted scan was also acquired before the functional scans. Prior to imaging session, anesthesia was induced in marmosets with 4% isoflurane in 2 l/min of oxygen in a plastic chamber. Isoflurane level was reduced to 2.5-3% for MRI preparation and further reduced to 1-1.3% during MRI acquisition, maintained throughout the scan by means of inhalation. Oxygen flow rate was kept between 2-2.5 l/min throughout the scan. Respiration, SpO₂, and heart rate were continuously monitored via pulse oximeter and were observed to be within the normal range throughout the scans. Temperature was also measured and recorded throughout, maintained using warm water circulating blankets, thermal insulation, and warmed air.

2.3.2 Macaque data acquisition

For comparative purposes, a group of 12 male rhesus macaque monkeys (*Macaca mulatta*), aged between 4 to 8 years and weighing 7 to 11 kg, were also studied. fMRI data was acquired on a 7T MRI scanner equipped with a 40-cm gradient coil set of 80 mT/m strength (Siemens, Erlangen, Germany). A 24-channel phased array receive coil with an 8-channel transmit coil was designed for macaque fMRI on this scanner (Gilbert et al. 2016). For each monkey, 4 runs of 600 functional volumes were acquired using a 2-dimensional multiBand EPI sequence with parameters: TR = 1000 ms, TE = 18 ms, and flip angle = 40° . Each functional volume comprised of 42 slices with a resolution of $1 \times 1 \times 1.1$ mm. The FOV was 96×96 mm, and the matrix size was 96×96 . A standard whole-brain 3-dimensional T1-weighted structural scan with 0.5-mm isotropic resolution and a T2-weighted 2-dimensional multi-slice turbo spin echo (TSE) were also acquired within the same imaging session with the same orientation as the functional scans

(0.4×0.4 mm in plane, 1 mm slice thickness), FOV of 128×128 , TR of 7500 ms, TE of 90 ms, and a flip angle of 120° . The anesthesia process was as follows: the animals were first sedated with 0.1-0.2 mg/kg acepromazine, followed by 7.5 mg/kg ketamine hydrochloride by intramuscular injection. Anesthetic induction was accomplished by the administration of 2.5mg/kg propofol via an intravenous catheter in the saphenous vein. Furthermore, anesthesia was maintained with 1 to 2% isoflurane with oxygen (1.5-2 l/min) through endotracheal intubation and it was reduced to 1% during fMRI acquisition. Heart rate and SpO₂ were monitored throughout via a pulse oximeter and end-tidal CO₂ and respiration rate were monitored via a capnometer. Temperature was recorded before and after the scans and was maintained within the normal range using heating discs, covers, and thermal insulation. Animals received subcutaneous fluids (10 ml/kg/hr) before and after the scan.

Isoflurane is a commonly used anesthetic agent in resting-state fMRI studies on rodents (e.g. Hutchison et al. 2010; Liu et al. 2011; Wang et al. 2011) as well as non-human primates (e.g. Vincent et al. 2007; Hutchison et al. 2011; Sallet et al. 2013). Beyond reducing physiological stress and motion, the use of anesthesia eliminates extensive training requirements necessary for animals to adapt to the scanner environment. Anesthetics can impact resting-state functional connectivity measures through alteration of underlying neural activity or the co-occurring effects on cerebral blood flow (CBF), blood volume (CBV), and metabolic rate (reviewed in Masamoto and Kanno 2012). Dose-dependent evaluation of isoflurane effects have been previously studied in macaques and suggested 1.0 to 1.5% as a suitable level in which to obtain coherent and stable patterns of distributed network activity (Hutchison et al. 2014) and as such this level was used as the safe range for both macaques and marmosets. It is important to

consider that temporal and spatial features of the network architecture are likely altered compared to the awake condition though data quality will be significantly improved.

2.3.3 Human data acquisition

The human resting-state fMRI dataset used in the present study was published previously (Hutchison et al. 2012; Hutchison et al. 2013) including ICA results (Hutchison and Everling 2012). The included 12 subjects (8 men, 4 women, average age = 26.2 years) scanned on a 3T Siemens TIM MAGNETOM Trio MRI Scanner. For each subject, 1 run of 360 functional volumes were acquired with a T2*-weighted EPI acquisition sequence with the following parameters: TR = 2000 ms, TE = 30 ms, slice thickness = 3.5 mm, in-plane resolution = 3mm \times 3mm, FOV = 240 \times 240, matrix size = 80 \times 80, and flip angle = 90°. A T2*-weighted structural scan was also acquired with FOV of 192 \times 240 \times 256, TR of 2300 ms, TE of 2.98 ms, and a flip angle of 9°. The subjects were instructed to remain as still as possible and to fixate at a central location throughout the scan.

2.3.4 Image preprocessing

fMRI data was preprocessed using modules contained within the FSL software package (fMRI Software Library: <http://www.fmrib.ox.ac.uk>). These included motion correction, slice timing correction, high-pass and low-pass temporal filtering, registration, normalization and spatial smoothing. The brain was manually extracted from skull and soft tissue using the FSL Brain Extraction Tool (BET) and the BrainSuite toolbox (<http://brainsuite.usc.edu>), to be used in parts of the registration process. The averaged EPI image for each subject was registered to its

corresponding anatomical image using linear and non-linear registration methods provided in FSL. The data from individual subjects was further co-registered to the common standard brain templates in order to make it possible for higher-level within-subject and between-subject analysis. The high-resolution standard brain template by Hikishmia (2011; see http://brainatlas.brain.riken.jp/marmoset_html) was used for marmoset registration, while the F99 atlas template (Van Essen 2004; see <http://sumsdb.wustl.edu/sums/macaquemore.do>) was used for macaques and the standard 152-brain MNI template for humans. Data were smoothed by Gaussian blurring with FWHM value of 1.5 mm in the case of marmosets, 3 mm in the case of macaques, and 6 mm for the humans.

2.3.5 Independent component analysis

Group-level independent component analysis was implemented using the MELODIC (Multivariate Exploratory Linear Optimized Decomposition into Independent Components: <http://fsl.fmrib.ox.ac.uk/fsl/fslwiki/MELODIC>) ICA module of the FSL software package in order to extract meaningful components that can be representative of the possible resting-state networks (RSNs). ICA assumes that fMRI data consist of a set of spatially or temporally overlapping components in addition to artifactual effects (such as head motion, respiratory and pulsation movements) that each has an independent spatial pattern and an associated timecourse. The spatial ICA algorithm aims to minimize the spatial overlap between components based on the independence of the signals. Prior to ICA decomposition the data was centered and whitened. ICA is a "model-free" algorithm that attempts to identify cortical activation patterns common to a group of voxels, rather than comparing the activation of individual voxels with a hypothesized time course, as in the seed-based analysis (Hyvärinen

and Oja 2000). However, controversy exists as to the optimal number of independent components (ICs) to extract from a data sample to best delineate human RSNs. Some studies have tried to determine an optimal number through developing a template-matching algorithm (Demertzi et al. 2014), but standardized approaches are lacking, particularly for non-human primates. Previous reports have indicated that the optimal number of ICs for non-human primates falls in the range of 20 to 30 components, which allows for detection of RSNs before fractionation occurs (Hutchison et al. 2011; Belcher et al. 2013; Mantini et al. 2013). In the current study, ICA was implemented seven times for each primate group, corresponding to the decomposition of the data into 5, 10, 15, 20, 25, 30 and 35 ICs to evaluate the robustness of the identification. After visual inspection, and in keeping with previous reports, the result from the extraction of 20 ICs was selected to be an appropriate representative of all meaningful components that corresponded well across the three groups. Group-level results were overlaid onto high-resolution standard brain templates and were visually inspected to identify relevant components associated with possible RSNs with reference to previously reported functional networks in macaques and humans (van den Heuvel and Hulshoff Pol 2010; Hutchison et al. 2011; Hutchison and Everling 2012).

2.3.6 Region of interest analysis

Frontoparietal networks underlying the primate saccade system were also investigated via a seed-based analysis of resting-state data. This was done on the basis of the general linear model (Wickens 2004), provided through the FEAT (fMRI Expert Analysis Tool: <http://fsl.fmrib.ox.ac.uk/fsl/fslwiki/FEAT>) module of the FSL toolbox. For marmosets and macaques, the regions of interest were initially drawn on the left and right SC of the template

volume image using MRICron software (<http://www.mricron.com/mricron/install.html>) based on standard atlases and previous studies (Paxinos et al. 2000; Paxinos et al. 2012). The lower resolution of functional data prevented us to perform a similar analysis on the human dataset. The mean time series signal of these seed regions was extracted for each monkey and regressed against the rest of the brain. This was done by using a multiple regression model of individual fMRI runs of every subject in order to find correlations among the time series of every brain voxel. This model also accounted for white matter and cerebrospinal fluid, as confound variables. A fixed-effects analysis was then implemented across all scans obtained for each subject in order to acquire a single z-statistic map of significant connectivity patterns. Finally, a group-level fixed-effects analysis was conducted to obtain functional connectivity maps across all subjects. Multiple-comparison corrections were done at cluster level by Gaussian random field theory with $z > 2.3$ and cluster significance: $p < 0.05$. As a result, a thresholded z-statistic map was obtained for the SC functional connectivity in marmosets and macaques, representing brain regions that significantly correlated with the left or right SC seed. Moreover, the putative marmoset FEF was identified as the frontal region with the largest functional connectivity with the SC as a cortical region of interest fundamental to the primate oculomotor system (Schall 2015). Macaque FEF was located on the anterior bank of the arcuate sulcus in each hemisphere (Bruce, 2004; Bruce & Goldberg, 1985). A similar seed-based analysis was implemented by calculating the correlation of the FEF time series signal with all other brain voxels, resulting in FEF-connectivity maps in marmosets and macaques. In the human data, results obtained from Hutchison et al. (2012) were used, with FEF located at the junction of the superior frontal sulcus and the anterior bank of the precentral sulcus (Luna et al. 1998; Ford et

al. 2005; Amiez 2006; Hutchison et al. 2012). Multiple-comparison corrections were achieved at cluster level by Gaussian random field theory with $z > 3.7$ and cluster significance: $p < 0.05$.

2.3.7 Surface-based registrations

The finalized volume-based connectivity maps resulting from the ICA as well as the final group z-score results obtained from the SC and FEF correlation analysis were further projected onto associated brain cortical surface models for each species provided through the CARET toolbox (<http://www.nitrc.org/projects/caret>) for surface or flat-map visualization purposes. The updated surface-based registrations that included the marmoset in addition to the macaque and human, were provided by Chaplin et al. (2013), who reconstructed a surface-based three-dimensional model of the marmoset cortex from coronal sections using the atlas by Paxinos and colleagues (2012). In order to achieve a more direct mean of comparing the seed-based results across species, we also projected the resulting marmoset z-statistic maps onto the macaque and human brain surface maps and vice versa using landmark-based inter-species surface registrations (Orban et al. 2004; Van Essen and Dierker 2007; Chaplin et al. 2013). The inter-species registration between the marmoset, macaque, and human models was implemented based on a landmark vector difference algorithm in CARET (Van Essen et al. 2001) and using a registration package described by Chaplin et al. 2013 (http://sumsdb.wustl.edu/sums/directory.do?id=8294741&dir_name=Expansion). This algorithm has been explained in full details by Van Essen and colleagues (2001) but in short, it deforms one species' spherical map to another, by aligning the corresponding landmark borders after they have been projected onto their respective spherical maps. The alignment process involves several stages, each of which includes multiple cycles. During each of the cycles, a

vector difference is calculated between the current location of the landmark in the source map and its corresponding location in the target and it is this vector difference that drives the deformation process (Van Essen et al, 2001; Orban et al. 2004; Chaplin et al. 2013; Mantini et al. 2013). After inter-species registration of the surface maps, a spatial correlation coefficient of thresholded z maps was eventually calculated to quantify the degree of similarity of the obtained functional connectivity maps across species.

2.3.8 Assessing functional hubs in the marmoset

Assessment of functional and structural brain organization has revealed that the cortex contains a small number of nodes referred to as hubs that have a disproportionately high number of connections (Honey et al. 2007; Sporns et al. 2007; Hagmann et al. 2008; Buckner et al. 2009; Tomasi and Volkow 2011; van den Heuvel and Sporns 2013; Belcher et al. 2016). The densely connected regions found in humans, macaques, and marmosets are topologically positioned to serve flexible and integrative roles across different functional subnetworks and enable globally efficient information flow (Sporns et al. 2007). To explore hub organization in the marmoset we computed the correlation matrix of 115 cortical regions within the right hemisphere defined by Paxinos et al. (2012) for every run. Fisher transformed matrices were then averaged within session, then within subject, and finally across subjects. The group average matrix was transformed back into correlation values and binarized with a threshold of $r > 0.2$ - values greater than this threshold indicating a connection (edge) between the regions (nodes). Betweenness centrality (BC; the number of shortest path lengths that pass through that node) was calculated using the Brain Connectivity Toolbox (BCT; <http://www.brain-connectivity->

toolbox.net; Rubinov and Sporns 2010). To assess the probability of obtaining BC values by chance, the binarized averaged graph was rewired 10000 times while preserving node degree distribution and values within the matrix was used to create a distribution. BC values occurring less than 5%, 1%, or 0.1% of the time in the null distribution were identified.

2.4 Results

2.4.1 Resting-state networks

After the implementation of group-level ICA on marmoset resting-state fMRI data with a model order of 20, 12 components appeared to reflect physiological noise, including cardiac and respiratory artifacts, or CSF and white matter. The remaining 8 components detected demonstrated considerable correspondence to possible RSNs, with visually identifiable connectivity patterns significantly overlapping with those previously described in macaques and humans (Figure 2-1 and 2-2). Identified marmoset brain networks, with their constituent brain areas determined according to the marmoset brain atlas by Paxinos and colleagues (2012) included:

- RSN 1 (Fig. 2-1A): A higher order midline visual network involving visual areas V1, V2, and dorsolateral area V6. This network has been previously reported in awake marmosets (Belcher et al. 2013).
- RSN 2 (Fig. 2-1B): A dorsal medial somatomotor network involving the anterior and posterior cingulate cortices (areas 24 and 23), primary motor area (4) as well as area 3 of somatosensory cortex. This network closely resembles a somatomotor network identified in awake marmosets characterized by connectivity between primary and secondary somatosensory areas, primary

motor area and cingulate cortex (Belcher et al. 2013). It also significantly corresponds with dorsal somatomotor network patterns in macaques and humans, as reported in previous studies (Vincent et al. 2007; Hutchison et al. 2011; Mantini et al. 2013).

- RSN 3 (Fig. 2-1C): A ventral somatomotor network that encompasses the primary motor cortex (area 4) and somatosensory cortex. This network, which has also been reported in awake marmosets (Belcher et al. 2013) as well as in anesthetized macaques (Hutchison et al. 2011), corresponds well with a ventral somatomotor network in macaques and humans in the present study.

- RSN 4 (Fig. 2-1D): a network encompassing the anterior cingulate cortex as well as the frontal operculum corresponding to a cingulo-operculum network in macaques and humans.

- RSN 5 (Fig. 2-1E): A network involving the rostral subdivision of the dorsal premotor area 6DR, prefrontal areas 8C, 8aV, 8aD, 45, 47, and parietal areas PGM, PEC, PE, LIP, VIP, MIP, AIP, PG. A similar network was also detected in RSN studies of awake marmosets and was designated as the default mode network (Belcher et al. 2013). However, our results suggest a better correspondence to a dorsal attention/control network in macaques and humans. This network has been previously reported in RSN studies of anesthetized macaques and identified as a frontoparietal network controlling saccades (Hutchison et al. 2011).

- RSN 6 (Fig. 2-1F): A network including the anterior cingulate cortex (area 24), anterior insula, auditory cortex, as well as area PFG and area TP. In the awake marmoset, Belcher et al. (2013) identified a very similar network with similar connectivity patterns, and they designated it as a salience-like network. Hutchison (2011) also identified a cingulo-insular component in

anesthetized macaques that encompassed some of the areas identified in the present study. The network may correspond to the salience network in macaques and humans.

- RSN 7 (Fig. 2-1G): A frontal pole network involving area 10, which was also distinguishable in the awake marmoset (Belcher et al. 2013), and which could represent a fractionated portion of the marmoset default mode network.

- RSN 8 (Fig. 2-2): A basal ganglia network including, most notably, the caudate and putamen. This network was identical to that reported in awake marmosets and anesthetized macaques, with the same brain regions being functionally connected to one another (Hutchison et al. 2011; Belcher et al. 2013). Among the RSNs identified through the group-level ICA, RSN 5 (corresponding to a dorsal attention/control network in humans (Fig. 2-1E)) encompassed significant frontal and parietal brain areas. Figure 2-3 displays a flat map cortical representation of the frontoparietal patterns of functional connectivity in RSN 5 (from Fig. 2-1E) in marmosets (left) and macaques (right). Considerable similarity is observed in the corresponding RSN 5 in these species. Both primate species show strong functional connectivity in posterior parietal cortex (including areas PGM, PEC, LIP, MIP, VIP, and AIP) and in dorsal premotor (area 6

DR) and prefrontal areas (area 8 complex). This pattern overlaps with previously reported findings of FEF connectivity patterns in macaques (Hutchison et al. 2013).

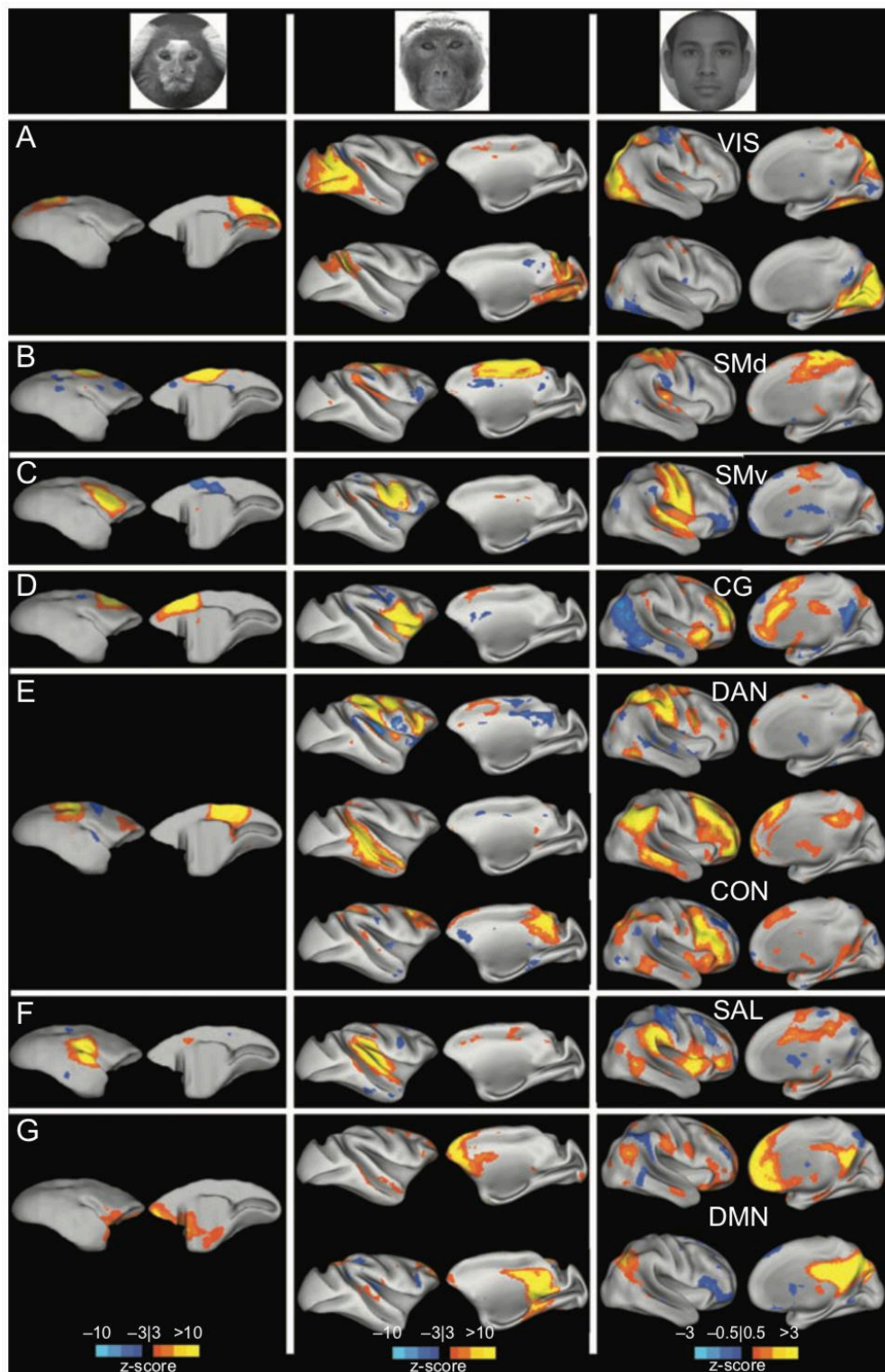


Figure 2-1. Homologous core resting-state networks of primate species. Note that the z-statistic maps are thresholded according to the z-score color bars provided for each species. The resulting z-statistic maps of the networks were projected onto each species respective surface model. These networks correspond to the following human RSNs: (A) visual network (VIS), (B) dorsal somatomotor network (SMd), (C) ventral somatomotor network (SMv), (D) cingulo-operculum network (SG), (E) dorsal attention network (DAN)/cognitive control network (CON), (F) salience network (SAL), and (G) default mode network (DMN). Human connectivity maps were taken from Hutchison and Everling (2012).

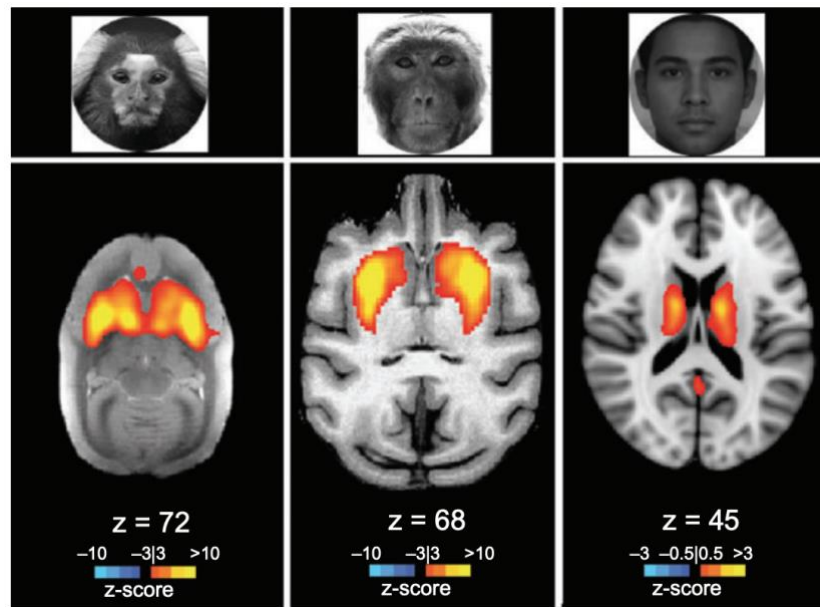


Figure 2-2. Basal ganglia network in the common marmoset (left), macaque (middle), and human (right). The z-statistic map of each species was overlaid onto the respective high-resolution template. Note that the z-statistic maps are thresholded according to the z-score color bars provided.

2.4.2 Seed-based connectivity patterns

To further delineate the observed frontoparietal functional connectivity patterns, this network was further investigated through seed-based analysis on volume data. Figures 2-4A and 2-4C display the functional connectivity of the right SC within the right hemisphere in the macaque and marmoset, respectively after being projected onto the surface maps. The results from the left and right SC seed were qualitatively very similar but stronger for the right SC in macaque monkeys. The results revealed strong functional connectivity between the right SC and frontoparietal and temporal brain areas in both primate species. In macaques, these areas correspond with visual areas V1, V2, V3, V4 as well medial temporal (MT) and medial superior temporal (MST) regions. Functional connectivity in temporal areas overlapped with the location of several known face patches in macaques (Fig. 4A; Schwiedrzik et al. 2015). Considerable functional connectivity was observed in parietal areas surrounding the intraparietal sulcus and area PG. Within frontal cortex, strong functional connectivity was observed in areas at the anterior bank of the arcuate sulcus, which corresponds to the location of FEF. This functional connectivity pattern had considerable correspondence with the SC connectivity in marmosets, where there was also strong functional connectivity between the right SC and V1, V2, V3, V4, MT, MST and FST. Areas 6DC, 6DR, 8B, 8aD, 8aV, 8C and 46D were strongly functionally connected areas within frontal cortex, with the caudal portion of area 8aD at the border to area 6DR having the strongest functional connectivity, likely corresponding to the FEF in marmosets. This region was identified as area 8aD based on the anatomical distance from the anterior commissure in the volume data using the marmoset atlas by Paxinos and colleagues (2012). The superimposed cortical borders on the surface maps also marked this region as area 8aD, overlapping with sites where Blum and colleagues (1982) were

able to evoke saccades and slow eye movements in anesthetized marmosets (open circles in Fig. 8, first panel) (Blum et al. 1982).

Although the functional connectivity of the SC suggests that area 8AD may correspond to the FEF in marmosets, tracer studies on marmoset monkeys have suggested that area 8aV may correspond to the FEF in marmosets (Burman et al. 2006; Reser et al., 2013). Therefore, we performed identical seed-analyses on the volume-data for the voxel with the strongest functional connectivity with the SC in the posterior part of area 8aD and for a voxel in area 8aV, identified based on the volume data using the marmoset atlas by Paxinos and colleagues (2012). Figure 2-4 depicts the lateral (left) and medial (right) view of the SC (first row), area 8aD (second row) and area 8aV (third row) functional connectivity z-statistic maps in marmosets projected onto the cortical surface model. The smaller cortical maps shown at the bottom left and right corners of area 8aD and 8aV maps of Fig 2-4, represent the lateral (left) and medial (right) views of the major projections to these areas that were reported by Reser and colleagues (2013) based on retrograde tracer injections in marmosets (Reser et al. 2013). The areas are color-coded according to the percentage of the projections found from the labeled neurons, ranging from the weakest projections shown in lighter yellow from more than 0.5 % of the labeled neurons to the strongest projections represented in darker red from more than 16 % of them. There was a strong correspondence of our observed functional connectivity patterns with the findings of the tracer studies regarding the afferent connections of area 8aD, reflecting a considerable agreement between the functional and structural connectivity patterns. To directly compare the functional connectivity maps of area 8aD and 8aV, we performed a higher-level analysis using a fixed effect with multiple-comparison corrections at a cluster level of $z > 2.3$ and cluster significance $p < 0.05$.

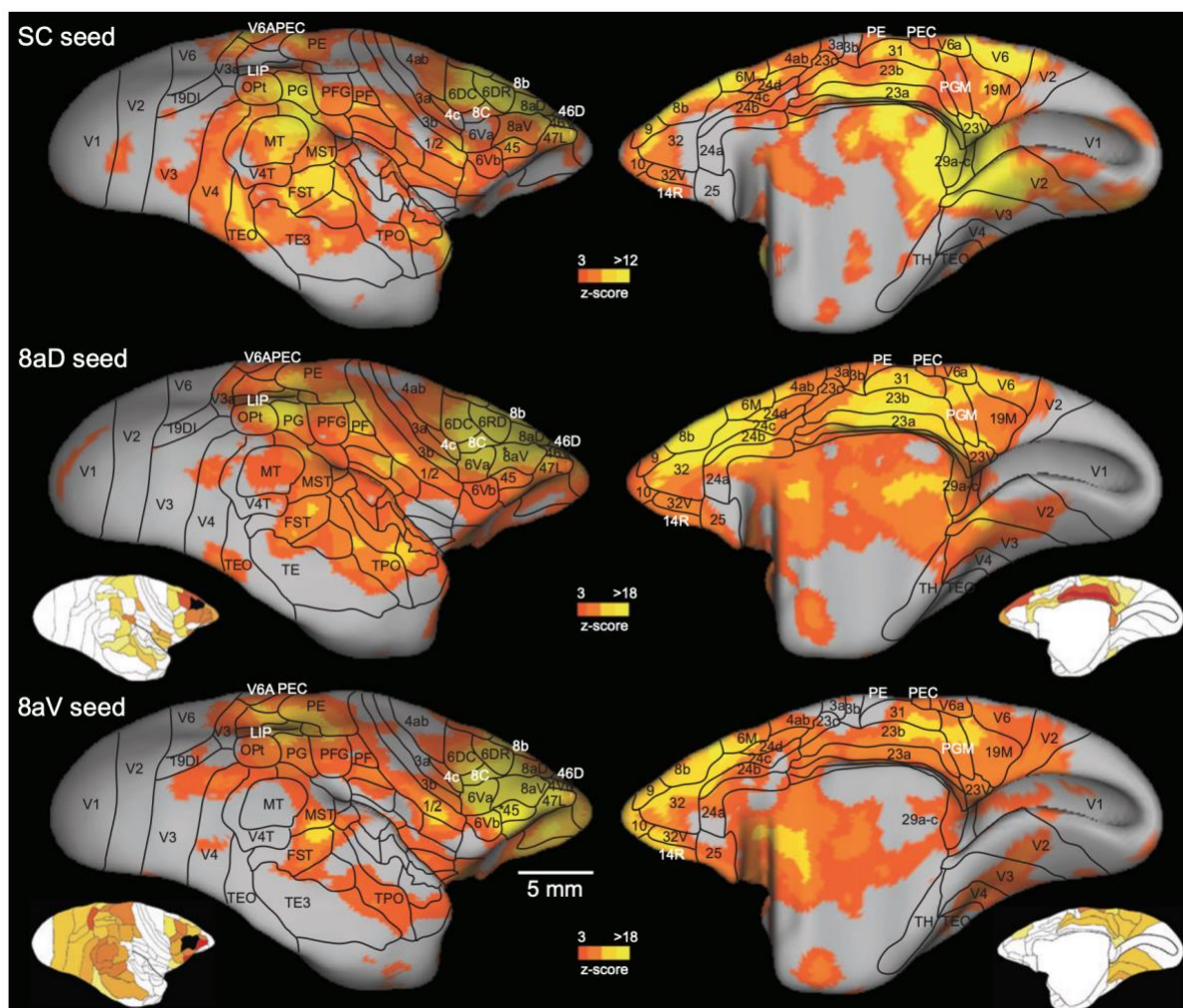


Figure 2-4. Lateral (left) and medial (right) views of the brain showing the functional connectivity patterns of the SC (first row), area 8aD (second row) and area 8aV (third row) in common marmosets projected onto marmoset cortical surface model with cortical borders superimposed. z-Statistic maps are thresholded according to the z-score color bar provided, displaying only the positive functional connectivity. Asterisk indicates the location of the seed. The figures at the bottom left and right corners of 8aD and 8aV maps represent the lateral (left) and medial (right) views of principal projections to area 8aD and 8aV, respectively, reported by Reser et al. (2013) based on fluorescent tracer injections from more than 0.5% of the labeled neurons (light yellow) to more than 16% (dark red) (Reser et al. 2013).

The results show that area 8aD had significantly stronger functional connectivity with areas 8b, 6DR, 23a, 23b, 24b, 24c, 31, 29a-c, PF, TPO, TEO, V1, V2, and V6, while area 8aV had stronger functional connectivity with areas 6Va, 45, and V4 (see Supplementary Fig. 2-1A in section 2.8- Supplementary Material). At the subcortical level, the SC exhibited significantly stronger functional connectivity with area 8aD than area 8aV (Supplementary Fig. 2-1B in section 2.8- Supplementary Material). Considering the strong projections from macaque FEF to the SC in macaque monkeys, we propose that 8aD corresponds to the putative marmoset FEF.

To compare the functional connectivity of FEF between marmosets and macaques, we conducted a seed-based analysis on the volume data after seeding macaque FEF in the anterior bank of the accurate sulcus in the right hemisphere. Similar to the SC-connectivity maps, the obtained FEF maps were also visualized on flat cortical representation maps of the right hemisphere as displayed in figure 2-5B and 5C for macaques and marmosets, respectively. In both macaques and marmosets, FEF exhibited strong functional connectivity with anterior and posterior cingulate cortex, PG, LIP and PF as well as various areas within posterior parietal cortex. Within prefrontal cortex, strong functional connectivity was observed with area 46 in marmosets and area 9/46 in macaques. Areas 6DC, 6DR, 6Va and 8aD also showed significant functional connectivity with the seed region.

Coronal views of specific slices within the resulting SC and FEF connectivity maps depict strong functional connectivity with subcortical and cortical areas including: the SC, parietal areas LIP, PG, PFG; temporal areas MT, FST, TE2, TPO; pulvinar, amygdala, area 23b, S2E, the caudate nucleus, and frontal areas including areas 8aV, 45, and 6DR (Fig. 2-6). The SC also showed functional connectivity with regions in the brain stem that overlapped with the

oculomotor (3N), trochlear (4N), and abducens nucleus (6N). Although a functional connectivity of the SC with oculomotor nuclei would make sense, our functional imaging resolution was too low to identify these small nuclei with certainty.

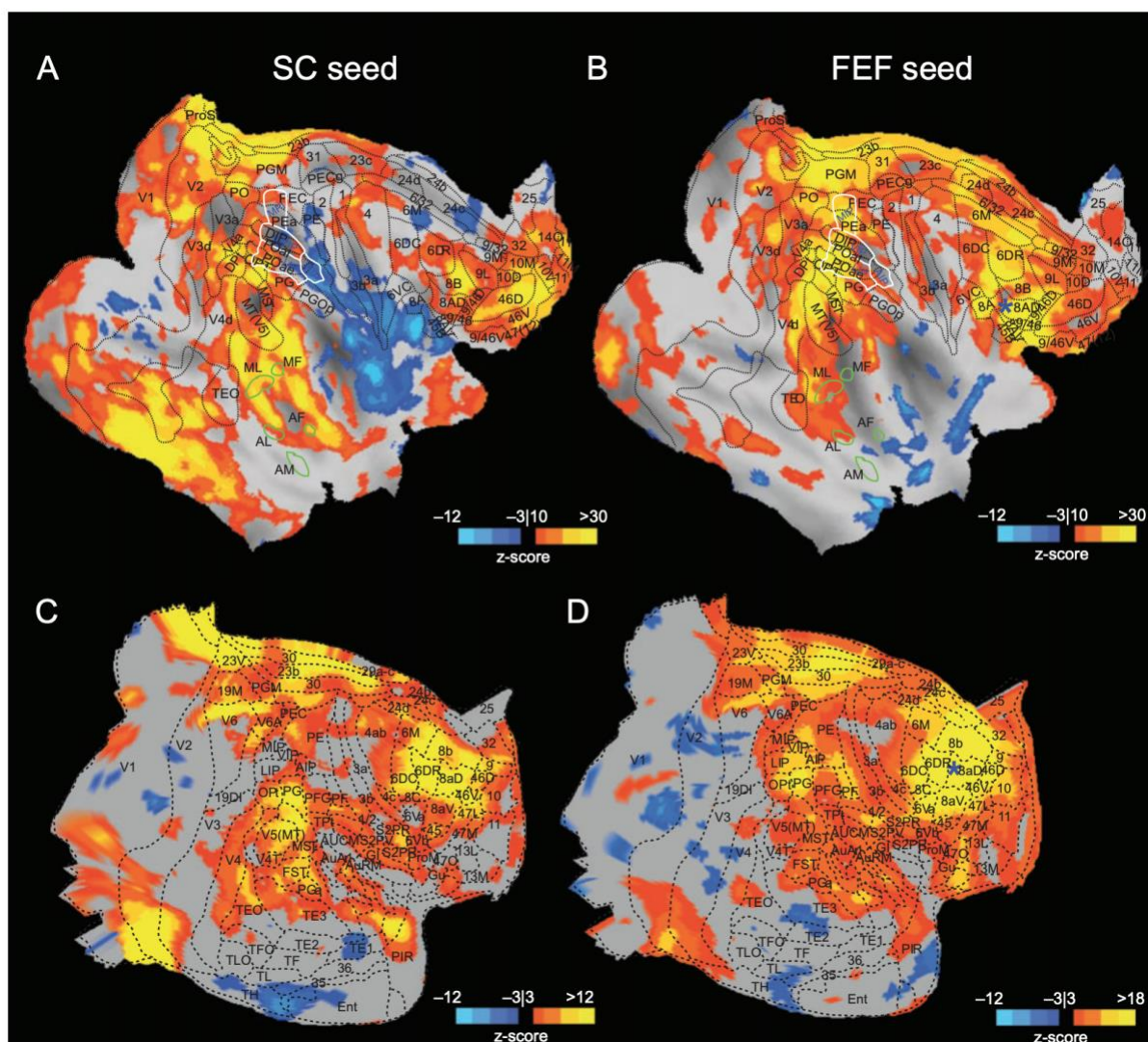


Figure 2-5. Functional connectivity patterns in the right hemisphere of macaques and common marmosets. Group averaged connectivity patterns of the SC (left column) and FEF (right column) are shown on flattened cortical representations of the macaque (top) and marmoset (bottom). Asterisks indicate the location of the FEF seed. The SC is not visualized in a cortical representation. Note that the z-statistic maps are thresholded according to the z-score color bars provided and they differ for each

map. The z-statistic maps were averaged across each group with multiple-comparison corrections achieved at cluster level with $z > 2.3$ and cluster significance: $p < 0.05$ and were projected onto the cortical flat-map models of macaques and marmosets. Areas marked in green represent cortical face patches in macaques (Schwiedrzik et al. 2015). White lines marked on the map refer to the location of LIP, VIP, MIP, and AIP macaques (from Felleman and Van Essen 1991).

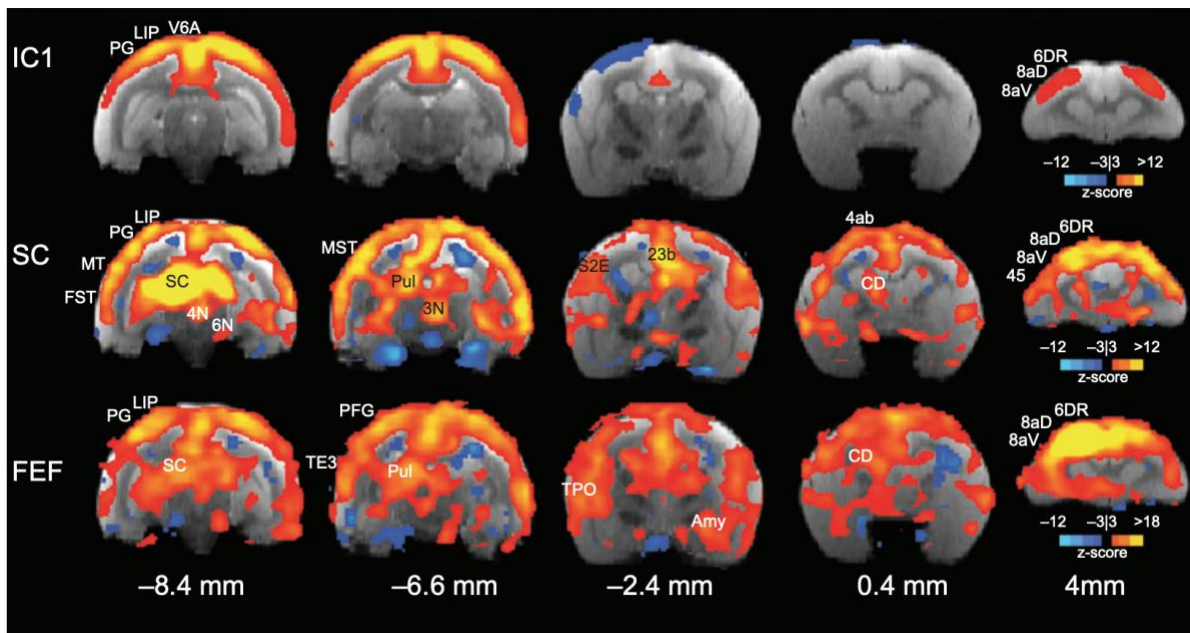


Figure 2-6. Coronal view of the functional connectivity patterns in frontal, parietal, temporal and subcortical areas in the common marmoset, obtained from ICA (first row), SC-based (second row), and FEF-based (third row) analysis. The numbers at the bottom of the figure represent the distance from the anterior commissure. The z-statistic maps were averaged across the group with multiple-comparison corrections achieved at cluster level with $z > 2.3$ and cluster significance: $p < 0.05$. SC: superior colliculus, Amy: amygdala, CD: caudate nucleus, LIP: lateral intraparietal, PG: postcentral gyrus, MT: medial temporal, FST: fundal area of the superior temporal sulcus, Pul: pulvinar, 3N: oculomotor nucleus, 4N: trochlear nucleus, 6N: abducens nucleus, TPO: temporo-parietooccipital, 8aV: anterior ventral area 8, 6DR: rostral dorsal area 6, TE3: temporal area TE2, S2E: secondary somatosensory cortex-external part, V6A: visual area V6.

In order to further compare FEF functional connectivity across species, the marmoset functional connectivity z-statistic maps were projected onto the macaque and human brain surface, and vice versa, using the inter-species surface registrations provided in CARET (Van Essen et al. 2001; Chaplin et al. 2013). Figure 2-7 displays the inter-species surface mapping of the SC-connectivity patterns in marmosets and macaques. In this matrix representation, the sources are the functional connectivity z-statistic maps of the species of interest (first row: marmoset, second row: macaque) and the targets are the cortical surface models of the species of interest that the z-statistic maps are going to be projected onto (first column: marmoset, second column: macaque). The results demonstrate a significant degree of homology for the SC functional connectivity patterns across marmosets and macaques when projected onto each other's cortical surface. However, notable differences include stronger functional connectivity of the SC with frontal cortical areas in marmosets, as compared to macaques. Similar interspecies surface-based registration was performed to compare FEF functional connectivity patterns across marmosets, macaques and humans. Figure 2-8 displays a similar matrix representation for projecting the marmoset (first row), macaque (second row) and human (third row) FEF-connectivity z-statistic maps as sources onto the cortical surface model of the species of interest (first column: marmoset cortical surface, second column: macaque inflated cortical surface, third column: human inflated cortical surface). The asterisk marks the approximate location of the FEF seed in each species. The resulting interspecies registrations reflect a remarkable correspondence for the FEF functional connectivity patterns across the 3 species when mapped onto each other's surface model. Areas involved in the marmoset FEF connectivity pattern correspond with similar frontoparietal brain areas in macaques and humans, and vice versa. Therefore, a very similar frontoparietal pattern of connectivity was consistently observed,

supporting the existence of a well preserved frontoparietal network underlying the saccadic eye movement circuitry across New World and Old World primates. To derive a quantitative assessment of the degree of overlap between the resulting seed region connectivity maps across species, a spatial correlation coefficient was calculated based on the z-statistic maps from each species projected onto the respective surface. The thresholds were set to account for both positive and negative patterns of connectivity. The FEF-connectivity map in marmosets correlated with that of macaques at an r-value of 0.53, and 0.50 with that of humans. Macaque FEF-connectivity maps correlated with that in the human at a correlation coefficient of 0.38. The spatial z-statistic maps were further binarized, where z-scores above the threshold were set to 1 while those below the threshold were set to 0, and the spatial correlation coefficients were re-calculated. In this case, the marmoset FEF functional connectivity map correlated with that of the macaque at an r-value of 0.35, and with that of the human at an r-value of 0.22. Macaque and human FEF functional connectivity maps correlated at an r-value of 0.30. All r-values calculated were significant with $p < 0.05$. These cross-species findings further emphasize the existence of a homologous frontoparietal putative saccade network in marmoset monkeys.

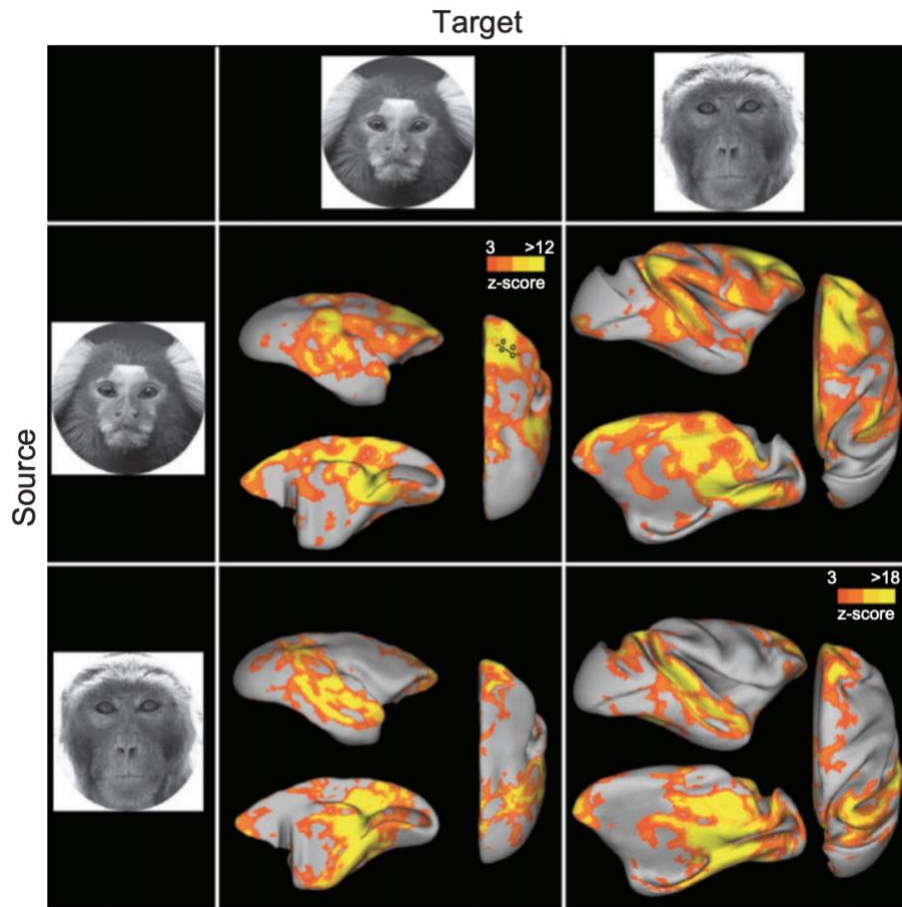


Figure 2-7. Inter-species surface-based registration of the SC functional connectivity maps between common marmosets and macaques. The top left panel displays the marmoset SC-connectivity map projected onto the marmoset brain surface while the top right panel shows the marmoset SC-connectivity map projected onto the macaque brain surface. The bottom left panel displays the macaque SC-connectivity map projected onto the marmoset brain surface while the bottom right panel shows the macaque SC-connectivity map projected onto the macaque brain surface. The black circles marked in marmoset SC-connectivity map projected onto marmoset brain surface (top left panel) indicates the locations at which Blum et al. (1982) were able to evoke saccadic eye movements in anesthetized marmosets using microstimulation. Note that the z-statistic maps are thresholded according to the z-score color bars provided and they differ for each map. The z-statistic maps were averaged across each group with multiple-comparison corrections achieved at cluster level with $z > 2.3$ and cluster significance: $p < 0.05$ and were projected on to the cortical surface models of macaques and marmosets (Chaplin et al. 2013; Van Essen 2005).

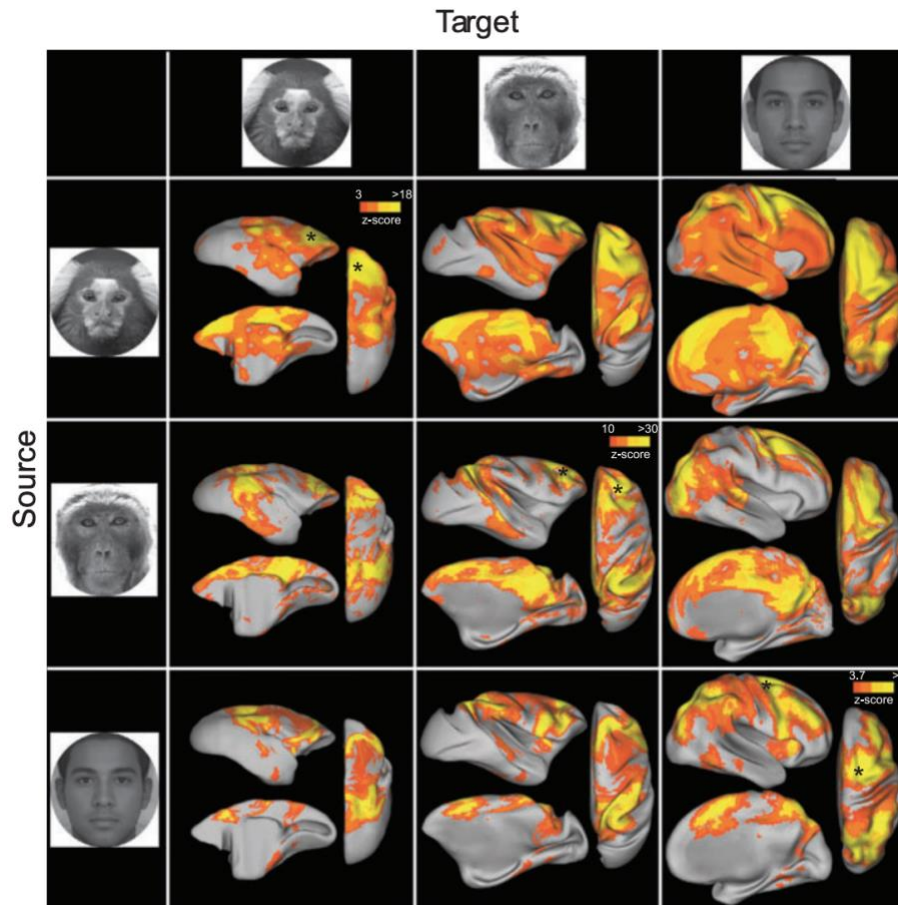


Figure 2-8. Inter-species surface-based registration of the FEF functional connectivity maps between common marmosets, macaques and humans. The first row displays the marmoset FEF-connectivity map projected onto the marmoset brain surface (left), macaque brain surface (middle) and human brain surface (right), respectively. The second row displays the macaque FEF-connectivity map projected onto the marmoset (left), macaque (middle), and human (right) brain surface, respectively. The third row displays the human FEF-connectivity map projected onto the marmoset (left), macaque (middle) and human (right) brain surface, respectively. The asterisks mark the location of the FEF seed in each species. Note that the z-statistic maps are thresholded according to the zscore color bars provided and they differ for each map. The z-statistic maps were averaged across each group with multiple-comparison corrections achieved at cluster level with $z > 2.3$ and cluster significance: $p < 0.05$ for marmosets and macaques and $z > 3.7$, cluster significance: $p < 0.05$ for humans, and were projected onto the cortical surface models of humans, macaques and marmosets (Chaplin et al. 2013; Van Essen 2005).

2.4.3 Functional hubs

The region-wise evaluation of betweenness centrality (BC) of the marmoset cortex is displayed in Figure 2-9. Of the 115 cortical areas, 14 were found to have significant BC values that indicate their position as functional hubs. These were: Area 8aD, PG, TPO, DI, TE2, area 11, LPro, 8aV, TE3, AuCPB, V4, PFG, PGA & IPa, and OPAI. The regions, and their relative “hubness” matched the pattern of cortical connectivity observed when evaluating the functional connectivity of SC and FEF.

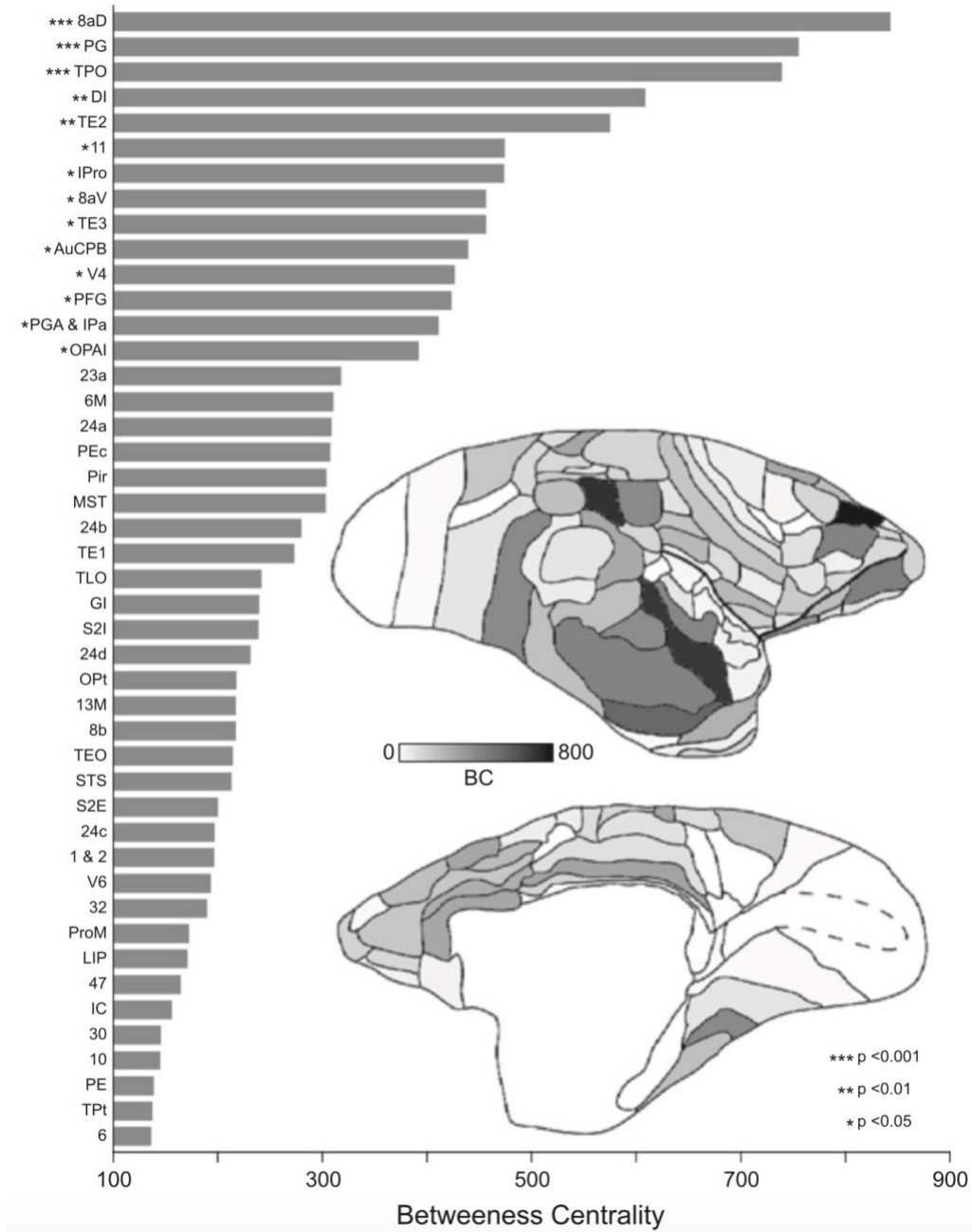


Figure 2-9. Hub identification in the common marmoset. The BC was evaluated for 115 cortical regions of the right hemisphere (Paxinos et al. 2012) calculated from the group-averaged and binarized functional connectivity matrix. The values for the highest 45 regions are rank ordered with significant regions are indicated with asterisks. The inset image displays the lateral and medial views with regions color-coded according to the BC value.

2.5 Discussion

Anesthetized New World common marmosets have been used for several decades as subjects in electrophysiological recording studies throughout the visual system (Yeh et al. 1995; Wilson et al. 1999). Only recently has it been shown that it is possible to record eye movements in awake behaving marmosets during visual tasks (Mitchell et al. 2014; Mitchell et al. 2015), by adopting an experimental approach that has been successful for almost 50 years in Old World macaques (Wurtz 1968). Combined with the marmoset's potential for molecular and genetic manipulations, and its lissencephalic cortex that allows laminar recordings in all key frontoparietal areas, this small primate is poised to become an important model not just for the study of oculomotor control, but for many areas of systems neuroscience (Izpisua Belmonte et al. 2015; Miller et al. 2016).

Here, we employed resting-state fMRI to compare functional networks between marmosets, macaques, and humans using the same imaging techniques and analysis approach. The aim of the present study was to evaluate whether the frontoparietal pattern of functional connectivity underlying the saccade circuitry is preserved across Old World (macaques and humans) and New World (marmosets) species, thereby identifying putative saccade-related areas in the marmoset for future invasive investigations of this circuitry.

Our ICA results demonstrate homologous RSNs between marmosets, macaques, and humans. This includes the identification of a frontoparietal RSN in marmosets that might reflect an ancestral frontoparietal predecessor to that observed in macaques and humans. Seed-based analysis of the superior colliculus (SC) demonstrated a similar functional connectivity pattern with cortical and subcortical areas between marmosets and macaques. The resolution of human data precluded accurate seeding of the SC in human subjects. However, correlation patterns of

the frontal eye fields (FEF) exhibited remarkably consistent patterns across marmosets, macaques, and humans. Taken together, our results strengthen the hypothesis that the strong frontoparietal functional connectivity underlying saccade control represents a preserved network among primates (Huerta et al. 1986; Huerta et al. 1987; Preuss 2007), which provides a foundation for the use of marmosets as an additional model for the study of the saccade circuitry in primates.

2.5.1 Exploratory analysis of RSN homologies

The goal of applying ICA was to identify homologous RSNs between marmosets, macaques, and humans. In lightly anesthetized marmosets, ICA extracted brain networks similar to those previously described in awake marmosets by Belcher and colleagues (2013) (Fig. 2-1 and 2-2). This finding supports our previous work in macaques, which showed stable and robust functional connectivity patterns in the isoflurane range between 1.0 and 1.5% (Hutchison et al. 2013). The Belcher et al. (2013) study described visual, basal ganglia, dorsal somatomotor, default-mode, salience, orbitofrontal, cerebellar, ventral somatomotor, and frontal pole RSNs that were mostly composed of connectivity between bilaterally homologous regions. A notable difference between our data and the awake marmoset study is that we found only one visual network (Fig. 2-1A), whereas Belcher and colleagues reported four different networks, including a primary visual, two higher-order visual, and a higher-order midline visual network. All these four networks were included in our visual network (Fig. 2-1A). Models with more components (25, 30) also did not show these four visual networks, but a model with 35 components contained left and right primary visual networks and a higher-order visual network. Another difference was that our 20 model-order decomposition did not contain a separate

cerebellar network. However, such an isolated cerebellar component was present in a model with 30 components. We found several components that resembled the orbitofrontal network described by Belcher and colleagues (2013), but we excluded these components as likely artifacts. A prominent network in our study that was absent in the Belcher et al. (2013) study is a pre-supplementary motor/anterior cingulate cortex RSN (Fig. 2-1D).

The dorsal somatomotor (Fig. 2-1B), ventral somatomotor (Fig. 2-1C), salience (Fig. 2-1F), frontal pole (Fig. 2-1G) and basal ganglia (Fig. 2-2) RSNs are virtually identical between the present results and the Belcher et al. (2013) study. It should be noted that the salience RSN includes area PFG, area TP, and several auditory areas; and thus, might also be identified as an auditory network. Belcher and colleagues identified one of their components as the default mode network (Fig. 2G, Belcher et al., 2013), a set of distributed areas that in humans is linked to a variety of cognitive processes such as autobiographical memory retrieval, envisioning the future, and mentalizing (Buckner et al. 2008). We identified the same frontoparietal RSN, but a projection on the flattened marmoset cortex showed that the frontal component included rostral premotor area 6DR, and prefrontal areas 8C, 8aV, 45, and 47; and the parietal component included areas PGM, PEC, PE, LIP VIP, MIP, AIP, and PG. Therefore, we believe that this component is better described as a dorsal attention network/control network, but its posterior medial parietal component area PGM is also a characteristic region of the default mode network in humans – though this region can have multiple network memberships (Leech et al. 2012). We hypothesize that the frontal pole network may also be part of the marmoset default-mode network.

ICA of lightly anaesthetized macaques confirms, but also improves the results from our first resting-state fMRI study of macaques (Hutchison et al. 2011). The present data show much

stronger and also more distributed networks than that of our previous study. These differences are likely the result of an increased number of animals (12 versus 6), more scans per subject (4 versus 2), and most importantly, substantial technical improvements in image acquisition (8-channel transmit/24-channel receive versus a 5-channel transceive coil, 1s TR versus 2s TR achieved using simultaneous multi-slice imaging).

The lower-order visual and somatomotor core networks showed the largest similarities between macaques, marmosets, and humans. Both a ventral and dorsal somatomotor RSN were present in all three species. It is more difficult to identify homologies between the higher order RSNs. This is not surprising as regions within the somatomotor and visual networks are functionally isolated in humans, whereas many higher order regions (e.g. precuneus, medial prefrontal cortex, posterior parietal cortex, FEF, and lateral intraparietal areas homologues) belong to multiple RSNs in humans and are associated with a broader range of functions (Yeo et al. 2014). Our ICA analysis in marmosets identified only one frontoparietal network (Fig. 2-1E, first panel), whereas the ICA in macaques identified three RSNs with frontal and parietal components (Fig. 2-1E, second panel) plus a frontal component (Fig. 2-1A, second panel) in one of the visual networks. More distributed networks were present in the awake human subjects, consistent with previous reports (Beckmann et al. 2005; Power et al. 2011; Yeo et al. 2011). In our human dataset, seven RSNs showed clear frontoparietal connectivity (third panel in Fig. 2-1E, 2-1D, 2-1F, 2-1G). ICA analysis in awake macaque monkeys at 3T (Mantini et al. 2013) previously identified only two (labeled as dorsal attention and DMN) frontoparietal networks, suggesting that the use of anesthesia cannot account for the differences between macaques and humans. Instead, these data suggest that RSNs may have become more distributed during primate evolution and that the single frontoparietal RSN in marmosets might

have originated from an ancestral frontoparietal network prior to the divergence between New World and Old World primates 40 million years ago. This frontoparietal network might then have given rise to the multiple and partially overlapping frontoparietal networks in Old World primates that also include cortical areas outside of the frontoparietal cortices.

2.5.2 Functional connectivity of the superior colliculus

Electrophysiological, lesion, and tracer studies have established an important role for the macaque SC in the control of saccadic eye movements. As expected, based on tracer studies (Leichnetz et al. 1981; Fries 1984; Lock et al. 2003), the SC showed positive functional connectivity with visual (V1, V2, V3, V4, MT, MST) and parietal areas (PGM, PO, PG, LIP, MIP). In frontal cortex, the SC seed showed functional connectivity with the upper arm of the anterior bank of the arcuate sulcus. Functional connectivity was also very strong with area 8B where microstimulation evokes ear and/or eye movements (Lanzilotto et al. 2013) and into the most anterior part of area 8aD, where the threshold for evoking neck EMG responses is lower than the threshold for evoking a saccade (Elsley et al. 2007). Considerable functional connectivity was also present with area 9/46D and area 46 (Fig. 2-4). Cooling of this region increases reaction times and decreases velocities of contralateral pro- and anti-saccades (Johnston et al. 2013).

Functional connectivity of the macaque SC included cortical face patch areas ML, MF, AL, AF, and also the amygdala (Fig. 2-5 marked by green circles, and Fig. 2-6). This finding is compatible with the notion of a subcortical face-processing system, consisting of the SC, the pulvinar, and the amygdala (Johnson MH 2005). We also found functional connectivity with areas that are involved in reaching movements in primates (Wise et al. 1997; Grefkes and Fink

2005), in particular with dorsal premotor (6DC, 6DR) and parietal cortical areas (e.g., area MIP) (Fig. 2-5). These results are consistent with tracer studies and with electrophysiological studies that have demonstrated gaze-dependent reach-related neural activity in the deep macaque SC layers that is highly correlated with EMG activity of shoulder, arm, and trunk muscles (Stuphorn et al. 1999). Recently, it has also been demonstrated that electrical microstimulation of the SC at depths (from the SC surface) of between 2600-4600 μm elicits a variety of arm movements (twitches, lifts, and extensions) in naïve animals (Philipp and Hoffmann 2014). In a highly trained monkey, Phillip and Hoffmann (2014) observed full reaches towards a touch screen. While we found functional connectivity with reach-related cortical areas, we found negative functional connectivity in parietal area AIP and in ventral premotor cortex (area 6VC) (Fig. 2-5). These areas are functionally connected with lateral FEF (Babapoor-Farrokhran et al. 2013) and are involved in grasping movements (Sakata et al. 1995; Murata et al. 2000; Fogassi 2001; Raos 2006).

In the marmoset, cortical neurons projecting to the SC have been identified and quantified by retrograde tracer injections in the SC by Collins et al. (2005). The most labeled neurons (together 40%) were identified in areas V1, V2, and MT. This was followed by neurons in areas V3, V4, and FST (20%). The study also showed dense labeling in the posterior parietal cortex and 8% of the labeled neurons were located in two frontal areas that the authors identified as FEF and FV (area ventral to the FEF with inputs from MT (Krubitzer and Kaas 1990)). They also reported labeled neurons in the medial wall and throughout the frontal cortex. The functional connectivity pattern of the SC we observed shows a very similar qualitative pattern as the retrograde tracer data. We found functional connectivity in V1, V2, V3, V4, MT, MST, FST, posterior parietal cortex, frontal cortex, and along the medial wall. The biggest difference

is that functional connectivity in marmosets (and also in macaques) was substantially weaker in early visual areas than one would have expected from the tracer data. As in macaques, the functional connectivity of the SC likely overlapped with putative face patches in the marmoset (Hung et al. 2015).

In frontal cortex, we found a strong cluster of functional connectivity with areas 6DR, 8B, 8aD, 8aV, 8C, and 46D. The strongest functional connectivity was in the caudal part of area 8aD, at the border to area 6DR (Fig. 2-4 and 2-5). We hypothesize that area 8aD and not neighbouring area 8aV (Burman et al. 2006) corresponds to the FEF in marmosets. In the macaque, area 8aD lies in the anterior bank of the upper arm of the arcuate sulcus in macaques, where larger amplitude saccades are represented (Bruce and Goldberg 1985; Schall 1997). Rosa and colleagues also suggested that the rostral part of area 6DR is involved in oculomotor control and that area 6DR plans goal-directed actions (Bakola et al. 2015). This location also seems to be in agreement with prediction that FEF is located approximately 4mm rostral to area 3b (Krubitzer and Kaas 1990) and that areas 3a, M1, and premotor areas lie between area 3b and FEF in the marmoset (Collins et al. 2005). This location also corresponds to sites where microstimulation evoked saccadic eye movements in anesthetized marmosets (Blum et al. 1982) (Fig. 7, open circles).

2.5.3 Locations of the frontal eye fields in marmosets

When we investigated the functional connectivity of the frontal voxel with the largest SC functional connectivity in marmosets, we obtained a functional connectivity map that largely corresponded to cortical areas labeled after retrograde tracer injections in area 8aD (Reser et al. 2013). This map shows strong functional connectivity with parietal area PG, LIP, and PF, areas

23a, 23b, 29a-c, anterior parts of area 24bm 23c, area 8b on the medial wall, and areas 6DC, 6DR, 6Va, 8aV, 46D, 8aD around the seed location (Fig. 2-4). The strong overlap between the functional and structural connectivity of area 8aD supports previous findings showing that a large part of functional connectivity is mediated by structural connectivity (Fig. 2-5) (Vincent et al. 2007; Damoiseaux and Greicius 2009; Greicius et al. 2009; Van Den Heuvel et al. 2009; Honey et al. 2009). Contrary to the present findings, Reser and colleagues (2013) had reported area 8aV as a putative FEF in marmosets based on tracer injection studies. In order to address these conflicting results, we conducted a similar seed analysis targeting area 8aV. The results demonstrated a similar pattern of functional connectivity to that of area 8aD; however, the overall strength of the functional connectivity was lower for area 8aV than 8AD, with a noticeable significant reduction of functional connectivity with the SC (Supp. Fig. 2-1). Considering the prominent role of the SC in the saccadic eye movement circuitry and the extensive amount of projections it receives from the FEF in macaques (Fries, 1984; Leichnetz et al. 1981), we hypothesize that the findings of the present study support the designation of area 8aD, and not 8aV, as a putative FEF in marmoset monkeys. Another possibility is that area 8aV may correspond to the FEF region encoding small amplitude saccades, whereas 8aD may correspond to the area encoding large amplitude saccades. Such an interpretation would be consistent with the finding that only medial FEF (area 8aD), but not lateral FEF (area 8aV) exhibited functional connectivity with the SC in macaque resting-state data (Babapoor-

Farrokhman et al. 2013). Electrophysiological recording and stimulation studies are required to distinguish the roles of areas 8aD and 8aV in saccade control in marmosets.

2.5.4 Functional connectivity of the frontal eye fields

The functional connectivity of the macaque FEF confirms data from a previous study in which we compared functional connectivity of FEF (area 8aD) between macaques and humans revealing a similar organization between the species (Hutchison et al. 2012). Our present study extends this finding to the New World common marmoset in addition to other New World species studies before (Huerta et al. 1986; Huerta et al. 1987). All three primate species show a clear frontoparietal network after seeding the (putative) FEF, with functional connectivity in the anterior cingulate cortex/pre-supplementary motor cortex, posterior cingulate cortex/precuneus, posterior parietal cortex, and prefrontal cortex (46 in marmosets, 9/46 and 46 in macaques, and 46 and 9/46 in humans (Fig. 2-8).

2.5.5 Hubs

Hub regions have been suggested to facilitate the coexistence of integration and segregation of brain function (Sporns et al. 2007) while also serving to minimize wiring and metabolic costs (Bassett and Bullmore 2006). The evaluation of hubs in humans using functional imaging and diffusion tract tracing techniques has converged on regions throughout heteromodal areas of association cortex including the PCC, medial and lateral PFC, lateral parietal cortex, and middle temporal cortex - regions assigned to the default-mode network (Hagmann et al. 2008; Buckner et al. 2009). Hubs in the macaque derived from the CoCoMac database (Stephan et al. 2001) of

post-mortem tract tracing studies (Sporns et al. 2007; Shen et al. 2012) or resting-state analysis (Shen et al. 2012) have suggested a slightly different pattern that encompasses similar PCC/Rsp, lateral parietal, temporal, and lateral PFC regions, but also areas V4, FEF, and MT that appears to reflect a combination of both default and attention network regions (Miranda-Dominguez et al. 2014).

A recent study exploring hub regions in the marmoset applying a local functional connectivity density metric in awake animals (Belcher et al. 2016) implicated visual regions (V1, V2, V6), posterior parietal cortex, posterior and anterior cingulate cortex, as well as subcortical regions (thalamus and striatum). While our measurement of betweenness centrality does suggest high connectedness of some midline cingulate regions, the highest values fell within frontal area 8aD, parietal cortex (PG), and temporal cortex (TPO, TE2, TE3) (Fig. 2-9). The pattern of centrally connected regions tightly overlaps with the frontoparietal network pattern revealed when examining the connectivity patterns of the FEF or SC and suggests that these brain areas, and by extension the network, make up the functional core of the marmoset brain. The location of the distributed frontoparietal network nodes within association cortex and the absence of DMN and control network homologues suggests that this core network may be the evolutionary precursor to the multiple association networks that are present in both macaques and humans, the later possessing an additional level of specialization through the lateralization of connectivity patterns. Over the 40 million years since the divergence of New and Old world primates, adjacent regions may have become functionally segregated and specialized, building on the neural circuitry responsible for the control of eye, body, and attentional processes to facilitate and regulate higher order cognitive processes such as introspection and switching between internal and external awareness. While the spatial abutting of functional nodes across

higher order networks across the cortical sheet (Vincent et al. 2007; Power et al. 2011; Yeo et al. 2011) does support the notion of a common origin from the phylogenetically old frontoparietal system, more evidence is needed including task-based functional imaging studies of marmoset to determine whether cognitive processing requirements that are typically split in macaques and human converge within the modes of this possible multi-modal network of the marmoset.

2.6 Conclusion

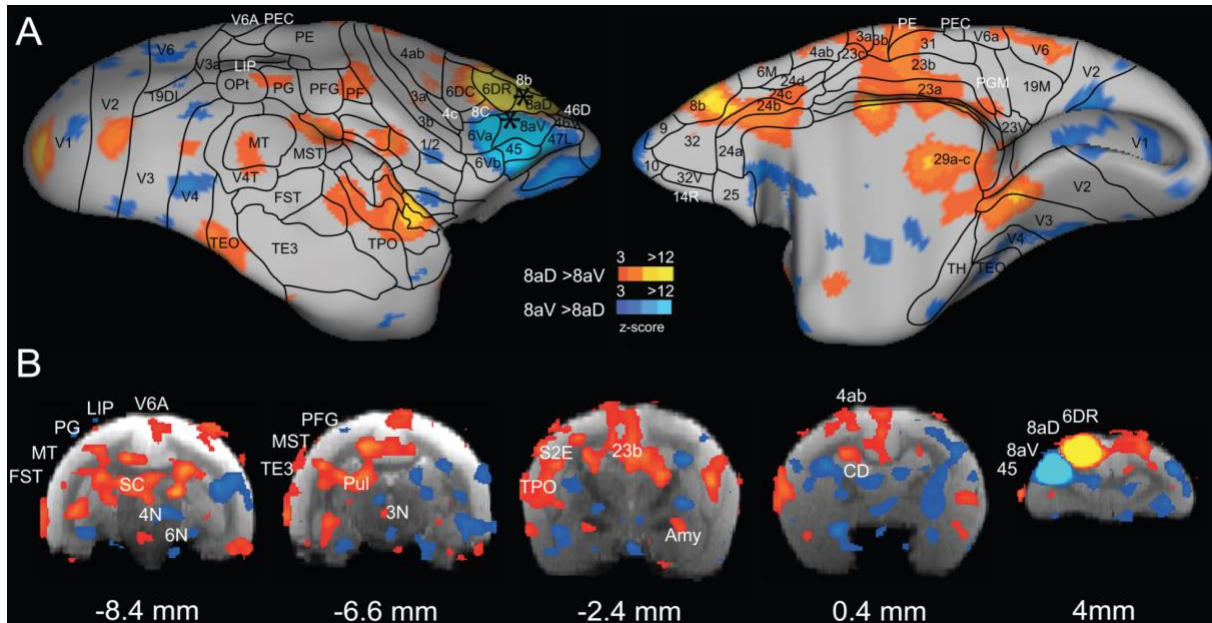
Our findings demonstrate strong similarities in the organization of RSNs between marmosets, macaques, and humans. The results also support the existence of a largely evolutionarily preserved frontoparietal saccade network in Old and New World primates and provide a solid foundation for guiding invasive neurophysiological studies of the saccade system in marmosets that can take advantage of their lissencephalic cortex. Such tangible investigations will not only further validate the functional connectivity findings of the present study, but also contribute to our understanding of this network across primate species.

2.7 Acknowledgements

This research was supported by the Natural Sciences and Engineering Research Council of Canada. RMH is supported by a Canadian Institute of Health Research (CIHR) Banting fellowship and a Brain and Behavior Research Foundation NARSAD/Evelyn Toll Family Young Investigator Grant. We wish to thank Nicole Hague, Ashley Kirley, Alex Li, and

Miranda Bellyou for their outstanding technical support. We are also extremely grateful to Kyle Gilbert for designing and building the marmoset and macaque coils.

2.8 Supplementary Material



Supplementary figure 2-1. Direct comparison of the functional connectivity maps of areas 8aD and 8aV at cortical (A) and subcortical (B) levels. Warm z-score colors refer to regions where area 8aD had significantly higher functional connectivity than 8aV, while cold z-score colors reflect areas where area 8aV had significantly higher functional connectivity than 8aD. The z-statistic maps were corrected for multiple-comparison at a cluster level of $z > 2.3$ with cluster significance $p < 0.05$.

2.9 References

- Amiez C. 2006. Local morphology predicts functional organization of the dorsal premotor region in the human brain. *J. Neurosci.* 26:2724–2731.
- Babapoor-Farrokhran S, Hutchison RM, Gati JS, Menon RS, Everling S. 2013. Functional connectivity patterns of medial and lateral macaque frontal eye fields reveal distinct visuomotor networks. *J. Neurophysiol.* 109:2560–2570.
- Baker JT, Patel GH, Corbetta M, Snyder LH. 2006. Distribution of activity across the monkey cerebral cortical surface, thalamus and midbrain during rapid, visually guided saccades. *Cereb. Cortex* 16:447–459.
- Bakola S, Burman KJ, Rosa MGP. 2015. The cortical motor system of the marmoset monkey (*Callithrix jacchus*). *Neurosci. Res.* 93:72–81.
- Bassett DS, Bullmore E. 2006. Small-world brain networks. *Neuroscientist* 12:512–23.
- Beckmann CF, DeLuca M, Devlin JT, Smith SM. 2005. Investigations into resting-state connectivity using independent component analysis. *Philos. Trans. R. Soc. Lond. B. Biol. Sci.* 360:1001–1013.
- Belcher AM, Yen CC, Stepp H, Gu H, Lu H, Yang Y, Silva AC, Stein EA. 2013. Large-scale brain networks in the awake, truly resting marmoset monkey. *J. Neurosci.* 33:16796–16804.
- Belcher AM, Yen CC-C, Notardonato L, Ross TJ, Volkow ND, Yang Y, Stein EA, Silva AC, Tomasi D. 2016. Functional connectivity hubs and networks in the awake marmoset brain. *Front. Integr. Neurosci.* 10:1–9.
- Blum B, Kulikowski JJ, Carden D, Harwood D. 1982. Eye movements induced by electrical stimulation of the frontal eye fields of marmosets and squirrel monkeys. *Brain. Behav. Evol.* 21:34–41.
- Bruce CJ, Friedman HR, Kraus MS, Stanton GB. 2004. The primate frontal eye field. *Vis. Neurosci.*:1428–1448.
- Bruce CJ, Goldberg ME. 1985. Primate frontal eye fields. I. single neurons discharging before saccades. *J. Neurophysiol.* 53:603–635.
- Buckner RL, Andrews-Hanna JR, Schacter DL. 2008. The brain's default network: anatomy, function, and relevance to disease. *Ann. N. Y. Acad. Sci.* 1124:1–38.
- Buckner RL, Krienen FM, Yeo BTT. 2013. Opportunities and limitations of intrinsic functional connectivity MRI. *Nat. Publ. Gr.* 16:832–837.

- Buckner RL, Sepulcre J, Talukdar T, Krienen FM, Liu H, Hedden T, Andrews-Hanna JR, Sperling RA, Johnson KA. 2009. Cortical hubs revealed by intrinsic functional connectivity: mapping, assessment of stability, and relation to Alzheimer's Disease. *J. Neurosci.* 29:1860–1873.
- Burman KJ, Palmer SM, Gamberini M, Rosa MGP. 2006. Cytoarchitectonic subdivisions of the dorsolateral frontal cortex of the marmoset monkey (*Callithrix jacchus*), and their projections to dorsal visual areas. *J. Comp. Neurol.* 495:149–172.
- Chaplin TA, Yu H, Soares JGM, Gattass R, Rosa MGP. 2013. A Conserved pattern of differential expansion of cortical areas in simian primates. *J. Neurosci.* 33:15120–15125.
- Collins CE, Lyon DC, Kaas JH. 2005. Distribution across cortical areas of neurons projecting to the superior colliculus in new world monkeys. *Anat. Rec. A. Discov. Mol. Cell. Evol. Biol.* 285:619–27.
- Corbetta M, Shulman GL. 2002. Human cortical mechanisms of visual attention during orienting and search. *Philos. Trans. R. Soc. Lond. B. Biol. Sci.* 353:1353–1362.
- Damoiseaux JS, Greicius MD. 2009. Greater than the sum of its parts: a review of studies combining structural connectivity and resting-state functional connectivity. *Brain Struct. Funct.* 213:525–33.
- Demertzi A, Gómez F, Crone JS, Vanhauzenhuysse A, Tshibanda L, Noirhomme Q, Thonnard M, Charland-Verville V, Kirsch M, Laureys S, et al. 2014. Multiple fMRI system-level baseline connectivity is disrupted in patients with consciousness alterations. *Cortex* 52:35–46.
- Elsley JK, Nagy B, Cushing SL, Corneil BD. 2007. Widespread presaccadic recruitment of neck muscles by stimulation of the primate frontal eye fields. *J. Neurophysiol.* 98:1333–1354.
- Van Essen DC, Dierker DL. 2007. Surface-based and probabilistic atlases of primate cerebral cortex. *Neuron* 56:209–225.
- Van Essen DC, Drury H a., Dickson J, Harwell J, Hanlon D, Anderson CH. 2001. An integrated software suite for surface-based analyses of cerebral cortex. *J. Am. Med. Informatics Assoc.* 8:443–459.
- Fogassi L. 2001. Cortical mechanism for the visual guidance of hand grasping movements in the monkey: a reversible inactivation study. *Brain* 124:571–586.
- Ford KA, Gati JS, Menon RS, Everling S. 2009. BOLD fMRI activation for anti-saccades in nonhuman primates. *Neuroimage* 45:470–476.

- Ford KA, Goltz HC, Brown MRG, Everling S. 2005. Neural processes associated with antisaccade task performance investigated with event-related fMRI. *J. Neurophysiol.* 94:429–440.
- Fries W. 1984. Cortical projections to the superior colliculus in the macaque monkey: a retrograde study using horseradish peroxidase. *J. Comp. Neurol.* 230:55–76.
- Gilbert KM, Gati JS, Barker K, Everling S, Menon RS. 2016. Optimized parallel transmit and receive radiofrequency coil for ultrahigh-field MRI of monkeys. *Neuroimage* 125:153–161.
- Grefkes C, Fink GR. 2005. The functional organization of the intraparietal sulcus in humans and monkeys. *J. Anat.* 207:3–17.
- Greicius MD, Supekar K, Menon V, Dougherty RF. 2009. Resting-state functional connectivity reflects structural connectivity in the default mode network. *Cereb. Cortex* 19:72–78.
- Hagmann P, Cammoun L, Gigandet X, Meuli R, Honey CJ, Van Wassenhove J, Sporns O. 2008. Mapping the structural core of human cerebral cortex. *PLoS Biol.* 6:1479–1493.
- Hashikawa T, Nakatomi R, Iriki A. 2015. Current models of the marmoset brain. *Neurosci. Res.* 93:116–127.
- van den Heuvel MP, Hulshoff Pol HE. 2010. Exploring the brain network: a review on resting-state fMRI functional connectivity. *Eur. Neuropsychopharmacol.* 20:519–534.
- Van Den Heuvel MP, Mandl RCW, Kahn RS, Hulshoff Pol HE. 2009. Functionally linked resting-state networks reflect the underlying structural connectivity architecture of the human brain. *Hum. Brain Mapp.* 30:3127–3141.
- van den Heuvel MP, Sporns O. 2013. Network hubs in the human brain. *Trends Cogn. Sci.* 17:683–696.
- Honey, C J, Sporns O, Cammoun L, Gigandet X, Thiran J P, Meuli R HP. 2009. Predicting human resting-state function connectivity from structural connectivity. *Pnas* 106:2035–2040.
- Honey CJ, Kotter R, Breakspear M, Sporns O. 2007. Network structure of cerebral cortex shapes functional connectivity on multiple time scales. *Pnas* 104:10240–10245.
- Huerta MF, Krubitzer L a, Kaas JH. 1986. Frontal eye field as defined by intracortical microstimulation in squirrel monkeys, owl monkeys, and macaque monkeys: I. Subcortical connections. *J. Comp. Neurol.* 253:415–439.
- Huerta MF, Krubitzer LA, Kaas JH. 1987. Frontal eye field as defined by intracortical microstimulation in squirrel monkeys, owl monkeys, and macaque monkeys. II. Cortical connections. *J. Comp. Neurol.* 265:332–361.

- Hung C-C, Yen CC, Ciuchta JL, Papoti D, Bock NA, Leopold DA, Silva AC. 2015. Functional mapping of face-selective regions in the extrastriate visual cortex of the marmoset. *J. Neurosci.* 35:1160–1172.
- Hutchison RM, Everling S. 2012. Monkey in the middle: why non-human primates are needed to bridge the gap in resting-state investigations. *Front. Neuroanat.* 6:1–19.
- Hutchison RM, Gallivan JP, Culham JC, Gati JS, Menon RS, Everling S. 2012. Functional connectivity of the frontal eye fields in humans and macaque monkeys investigated with resting-state fMRI. *J. Neurophysiol.* 107:2463–2474.
- Hutchison RM, Hutchison M, Manning KY, Menon RS, Everling S. 2014. Isoflurane induces dose-dependent alterations in the cortical connectivity profiles and dynamic properties of the brain's functional architecture. *Hum. Brain Mapp.* 35:5754–5775.
- Hutchison RM, Leung LS, Mirsattari SM, Gati JS, Menon RS, Everling S. 2011. Resting-state networks in the macaque at 7T. *Neuroimage* 56:1546–1555.
- Hutchison RM, Mirsattari SM, Jones CK, Gati JS, Leung LS. 2010. Functional networks in the anesthetized rat brain revealed by independent component analysis of resting-state fMRI. *J. Neurophysiol.* 103:3398–3406.
- Hutchison RM, Womelsdorf T, Gati JS, Everling S, Menon RS. 2013. Resting-state networks show dynamic functional connectivity in awake humans and anesthetized macaques. *Hum. Brain Mapp.* 34:2154–2177.
- Hyvärinen A, Oja E. 2000. Independent component analysis: algorithms and applications. *Neural Netw.* 13:411–30.
- Izpisua Belmonte JC, Callaway EM, Churchland P, Caddick SJ, Feng G, Homanics GE, Lee KF, Leopold DA, Miller CT, Mitchell JF, et al. 2015. Brains, genes, and primates. *Neuron* 86:617–631.
- Johnston K, Everling S. 2008. Neurophysiology and neuroanatomy of reflexive and voluntary saccades in non-human primates. *Brain Cogn.* 68:271–283.
- Johnston K, Everling S. 2011. Frontal cortex and flexible control of saccades. Liversedge SP, Gilchrist ID ES, editor. Oxford, UK: Oxford University Press.
- Johnston K, Koval MJ, Lomber SG, Everling S. 2013. Macaque dorsolateral prefrontal cortex does not suppress saccade-related activity in the superior colliculus. *Cereb. Cortex* 24:1373–1388.
- Kagan I, Iyer A, Lindner A, Andersen RA. 2010. Space representation for eye movements is more contralateral in monkeys than in humans. *Proc. Natl. Acad. Sci. U. S. A.* 107:7933–7938.

- Kishi N, Sasaki E, Okano H. 2014. Common marmoset as a new model animal for neuroscience research and genome editing technology. :53–62.
- Koyama M, Hasegawa I, Osada T, Adachi Y, Nakahara K, Miyashita Y. 2004. Functional magnetic resonance imaging of macaque monkeys performing visually guided saccade tasks: comparison of cortical eye fields with humans. *Neuron* 41:795–807.
- Krubitzer LA, Kaas JH. 1990a. Cortical connections of MT in four species of primates: areal, modular, and retinotopic patterns. *Vis. Neurosci.* 5:165–204.
- Krubitzer LA, Kaas JH. 1990b. The organization and connections of somatosensory cortex in marmosets. *J. Neurosci.* 10:952–74.
- Laird AR, Fox PM, Eickhoff SB, Turner JA, Ray KL, McKay DR, Glahn DC, Beckmann CF, Smith SM, Fox PT. 2011. Behavioral interpretations of intrinsic connectivity networks. *J. Cogn. Neurosci.* 23:4022–37.
- Lanzilotto M, Perciavalle V, Lucchetti C. 2013. Auditory and visual systems organization in Brodmann Area 8 for gaze-shift control: where we do not see, we can hear. *Front. Behav. Neurosci.* 7:1–3.
- Leech R, Braga R, Sharp DJ. 2012. Echoes of the brain within the posterior cingulate cortex. *J. Neurosci.* 32:215–222.
- Leichnetz GR, Spencer RF, Hardy SGP, Astruc J. 1981. The prefrontal corticotectal projection in the monkey; an anterograde and retrograde horseradish peroxidase study. *Neuroscience* 6:1023– 1041.
- Liu X, Zhu XH, Zhang Y, Chen W. 2011. Neural origin of spontaneous hemodynamic fluctuations in rats under burst-suppression anesthesia condition. *Cereb. Cortex* 21:374–384.
- Lock TM, Baizer JS, Bender DB. 2003. Distribution of corticotectal cells in macaque. *Exp. Brain Res.* 151:455–470.
- Luna B, Thulborn KR, Strojwas MH, McCurtain BJ, Berman RA, Genovese CR, Sweeney JA. 1998. Dorsal cortical regions subserving visually guided saccades in humans: an fMRI study. *Cereb. Cortex* 8:40–47.
- Mantini D, Corbetta M, Romani GL, Orban G a., Vanduffel W. 2013. Evolutionarily novel functional networks in the human brain? *J. Neurosci.* 33:3259–3275.
- Mantini D, Corbetta M, Romani GL, Orban GA, Vanduffel W. 2012. Data-driven analysis of analogous brain networks in monkeys and humans during natural vision. *Neuroimage* 63:1107– 1118.

- Margulies DS, Vincent JL, Kelly C, Lohmann G, Uddin LQ, Biswal BB, Villringer A, Castellanos FX, Milham MP, Petrides M. 2009. Precuneus shares intrinsic functional architecture in humans and monkeys. *Proc. Natl. Acad. Sci. U. S. A.* 106:20069–20074.
- Masamoto K, Kanno I. 2012. Anesthesia and the quantitative evaluation of neurovascular coupling. *J. Cereb. Blood Flow Metab.* 32:1233–47.
- Menon V. 2011. Large-scale brain networks and psychopathology: a unifying triple network model. *Trends Cogn. Sci.* 15:483–506.
- Miller CT, Freiwald WA, Leopold DA, Mitchell JF, Silva AC, Wang X. 2016. Marmosets: A Neuroscientific Model of Human Social Behavior. *Neuron* 90:219–233.
- Miranda-Dominguez O, Mills BD, Grayson D, Woodall A, Grant KA, Kroenke CD, Fair DA. 2014. Bridging the gap between the human and macaque connectome: a quantitative comparison of global interspecies structure-function relationships and network topology. *J. Neurosci.* 34:5552–5563.
- Mitchell JF, Leopold DA. 2015. The marmoset monkey as a model for visual neuroscience. *Neurosci. Res.* 93:20–46.
- Mitchell JF, Priebe NJ, Miller CT. 2015. Motion dependence of smooth pursuit eye movements in the marmoset. *J. Neurophysiol.* 113:3954–3960.
- Mitchell JF, Reynolds JH, Miller CT. 2014. Active vision in marmosets: a model system for visual neuroscience. *J. Neurosci.* 34:1183–1194.
- Moore T, Armstrong KM. 2003. Selective gating of visual signals by microstimulation of frontal cortex. *Nature* 421:370–373.
- Murata a, Gallese V, Luppino G, Kaseda M, Sakata H. 2000. Selectivity for the shape, size, and orientation of objects for grasping in neurons of monkey parietal area AIP. *J. Neurophysiol.* 83:2580–601.
- Neubert FX, Mars RB, Thomas AG, Sallet J, Rushworth MFS. 2014. Comparison of human ventral frontal cortex areas for cognitive control and language with areas in monkey frontal cortex. *Neuron* 81:700–713.
- Okano H, Hikishima K, Iriki A, Sasaki E. 2012. Seminars in Fetal & Neonatal Medicine The common marmoset as a novel animal model system for biomedical and neuroscience research applications. *Semin. Fetal Neonatal Med.* 17:336–340.
- Orban GA, Van Essen D, Vanduffel W. 2004. Comparative mapping of higher visual areas in monkeys and humans. *Trends Cogn. Sci.* 8:315–324.
- Paxinos G, Huang XF, Toga AW. 2000. The rhesus monkey brain in stereotaxic coordinates. 1st ed. San Diego: Academic Press.

- Paxinos G, Watson C, Petrides M, Rosa M, Tokuno H. 2012. The marmoset brain in stereotaxic coordinates. Oxford, UK: Elsevier.
- Philipp R, Hoffmann K-P. 2014. Arm movements induced by electrical microstimulation in the superior colliculus of the macaque monkey. *J. Neurosci.* 34:3350–63.
- Power JD, Cohen AL, Nelson SM, Wig GS, Barnes KA, Church JA, Vogel AC, Laumann TO, Miezin FM, Schlaggar BL, et al. 2011. Functional network organization of the human brain. *Neuron* 72:665–678.
- Preuss TM. 2007. Evolutionary specializations of primate brain systems. *Primate Orig. Adapt. Evol.*:625–675.
- Raichle ME. 2011. The restless brain. *Psychologist* 22:836–839.
- Raos V. 2006. Functional properties of grasping-related neurons in the ventral premotor area F5 of the macaque monkey. *J. Neurophysiol.* 95:709–729.
- Reser DH, Burman KJ, Yu HH, Chaplin TA, Richardson KE, Worthy KH, Rosa MGP. 2013. Contrasting patterns of cortical input to architectural subdivisions of the area 8 complex: a retrograde tracing study in marmoset monkeys. *Cereb. Cortex* 23:1901–1922.
- Rubinov M, Sporns O. 2010. Complex network measures of brain connectivity: uses and interpretations. *Neuroimage* 52:1059–1069.
- Sakata H, Taira M, Murata A, Mine S. 1995. Neural mechanisms of visual guidance of hand action in the parietal cortex of the monkey. *Cereb. Cortex* 5:429–438.
- Sallet J, Mars RB, Noonan MP, Neubert F-X, Jbabdi S, O'Reilly JX, Filippini N, Thomas AG, Rushworth MF. 2013. The organization of dorsal frontal cortex in humans and macaques. *J. Neurosci.* 33:12255–12274.
- Sasaki E. 2015. Prospects for genetically modified non-human primate models, including the common marmoset. *Neurosci. Res.* 93:110–115.
- Sasaki E, Suemizu H, Shimada A, Hanazawa K, Oiwa R, Kamioka M. 2009. with germline transmission Generation of transgenic non-human primates with germline transmission. *Nature* 459:523–527.
- Schall JD. 1997. Visuomotor areas of the frontal lobe. *Cereb. Cortex* 12:527–638.
- Schall JD. 2004. On the role of frontal eye field in guiding attention and saccades. *Vision Res.* 44:1453–1467.
- Schall JD. 2015. Visuomotor functions in the frontal lobe. In: *Annual Review of Vision Science*. Vol. 1. p. 469–498.

- Schwiedrzik CM, Zarco W, Everling S, Freiwald WA. 2015. Face patch resting state networks link face processing to social cognition. *PLoS Biol.* 13:1–27.
- Shen K, Bezgin G, Hutchison RM, Gati JS, Menon RS, Everling S, McIntosh AR. 2012. Information processing architecture of functionally defined clusters in the macaque cortex. *J. Neurosci.* 32:17465–76.
- Smith SM, Fox PT, Miller KL, Glahn DC, Fox PM, Mackay CE, Filippini N, Watkins KE, Toro R, Laird AR, et al. 2009. Correspondence of the brain's functional architecture during activation and rest. *Proc. Natl. Acad. Sci. U. S. A.* 106:13040–5.
- Sporns O, Honey CJ, Kötter R. 2007. Identification and classification of hubs in brain networks. *PLoS One* 2:1–14.
- Stephan KE, Kamper L, Bozkurt A, Burns GA, Young MP, Kötter R. 2001. Advanced database methodology for the collation of connectivity data on the macaque brain (CoCoMac). *Philos. Trans. R. Soc. London Ser. B, Biol. Sci.* 356:1159–1186.
- Stuphorn V, Hoffmann KP, Miller LE. 1999. Correlation of primate superior colliculus and reticular formation discharge with proximal limb muscle activity. *J. Neurophysiol.* 81:1978–1982.
- T'hart BA, Abbott DH, Nakamura K, Fuchs E. 2012. The marmoset monkey: a multi-purpose preclinical and translational model of human biology and disease. *Drug Discov. Today* 17:1160–1165.
- Tomasi D, Volkow ND. 2011. Association between functional connectivity hubs and brain networks. *Cereb. Cortex* 21:2003–2013.
- Toro R, Fox PT, Paus T. 2008. Functional coactivation map of the human brain. *Cereb. Cortex* 18:2553–2559.
- Vincent JL, Patel GH, Fox MD, Snyder AZ, Baker JT, Van Essen DC, Zempel JM, Snyder LH, Corbetta M, Raichle ME. 2007. Intrinsic functional architecture in the anaesthetized monkey brain. *Nature* 447:83–86.
- Wang K, Van Meer MPA, Van Der Marel K, Van Der Toorn A, Xu L, Liu Y, Viergever MA, Jiang T, Dijkhuizen RM. 2011. Temporal scaling properties and spatial synchronization of spontaneous blood oxygenation level-dependent (BOLD) signal fluctuations in rat sensorimotor network at different levels of isoflurane anesthesia. *NMR Biomed.* 24:61–67. Wickens TD. 2004.
- The general linear model. *Math. Brain Imaging*:1–13.
- Wilson P, Kitchener PD, Snow PJ. 1999. Cutaneous receptive field organization in the ventral posterior nucleus of the thalamus in the common marmoset. *J. Neurophysiol.* 82:1865–1875.

- Wise SP, Boussaoud D, Johnson PB, Caminiti R. 1997. Premotor and parietal cortex: corticocortical connectivity and combinatorial computations. *Annu. Rev. Neurosci.* 20:25–42.
- Wurtz R, Goldberg M. 1989. *The neurobiology of saccadic eye movements*. Amsterdam: Elsevier.
- Wurtz RH. 1968. Visual cortex neurons: response to stimuli during rapid eye movements. *Science.* 162:1148–1150.
- Yeh T, Lee BB, Kremers J, Cowing JA, Hunt DM, Martin PR, Troy JB. 1995. Visual responses in the lateral geniculate nucleus of dichromatic and trichromatic marmosets (*Callithrix jacchus*). *J. Neurosci.* 15:7892–7904.
- Yeo BTT, Krienen FM, Chee MWL, Buckner RL. 2014. NeuroImage estimates of segregation and overlap of functional connectivity networks in the human cerebral cortex. *Neuroimage* 88:212–227.
- Yeo BTT, Krienen FM, Sepulcre J, Sabuncu MR, Lashkari D, Hollinshead M, Roffman JL, Smoller JW, Zollei L, Polimeni JR, et al. 2011. The organization of the human cerebral cortex estimated by intrinsic functional connectivity. *J. Neurophysiol.* 106:1125–1165.

CHAPTER 3

3 Electrical microstimulation evokes saccades in posterior parietal cortex of common marmosets²

3.1 Abstract

The common marmoset (*Callithrix jacchus*) is a small-bodied New World primate increasing in prominence as a model animal for neuroscience research. The lissencephalic cortex of this primate species provides substantial advantages for the application of electrophysiological techniques such as high-density and laminar recordings, which have the capacity to advance our understanding of local and laminar cortical circuits and their roles in cognitive and motor functions. This is particularly the case with respect to the oculomotor system, as critical cortical areas of this network such as the frontal eye fields (FEF) and lateral intraparietal area (LIP) lie deep within sulci in macaques. Studies of cytoarchitecture and connectivity have established putative homologies between cortical oculomotor fields in marmoset and macaque, but physiological investigations of these areas, particularly in awake marmosets, have yet to be carried out. Here we addressed this gap by probing the function of posterior parietal cortex of the common marmoset with electrical microstimulation. We implanted two animals with 32-channel Utah arrays at the location of the putative area LIP and applied microstimulation while they viewed a video display and made untrained eye movements. Similar to previous studies in macaques, stimulation evoked fixed-vector and goal-directed saccades, staircase saccades, and

² A version of Chapter 3 is published as: Electrical microstimulation evokes saccades in posterior parietal cortex of common marmosets, Maryam Ghahremani, Kevin D. Johnston, Liya Ma, Lauren K. Hayrynen, Stefan Everling, *J of Neurophysiol.* 122 (4), 1765-1776.

eyeblinks. These data demonstrate that area LIP of the marmoset plays a role in the regulation of eye movements, provide additional evidence that this area is homologous with that of the macaque, and further establish the marmoset as a valuable model for neurophysiological investigations of oculomotor and cognitive control.

3.2 Introduction

The common marmoset (*Callithrix jacchus*) has recently gained considerable attention as a model for biomedical research in general (Mansfield, 2003) and neuroscience research in particular (Belmonte et al., 2015; Mitchell et al., 2015; Miller et al., 2016; French, 2019). Accordingly, considerable effort has been directed toward mapping the marmoset brain (Okano and Mitra, 2015), and establishing homologies between cortical areas in this species and the macaque (Paxinos et al., 2012; Solomon and Rosa, 2014; Bakola et al., 2015), which to date has been the most commonly used primate model. The marmoset model also holds substantial promise for the study of oculomotor control. Marmosets are highly visual, foveate animals that make both saccadic and smooth pursuit eye movements (Mitchell et al., 2014, 2015), and possess a lissencephalic cortex well-suited to laminar and high-density recordings (Mitchell and Leopold, 2015). In comparison to the macaque model, however, our knowledge of marmoset oculomotor areas is currently at an emergent stage, and it remains to establish the anatomical and physiological correspondences between cortical eye fields in the two species. The cortical and subcortical circuitry controlling saccadic eye movements is perhaps the most thoroughly understood sensorimotor system in the primate brain (Munoz et al., 2000; Schiller and Tehovnik, 2001). In the macaque, these areas include the frontal eye fields (FEF) (Bruce and Goldberg, 1985) and lateral intraparietal area (LIP) (Andersen et al., 1987), both of which

send direct projections to the midbrain superior colliculus (SC) (Selemon and Goldman-Rakic, 1988), an area critical for saccade generation. These cortical areas are buried deep within sulci in this species which highlights the advantages of marmosets with their smooth cortex. Here, we investigated the oculomotor properties of the marmoset posterior parietal cortex. In this species, the picture with respect to the parcellation and homology of the marmoset posterior parietal cortex (PPC) is thus far considerably less clear than is understood in the macaque. Using cyto and myeloarchitecture, Rosa et al. (2009) separated the marmoset PPC into two main subdivisions, PPD (dorsal posterior parietal) and PPv (ventral posterior parietal) (Rosa et al., 2009). Based on the similar pattern of myelination within marmoset PPD and macaque parietal cortex (Blatt et al., 1990), and the presence of large layer V pyramidal neurons, they proposed that this subregion contained the likely homologue of macaque LIP. Subsequent anatomical (Collins et al., 2005; Reser et al., 2013) and resting-state fMRI (Ghahremani et al., 2017) investigations have supported this view as they have shown triangulated connectivity of this area with the putative FEF and SC. As has been previously noted by other authors however (Solomon and Rosa, 2014), the identification of area LIP requires confirmation with electrophysiological techniques in awake animals to establish common functional properties.

Intracortical microstimulation has long been used as a tool to characterize the properties of brain areas by activating neuronal populations (see for review Tehovnik et al., 2006; Clark et al., 2011). Microstimulation of PPC in the awake behaving macaque has been shown to evoke body movements, eye blinks, and both saccadic and smooth eye movements (Fleming and Crosby, 1955; Keating et al., 1983; Shibutani et al., 1984; Kurylo and Skavenski, 1991). Thier & Andersen (1998) subsequently found that the region from which saccades could be evoked was restricted to area LIP within the lateral bank of the intraparietal sulcus, from which they

observed both fixed-vector saccades, for which amplitude and direction were invariant with respect to initial eye position, and convergent or goal-directed saccades which tended to drive the eyes to a fixed goal location in space (Thier and Andersen, 1998). To date, no studies have investigated the oculomotor properties of the cytoarchitectonically defined region LIP in the common marmoset. Here, we applied for the first time electrical microstimulation to the putative area LIP within the PPC of awake behaving marmosets and monitored eye position while the animals were allowed to make unrestricted eye movements. To ensure maximal coverage of the cortical area, we implanted 32 channel Utah arrays in area LIP of two marmosets and applied stimulation trains of varying currents. Similar to previous findings in macaque monkeys, we observed eye blinks as well as both fixed-vector and convergent saccades. These data suggest that area LIP of marmoset plays a similar role to that of the macaque in the modulation of eye movements.

3.3 Methods

3.3.1 Subjects

Two male common marmoset (*Callithrix jacchus*) monkeys weighing 440 g and 451g each, and aged 2.5 and 4 years were subjects in the experiment. All experimental procedures conducted were in accordance with the Canadian Council of Animal Care policy on the care and use of laboratory animals and an ethics protocol approved by the Animal Care Committee of the

University of Western Ontario. The health and welfare of animals was under the close supervision of university veterinarians.

Details of surgical procedures and training methods involved in preparation of the animals for awake behaving experiments have been previously described (Johnston et al., 2018). Briefly, each animal was acclimated to restraint within a custom-designed primate chair and subsequently underwent an aseptic surgical procedure in which a combination recording chamber/head holder was attached to the skull using dental resin and adhesive (Bisco All-Bond, Bisco Dental Products, Richmond, BC, Canada). This allowed restraint of the head within a custom-designed stereotaxic frame during experimental sessions. Following subsequent additional training to acclimate the animals to head restraint, a second aseptic surgery was carried out in which a 32 channel Utah array (Blackrock Microsystems, Salt Lake City, UT, USA) was inserted into the putative area LIP within the posterior parietal cortex (PPC) of each monkey. Electrodes within these arrays were 1mm in length and had an inter-electrode spacing of 400 μm . During this surgery, a microdrill was used to open 4mm burr holes in the skull to allow access to PPC at locations based upon the stereotaxic coordinates of area LIP (1.4 mm anterior, 6 mm lateral) (Paxinos et al., 2012) which corresponds to the location of a posterior parietal region previously shown to have strong resting-state connectivity with the midbrain superior colliculus (SC) (Ghahremani et al., 2017). We additionally confirmed these locations visually by noting the location of a small blood vessel corresponding to the location of a shallow sulcus believed to be homologous to the intraparietal sulcus of other primate species. Arrays were manually inserted such that the width of the array straddled the sulcus and the array length covered as much of the sulcus length as possible. Following array insertion, the array wires and connector were fixed in place within the recording chamber using dental adhesive, and the array

and remaining exposed cortical surface within the burr hole were covered with medical-grade silicone elastomer adhesive (World Precision Instruments, Sarasota, FLA, USA). A screw-hole was drilled into the skull posterior to the location of the implanted array to place the ground screw. The ground wire of the array was then tightly wound around the base of the screw to ensure good electrical connection. Any remaining exposed wire was then covered with additional protective layers of dental adhesive as required. After full curing of the adhesive, a removable protective cap was fixed in place on the recording chamber.

3.3.2 Microstimulation Protocol

Prior to applying microstimulation, we first verified that individual sites in the microelectrode array were within cortex by monitoring for extracellular neural activity using the Open Ephys acquisition board (<http://www.open-ephys.org>) and digital headstages (Intan Technologies, Los Angeles, CA, USA). For both animals, spike activity began about 2 weeks following array implant surgery. Microstimulation pulses were delivered using the Intan RHS2000 Stimulation/Recording Controller system and digital stimulation/recording headstages (Intan Technologies, Los Angeles, CA, USA). Stimulation trains consisted of 0.3ms biphasic current pulses delivered at 300 Hz for a duration of 100-300ms, at current amplitudes varying between 40 and 240 μ A. For those sites at which saccades were evoked, we additionally determined the threshold current, defined as the minimum current at which saccades could be evoked on 50% of stimulation applications. In sessions investigating whether saccades could be evoked at individual array sites, eye movements were uncontrolled and microstimulation trains were triggered manually by the experimenter. In those on which we investigated effects of initial eye position on saccade direction and amplitude, stimulation trains were triggered by behavior

control software based on fixation location and duration criteria (see Eye Movement Recording, below).

3.3.3 Eye Movement Recording

Animals were seated in a primate chair that was integrated with a custom designed stereotaxic frame for head restraint and eye movement recording. The chair/frame system was mounted on a table within a sound-attenuating chamber (Crist Instruments Co., Hagerstown, MD, USA). Their heads were restrained, and a liquid spout placed at their mouth for reward delivery. Rewards consisted of acacia gum and were delivered via infusion pump (Model NE-510, New Era Pump Systems, Inc., Farmingdale, New York, USA). Eye positions were monitored via high-speed (1000 Hz) infrared video oculography which monocularly tracked pupil location (EyeLink 1000, SR Research, Ottawa, ON, Canada), and recorded together with microstimulation parameters using the Intan Simulation/Recording controller. Eye position was calibrated in each session by requiring marmosets to fixate on images of marmoset faces presented at several predetermined locations, in order to receive a liquid reward. All stimuli were presented on a CRT monitor (ViewSonic Optiquest Q115, 76 Hz non-interlaced, 1600 x 1280 resolution) at a viewing distance of 42cm. Stimulus presentation and reward delivery were carried out under computer control using the CORTEX real-time operating system (NIMH, Bethesda, MD, USA).

In the initial series of microstimulation sessions, animals freely viewed video images on the CRT monitor while we manually applied stimulation trains at single array sites and monitored the animals' horizontal and vertical eye positions to determine whether saccades could be evoked at a given site. For those sites at which saccades could be reliably evoked, we

carried out stimulation current series to determine saccade thresholds. Rewards were given manually by the experimenters to maintain the animals' level of alertness throughout the session but were not contingent on any oculomotor behavior. To further investigate effects of initial eye position on saccade directions and amplitudes, in a subsequent series of sessions we revisited many of the sites at which saccades could be evoked and applied stimulation under computer control while the animal's initial eye positions were at each of a set of predetermined locations. In these sessions, animals freely viewed the same video images and stimulation trains were triggered by the CORTEX real-time operating system when their eye positions were maintained within $5 \times 5^\circ$ electronic windows centered on one of a series of predetermined locations for a period of 100 ms. Locations were at an eccentricity of 7 degrees at the upper left, lower left, upper right, and lower right quadrants of the display monitor, or at the monitor center.

3.3.4 Confirming Array Location

Ex vivo MRI for marmoset B and in vivo micro-CT scan for marmoset W were conducted to confirm the positioning of the array with respect to local landmarks and the putative area LIP. As marmoset W was involved in further data experiments, a micro-CT scan was carried out to determine the array location brain of this animal.

3.3.5 Ex vivo MRI scan

Marmoset B was sacrificed at the end of the data acquisition process to prepare the brain for ex vivo MRI scan. The animal was deeply anesthetized with 20 mg/kg of ketamine plus 0.025 mg/kg Medetomidine and 5% isoflurane in 1.4-2% oxygen to reach beyond the surgical plane

(i.e. no response to toe pinching or cornea touching). It was then transcidentally perfused with 200 ml of phosphate buffered saline, followed by 200 ml of 10% buffered formalin. The brain was then extracted and stored in 10% buffered formalin for more than a week prior to performing the ex vivo scan. On the day of the scan, the brain was transferred to another container for imaging and immersed in a fluorine-based lubricant, Christo-lube (Lubrication Technology, Inc), to improve homogeneity and avoid susceptibility artifacts at the boundaries. The ex vivo image was then acquired using a 9.4T, 31 cm horizontal bore magnet (Varian/Agilent) and Bruker BioSpec Avance III console with the software package Paravision-6 (Bruker BioSpin) and a custom-built 15-cm-diameter gradient coil with 400 mT/m maximum gradient strength (xMR, London, Ontario, Canada; Peterson et al., 2018). An ex vivo T2-weighted image was acquired with the following scanning parameters: repetition time (TR) = 5s, echo time (TE) = 45 ms, field of view (FOV) = 40×32 , image size = 160×128 , slice thickness = 0.5 mm.

To identify the location of the previously implanted array, the resulting T2-weighted image was registered to the NIH marmoset brain template (Liu et al., 2018) using the registration packages of the FSL software (fMRI Software Library: <http://www.fmrib.ox.ac.uk>). This registration process inherently involved two steps: the NIH template was based on registration of a brain to the Paxinos et al (2012) brain; then the experimental brains were registered to the NIH template to provide the final image. Upon visual examination of the image, an indentation of comparable size to the array (2.4 mm) was identified on the surface of the cortex within the PPC that represented the array location. The location of this region of interest was interpolated on the cortical surface to create a mask across this indentation. The mask was then projected on to the surface space in CARET toolbox (Van Essen et al., 2001), using a surface-based version of the

NIH volume template that was kindly provided by the authors of the NIH marmoset brain template (Liu et al., 2018). The array mask was then compared to the area LIP as defined by the parcellated regions of the NIH template, that was also projected on CARET surface space.

3.3.6 In vivo micro-CT scan

Marmoset W was imaged on a live-animal micro-CT scanner (eXplore Locus Ultra, GR Healthcare Biosciences, London, ON) to identify the location of the array on the brain. Prior to the scan, the animal was anesthetized with 15mg/kg Ketamine mixed with 0.025mg/kg Medetomidine. It was then placed on the CT bed in supine position with arms along its sides. X-ray tube potential of 120 kV and tube current of 20 mA were used for the scan, with the data acquired at 0.5° angular increment over 360°, resulting in 1000 views. The resulting CT images were then reconstructed into 3D with isotropic voxel size of 0.154 mm. Heart rate and SpO₂ were monitored throughout the session. At the end of the scan, the injectable anesthetic was reversed with an IM injection of 0.025mg/kg Ceptor.

To find the location of the array with respect to the NIH template, the acquired CT image was similarly registered to the NIH marmoset brain atlas (Liu et al., 2018) using the FSL software (fMRI Software Library: <http://www.fmrib.ox.ac.uk>). Similar to the ex vivo MRI data, an ROI mask was created over the traces of the array across the surface of the cortex to represent the location of the array. This mask was projected on the surface space using CARET.

3.3.7 Data Analysis

All eye movement analyses were carried out using custom-written codes in MATLAB software (The Mathworks, Natick, MA). Horizontal and vertical eye traces were low-pass filtered at 30 Hz and horizontal and vertical eye traces were then aligned with the stimulation onset to detect changes in eye movements following the stimulation pulse. We only considered changes in eye position that were greater than 2° and fell within a window of 200ms from the onset of microstimulation. Saccades were detected based on first order derivative, corresponding to the velocity of eye movements. The start of a saccade was defined by the first time point in which the speed of the eye movement reached 30 °/s and the first time point at which the speed went back to zero marked the end point of saccade. All saccades were normalized to the baseline by subtracting the mean of the eye position within a 50ms window before the onset of stimulation. Saccade amplitudes were defined based on the start and endpoints of saccades, as determined by the velocity criteria. The obtained values per trial were then averaged across all saccadic trials for each site of the array. Saccade latency was defined as the time from the onset of microstimulation to the onset of the saccade. The duration of saccades was calculated based on the difference between the time point of the start and end of saccades. The same procedures were employed in those sessions in which we investigated the effect of initial eye position, except that in this case saccades were not normalized to baseline (i.e. pre-saccadic eye position). To quantify the effect of initial eye position on microstimulation-evoked saccades, we applied the linear regression modeling technique proposed by Russo and Bruce (1993). For every site of interest, the size of saccades defined as the difference of saccade offset and onset, was plotted versus all different initial eye positions to produce scatter plots for horizontal and vertical saccade components, separately. A line of regression was fit into each scatter plot, the slope of which represented the effect of initial eye position on elicited saccades. A value that was closer

to zero indicated that the elicited saccades had mostly unchanged trajectories, independent of the initial eye position. This is referred to as fixed-vector saccades. A value close to 1 or -1 implied that the elicited saccades changed trajectory depending on the initial eye position and converged towards a common orbital position irrespective of where the eye started. Such saccade vectors are defined as convergent or goal-directed saccades (Russo and Bruce, 1993).

3.4 Results

3.4.1 Confirming the location of the array

The results of the *ex vivo* MRI for marmoset B and *in vivo* micro-CT scan for marmoset W are demonstrated in Figure 3-1. The Figure on the left displays the location of the array for both marmoset B (red patch) and marmoset W (blue patch) registered on the surface space of the left hemisphere of the marmoset brain using CARET surface registration toolbox, with registration-based estimates of the cytoarchitectonic boundaries overlaid in white. The Figure on the right displays the location of the arrays in more details, by zooming into the area enclosed within the blue box as shown on the left Figure, with all the overlapping and neighboring areas labelled according to the NIH brain parcellation map (Liu et al., 2018). The purple patch in these Figures demonstrates the overlapping area between the arrays from both animals. As can be observed, the array location mostly fell within the boundaries of area LIP, while covering parts of areas MIP and VIP in both animals.

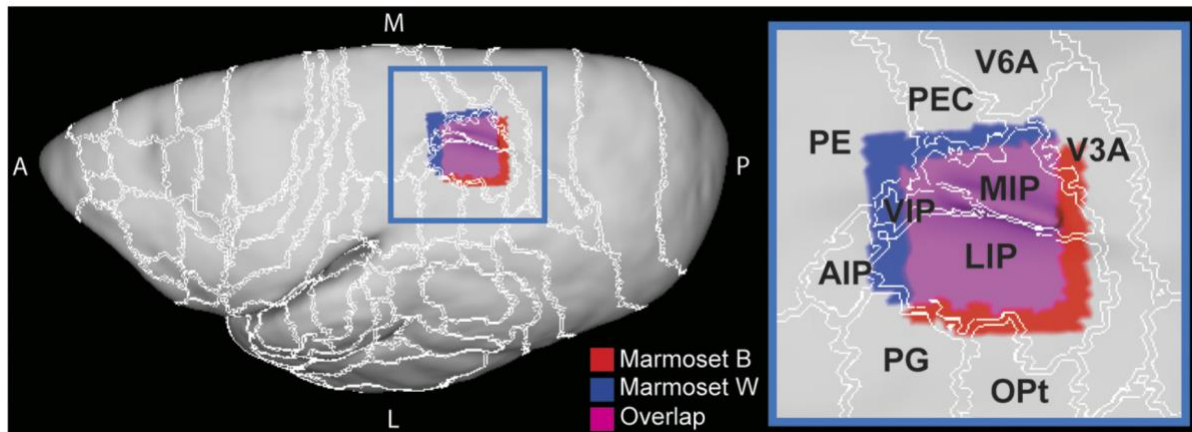


Figure 3-1. Identification of the positioning of the array with ex vivo MRI for *marmoset B* and in vivo micro-CT scan for *marmoset W*. *Left*: the location of the array for both *marmoset B* and *marmoset W* registered on the surface space of the left hemisphere of the marmoset brain, with cortical boundaries overlaid in white. *Right*: the location of the arrays is displayed in more detail by zooming into the area enclosed within the blue box at *left*, with all the overlapping and neighboring areas labeled according to the NIH brain parcellation map (Liu et al. 2018). The purple patches demonstrate the overlapping area between the arrays from both animals. LIP, lateral intraparietal area; MIP, medial intraparietal area; VIP, ventral intraparietal area; AIP, anterior intraparietal area; PE, parietal area PE; PEC, caudal part of parietal area PE; PG, parietal area PG; OPt, occipito-parietal transitional area; V6A, visual area 6A; V3A, visual area 3A; M, medial; L, lateral; P, posterior; A, anterior.

3.4.2 Oculomotor Effects of LIP Microstimulation

In both animals, microstimulation of putative area LIP evoked saccades and eye blinks at multiple sites of the implanted array. For Marmoset B, we observed saccades at 21/32 sites, and eye blinks at 2/32 sites. For Marmoset W, we observed saccades at 23/32 sites, and eye blinks at 9/32 sites. Figure 3-2A depicts this pattern of observations across all sites of the array for both animals. As can be seen from the Figure, saccades were evoked at many array sites, with the exception of the most anterior sites, from which we obtained either blinks (Marmosets W and B), or no response (Marmoset B). At some of these no response sites in Marmoset B we also never recorded any spiking activity in separate sessions (circles with cross sign in Fig. 3-2A). Thus, we cannot exclude the possibility that these electrodes were not in grey matter or that the cortex was damaged at those sites. The dashed line in Fig. 3-2 marks the approximate border line of area MIP based on the location of the shallow intraparietal sulcus (IPS) from the NIH atlas, as depicted in Fig. 3-1A considerable portion of the sites that elicited saccades fell on the medial side of the IPS, overlapping with the location of putative area MIP and most of the sites eliciting eye blinks overlapped with area VIP. For most sites at which microstimulation evoked saccades, we carried out current series to determine saccade thresholds, which we defined as the current at which saccades could be evoked on 50% of trials. Thresholds ranged from 40 to 240 μ A. The topography of saccade thresholds is depicted in Figure 3-2B. We generally noted higher thresholds in Marmoset B, which was most likely attributable to the depth of the electrodes within cortex for this animal. We did not observe a clear pattern of threshold topography in either animal.

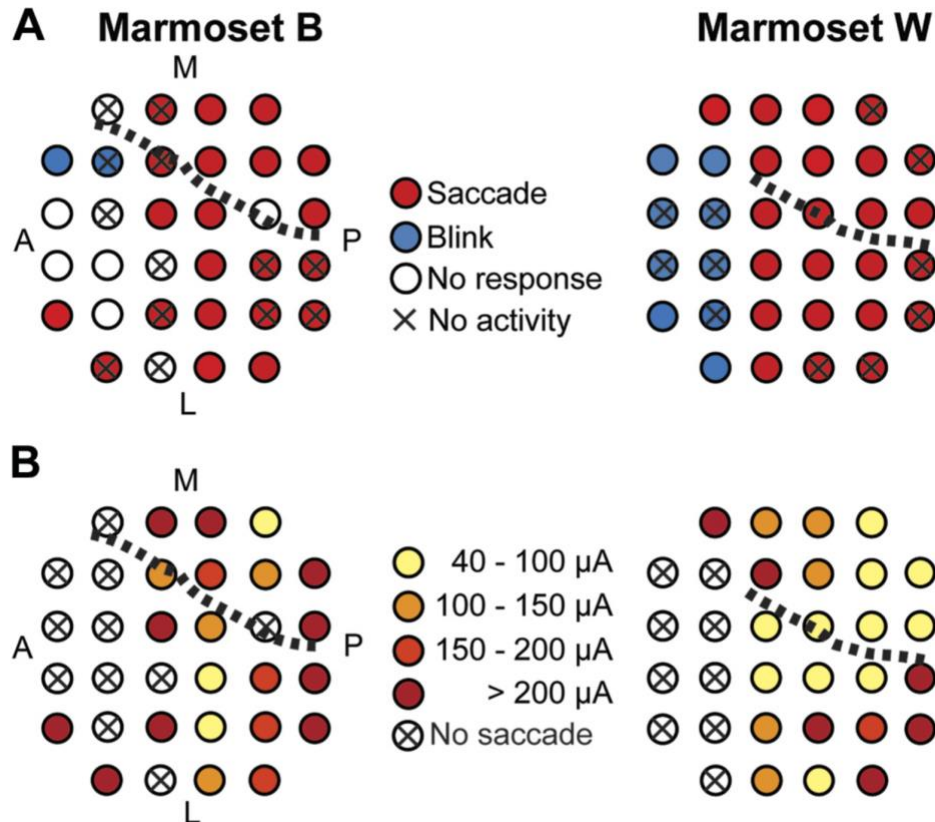


Figure 3-2. *A*: mapping the results of electrical microstimulation on individual sites of the array implanted in left area LIP for *marmosets B* (left) and *W* (right). Each circle corresponds to an electrode channel within the array. Red circles indicate sites that elicited saccades upon microstimulation. Blue circles designate sites that elicited blinks, and open circles indicate sites in which no specific response was observed as a result of microstimulation. Circles with a cross sign refer to sites in which no spike activity was recorded. Dashed line marks the approximate border line of area MIP based on the location of the shallow intraparietal sulcus from the NIH atlas, as depicted in Fig. 1. *B*: mapping the distribution of saccade onset thresholds with gradients of red. Circles with a cross sign refer to sites whose microstimulation did not evoke saccades. Dark red circles are sites with the highest saccade onset thresholds of >200 μA . Light red marks sites with thresholds in the range of 150–200 μA . Orange marks sites with thresholds of 100–150 μA . Light yellow marks sites with the lowest saccade thresholds in the range of 40–100 μA . A, anterior; P, posterior; M, medial; L, lateral.

An example of a microstimulation-evoked saccade is presented in Figure 3-3 from a representative site in Marmoset W (marked in grey within the array grid on the top right of Fig. 3-3). Here, microstimulation currents of varying amplitudes (75, 100, 200 μA) elicited contralateral saccades with an upward vertical component (Fig. 3-3A). In general, we noted that the probability of evoking a saccade at a responsive site increased as a function of stimulation current (Fig. 3-3B left). Moreover, the amplitude of the evoked saccades was nearly constant across varying current amplitudes, especially past the current threshold, and fell in the range of 7.5 to 9 degrees (Fig. 3-3B right).

3.4.3 Saccade Latency and Duration

Saccade onset latency was defined as the time from the onset of the microstimulation pulse to saccade onset. Latency values were averaged across all trials of all saccade-eliciting sites for both animals and plotted as a function of the stimulation current, ranging from 50 to 240 μA (Fig. 3-4A). Onset latencies declined as a function of the stimulation current. Mean latencies ranged from 64 ms at 200-250 μA to 87 ms when currents were in the range of 50-100 μA . Error bars were calculated based on the standard error from the mean.

Saccade duration was defined as the time from saccade onset to the end of saccade. This parameter was similarly averaged across all trials of all saccade-eliciting sites of the array for both monkeys and plotted against stimulation current amplitude. As demonstrated in Figure 3-4B, saccade duration was 20 ms on average and there was no significant difference in saccade duration across different stimulation current amplitudes. Error bars were calculated based on the standard error from the mean.

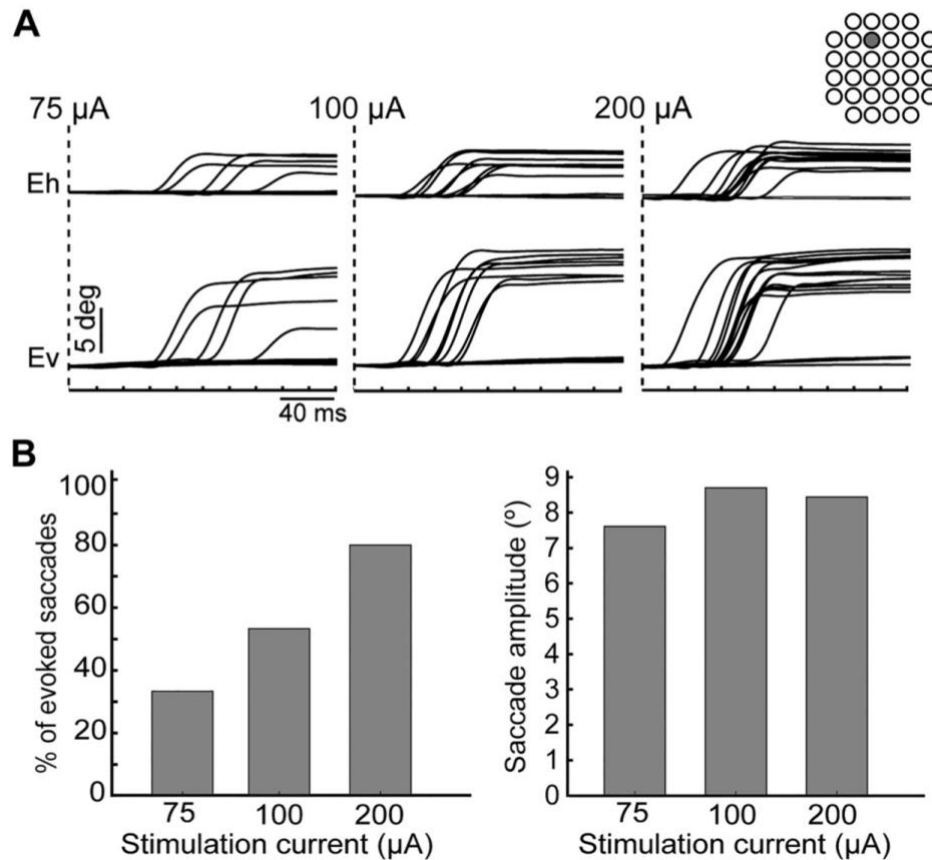


Figure 3-3. A: examples of saccades from a representative site (marked on the array grid at top right) of the array that was microstimulated at 3 different current amplitudes: 75 μA (left), 100 μA (center), and 200 μA (right). For each plot, the dashed line marks the onset of microstimulation, and the x-axis represents time in milliseconds with a calibration bar of 40 ms. The traces at top refer to the horizontal eye movements (Eh), and the traces at bottom refer to the vertical eye movements (Ev). The calibration bar for the amplitude of these traces is given at 5° for all plots. B: bar plots representing % of elicited saccades (left) and their amplitude (right) at each microstimulation current amplitude (x-axis) from the same representative site.

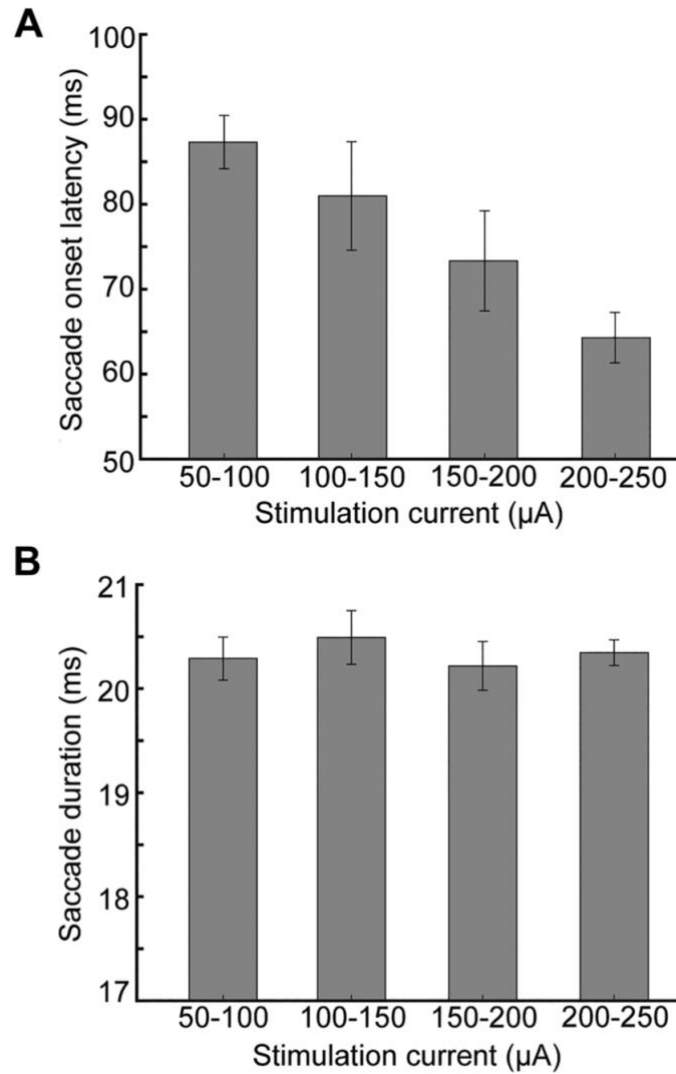


Figure 3-4. A: saccade onset latency from all saccadic sites of the array for both marmosets as a function of the amplitude of the microstimulation current. B: the duration of all saccades for both animals as a function of the amplitude of the microstimulation current. Error bars were calculated based on the standard error from the mean.

3.4.4 Staircase saccades

At some sites within the array, we found trials in which prolonged (300 ms) stimulation was able to evoke staircase saccades, separated by intervals of variable duration (80 to 140 ms). There were four such sites identified in marmoset W that exactly overlapped with sites from which fixed-vector saccades were elicited. There was only one site with staircase saccade identified in marmoset B. Two examples of such staircase saccades in marmoset W are shown in Figure 3-5 from two individual sites that were stimulated at current amplitudes of 150 and 225 μA , respectively. The amplitude of the saccades within the staircase sequence decreased in some cases (Fig. 3-5 left) and was less variable in other cases (Fig. 3-5 right), while the direction of the saccades within the staircase remained the same in most cases observed.

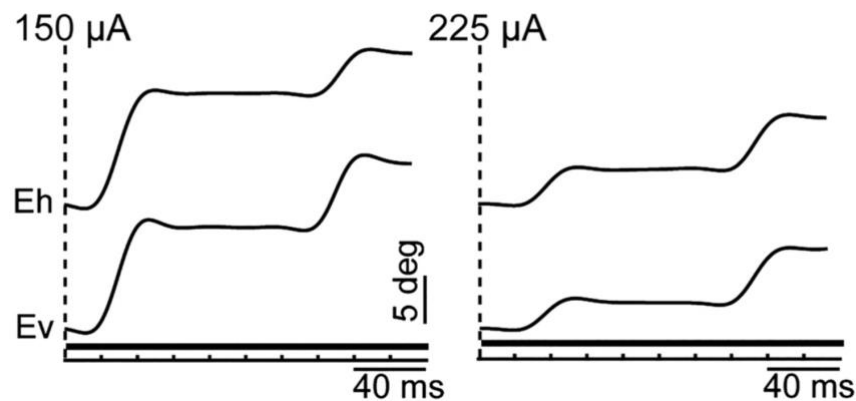


Figure 3-5. Representative examples of staircase saccades from 2 individual sites of the array stimulated at 150 μA (left) and 225 μA (right), respectively. Dashed line refers to the onset of stimulation, and the solid horizontal bar shows the duration of stimulation. x-Axis refers to time with a calibration bar of 40 ms. The traces at top display horizontal eye movements (Eh) and the traces at bottom vertical eye movements (Ev) with an amplitude calibration bar of 5°.

3.4.5 Effects of initial eye position

Based on the previous literature on macaque LIP, it has been reported that one of the factors influencing the direction or amplitude of saccades induced by LIP microstimulation is the initial position of the eye at the time of microstimulation (Shibutani et al., 1984; Kurylo and Skavenski, 1991; Thier & Andersen, 1996; Their & Andersen, 1998). To investigate this in the marmoset PPC, in a subset of sessions and sites we applied microstimulation whenever the animal's eye position fell within one of 7 predefined zones. Next, we applied regression analysis to each of these sites for horizontal and vertical saccade components individually, to examine the impact of initial eye position on the convergence of the elicited saccades. The slope of the regression line was calculated and used as an index to indicate the level of the impact (Russo and Bruce, 1993). Out of the 10 saccadic sites investigated, three sites exhibited saccades for which amplitude and direction were modified such that eye position was driven to converge on a common location, from any starting position across the display. An example of such sites is shown in Figure 3-6A (right) from a representative site of the array in marmoset W with its corresponding regression analysis plots (3-6B, right). The location of these sites is marked within the array grid as displayed on the top right of each plot. The preferred "goal zone" was generally located in the contralateral upper visual field as demonstrated in the representative example of Figure 3-6A (right). The slope of the regression line for horizontal saccade component (K_h , blue) in this site was 0.24 and for vertical component (K_v , red) was 0.65. Most of the remaining sites exhibited fixed-vector saccades that maintained similar amplitudes and directions irrespective of the starting position of the eye at the onset of microstimulation. A representative site that elicited such fixed-vector saccades in marmoset W is shown in Figure 3-6A (left) with its corresponding regression analysis plot (3-6B, left). Here, the slope of the

regression line for horizontal saccade component (K_h , blue) in this site was 0.02 and for vertical component (K_v , red) was -0.03, which were much closer to 0 compared to the representative site for the goal-directed saccade (Fig. 3-6A, right). There were few sites that exhibited saccades that did not exactly belong to either category. However, all evoked saccades (vector or goal-directed) exhibited an upward bias, contralateral to the site of stimulation. Figure 3-7 displays the slopes of the regression line for horizontal (left, K_h) and vertical (right, K_v) saccade components plotted as bar graphs for all the 10 sites in which the effect of initial eye position was investigated. The location of these sites is marked on the array grid as shown on the top right of Figure 3-7. For the three sites that seemed to elicit goal-directed saccades, K_h was in the range of 0.14 to 0.25, which was comparable to other sites (Fig. 3-7A). However, in these three sites K_v varied from 0.5 to 0.6 which was considerably higher than the slope of the vertical saccade components of all the other sites (Fig. 3-7B). In the case of remaining sites, the slope of the regression line for horizontal saccade components (K_h) ranged from 0.01 to 0.2 and for vertical saccade components (K_v) ranged from -0.1 to 0.37.

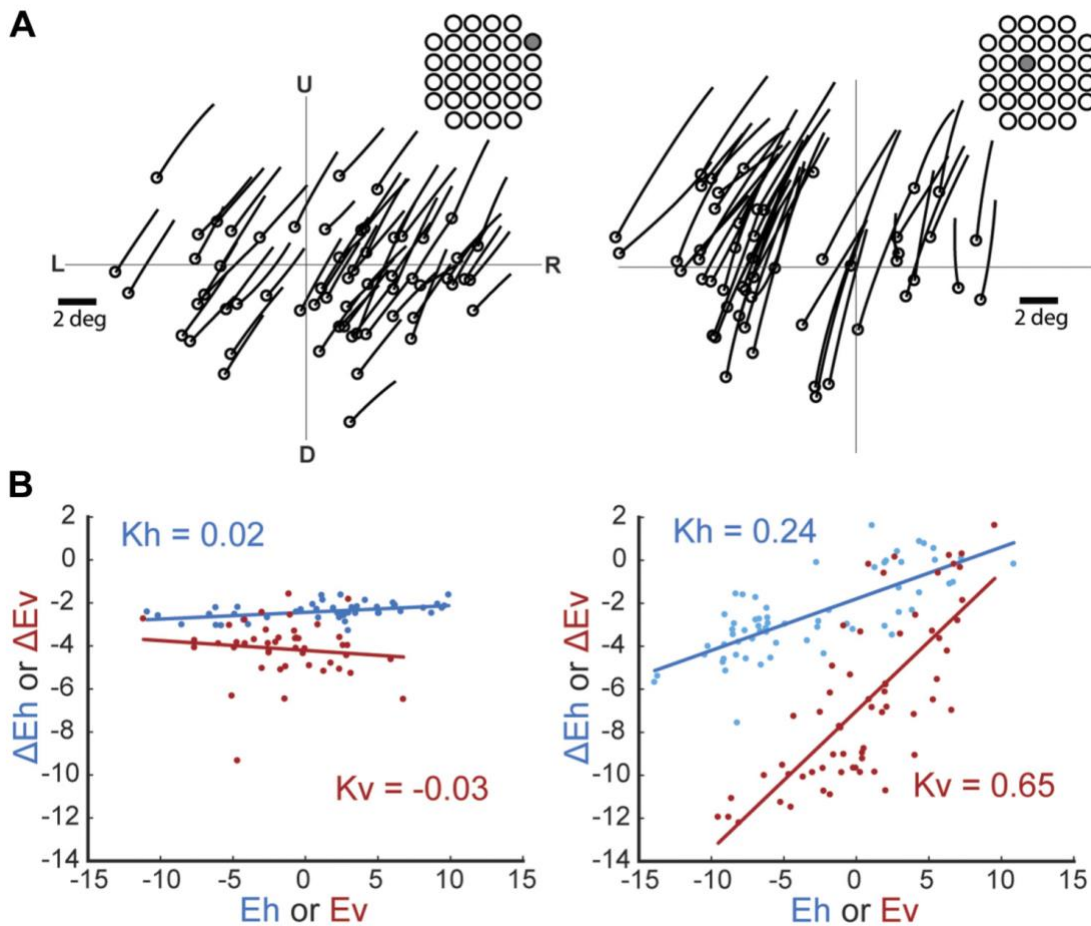


Figure 3-6. Effect of initial eye position on stimulation-evoked saccades. A: examples of the effect of initial eye position on evoked saccades from 2 representative sites of the array as marked on the array grids at top. Left: fixed-vector saccades. Right: goal-directed saccades. Circles indicate the starting position of saccades. Vertical and horizontal axes illustrate the distribution of starting position of saccades across the display. L, left; R, right; U, up; D, down. Saccade amplitude calibration bar is given for 2° . B: corresponding regression plots for the representative sites displayed in A. Each panel displays 2 scatterplots for each of the horizontal (K_h) and vertical (K_v) saccade components, with the y-axis being the size of saccades defined as the difference of saccade offset and onset (ΔE_h , horizontal; ΔE_v , vertical), vs. different initial eye positions (E_h , horizontal; E_v , vertical). Dots represent saccade trials from that representative site, and the line represents the regression line of best fit.

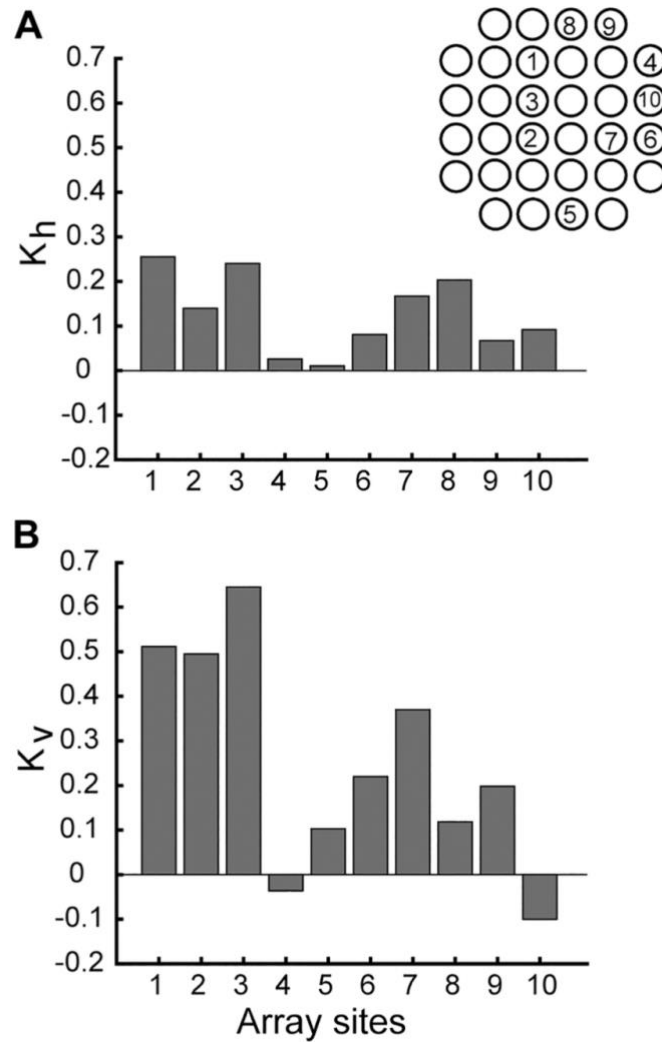


Figure 3-7. The results of regression analysis from all 10 sites of the array in which the effect of initial eye position was examined. These specific sites are marked on the array grid as shown at top right. A: slopes of horizontal saccade components (K_h). B: slopes of vertical saccade components (K_v). x-Axis represents individual sites, and y-axis represents slopes.

3.4.6 Saccade Direction and Amplitude

Saccade direction and amplitude were calculated based on the slope and amplitude of horizontal and vertical eye traces, between the start point and end point of saccades for each saccadic site of the array. These parameters were represented as arrows with their associated direction and amplitude. To determine the general topography of saccade directions and amplitudes, all saccades evoked at each specific site were averaged together, resulting in an average saccade vector for that site. This procedure was repeated for all saccadic sites of the array for each animal and the resulting saccade vectors were mapped onto their associated location within the array (Figure 3-8A). The result demonstrated that the majority of microstimulation-evoked saccades exhibited a prominent upward bias, contralateral to the site of stimulation, in both animals across most sites of the array (Figure 3-8A). There were few sites in Marmoset B that exhibited downward saccades. However, the horizontal component of the evoked saccades was always contralateral to the site of stimulation. In terms of the saccade amplitude, varying amplitudes were observed across array sites in both animals with more centrally located sites having larger amplitudes in general.

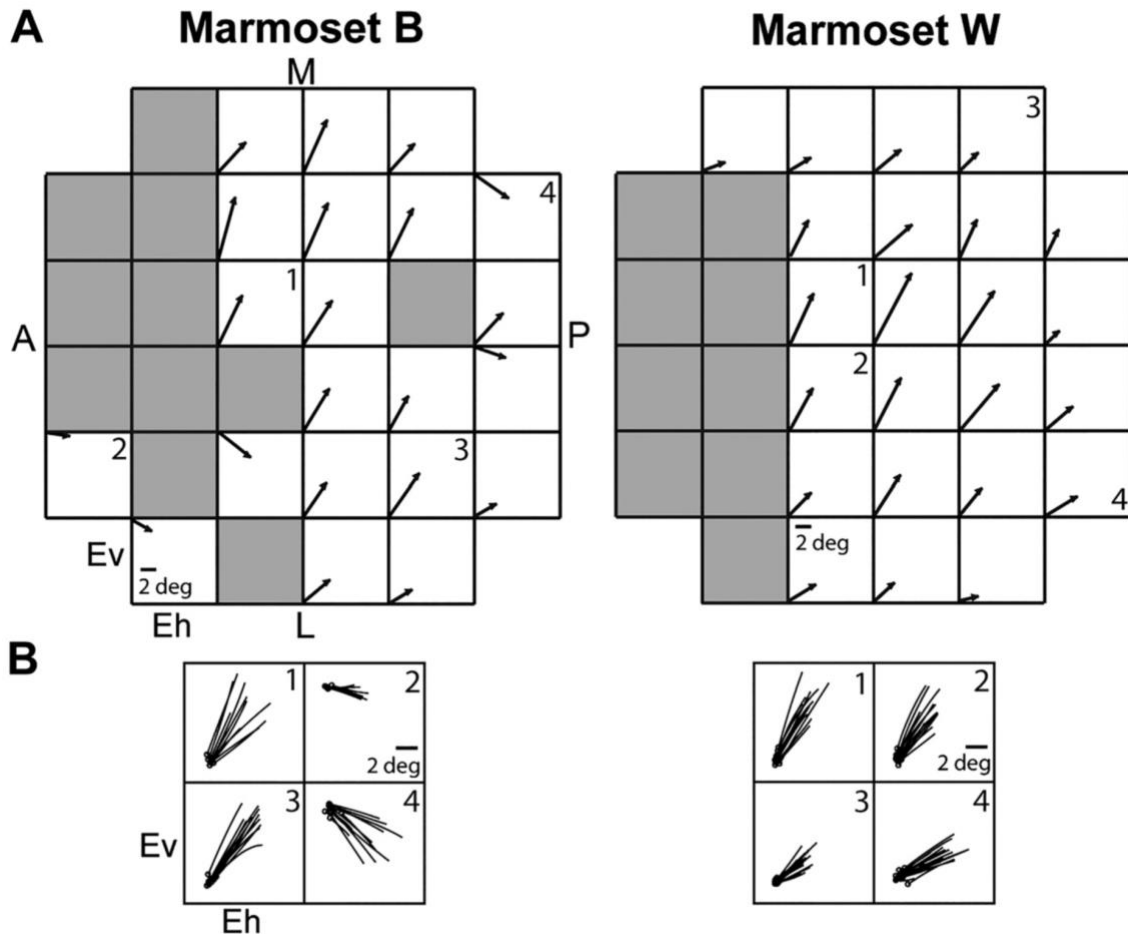


Figure 3-8. A: mapping the average saccade vectors across all saccadic sites of the array for marmosets B (left) and W (right). Each square corresponds to an array electrode. Gray squares refer to sites that did not elicit saccades upon microstimulation. Each arrow represents the average saccade vector evoked across all saccade trials, with its associated amplitude and direction. The amplitude of the saccades is measured by the calibration bar given for 2° . Each arrow is plotted based on vertical and horizontal axes that represent vertical (Ev) and horizontal (Eh) eye movements, respectively. B: examples of individual saccades constituting an average saccade vector from 4 representative array sites per animal, marked by 1, 2, 3, and 4 in A. Saccade amplitude calibration bar is given for 2° . Circles indicate the starting position of saccades. For each site, vertical and horizontal axes refer to vertical (Ev) and horizontal (Eh) eye movements, respectively. A, anterior; P, posterior; M, medial; L, lateral.

3.5 Discussion

Here, we applied intracortical microstimulation to a subregion of the PPC, putative area LIP, to investigate the oculomotor properties of this area in common marmosets. We observed a suite of oculomotor responses including fixed-vector saccades, goal-directed craniocentric saccades, and staircases of saccades. In all cases, saccades were directed toward the hemifield contralateral to the site of stimulation, and predominantly toward the upper visual field. In some cases, we also observed eye blinks. These findings are consistent with previous electrical stimulation studies of PPC in the macaque model (Shibutani et al., 1984; Kurylo and Skavenski, 1991; Thier and Andersen, 1996, 1998), and support the view that LIP of the marmoset has similar oculomotor properties as that of macaque.

A consistent finding of microstimulation experiments in macaque LIP is the presence of two broad classes of saccades: so-called “modified vector” or retinotopic saccades with relatively consistent directions and amplitudes regardless of the initial position of the eyes, and “goal-directed” or craniocentric saccades, the amplitudes and directions of which vary with initial eye position such that they tend to be driven toward a particular goal location (Kurylo and Skavenski, 1991; Thier and Andersen, 1996, 1998). Sites at which these saccade types can be evoked have a topographic distribution, such that vector saccades are evoked at more caudal sites, while goal-directed saccades are confined to a small rostral region in the floor of the of the intraparietal sulcus and extending into the medial bank, termed the “intercalated zone” (Thier and Andersen, 1996, 1998). We similarly observed both classes of saccades following microstimulation of marmoset putative area LIP. We found, however that goal-directed saccades were rare and not restricted to a specific cluster of sites. One possible explanation for the relative lack of goal-directed sites we observed is the limited oculomotor range of the

marmoset. In some cases, the goal-directed saccades evoked from macaque intraparietal sulcus drove the eyes to a goal location beyond the range of ocular motility (Kurylo and Skavenski, 1991; Thier and Andersen, 1996). In marmosets, very few saccades occur beyond about 12 degrees during head-fixed free viewing (Mitchell et al., 2014; Mitchell and Leopold, 2015), which is considerably less than the approximately 30° eccentric range of the macaque (Tomlinson and Bahra, 1986; Heiney and Blazquez, 2011). Marmosets also rely more on movements of the head to shift gaze (Mitchell et al., 2014). It thus seems possible that we failed to observe convergent eye movements due to the fact that we were able to analyze only the initial few degrees of the eye trajectories of gaze shifts converging well outside the oculomotor range, and thus underestimated the number of sites at which goal-directed saccades could be evoked. Alternatively, such sites may simply be more rare and widely distributed in marmoset PPC. Consistent with this idea, we found that eye blinks but not goal-directed saccades could be evoked at the most rostral sites in both animals. In contrast, in macaque eye blinks and goal-directed saccades could both be evoked from the intercalated zone in the rostral portion of area LIP (Thier and Andersen, 1996, 1998). Whether this difference in co-localization of responses represents a real phylogenetic difference in modularity of PPC organization (Krubitzer et al., 1995) between these primate species remains to be definitively determined, though we noted also a continuity of sites from which saccades could be evoked in marmosets, contrasting with the typical “fractured” distribution of sites in macaque LIP, in which sites from which saccades can be evoked are organized in clusters separated by non-responsive bands of cortex (Thier and Andersen, 1996).

In contrast to differences in the distribution of goal-directed saccades, we observed a similar topography of saccade directions in marmoset area LIP to previous findings in macaques

(Thier and Andersen, 1998). The directions of evoked saccades were toward the contralateral hemifield in all cases in both animals, and in the vast majority of cases these saccades had an upward component. A small number of sites with a downward component were observed in marmoset B, either at the most rostral or caudal sites. Amplitudes of evoked saccades varied from 3 to 12 degrees. In neither animal did we observe a clear topographic organization of either of these saccade parameters. In macaque LIP, microstimulation has been shown to evoke contralateral saccades with a strong upward bias and no clear organization with respect to direction or amplitude (Kurylo and Skavenski, 1991; Thier and Andersen, 1996, 1998). One potential explanation for how rarely downward saccades were evoked is that these types of saccades may be encoded in a different area within the marmoset PPC that was not covered by our implanted array. Another possibility is that many of small marmosets' predators like raptors attack from above (Oliveira and Dietz, 2011) and therefore there might be a stronger and faster upper visual field representation in these primates' oculomotor regions. Such over-representation of the upper visual field has been previously reported in rodents (Drager and Hubel, 1976) and more recently in primates (Hafed and Chen, 2016). Hafed and Chen (2016) reported sharper, stronger, and faster upper visual field representation in the SC of macaque monkeys. They hypothesized that SC organization is in tune with environmental constraints on eye movement exploration between the upper and lower visual fields. This was evident by a significant asymmetry observed across the horizontal meridian, such that the SC generated more accurate and lower latency saccades towards the upper visual fields (Hafed and Chen, 2016). Another study characterizing response fields of FEF neurons reported that about 70% of them were upper visual field neurons (Mayo et al., 2015). These findings suggest that the over-

representation of the upper visual field may be common in other areas involved in saccade and visual exploration such as area LIP in primates.

Previous studies investigating the effects of intracortical microstimulation on motor responses in marmosets have reported that the thresholds for evoking movements is greater in this species than macaques (Burman et al., 2008), possibly due to the smaller soma size and hence decreased electrical excitability of pyramidal neurons in marmosets (Nudo et al., 1995). We systematically obtained thresholds at most PPC sites from which we were able to evoke eye movements and found that thresholds varied from 40 to 240 μA , values similar to those observed in previous studies of macaque PPC which in the literature have typically ranged from 25- 200 μA (Shibutani et al., 1984; Kurylo and Skavenski, 1991; Thier and Andersen, 1998). This similarity is perhaps surprising as the Utah arrays we used here did not allow us to optimize the cortical depths at which stimulation was applied by moving individual electrodes. However, the higher current threshold seems to be a characteristic feature of marmoset area LIP compared to other oculomotor frontal areas. In fact, in a recent microstimulation study by Selvanayagam et al (2019) from our group, 1mm-length Utah arrays were implanted in frontal cortical areas of marmosets and microstimulation within the putative area FEF could elicit saccades at current thresholds as low as 12 μA . Thus, although the fixed length of Utah electrode arrays did not allow optimal targeting of layer V output neurons in either study, marmoset area LIP seems to have a higher saccade threshold than marmoset FEF (Selvanayagam et al., 2019). We also observed that the amplitude of evoked saccades did not vary greatly across varying amplitudes of the stimulation current, especially above the threshold current. Similar findings were reported in microstimulation studies of area LIP (Shibutani et al., 1984; Kurylo and Skavenski, 1991), as well as the SC (Schiller and Stryker, 1972), and FEF (Robinson and Fuchs, 1969) in

macaques. We did note however that the latencies of evoked saccades were greater following stimulation of marmoset LIP than most prior studies in macaque. We obtained latencies of 64-87ms, in comparison to the mean latencies of 30 and 50 ms found by Thier & Andersen (1998), and Shibutani et al. (1984), respectively. Whether this represents a true species difference in the role of area LIP in the control of saccades or is simply a reflection of reduced soma and axon sizes in the smaller New World marmoset remains to be determined. Studies investigating the response properties of single LIP neurons during saccades, as well as studies in the marmoset FEF should prove illuminating in this regard. Saccade duration in the present study was around 20 ms which greatly overlaps with the duration of spontaneous saccades previously reported for common marmosets (Mitchell et al., 2014), though it most closely resembles faster spontaneous saccades. Kurylo and Skavenski (1991) obtained similar findings in macaque monkeys, where there was substantial overlap in the duration of spontaneous and electrically induced saccades. They claimed that the larger spread in the duration of spontaneous saccades compared to stimulation-evoked saccades can explain the small differences in duration.

Many previous studies applying microstimulation to macaque PPC have observed evoked movements of not only the eyes, but also the pinnae, face, arms, and shoulders (Fleming and Crosby, 1955; Shibutani et al., 1984; Kurylo and Skavenski, 1991; Thier and Andersen, 1998; Cooke et al., 2003). Although we monitored the animals here for these effects, we did not observe any such movements following stimulation, even at higher current amplitudes. This may be at least partially explained by the size and locations of the implanted microelectrode arrays. Each array was implanted on the basis of resting-state fMRI and the local sulcal landmark such that it was placed roughly straddling the sulcus in mediolateral extent and centred with respect to the sulcus in rostrocaudal extent, in order to cover as much of the

putative area LIP as possible. In marmoset, area LIP extends approximately 3.5 – 4mm rostro-caudally, and 2 mm medio-laterally. The dimensions of our arrays were 2.4×2.4 mm and seemed to be rostrocaudally located predominantly within the borders of area LIP, and mediolaterally overlapping with area MIP on the medial side of the intraparietal sulcus (Fig. 3-1). Thier and Andersen (1998), found that within macaque area LIP itself, movements other than those of the eyes were evoked only in the intercalated zone from which goal-directed saccades could be evoked, at the most rostral extent of LIP. While the medial side of the IPS (area MIP) in macaques have been implicated to specifically hold a representation of hand or reaching movements towards a visual target, there is a small percentage of neurons within macaque MIP that also respond in relation to saccadic eye movements (Snyder et al., 1997, 2000). In the present study, even though the implanted array covered parts of area MIP according to the Paxinos et al. (2012), no movements other than those of the eyes were evoked at the more caudal sites from which fixed-vector saccades were evoked. Since we found that fixed-vector saccades were evoked at the majority of sites in both animals, it seems reasonable to suggest that most of our stimulation sites were restricted to the region specific to fixed-vector eye movements, and simply did not reach cortex from which non-eye movements could be evoked. This observed discrepancy between marmosets and macaques may be due to the variations of borders across individuals and the imprecisions inherent to the registration process. It can also imply that the region designated as the putative area MIP in marmosets according to Paxinos et al. (2012), is actually an extension of area LIP, since it does not seem to serve a different function compared to the LIP. In macaque monkeys, area LIP is the only parietal area with direct projections to the SC (Lynch et al., 1985; Andersen et al., 1990) and there are reciprocal connections between the FEF and the LIP and VIP, but not MIP (Stanton

et al., 1995, 2005). However, previous tracing and functional connectivity studies in marmosets have demonstrated that all three intraparietal areas LIP, VIP and MIP are reciprocally connected with the putative marmoset FEF (Reser et al., 2013; Majka et al., 2016; Ghahremani et al., 2017). Accordingly, corticotectal neurons in marmoset PPC seem to be more distributed compared to the macaque (Collins et al., 2005). Although tracer studies supporting the identity of marmoset area LIP have been based on injections placed in other areas (Rosa et al., 2009) and no study involving direct injections into LIP has been published yet, open access data provided by Majka et al (2016) (marmosetbrain.org) confirm that the putative area LIP in marmosets is indeed mostly connected to visual and frontal oculomotor areas such as the FEF. Therefore, a macaque LIP homologue certainly exists within the marmoset PPC, but its precise boundaries remain unclear, such that the physiological area LIP as defined by Paxinos et al (2012) may be larger than what was originally proposed. On the other hand, we did observe eye blinks at a few stimulation sites in both animals that possibly covered parts of area VIP, consistent with observations in area VIP in macaques, a region from which defensive movements of the arms and face can also be evoked (Cooke et al., 2003). Future work using larger arrays covering a greater extent of PPC or greater cortical sampling by other means would definitely address this discrepancy in findings.

The recent increase in popularity of the marmoset model has been paralleled by anatomical studies aiming to establish homologies between cortical areas of the marmoset and rhesus macaques, which historically have been the most commonly used primate model in neuroscience research (Solomon and Rosa, 2014). In a similar vein, behavioural work has demonstrated that marmosets display many similarities with macaques with respect to their visual and oculomotor behaviour (Mitchell et al., 2014; Johnston et al., 2018, 2019). To date

however, few studies have investigated the properties of cortical areas involved in oculomotor control in awake behaving marmosets, which is a critical step in determining the function of these areas and relating them to macaques and ultimately human brain function. It has been proposed that homology between cortical fields can be established on the basis of three primary criteria: cytoarchitecture, connectivity, and neural response properties (Kaas, 1987; Krubitzer, 1995). With respect to area LIP, corresponding aspects of cytoarchitecture between macaques and marmosets such as dense myelination and the presence of large layer V pyramidal neurons have been established (Bock et al., 2009; Rosa et al., 2009). Similarly, area LIP shares a common pattern of connectivity across species. This area was originally defined in macaques as a subregion within the intraparietal sulcus with extensive interconnections to the FEF and SC (Andersen et al., 1985). Such connectivity has been established in marmoset on the basis of anatomical (Collins et al., 2005; Reser et al., 2013) and resting-state fMRI (Ghahremani et al., 2017). Our data here suggest that the functional properties of LIP in both species are also similar. Although we noted some differences in the proportions and distributions of the two types of microstimulation-evoked saccades in the two species, we found that saccades could be evoked at similar currents, at marginally longer latencies, and with a similar direction bias toward the upper contralateral visual field as previous studies in macaques. Although single neuron recordings in area LIP of marmosets trained to perform oculomotor tasks are needed to definitively establish correspondence in neuronal response properties, taken together, these three existing lines of convergent evidence provide compelling support for the notion that

marmoset LIP is homologous with that of macaque monkeys, and establish further the marmoset as a promising new model for the study of oculomotor and cognitive control.

3.6 Acknowledgements

We thank N. Hague, C. Vander Tuin, W. Froese, and K. Faubert for surgical assistance and care of the experimental animals. This research was supported by the Canadian Institutes of Health Research grant FRN148365 to S.E. and the Canada First Research Excellence Fund to BrainsCAN.

3.7 References

- Andersen R, Bracewell R, Barash S, Gnadt J, Fogassi L (1990) Eye position effects on visual, memory, and saccade-related activity in areas LIP and 7a of macaque. *J Neurosci* 10:1176–1196.
- Andersen RA, Asanuma C, Cowan WM (1985) Callosal and prefrontal associational projecting cell populations in area 7A of the macaque monkey: A study using retrogradely transported fluorescent dyes. *J Comp Neurol* 232:443–455.
- Andersen RA, Essick GK, Siegel RM (1987) Neurons of area 7 activated by both visual stimuli and oculomotor behavior. *Exp Brain Res* 67:316–322.
- Bakola S, Burman KJ, Rosa MG (2015). The cortical motor system of the marmoset monkey (*Callithrix jacchus*). *Neurosci Res* 93: 72– 81.
- Belmonte JCI et al. (2015) Brains, genes, and primates. *Neuron* 86:617–631.
- Blatt GJ, Andersen RA, Stoner GR (1990) Visual receptive field organization and cortico-cortical connections of the lateral intraparietal area (area LIP) in the macaque. *J Comp Neurol* 299:421–445.
- Bock NA, Kocharyan A, Liu J V., Silva AC (2009) Visualizing the entire cortical myelination pattern in marmosets with magnetic resonance imaging. *J Neurosci Methods* 185:15–22.

- Bruce CJ, Goldberg ME (1985) Primate frontal eye fields. I. Single neurons discharging before saccades. *J Neurophysiol* 53:603–635.
- Burman KJ, Palmer SM, Gamberini M, Spitzer MW, Rosa MGP (2008) Anatomical and physiological definition of the motor cortex of the marmoset monkey. *J Comp Neurol* 506:860–876.
- Clark KL, Armstrong KM, Moore T (2011) Probing neural circuitry and function with electrical microstimulation. *Proc R Soc B Biol Sci* 278:1121–1130.
- Collins CE, Lyon DC, Kaas JH (2005). Distribution across cortical areas of neurons projecting to the superior colliculus in new world monkeys. *Anat Rec A Discov Mol Cell Evol Biol* 285A: 619 – 627.
- Cooke DF, Taylor CSR, Moore T, Graziano MSA (2003) Complex movements evoked by microstimulation of the ventral intraparietal area. *Proc Natl Acad Sci* 100:6163–6168.
- Drager UC, Hubel DH (1976) Topography of visual and somatosensory projections to mouse superior colliculus. *J Neurophysiol* 39:91–101.
- Fleming JFR, Crosby EC (1955) The parietal lobe as an additional motor area. The motor effects of electrical stimulation and ablation of cortical areas 5 and 7 in monkeys. *J Comp Neurol* 103:485–512.
- French JA (2019) The marmoset as a model in behavioral neuroscience and psychiatric research. In: *The Common Marmoset in Captivity and Biomedical Research*. Amsterdam: Elsevier.
- Ghahremani M, Hutchison RM, Menon RS, Everling S (2017) Frontoparietal Functional Connectivity in the Common Marmoset. *Cereb Cortex*:1–16.
- Hafed ZM, Chen CY (2016) Sharper, Stronger, Faster Upper Visual Field Representation in Primate Superior Colliculus. *Curr Biol* 26:1647–1658.
- Heiney SA, Blazquez PM (2011) Behavioral responses of trained squirrel and rhesus monkeys during oculomotor tasks. *Exp Brain Res* 212:409–416.
- Johnston K, Ma L, Schaeffer L, Everling S (2019) Alpha Oscillations Modulate Preparatory Activity in Marmoset Area 8Ad. *J Neurosci* 39:1855–1866.
- Johnston KD, Barker K, Schaeffer L, Schaeffer DJ, Everling S (2018) Methods for chair restraint and training of the common marmoset on oculomotor tasks. *J Neurophysiol*. 119: 1636 –1646.
- Kaas J (1987) The organization of neocortex in mammals: implications for theories of brain function. *Annu Rev Psychol* 38:129–151.

- Keating EG, Gooley SG, Pratt SE, Kelsey JE (1983) Removing the superior colliculus silences eye movements normally evoked from stimulation of the parietal and occipital eye fields. *Brain Res* 269:145–148.
- Krubitzer L (1995) The organization of neocortex in mammals: are species differences really so different? *Trends Neurosci* 18:408–417.
- Krubitzer L, Clarey J, Tweedale R, Elston G, Calford M (1995) A redefinition of somatosensory areas in the lateral sulcus of macaque monkeys. *J Neurosci* 15:3821–3839.
- Kurylo DD, Skavenski AA (1991) Eye movements elicited by electrical stimulation of area PG in the monkey. *J Neurophysiol* 65:1243–1253.
- Liu C, Ye FQ, Yen CCC, Newman JD, Glen D, Leopold DA, Silva AC (2018) A digital 3D atlas of the marmoset brain based on multi-modal MRI. *Neuroimage* 169:106–116.
- Lynch JC, Graybiel AM, Lobeck LJ (1985) The differential projection of two cytoarchitectonic subregions of the inferior parietal lobule of macaque upon the deep layers of the superior colliculus. *J Comp Neurol* 235:241–254.
- Majka P, Chaplin TA, Yu HH, Tolpygo A, Mitra PP, Wójcik DK, Rosa MGP (2016) Towards a comprehensive atlas of cortical connections in a primate brain: Mapping tracer injection studies of the common marmoset into a reference digital template. *J Comp Neurol* 524:2161–2181.
- Mansfield K (2003) Marmoset models commonly used in biomedical research. *Comp Med* 53:383–392.
- Mayo JP, DiTomaso AR, Sommer MA, Smith MA (2015) Dynamics of visual receptive fields in the macaque frontal eye field. *J Neurophysiol* 114:3201–3210.
- Miller CT, Freiwald WA, Leopold DA, Mitchell JF, Silva AC, Wang X (2016). Marmosets: a neuroscientific model of human social behavior. *Neuron* 90: 219–233.
- Mitchell JF, Leopold DA (2015). The marmoset monkey as a model for visual neuroscience. *Neurosci Res* 93: 20 – 46.
- Mitchell JF, Priebe NJ, Miller CT (2015). Motion dependence of smooth pursuit eye movements in the marmoset. *J Neurophysiol* 113: 3954 –3960.
- Mitchell JF, Reynolds JH, Miller CT (2014). Active vision in marmosets: a model system for visual neuroscience. *J Neurosci* 34: 1183–1194.
- Munoz DP, Dorris MC, Paré M, Everling S (2000) On your mark, get set: Brainstem circuitry underlying saccadic initiation. *Can J Physiol Pharmacol* 78:934–944.
- Nudo RJ, Sutherland DP, Masterton RB (1995) Variation and evolution of mammalian corticospinal somata with special reference to primates. *J Comp Neurol* 358:181–205.

- Okano H, Mitra P (2015) Brain-mapping projects using the common marmoset. *Neurosci Res* 93:3–7.
- Oliveira LC, Dietz JM (2011) Predation risk and the interspecific association of two brazilian atlantic forest primates in cabruca agroforest. *Am J Primatol* 73:852–860.
- Paxinos G, Watson C, Petrides M, Rosa M, Tokuno H (2012) The marmoset brain in stereotaxic coordinates. Oxford, UK: Elsevier.
- Reser DH, Burman KJ, Yu HH, Chaplin TA, Richardson KE, Worthy KH, Rosa MGP (2013) Contrasting patterns of cortical input to architectural subdivisions of the area 8 complex: a retrograde tracing study in marmoset monkeys. *Cereb Cortex* 23:1901–1922.
- Robinson DA, Fuchs AF (1969) Eye movements evoked by stimulation of frontal eye fields. *J Neurophysiol* 32:637–648.
- Rosa MGP, Palmer SM, Gamberini M, Burman KJ, Yu H-H, Reser DH, Bourne JA, Tweedale R, Galletti C (2009) Connections of the Dorsomedial Visual Area: Pathways for Early Integration of Dorsal and Ventral Streams in Extrastriate Cortex. *J Neurosci* 29:4548–4563.
- Russo GS, Bruce CJ (1993) Effect of eye position within the orbit on electrically elicited saccadic eye movements: a comparison of the macaque monkey's frontal and supplementary eye fields. *J Neurophysiol* 69:800–818.
- Schiller PH, Stryker M (1972) Single-unit recording and stimulation in superior colliculus of the alert rhesus monkey. *J Neurophysiol* 35:915–924.
- Schiller PH, Tehovnik EJ (2001) Look and see: How the brain moves your eyes about. *Prog Brain Res* 134:127–142.
- Selemon L, Goldman-Rakic P (1988) Common cortical and subcortical targets of the dorsolateral prefrontal and posterior parietal cortices in the rhesus monkey: evidence for a distributed neural network subserving spatially guided behavior. *J Neurosci* 8:4049–4068.
- Selvanayagam J, Johnston KD, Schaeffer DJ, Hayrynen LK, Everling S, Mapping M, Mapping M (2019) Functional localization of the frontal eye fields in the common marmoset using microstimulation. *J of Neurosci* 39 (46) 9197-9206.
- Shibutani H, Sakata H, Hyvärinen J (1984) Saccade and blinking evoked by microstimulation of the posterior parietal association cortex of the monkey. *Exp Brain Res* 55:1–8.
- Snyder LH, Batista AP, Andersen RA (1997) Coding of intention in the posterior parietal cortex. *Nature* 286:167–170.
- Snyder LH, Batista AP, Andersen RA (2000) Saccade-Related Activity in the Parietal Reach Region. *J Neurophysiol* 83:1099–1102.

- Solomon SG, Rosa MGP (2014) A simpler primate brain: the visual system of the marmoset monkey. *Front Neural Circuits* 8: 96.
- Stanton GB, Bruce CJ, Goldberg ME (1995) Topography of projections to posterior cortical areas from the macaque frontal eye fields. *J Comp Neurol* 353:291–305.
- Stanton GB, Friedman HR, Dias EC, Bruce CJ (2005) Cortical afferents to the smooth-pursuit region of the macaque monkey's frontal eye field. *Exp Brain Res* 165:179–192.
- Tehovnik EJ, Tolias AS, Sultan F, Slocum WM, Logothetis NK (2006) Direct and Indirect Activation of Cortical Neurons by Electrical Microstimulation. *J Neurophysiol* 96:512–521.
- Thier P, Andersen RA (1996) Electrical microstimulation suggests two different forms of representation of head-centered space in the intraparietal sulcus of rhesus monkeys. *Proc Natl Acad Sci* 93:4962–4967.
- Thier P, Andersen RA (1998) Electrical Microstimulation Distinguishes Distinct Saccade-Related Areas in the Posterior Parietal Cortex. *J Neurophysiol*:1713–1735.
- Tomlinson RD, Bahra PS (1986) Combined eye-head gaze shifts in the primate. I. Metrics. *J Neurophysiol* 56:1542–1557.
- Van Essen DC, Drury H a., Dickson J, Harwell J, Hanlon D, Anderson CH (2001) An integrated software suite for surface-based analyses of cerebral cortex. *J Am Med Informatics Assoc* 8:443–459.

CHAPTER 4

4 Post-stimulus neuronal activity in marmoset frontal and parietal oculomotor areas during the pro/antisaccade task

4.1 Abstract

The antisaccade task is a popular paradigm that can probe executive control via investigating the voluntary control of eye movement. In this task, participants are instructed to suppress a prepotent stimulus-driven response and instead, generate a less potent saccadic response away from the stimulus. Electrophysiological evidence in macaque monkeys has revealed differences in neuronal activity in oculomotor areas between pro- and antisaccades, shedding light on the underlying mechanisms of the voluntary suppression of activity during the antisaccade task. Here, we investigated neuronal activity in two cortical oculomotor areas of the common marmoset monkey (*Callithrix jacchus*), trained to perform the pro/antisaccade task. We inserted linear electrode arrays into areas 8Ad and the lateral intraparietal area (LIP) of two male marmosets and recorded neural activity while they performed an adapted version of the conventional pro/antisaccade task. This version of the task involved alternating blocks of trials that required a saccade either toward a large bright stimulus or the inhibition of this reflexive response in favor of a saccade toward a small, dim stimulus. Area 8aD neurons were significantly more active for correct antisaccades in contralateral directions compared to erroneous antisaccades. We found neurons with significant stimulus-related activity in area LIP and neurons with significant saccade-related activity in both areas 8aD and LIP of common

marmosets. These findings demonstrate a potential role of marmoset frontal and parietal oculomotor areas in saccadic eye movements and support the marmosets as potential alternative primate models for the oculomotor system.

Key words: eye movement; prosaccade, antisaccade, marmoset, frontal cortex, parietal cortex.

4.2 Introduction

Measurements of saccadic eye movements have been known to reflect many aspects of human cognitive processing. In particular, the antisaccade task is a popular saccadic eye movement paradigm to probe executive control via investigating the voluntary control of eye movement. In this task, participants are instructed to generate a saccade away from the target once it appears on the display (Hallett, 1978; Munoz and Everling, 2004). Despite how simple it may seem, studies in both human (Hallett and Adams, 1980) and Old-World macaque monkeys (Amador et al., 1998; Everling and Munoz, 2000) have demonstrated that subjects often make an erroneous saccade towards the salient stimulus instead of looking away from it. The difficulty lies in the competition between the correct voluntary saccade that should be generated away from the stimulus, and an automatic incorrect saccade towards the stimulus. To make a correct response, participants must suppress this stimulus-driven automatic saccade and instead program a saccade to the mirror location away from the stimulus (Munoz and Everling, 2004). This ability to flexibly respond to an event is a hallmark of executive control (Miller and Cohen, 2001) and patients with neuropsychiatric disorders associated with impairments of executive control, often demonstrate poor performance on the antisaccade task (schizophrenia:

(Fukushima et al., 1990); Alzheimer's disease: (Currie et al., 1991); attention- deficit hyperactivity disorder (Munoz et al., 2003)). To have a point of comparison, the antisaccade task is often compared to a prosaccade task in which a correct response is defined as a saccade towards the stimulus (Munoz and Everling, 2004). Compared to prosaccades, antisaccades generally have longer saccade latency since an extra amount of time is taken to inhibit the reflexive saccade and to program a saccade in the mirror location of the stimulus (Munoz and Everling, 2004).

Neuroimaging and electrophysiological studies have shown that there is a network of frontal, parietal and subcortical brain areas that comprise the oculomotor circuitry in nonhuman primates, involving neurons that adjust their firing rate in response to anti- and prosaccade tasks (Everling and Fischer, 1998; Munoz and Everling, 2004). The superior colliculus (SC) is the main core of the saccade network, receiving projections from cortical areas involved in saccade control. The frontal eye field (FEF) is a significant frontal oculomotor area with direct projections to the SC, containing neurons that discharge on both pro- and antisaccade trials in macaques with a lower presaccadic activity on antisaccade trials (Everling and Munoz, 2000). The lateral intraparietal area (LIP) is a prominent parietal oculomotor area that sits at the interface between visual and sensorimotor processing and has been implicated to play a role in planning of saccades (Gnadt and Andersen, 1988; Andersen et al., 1997). LIP neurons in macaque tend to respond to salient visual stimuli and before saccades toward visible visual targets but seem less responsive to remembered visual targets (Gottlieb and Goldberg, 1999). Some studies have suggested that area LIP might play a role in the vector inversion process during an antisaccade trial. Gottlieb & Goldberg (1999) recorded from LIP neurons during pro- and antisaccade trials and reported that most LIP neurons represented the target vector, with

only a few representing the direction of movement (Gottlieb and Goldberg, 1999). Zhang and Barash (2000, 2004) also reported that macaque LIP neurons were firing early when the visual stimulus matched the contralateral receptive field, but these neurons also exhibited a “paradoxical activity” later when the visual target was presented on the ipsilateral receptive field (Zhang and Barash, 2000, 2004). Most of the previous studies on area LIP and antisaccade task have been unclear about the precise role of LIP neurons in cases where the saccade goal and the spatial location of the associated cue do not overlap (antisaccade).

Most of our understanding of the neuronal activity within oculomotor brain areas comes from electrophysiological recordings in the Old-World macaques but, many of these areas are buried within sulci in this species, making them harder to access for higher density or laminar electrophysiological recordings. Here, we took advantage of the lissencephalic cortex of the New World common marmoset monkeys to simultaneously record from single neurons within cortical layers of areas FEF and LIP, using laminar electrodes. Common marmosets (*Callithrix jacchus*) are small-bodied New World primates that are becoming a prominent animal model in neuroscience research. They are highly visual and foveate animals capable of making saccadic eye movements (Mitchel and Leopold, 2015) and neuroimaging studies have shown the existence of a homologue frontoparietal oculomotor network to that of the macaque in these species (Ghahremani et al, 2017). Their lissencephalic cortex provides direct access to prominent cortical oculomotor regions such as the FEF and LIP and our group has recently taken advantage of that to establish a mapping of saccade vectors across these parietal (Ghahremani et al., 2019) and frontal (Selvanayagam et al., 2019) oculomotor regions in marmosets using electrical microsimulation. These findings provided evidence towards identifying these areas in marmosets as potential homologues to FEF and LIP in macaques but

currently, our knowledge of the neuronal activity in marmoset oculomotor regions is limited in comparison to the macaques. A recent study from our group investigated pre-stimulus neural activity in area 8aD and area LIP of marmosets while the monkey performed the antisaccade task and reported prominent task-dependent activity in alpha/gamma bands in area 8aD (Johnston et al., 2019). Here, we investigated post-stimulus activity in the same dataset, involving the stimulus period when the stimulus signal reaches the brain and the perisaccadic period. This is another important epoch during the antisaccade task that can give us insight about visual and saccade-related activity. In both areas 8aD and LIP, we found increased saccade-related activity during the perisaccadic period of the pro/antisaccade task, while area LIP neurons also showed stimulus-related responses during the stimulus period.

4.3 Materials and Methods

4.3.1 Subjects

The present study was conducted on two male common marmoset (*Callithrix jacchus*) monkeys Marmoset M and Marmoset B who were 5 and 4 years old, respectively and weighted 360 g. All experimental procedures were conducted according to the Canadian Council of Animal Care policy on the care and use of laboratory animals and an ethics protocol approved by the Animal Care Committee of the University of Western Ontario. Animals were pair-housed in cages in colony rooms with a 12:12-h light-dark cycle, humidity level of 50-60%, and temperature maintained at 25-27°C. The health and welfare of animals was under the close supervision of university veterinarians. Before surgical preparations, animals were trained to acclimate to

restraint within a custom designed primate chair that was used during recordings on behavioral paradigms.

4.3.2 Surgical procedures

The surgical procedures applied in the present study have been described in a previous study from our group (Johnston et al., 2019). Briefly, each animal underwent an aseptic surgical procedure in which a custom-built oval-shaped recording chamber was attached to the skull, with four conical receptacles that allowed restraint of the head within a custom-designed stereotaxis frame during the recording sessions. The chamber was made to be sufficiently long and wide to allow access to a substantial part of the anteroposterior and mediolateral extent of the marmoset skull for simultaneous recordings in both frontal and parietal areas.

Prior to the surgery, anesthesia was induced with an intramuscular bolus of ketamine (15–20 mg/kg) and propofol (0.3–5 mg/kg in 0.9% saline) was infused at a continuous rate via a catheter placed in one of the lateral tail veins. General anesthesia was additionally applied throughout the surgery with gaseous isoflurane (0.5–3.0%) in oxygen delivered through a custom-designed mask. Temperature was maintained using a circulating water blanket, a forced-air warming blanket, and an intravenous fluid warmer and monitored throughout the surgery, along with heart rate and arterial O₂ saturation. The animal was then placed within a stereotaxic frame (Kopf Instruments model 1248) for precise localization of the chamber and the regions of interest. A midline incision was made along the cranium and the temporalis muscle was retracted to gain access to the underlying periosteum, which was carefully removed along with any tissue. The skull surface was then prepared for application of dental resin and

adhesive. After the application of adhesive cement (BISCO Duo-link, Schaumburg, IL) to the skull surface, the recording chamber was lowered onto the surface with the use of a stereotaxic manipulator to ensure correct location and orientation. Additional adhesive was added as needed to cover the skull surface inside the chamber and ensure an adequate seal around the chamber edges. The animals were then recovered and administered with an intraoperative dose of buprenorphine (0.01–0.02 mg/kg) about 1 h before the end of the surgery to ensure adequate analgesia during postsurgical recovery. A subsequent dose of buprenorphine was administered 12 h after the end of surgery, which was repeated for 2–3 days after surgery, along with administration of meloxicam (0.2 mg/kg) for up to 5 days and an antibiotic regimen, as directed by a University veterinarian.

Upon full recovery, animals were trained on the behavioral paradigm and then underwent a second surgery in which burr holes of 3 mm in diameter were drilled within the head chamber to provide access to areas 8aD (15 mm anterior, 4 mm lateral) and LIP (1.5 mm anterior 6 mm lateral) at their corresponding stereotaxic coordinate in accordance with Paxinos marmoset atlas (Paxinos et al, 2012) and previous fMRI findings of the strong frontoparietal network nodes in marmosets (Ghahremani et al., 2017).

4.3.3 Behavioral task

The behavioral task paradigm was presented under the control of the CORTEX real-time operating system (National Institutes of Mental Health–National Institutes of Health, Bethesda, MD) that monitored both animal behavior and reward delivery. Stimuli were presented on a CRT monitor (ViewSonic Optiquest Q115, 76 Hz noninterlaced, 1,600 × 1,280 resolution) at a

viewing distance of 42 cm. The behavioral task adapted for marmosets in the present study is identical to what was previously explained by Johnston et al (2019). The conventional interleaved prosaccade/antisaccade task that is commonly used for macaques (Munoz and Everling, 2004) was adjusted for marmoset performance level, resorting the task into blocks of prosaccade and antisaccade. Moreover, marmosets had a poor performance making an antisaccade to a blank location in the display monitor. Consequently, we used antisaccade trials that are used in the final stage of macaque antisaccade training protocol, in which a small dim stimulus indicates the target location for an antisaccade (Johnston and Everling, 2011). In this case, the antisaccade task still involves the cognitive aspect of inhibiting the automatic saccade response and generating a voluntary saccade in the opposite direction to a prosaccade.

The task started by fixating on a central instruction cue that was presented on the dark background CRT display (0.01 cd/m²) within an electronic window of 4° x 4°, for a duration of 500-700 ms. This instruction cue was either a cross (1° x 1°, 10 cd/m²) or a filled circle (0.55°, 10 cd/m²) depending on the trial type, prosaccade or antisaccade. For Marmoset M, the cross was the instruction cue for a prosaccade trial while the filled circle signaled an antisaccade trial and the reverse was used for Marmoset B. After this instruction period, two circular stimuli were displayed simultaneously to the left and right of the fixation at an eccentricity of 6.7°, with one being larger and brighter (20 cd/m²) than the other (0.2°, 1.5 cd/ m²). Depending on the shape of the central instruction cue that was presented before, the animals were required to make a single saccade towards the more salient stimulus for prosaccade trials or towards the less salient one for antisaccade trials (Fig. 4-1A). A liquid reward was given upon correct response. Since it was a block task design, the task block was reversed after 10 correctly performed trials. Task performance lasted between 25 to 45 min.

4.3.4 Electrophysiological recording

To record from the regions of interest, animals were first placed within a primate chair that was mounted on a table within a sound-attenuating chamber (Crist Instrument). The chair had an integrated custom-designed stereotaxic frame, with electrode micromanipulators (Kopf Instruments) attached to it at the beginning of each recording session. Animals' head was fixated within the stereotaxic using the conical receptacles on the head chamber and a liquid spout was placed at their mouths for computer-controlled reward delivery (Crist Instrument). Eye positions were monitored throughout the task using high-speed (1000 Hz) infrared video oculography tracking the pupil location (EyeLink 1000, SR Research, Ottawa, ON, Canada). The camera and infrared emitter were mounted directly below the CRT display on which stimuli were presented to the animal. Extracellular recordings were made from area 8aD within the frontal cortex, and area LIP within the posterior parietal cortex, using commercially available silicon-based laminar microelectrodes, each with 16 contacts and 150 μm of interelectrode spacing (ATLAS Neuroengineering). The electrode micromanipulators that were attached to the stereotaxis frame were used to insert the electrodes into the cortex, vertical to the interaural plane at the stereotaxic coordinates of each brain area. Each electrode was slowly advanced into area of interest (8aD or LIP) until most of the contacts were inside the brain (Fig. 4-1B), as reflected by the local field potentials (LFPs) that were monitored at each electrode contact and reported in a previous study from our group on this data (See Fig. 1D of Johnston et al., 2019). In this manner, there was no prescreening of the neurons involved in order to obtain a relatively unbiased sampling of neural activity. We waited for about 20 min after insertion of the electrodes, to allow them to settle before starting the behavioral and neural data acquisition.

Plexon multi-acquisition processor (MAP) system (Plexon, Dallas, TX, USA) for one monkey and the Open Ephys acquisition board (<http://www.openephys.org>) and digital head stages (INTAN, Los Angeles, CA) for the other were used to amplify, filter and store neural spiking activity data that were then converted offline to Neuroexplorer (nex) files. Plexon offline sorter (Plexon, Dallas, Texas) was used to isolate single units by applying principal component analysis (PCA) in 2D and 3D. We also sorted the occurrence of behavioral events which included start of a trial, onset of fixation, stimulus presentation, reward delivery, and performance along with the horizontal and vertical eye positions.

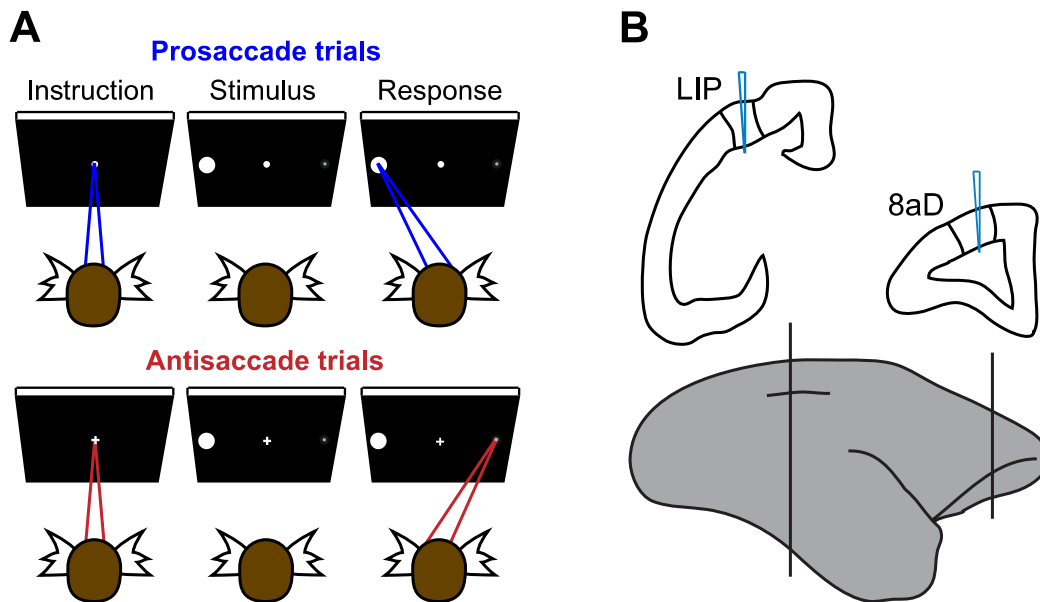


Figure 4-1. Task and the location of recording electrodes. (A) Blocked prosaccade and antisaccade task adapted for marmosets. Animals were presented with a central instruction cue (top: dot for Pro, bottom: cross for Anti) and had to generate a saccade toward a highly salient (top, Pro) or a small dim stimulus (bottom, Anti) to receive reward. (B) Recording locations. Top: coronal sections of parietal and frontal cortices depicting locations of electrode penetrations with respect to cytoarchitecturally defined regions of marmoset cortex. Bottom: lateral view of marmoset brain with parietal and frontal sections marked. *This figure was modified from Johnston et al (2019), J of Neurosci. 39(10):1855–1866.*

4.3.5 Data analysis

The acquire data were analyzed using custom MATLAB codes (The MathWorks) and the fieldtrip toolbox (<http://www.ru.nl/fcdonders/fieldtrip/>). The previously published work on this data analyzed neuronal activity in the preparatory period from 500 ms to 0 s before peripheral stimulus onset (Johnston et al., 2019). In the present study we focused all of our analysis on neuronal activity occurring after the peripheral stimulus onset until the end of the perisaccadic epoch.

4.3.6 Behavioral analysis

Horizontal and vertical eye traces were low-pass filtered at 30 Hz. we then filtered out blinks and corrected all saccadic reaction times (SRTs) across all trials and all sessions for both animals based on a velocity threshold of 30°/s for eye movements. Anticipatory saccades, identified as responses initiated before the visual target was processed, were excluded by setting the lower bound of the saccade window to 70 ms. The upper bound was set to 600 ms to exclude any behaviorally irrelevant saccade occurrences. To observe differences of SRT distribution between correct/error pro and correct/error antisaccade trials, we included both correctly and incorrectly performed trials for each trial type and made a histogram of their distribution for each animal. Two-sample t test was applied to identify statistically significant differences.

4.3.7 Neuronal classification analysis

For the analyses of neuronal activities, we focused on two behavioral epochs: stimulus period and perisaccadic period. The stimulus period was defined from the time that the visual stimulus signal reached neurons in the cortical area of interest, until 80 ms after. Based on the observation of stimulus related activity across all neurons, it appeared that it took about 35 ms for the visual stimulus to reach both areas 8aD and LIP in marmosets. We therefore defined the stimulus period to be from 30 to 80 ms after the stimulus onset. A previous study by Ma et al (2019) from our group, reported similar latency for visual target to reach area LIP (Ma et al., 2020). The perisaccadic period was defined as -70 to 100 ms around the saccade onset, covering the period of saccade preparatory activity just prior to saccade onset. Two-way analysis of variance (ANOVA) was used on each behavioral epoch to characterize the neuronal activity using combinations of stimulus location, saccade direction and task type as factors. ANOVA results yielded main effects per factor as well as interaction effects for each pair. Based on the results of the ANOVA analysis with significance at $p < 0.05$, neurons were classified into the following types: stimulus-related, saccade-related, task-related neurons, and visuomotor neurons. Stimulus-related neurons demonstrated a significant main effect ($p < 0.05$) of stimulus location at the stimulus period. Saccade-related neurons showed a significant main effect ($p < 0.05$) for saccade direction at the perisaccadic period. Visuomotor neurons exhibited both stimulus-related and saccade-related activities and thus, showed significant interaction effect ($p < 0.05$) for both stimulus location at the stimulus period and the saccade direction at the perisaccadic period. Task-related neurons demonstrated differences in activity for pro- versus antisaccade trials.

We also looked into the entire population of cells in areas 8aD and LIP with at least 5 correct trials per condition within the perisaccadic period, irrespective of any statistical significance of their perisaccadic activity, to have an idea of general preferences in terms of saccade direction and correct versus error antisaccades. To analyze population preferences in each brain area for contralateral versus ipsilateral saccade directions in pro- and antisaccade trials, we averaged each neuron's activity across all contralateral and all ipsilateral trials for each of pro- and antisaccade trials and used the obtained values as coordinates in a scatterplot of ipsi versus contra for all neurons. Similarly, to examine whether the neuronal population in each brain area of interest had general preference for correct or error antisaccades, we averaged each neuron's activity across all correct and all erroneous antisaccade trials and used these values as coordinates in a scatterplot of correct versus error for all neurons. In each scatterplot, a diagonal midline defined the boundary of differences in preference. Two-sample t test was applied for all scatterplots to identify any statistically significant differences.

4.3.8 Spike Density Function

To create line plots of single neuron or group averaged activity, we evaluated the relationship between neural activity and stimulus onset and saccade onset using continuous spike density functions. Each neuronal spike was convolved with an asymmetric function that resembled a postsynaptic potential (Hanes and Schall, 1995; Thompson et al., 1996), forming an activation waveform. This function is advantageous over the standard Gaussian functions (Richmond and Optican, 1987) since it accounts for the fact that spikes exert an effect forward, but not backward in time.

4.4 Results

4.4.1 Saccade behavior

Neural activity was recorded from areas LIP and 8aD of two trained common marmoset monkeys (Fig. 4-1B) on the block-design pro/antisaccade task (Fig. 4-1A), within 16 recording sessions for marmoset M and 13 sessions for marmoset B. Correct performance on prosaccade trials required the animal to make a saccade towards the larger more salient peripheral stimulus, while correct performance on antisaccade trials required a saccade away from the more salient peripheral stimulus (towards the dimmer smaller peripheral stimulus). Saccade reaction times (SRTs) were corrected across all sessions and all trials for both animals based on a velocity threshold criterion of 30 deg/s. Figure 4-2A demonstrates the distribution of SRTs for correct (blue) and error (red) prosaccade (left) and correct (blue) and error (red) antisaccade (right) trials averaged across both animals. Similar to what Johnston et al (2019) reported, there was a significantly higher percentage of error on antisaccade trials (1359/2567; 53%) than prosaccade trials (902/2132; 42%) for both marmosets (Chi-square test: $p = 3.78 \times 10^{-13}$). Reaction times were significantly shorter for prosaccades (193.64 (mean) \pm 101.97 (SD) ms) than antisaccades (216.42 \pm 100.97 ms) based on two-sample t-test with $p = 3.31 \times 10^{-8}$. In prosaccade trials, error trials (239.12 \pm 112.02) had longer SRTs than correct trials ($p = 4.98 \times 10^{-12}$), whereas in antisaccade trials, SRT was shorter for error trials (190.38 \pm 97.76) compared to correct ones ($p = 4.03 \times 10^{-11}$) (Johnston et al., 2019). These findings go in line with previous literature (Everling and Fischer, 1998; Everling et al., 1999) and indicate the shared difficulty of performing the antisaccade task across marmosets, macaques and humans. Prosaccade is a relatively easier task to learn, since a correct response is defined as the reflexive

saccade towards the more salient stimulus (bigger brighter dot), resulting in shorter SRT and lower percentage of error compared to antisaccade blocks. Figure 4-2B (left) shows an example of representative correct prosaccades performed by marmosets in the prosaccade block of the task. The first panel is an example of the correct saccade towards stimulus on the left, demonstrated by the rapid downward movement of the horizontal eye trace, while the second panel is a rightward saccade towards stimulus on the right as shown by the rapid upward movement of the eye trace. Antisaccade task is more prone to errors since correct performance requires suppressing the reflexive saccade towards the salient peripheral stimulus. Figure 4-2B (right) shows examples of incorrect antisaccades performed by marmosets during the antisaccade block of the task. First panel demonstrates an incorrect saccade towards the left where the stimulus was presented, followed by a corrective saccade towards the right, away from the stimulus. Second panel is an incorrect antisaccade towards the right when the stimulus was presented in the right, followed by a corrective saccade away from the stimulus (towards the left). These corrective subsequent saccades were observed in a proportion of antisaccade trials with a latency of about 200- 250 ms from the onset of the initial incorrect saccade. Figure 4-2C illustrates the percent accuracy in animals' performance in prosaccade (left) and antisaccade (right) blocks across three time periods within a block: beginning, middle and end. The beginning period started from the first time point of a block (pro or anti) until the end of the first one-third of time into the block. The middle period started just after the first one-third, until the end of the second one-third of time within the block. Similarly, the end period started just after the second one-third of the time within the block until the end of the block. The resulting accuracies within each time period of a certain block (pro or anti) were averaged across all trials within that block for both animals. As demonstrated by the bar plots (Fig. 4-2C),

accuracy was generally higher in prosaccade blocks (78%) compared to antisaccade (65%) blocks when averaged across the entire time within a block. We further divided the time spent within a block into three periods: the beginning period (first one-third of time within the block), the middle period (second one-third of time within the block), and the end period (last one-third of time spent within a block). For both prosaccade blocks and antisaccade blocks, the accuracy was the lowest within the beginning period (73% for prosaccade trials, 59% for antisaccade trials) and gradually increased with the highest accuracy within the end period (82% for prosaccade trials, 70% for antisaccade trials). The beginning period within a block can also be thought of as the transition period from one task block to the other (pro/anti), since the animal has just started a new block type based on the instruction cue and is in the process of transitioning into it as the block begins. This explains the observation of the lowest accuracy percentages that occurs in the beginning period for both pro and antisaccade blocks. The end period on the other hand, is when the animal has done enough trials within a block to be more familiar with the rule and be able to produce higher percentage of correct responses, as reflected by the highest accuracy percentages in the end period for both pro and antisaccade blocks (Fig. 4-2C). The percent accuracy within each individual time period (beginning, middle, end) was higher in prosaccade blocks compared to antisaccade blocks and even in the end period, the percent accuracy in antisaccade blocks (70%) still remained lower than that of prosaccade blocks (82%). However, the increasing trend in percent accuracy as the animal continued within a block in both pro and antisaccade trial types demonstrates the ability of the animal to understand the task demands and improve his performance accordingly.

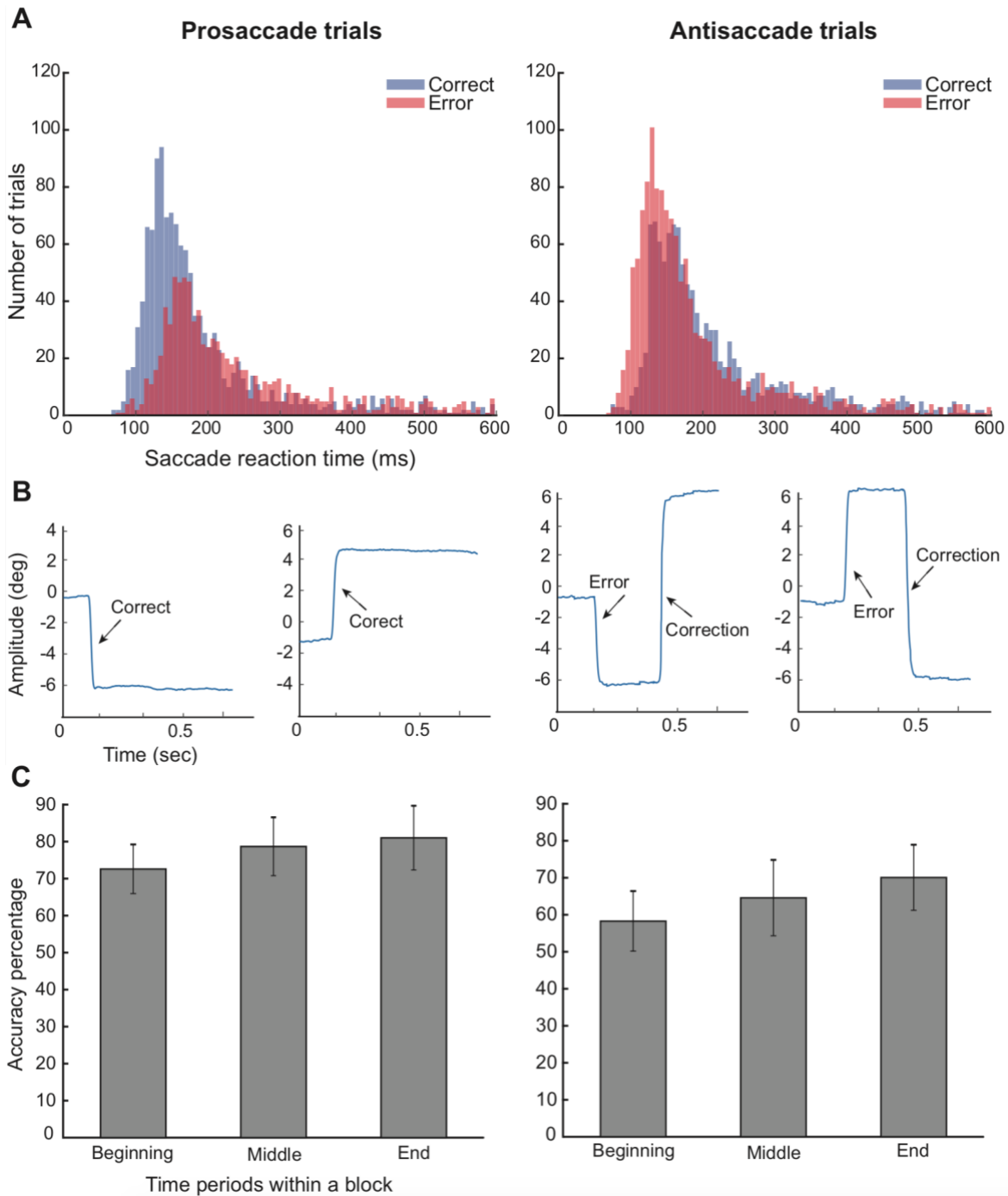


Figure 4-2. (A) Distribution of saccadic reaction times for correct (blue bars) and error (red bars) responses on prosaccade (left) and antisaccade (right) trials. (B) Examples of saccadic eye movement traces for prosaccades (left) and antisaccades (right). (C) Bar plots of the percent accuracy in prosaccade (left) and antisaccade (right) blocks, across three time periods within a block: the beginning, the middle and the end of the block. Error bars were calculated based on the standard error from the mean.

4.4.2 Single unit activity

In total, we recorded from 302 neurons across all sessions in both recording sites, area LIP and 8aD, with 149 neurons in area 8aD and 153 neurons in LIP. In this study we were interested in neuronal activity in marmoset areas LIP and 8aD during two behavioral epochs after the peripheral stimulus onset on the pro/antisaccade task: stimulus period and perisaccadic period. The stimulus period was defined from 30 to 80 ms after the onset of peripheral stimulus presentation. In line with previous study from our group (Ma et al., 2020), our findings indicated that 35 ms is about how long it took for the visual signal to reach marmoset cortical areas. The perisaccadic period was defined from -70 to 100 ms around saccade onset. Two-way ANOVA was applied on each epoch to characterize the neuronal activity using combinations of stimulus location, saccade direction and task type as factors.

The dataset from correct pro- and antisaccade trials was contrasted based on the direction of saccades: contralateral versus ipsilateral, defined with respect to the brain hemisphere we were recording from. This resulted in four conditions: Pro ipsi (ipsilateral prosaccades) with the salient stimulus presented at the ipsilateral location, Pro contra (contralateral prosaccades) with the salient stimulus at the contralateral location, Anti ipsi (ipsilateral antisaccades) with the salient stimulus at the contralateral location, Anti contra (contralateral antisaccades) with the salient stimulus at the ipsilateral location. For each brain area, neurons with significant activity during the stimulus and the perisaccadic period were detected based on the ANOVA and their spike activity was examined on a cell by cell basis to identify prominent patterns of activity in response to the stimulus location, saccade direction, or task type. Neuronal activity was also averaged together to plot average firing rate of all significant neurons across the four trial conditions, Pro ipsi, Pro contra, Anti ipsi, Anti contra. To observe activity after stimulus onset

and around saccade onset, we aligned the activity of significant neurons based on both stimulus onset to visualize stimulus-related activity (Stim aligned) and on saccade onset to demonstrate saccade related activity (Sacc aligned).

ANOVAs yielded significant main effects per factor and interaction effects with significance at $p < 0.05$. No significant effect of task was identified in either area LIP or 8aD in either period. Main classes of neurons identified from the ANOVA analysis were stimulus-related or visual neurons, saccade-related or motor neurons, and visuomotor neurons who responded around both stimulus onset and saccade onset.

4.4.2.1 Neuronal activity in area LIP

No significant task-related activity was detected in area LIP neurons in either stimulus or perisaccadic period. However, the ANOVA test applied on the stimulus period identified a total of 20 neurons in area LIP (13 %) with significant main effect for stimulus location ($p < 0.05$). The stimulus-related activity started around 35-40 ms after the stimulus onset (marked by the dotted line), reaching a peak at about 70 ms after stimulus onset. Neuronal activity from two representative LIP neurons is shown in Fig. 4-3A (left panel). These neurons exhibited increased firing rates for two trial conditions: contralateral prosaccades (Pro contra in red) and ipsilateral antisaccades (Anti ipsi in cyan), with the highest peak of activity for the latter. Since ipsi and contra refer to the direction of the saccade, what is common between a contralateral prosaccade (Pro contra) and ipsilateral antisaccade (Anti ipsi) in terms of the stimulus is that in both conditions, the salient stimulus was presented at the contralateral location. Thus, the identified LIP neurons with significant stimulus-related activity preferred contralateral stimulus

locations. The plot of the averaged firing rates across all the 20 LIP neurons with significant stimulus-related activity demonstrated similar findings (Fig. 4-3B (left panel)). Based on the ANOVA results, these neurons had main effect for stimulus location and no effect for saccade direction during the stimulus period. This was further evident when we temporally re-aligned the firing rate of the significant stimulus-related LIP neurons based on the saccade onset. The results are shown in the right panel of Fig. 4-3 (Saccade-aligned). As demonstrated by the activity of the 2 representative cells shown in Fig. 4-3A (right panel – Saccade-aligned), when aligned on the saccade onset, these LIP neurons did not demonstrate any prominent saccade-related activity around saccade onset time (marked by the dotted line). Looking at group-level activity (Fig. 4-3B- right panel), the observed patterns seemed to be the carry-over activities prior to saccade-related period, and not related to the saccade onset. Thus, the identified 20 LIP neurons were visual neurons.

We next applied two-factor ANOVAs on neuronal activity of area LIP during the perisaccadic period and identified 21 neurons with significant saccade related activity ($p < 0.05$), 7 of which also demonstrated significant interaction effect for saccade direction and stimulus location (Fig. 4-4). All the 21 neurons in area LIP of marmosets strongly preferred contralateral saccades in both pro- (Pro contra in red) and antisaccade (Anti contra in dark blue) trials, with a relatively stronger activity for contralateral prosaccades. Fig. 4-4A shows neuronal activity from four representative LIP neurons. The first two are examples of cells that only had significant saccade related activity and no interaction effect for stimulus location. This was evident by the sharp rise of activity for contralateral anti and pro conditions in the saccade-aligned plots (4-4A – right panel, first two cells) that started around saccade onset time (marked by the dotted line), and the absence of any stimulus related changes of activity on the stimulus-aligned plots (4-4A

- left panel, first two cells) shortly after the stimulus onset (marked by the dotted line). The third and fourth neuronal activity in fig. 4-4A are from two representative cells in area LIP that had both saccade related activity around saccade onset and stimulus related activity shortly after stimulus onset (Fig. 4-4A – third and fourth cells). As shown in the saccade-aligned activity (Fig. 4-4A – right panel, third and fourth cells), the rise of saccade-related activity in these cells was slightly delayed by about 10 to 20 ms for Pro contra trials and closer to 40 ms for Anti contra trials. When aligned based on stimulus onset time (Fig. 4-4A, left panel, third and fourth cells), these cells demonstrated a stimulus-related response within the stimulus period with preference for Pro contra (contralateral prosaccades in red) and Anti ipsi (ipsilateral antisaccades in cyan) conditions, reflecting preference for contralateral stimulus locations. In another words, while these cells appear to be saccade-related with preference for contralateral saccade directions in both anti and pro trials at the perisaccadic period, they also exhibited increased activity for contralateral stimulus locations at the stimulus period, indicating a visual response.

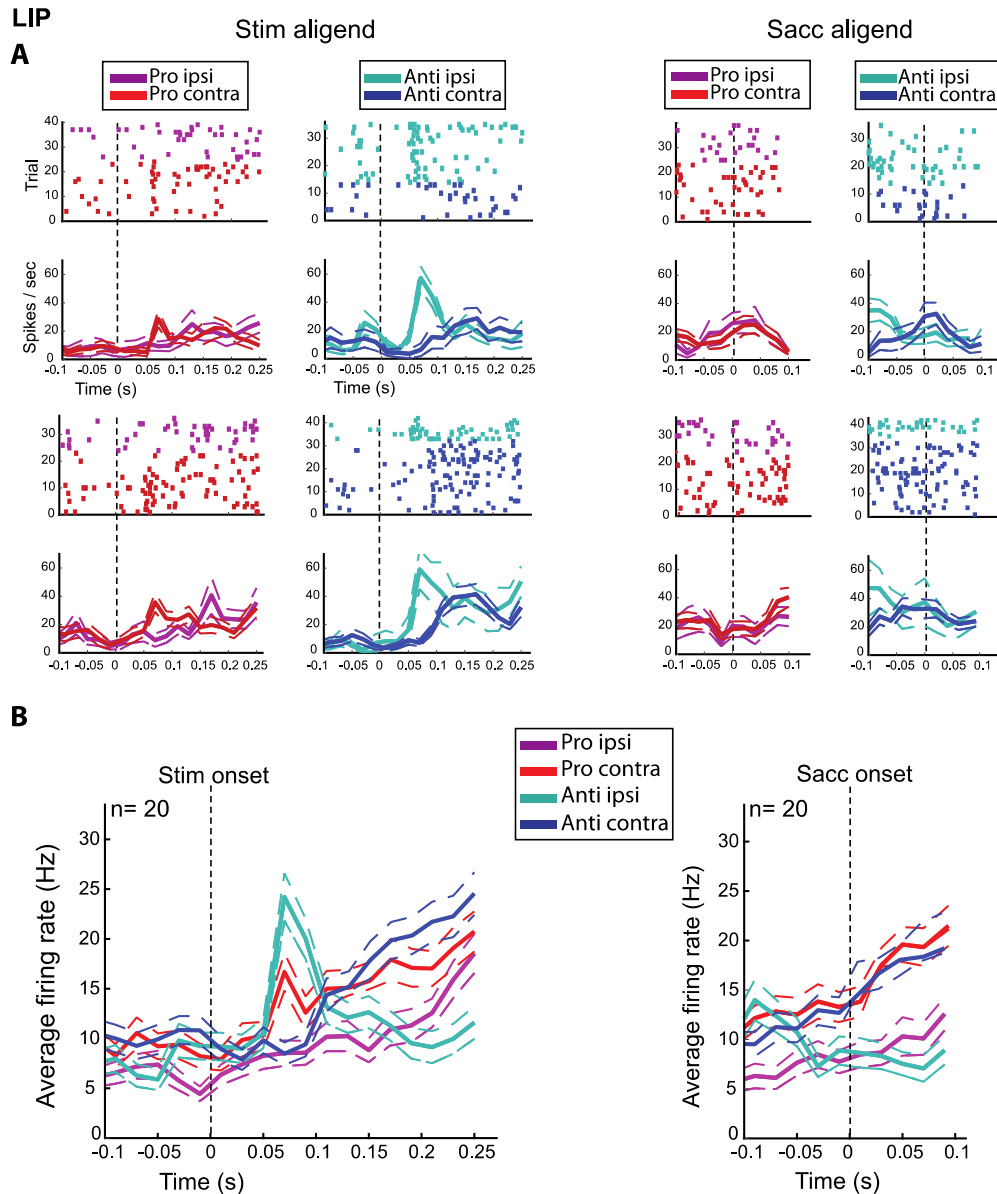


Figure 4-3. Average and single cell activity in area LIP of common marmosets based on stimulus period (30 to 80 ms after the stimulus onset) in the pro/antisaccade task. (A) Stimulus-aligned (left) and saccade-aligned (right) spike activity of representative single cells in area LIP significant activity during the stimulus period defined. (A) Stimulus-aligned (left) and saccade-aligned (right) average firing rate of LIP neurons with significant activity during the stimulus period. Dashed line in all plots on the left panel marks the onset of the salient stimulus while in the right panel it marks the onset of saccade. Pro ipsi: ipsilateral prosaccade, Pro contra: contralateral prosaccade, Anti ipsi: ipsilateral antisaccade, Anti contra: contralateral antisaccade.

All in all, it appeared from our findings that LIP cells with an earlier onset of saccade-related activity, had no stimulus-related response within the stimulus period, while cells for which the saccade-related activity was delayed further past saccade onset, also demonstrated a stimulus-related response within the stimulus period for contralateral stimulus locations. The preference of area LIP neurons for contralateral saccade directions in both pro- and antisaccade trials in the perisaccadic period, was consistently observed at the group level firing rates evident from the saccade-aligned plots (Fig. 4-4B, right panel). When aligned based on the stimulus onset, the preference for contralateral stimulus location was also present at group-level firing rate (Fig. 4-4B, left panel) with higher activity for Pro contra (red) and Anti ipsi (cyan) conditions.

4.4.2.2 Neuronal activity in area 8aD

There was no significant stimulus-related and task-related activity in area 8aD neurons in either the stimulus or the perisaccadic period. However, applying the two-factor ANOVA on neuronal activity of areas 8aD during the perisaccadic period identified a total of 23 neurons in area 8aD (15.4 %) with significant main effect for saccade direction ($p < 0.05$). Area 8aD neurons demonstrated significant saccade-related response within the perisaccadic period with strong preference for contralateral saccades on both pro- (Pro contra in red) and antisaccade (Anti contra in dark blue) trials (Fig. 4-5A, right panel). The increase of activity started at about 30 ms prior to saccade onset (marked by the dotted line in Fig. 4-5A, right panel) and reached a sharp peak at about 20 ms after saccade onset. The preference for contralateral saccades in area 8aD neurons during the perisaccadic period was also observed at the group level firing rate (Fig.

4-5B, right panel), with activity of contralateral pro- and anti- conditions rising prior to saccade onset and reaching a sharp peak about 20 ms after. ANOVA did not yield any stimulus related effects for area 8aD. Indeed, when the activity of these significant perisaccadic neurons was aligned on stimulus onset, there was no prominent change in activity observed around the stimulus onset, both at and single cell level (Fig. 4-5A left panel) and group level (Fig. 4-5B left panel). Thus, the identified neurons in area 8aD were saccade-related motor neurons.

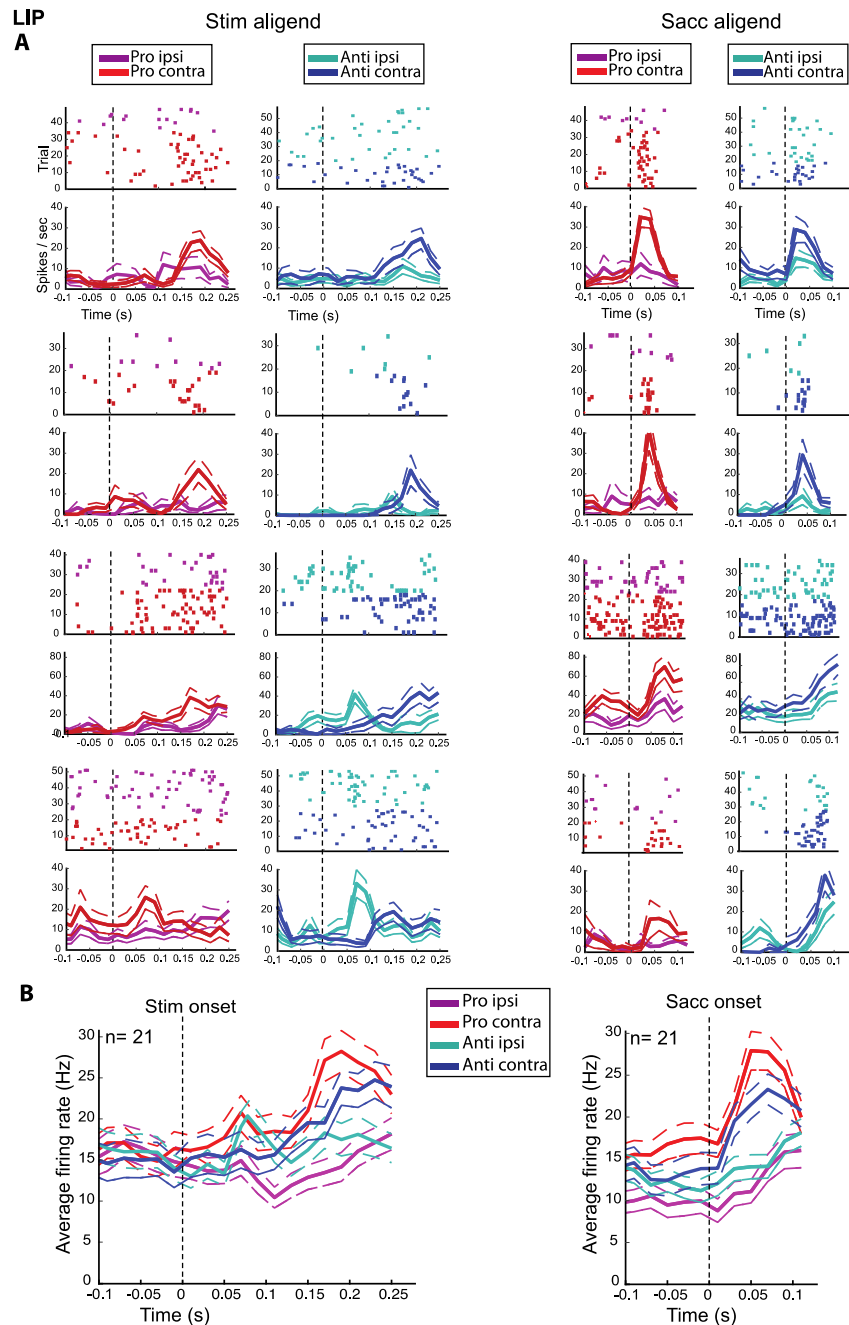


Figure 4-4. Average and single cell activity in area LIP of common marmosets based on perisaccadic period (from -70 to 100 ms around the saccade onset) in the pro/antisaccade task. (A) Stimulus aligned (left) and saccade-aligned (right) spike activity of representative single cells in area LIP with significant activity during the perisaccadic period. (B) Stimulus-aligned (left) and saccade-aligned (right) average firing rate of area LIP neurons with significant activity during the perisaccadic period. Dashed line in all plots on the left panel marks the onset

of the salient stimulus while in the right panel it marks the onset of saccade. Pro ipsi: ipsilateral prosaccade, Pro contra: contralateral prosaccade, Anti ipsi: ipsilateral antisaccade, Anti contra: contralateral antisaccade.

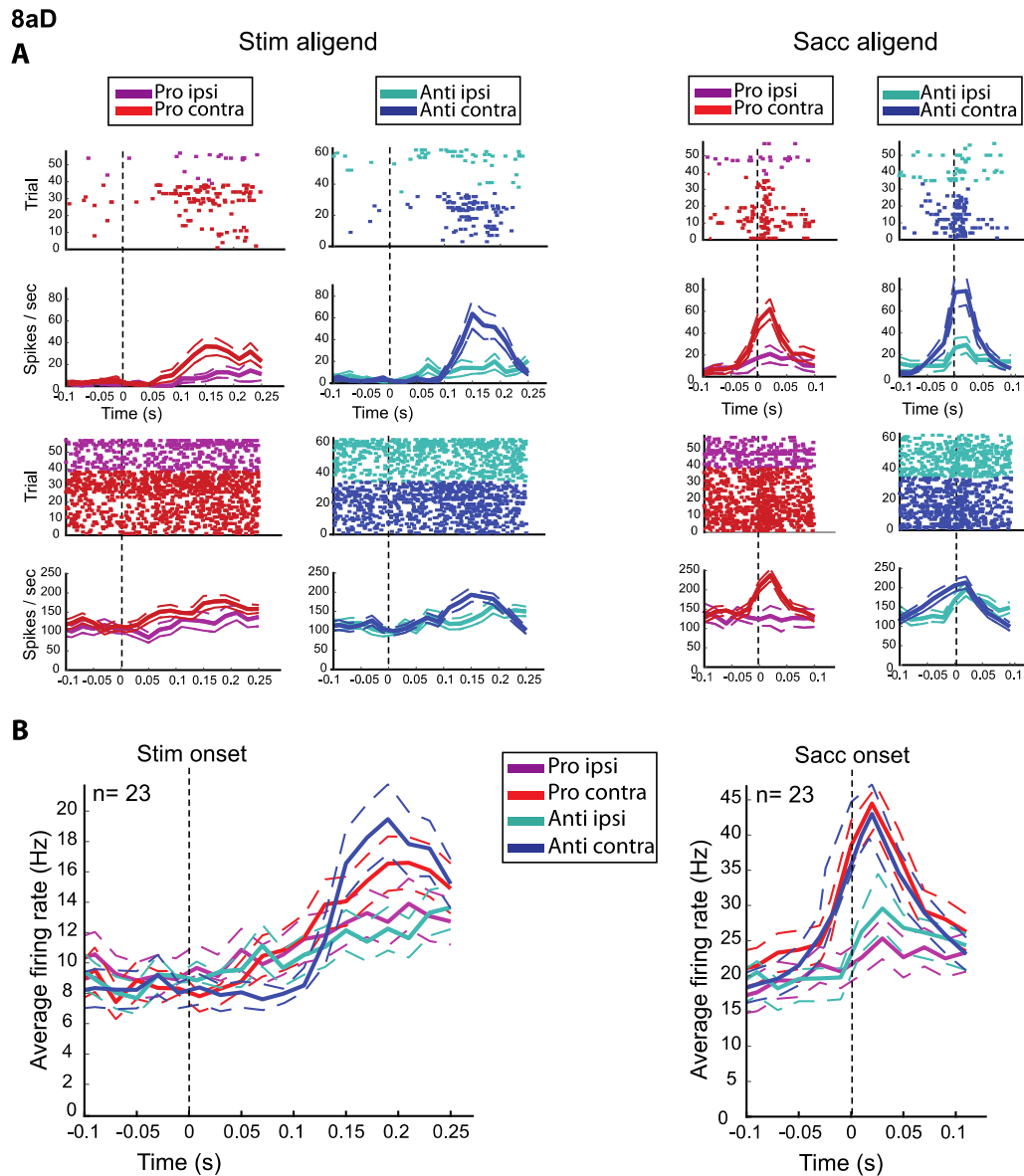


Figure 4-5. Average and single cell activity in area 8aD of common marmosets based on perisaccadic period (from -70 to 100 ms around the saccade onset) in the pro/antisaccade task. (A) Stimulus-aligned (left) and saccade-aligned (right) spike activity of representative single cells in area 8aD with significant activity during the perisaccadic period. (B) Stimulus-aligned

(left) and saccade-aligned (right) average firing rate of area 8aD neurons with significant activity during the perisaccadic period. Dashed line in all plots on the left panel marks the onset of the salient stimulus while in the right panel it marks the onset of saccade. Pro ipsi: ipsilateral prosaccade, Pro contra: contralateral prosaccade, Anti ipsi: ipsilateral antisaccade, Anti contra: contralateral antisaccade.

We also looked at the entire population of cells in areas 8aD and LIP with at least 5 correct trials per condition within the perisaccadic period, irrespective of the statistical significance of their perisaccadic activity, to have an idea of the general preference of cells. Most cells in areas 8aD, significantly preferred contralateral saccade directions in both Pro (Fig. 4-6A, left) (two-sample t-test, $p = 0.0006$) and Anti trials (Fig. 4-6A, right) (two-sample t-test, $p = 0.04$). Similarly, area LIP cells significantly preferred contralateral saccade directions in both Pro (Fig. 4-6B, left) (two-sample t-test, $p = 0.02$) and Anti trials (Fig. 4-6B, right) (two-sample t-test, $p = 0.03$).

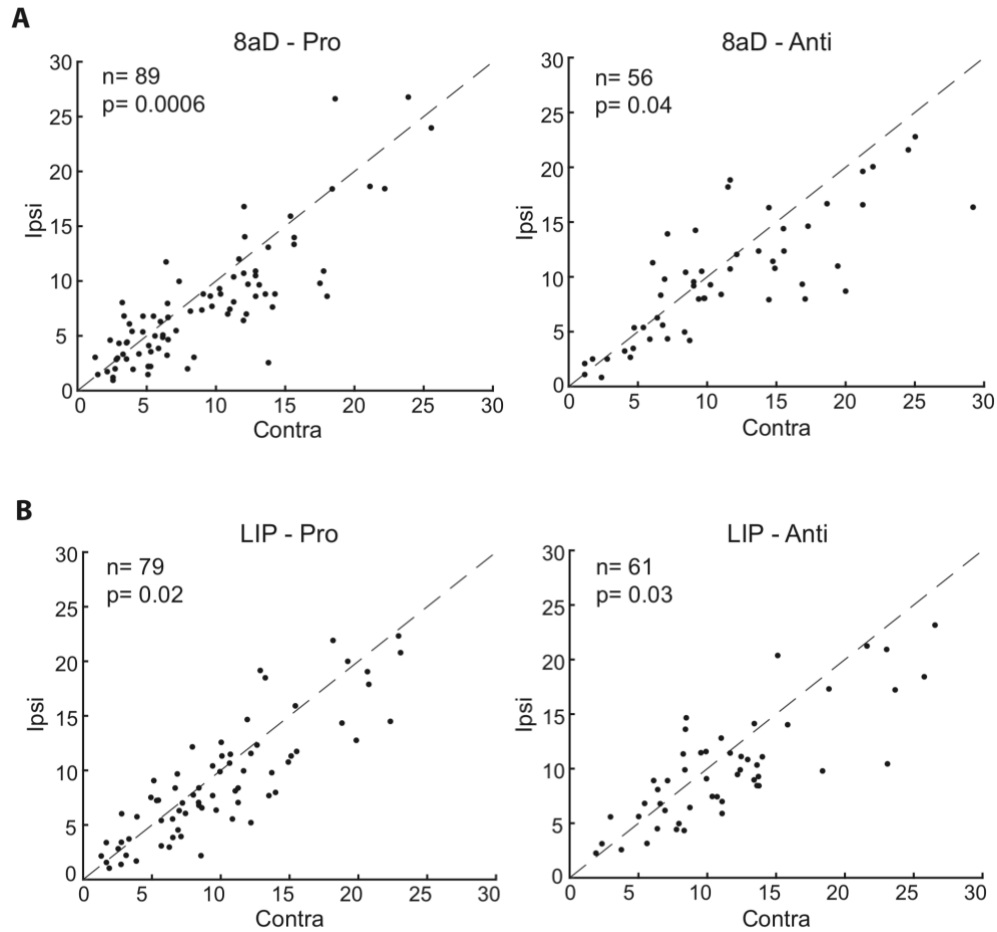


Figure 4-6. Discharge rate of single neurons in marmoset areas 8aD and LIP for ipsilateral versus contralateral prosaccades and antisaccades. (A) Scatter plots depicting relative discharge rates of area 8aD neurons in pro (left) and anti (right) trials on ipsilateral versus contralateral saccades. (B) Scatter plots depicting relative discharge rates of area LIP neurons in pro (left) and anti (right) trials on ipsilateral versus contralateral saccades.

In terms of the preference of neurons for correct versus error in antisaccade trials, neurons in area 8aD significantly preferred correct antisaccades in contralateral direction (two-sample t-

test, $p=0.046$) (Fig. 4-7, left). Area LIP neurons did not demonstrate any statistically significant difference between correct and error antisaccade trials (two-sample t-test, $p = 0.325$) (Fig. 4-7, right).

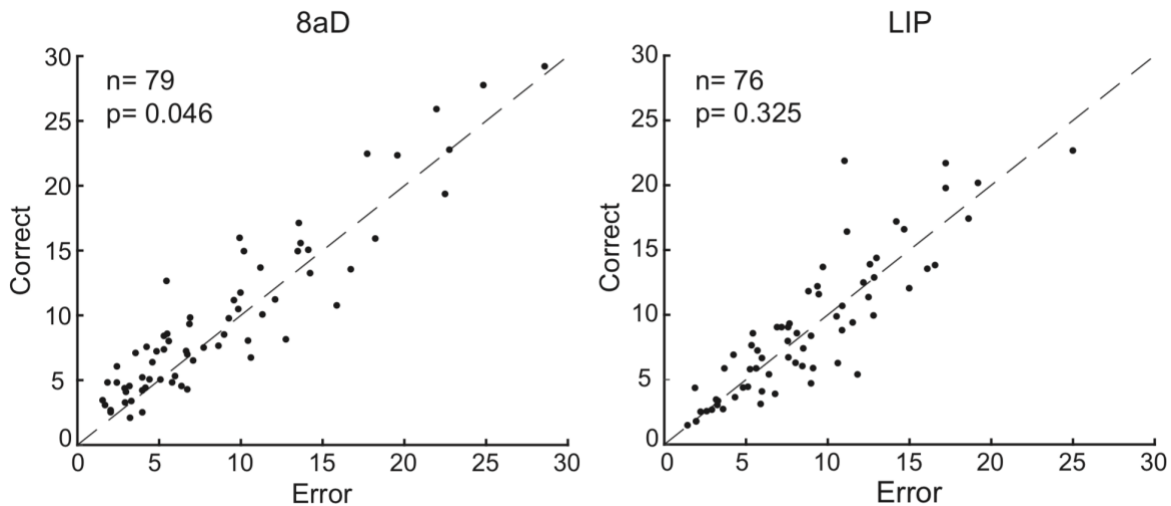


Figure 4-7. Scatter plots depicting the relative discharge rate of single neurons in marmoset areas 8aD (left) and LIP (right) for correct versus error contralateral antisaccade trials.

4.5 Discussion

In the present study, we investigated neuronal activity in areas 8aD and LIP of two common marmoset monkeys while performing the pro/antisaccade task. We focused the analysis on the stimulus (30 to 80 ms after stimulus onset) and perisaccadic periods (-70 to 100 ms around saccade onset). The results demonstrated behaviorally relevant differences between prosaccade and antisaccade trials in terms of the SRTs, proportions of error and percent accuracy. No task-related neuronal activity was found in either brain area in either stimulus or perisaccadic period. No prominent stimulus related activity was found in area 8aD neurons; however, area LIP

neurons demonstrated higher activity for contralateral stimulus locations during the stimulus period. Both areas exhibited saccade-related activity during the perisaccadic period, with a preference for contralateral saccades. This finding was consistent across the whole population of recorded neurons. Additionally, neurons in area 8aD preferred correct antisaccades over errors, whereas no significant differences were found for area LIP neurons.

4.5.1 Behavior

Both marmosets had a significantly higher percentage of errors on antisaccade than prosaccade trials. Correct prosaccades had significantly shorter SRTs than correct antisaccades. While erroneous prosaccades had longer SRTs than correct prosaccades, the SRTs were shorter for erroneous antisaccades than correct antisaccades. These findings go in line with previous literature on human, macaque performing a similar task (Everling and Fischer, 1998; Everling et al., 1999) and indicate that like macaques and humans, marmosets share the difficulty in performing the antisaccade task compared to prosaccade. In a prosaccade block, a correct response is equivalent to the automatic saccade that would naturally occur towards the more salient stimulus (bigger brighter dot), whereas in antisaccade blocks correct performance requires suppressing this reflexive saccade and program a saccade away from the salient stimulus. The antisaccade task is indicative of the top-down voluntary control of eye movements (Hallett, 1978; Munoz and Everling, 2004) and the observed direction errors are thought to reflect a failure in voluntary inhibition of the automatic saccade and not an inability to generate the voluntary antisaccade. This is evident from the fact that we observed a corrective antisaccade generated after a short intersaccadic interval following an erroneous antisaccade,

showing an understanding of task demands (Fig. 4-2). Such corrective saccades have also been observed in humans (Clementz, 1998) and macaques (Amador et al., 1998) performing similar antisaccade task. Marmosets' ability to understand task demands was also demonstrated by the percent accuracy in animals' performance in each of prosaccade and antisaccade blocks in our experiment. The percent accuracy was the lowest for both animals during the transition (beginning) period within a task block (pro/anti), since the animal had just started a new block and was in the process of transitioning and understanding the associated task rule. As the animals performed more trials within a block (pro or anti), the percent accuracy improved for both trial types, reaching its highest within the end period of the block. However, even in the end period, the percent accuracy in antisaccade blocks (70%) still lagged behind that of prosaccade blocks (82%). In comparison to macaques, common marmosets were generally harder to be trained on the antisaccade task. As mentioned in our methods section, the conventional interleaved prosaccade/antisaccade task that is commonly used for macaques (Munoz and Everling, 2004) had to be adjusted for marmoset performance level, by resorting the task into blocks of prosaccade and antisaccade trials. Additionally, compared to the macaques, it was difficult for marmosets to make an antisaccade to a blank location in the display and for this reason, a small dim stimulus had to be included in that blank location as the target for an antisaccade (Johnston and Everling, 2011). This form of antisaccade trials is used in the final stage of macaque antisaccade training protocol before they advance to the next level of difficulty of issuing an antisaccade to a blank space, which they eventually tend to master. The adjustments we made to the task, made it possible to train common marmosets on performing the antisaccade task in a few months.

4.5.2 Stimulus related neuronal activity

To identify any stimulus related neuronal activity in areas 8aD and LIP, we looked at any statistically significant (ANOVA) activity during the stimulus period defined from 30 to 80 ms after the peripheral stimulus onset. In line with a previous study (Ma et al., 2020), we found that 35 ms is about how long it took for the visual signal to reach marmoset cortical areas and no changes in neuronal activity were observed in either brain area from the stimulus onset until about 35 ms after.

Area 8aD - We did not observe any prominent stimulus related activity in area 8aD neurons that we had recorded from. Macaque studies have reported that visuomotor neurons of the FEF showed increased activity after the presentation of a visual stimulus in their response field (Bruce and Goldberg, 1985), especially when this stimulus was the target of saccade, as is the case in prosaccade task (Mohler and Wurtz, 1976). Everling and Munoz (2000) found that in all visuomotor FEF neurons, stimulus related responses were only present when the stimulus was presented in the neuron's response field and this was independent of the direction of the upcoming saccade (Everling and Munoz, 2000). We believe that the lack of any prominent stimulus-related activity in area 8aD in our study could be because the presented stimulus was not falling in neurons' response field. Since the neuronal data in the present study was acquired using linear electrode arrays, we could not map individual neurons' response field at the time of recording, and this is one of the shortcomings of the present study. Another possible explanation for our observation can be related to the actual location of the putative area FEF in common marmosets. We selected area 8aD bordering 6DR as the location of the putative area FEF in marmosets based on our observations in a resting-state fMRI study on common marmosets that found area 8aD bordering 6DR to have the strongest functional connectivity

with the SC, a pivotal node of the oculomotor network (Ghahremani et al., 2017). However, the exact location of putative marmoset FEF is still under debate. Few recent studies propose area 8aV, and not 8aD, to be the putative area FEF in common marmosets. Selvanayagam et al (2019) performed a systemic microstimulation study on marmoset frontal cortex and reported that microstimulation of area 8aV could elicit larger saccades often along with shoulder, neck and ear movements, which is closer to the characteristics of the macaque FEF (Selvanayagam et al., 2019). Based on a tract tracing study by Reser et al (2013), area 8aV was characterized by large pyramidal cells in the upper part of layer 5 and was also a more myelinated area in comparison to area 8aD. According to their findings, area 8aV was distinct from 8aD due to its widespread projections from various visual areas, especially the extrastriate visual areas. They then proposed that area 8aV may be more involved in the visual modality and the complex processing of visual information (Reser et al., 2013). Therefore, considering its heavier connections with visual areas, it is possible that neurons in area 8aV will demonstrate higher stimulus-related activity after the onset of the salient visual stimulus in a saccade task. Area 8aD may have more limited connection with visual areas and thus exhibit lower stimulus-related neuronal activity. Further electrophysiological recordings of marmoset area 8aV while the animal performs similar saccadic eye movement tasks, may help clarify the differences in the oculomotor function of these frontal areas in marmosets.

Area LIP - We found neurons in area LIP of marmosets with stimulus related activity occurring around 35 ms after the stimulus onset (Fig. 4-3), with preference for contralateral stimulus locations. Historically, area LIP neurons have been harder to characterize, since visual and saccade-related responses are more closely intertwined in LIP. The posterior parietal cortex (PPC) sits at the interface between frontal motor fields and occipital and temporal visual fields,

suggesting its potential role in visually guided behavior (Liversedge et al., 2011). What we know from macaque studies, is that a large percentage of neurons in area LIP are visually responsive cells that hold a coarse representation of the contralateral visual field (Ben Hamed et al., 2001). This was in line with our findings on marmoset LIP neurons having higher activity for contralateral stimulus locations.

4.5.3 Saccade related neuronal activity

To identify saccade related neuronal activity in areas 8aD and LIP, we looked at any statistically significant (ANOVA) activity during the perisaccadic period defined from -70 to 100 ms after the onset of peripheral stimulus.

Area 8aD - We found prominent saccade related activity in area 8aD of common marmoset monkeys during the perisaccadic period in the pro/antisaccade task. These neurons had a strong preference for prosaccades and antisaccades in contralateral direction (Fig. 4-5). The increase of activity started at about 30 ms prior to saccade onset (marked by the dotted line) and reached a sharp peak at about 20 ms after saccade onset. As discussed earlier, it is not clear yet whether area 8aD in marmosets is the putative FEF, but based on our findings in the present study, this area certainly contains saccade-related neurons that respond both before and after saccade onset, indicating their involvement in saccade preparation. This is in line with our fMRI findings in a previous study showing that area 8aD in marmosets had the strongest connection within the marmoset frontal cortex, with area SC (Ghahremani et al., 2017). Previous studies on macaques have demonstrated that, like area SC (Dorris and Munoz, 1998), area FEF is also involved in saccade initiation (Hanes and Schall, 1996). FEF deactivation in macaques has been

reported to result in reduced saccade preparation in the SC as well as increased contralesional SRTs (Dash et al., 2018). Human brain imaging studies have demonstrated increased activation in the FEF during the antisaccade compared with prosaccade task (O'Driscoll et al., 1995; Doricchi et al., 1997), which might be related to the increased activation of inhibitory interneurons in the FEF and not the saccade-related neurons (Everling and Munoz, 2000). Electrophysiological studies in macaque reported increased discharge of FEF neurons for both prosaccade and antisaccade trials, with lower discharge for antisaccade compared to prosaccade across all task epochs - instruction, stimulus and saccade (Everling and Munoz, 2000). They explained that the reduced preparatory activity of FEF neurons on antisaccade trials reduces the excitation of saccade neurons in the SC, thereby reducing the risk of generating an erroneous saccade towards the stimulus. Johnston et al (2019) from our group similarly reported that neurons in upper layers of area 8aD in marmosets were more active for prosaccades than antisaccades during the preparatory period (Johnston et al., 2019). In our investigations on the perisaccadic period, there was no difference in the strength of the saccade related activity between pro and antisaccade trials. This might be due to the fact that among individual neurons, there were different thresholds for pro and antisaccades that were averaged. Higher number of trials and recording sessions can provide access to higher number of recorded neurons which will be required to address such task related difference of saccade-related activity in more details. Finally, area 8aD neurons had a significant preference for correct antisaccades compared to error, indicating to a performance-related activity pushing the oculomotor system towards correct performance.

Area LIP - neurons in marmoset area LIP with statistically significant activity in the perisaccadic period, also showed strong saccade-related responses (Fig. 4-4). Similar to area

8aD neurons, neurons in area LIP of marmosets preferred contralateral saccades in both pro and antisaccade trials, with a relatively stronger preference for contralateral prosaccades. However, as opposed to area 8aD, the rise of activity in area LIP neurons was delayed towards the saccade onset time and after. In a study by Gottlieb and Goldberg (1999) in macaque LIP, it was found that most area LIP neurons encoded contralateral cue locations irrespective of the dictated saccade and only a few had saccade-related activities, encoding the direction of the upcoming saccade. Among the few saccade-related neurons, most of them responded more strongly to prosaccades to their response field compared with antisaccades and the response started before the onset of saccade (Gottlieb and Goldberg, 1999). In our study on marmosets, we also found stronger LIP activity for prosaccades, however the rise of activity was delayed toward saccade onset time or after. This delayed response may indicate that marmoset area LIP has no role in saccade initiation, preparation and generation. It might play a more important role in describing the salient world, but not in the decision-making process of how and when to act in that world. When looking at single cell activity of LIP neurons from both saccade-aligned and stimulus-aligned perspectives, it was evident that cells with a visual response (to contralateral stimulus locations) had a longer latency for saccade response, compared to those with no visual response. The delay was more pronounced for antisaccades which may have implications with regards to the role of marmoset area LIP in the vector inversion process. Such implication has been reported in macaques before in studies by Zhang and Barash (2000, 2004). They investigated macaque area LIP neurons using a memory-delayed version of the antisaccade task and found certain neurons that became active when the saccade vector but not the visual stimulus was aligned with their response field but they also responded about 50 ms after the stimulus onset which is the common latency for visual neurons in the macaque LIP. These authors argued that

the presence of such paradoxical activity in this subset of LIP neurons might indicate to a re-mapped visual response that could contribute to the saccade vector inversion in anti-saccade task (Zhang and Barash, 2000, 2004). We had a similar finding in a subset of area LIP neurons in common marmosets, indicating the potential involvement of this area in vector inversion during antisaccades in these species as well. It may be the case that the underlying processes in vector inversion, cause a delay in saccade-related response of such cells. Another potential cause for the delay is that the salient stimulus can act as a distractor in antisaccade trials. Finally, the higher activity of LIP neurons in prosaccade compared to antisaccade trials may imply that this area relies more heavily on the visual stimulus, compared to area FEF. This is in line with behavioral studies in the macaque, reporting that the magnitude of pre-saccadic activity is significantly reduced in area LIP when saccades are made in the absence of visual target, as is the case in antisaccade blocks (Ferraina et al., 2002).

Overall, this study demonstrated prominent stimulus-related and saccade-related activities in area LIP, and strong saccade-related response in area 8aD neurons in common marmoset monkeys. There was no prominent task-related response in either area. The results can be improved in future by having higher number of sessions and trials per session to have access to a larger population of cells. The antisaccade task is hard to learn for common marmosets compared to macaques, and therefore there wasn't a sufficiently high number of correct responses, especially correct antisaccade responses to properly detect task related differences in neuronal activity. Furthermore, as mentioned earlier, we were not able to optimize our neuronal recordings based on the response field of individual neurons, which can heavily impact neuronal response, especially stimulus-related visual responses. With regards to our findings on area 8aD, further clarifications on the precise location of the putative area FEF in common

marmosets are necessary to target more precisely the area within the marmoset frontal cortex with the heaviest involvement in saccadic eye movements. In spite of all the aforementioned shortcomings, the present study certainly laid a foundation for the potential oculomotor roles of area 8aD and LIP of common marmosets within the stimulus and perisaccadic periods of the pro/antisaccade task. This study further reflected that marmoset monkeys could be trained up to the final stage of antisaccade training for macaques within a few months. In the near future, more advanced and higher-density recording techniques such as Neuropixel (Jun et al., 2017) can be applied on marmosets performing the pro/antisaccade task, taking advantage of their lissencephalic cortex and providing access to a much larger population of neurons within marmoset oculomotor areas. Our study thus emphasized the great potential of using common marmosets as alternative primate models of the oculomotor system with such advanced recording techniques.

4.6 References

CHAPTER 5

5 General Discussion

The cortical and subcortical circuitry underlying saccadic eye movements is perhaps the most thoroughly understood sensorimotor system in the primate brain (Munoz et al., 2000; Schiller and Tehovnik, 2001). Most of our knowledge about the oculomotor system comes from neurophysiological studies in the Old-World macaque monkeys. Despite their prominent role as a nonhuman primate (NHP) model for saccade control and cognition, macaque monkeys have shortcomings that limits their application for more advanced high-density electrophysiology. Many of the key frontoparietal areas involved in the oculomotor system are deeply buried in sulci in macaques, making them difficult to access for high-density recording techniques. The common marmoset (*Callithrix jacchus*) is a small-bodied New World primate that has recently gained considerable attention as an alternative primate model for neuroscience research (Izpisua Belmonte et al., 2015; Mitchell and Leopold, 2015; Miller et al., 2016; French, 2019). Marmosets possess a lissencephalic cortex that offers great opportunity for high-density electrophysiology and optical imaging, accessing key oculomotor areas right at the surface of the cortex (Mitchell and Leopold, 2015). However, in comparison to the macaque, little is known about marmoset oculomotor areas and their role in saccade control and our knowledge of the functional organization of the saccade network in this species is more limited. My PhD research aimed to enhance our knowledge about the saccade circuitry in this species by using ultra-high field resting-state fMRI, intracortical microstimulation and electrophysiological recordings in common marmoset monkeys. What follows is a summary of the main findings and the limitations associated with each part of my studies as well as potential future directions.

5.1 The frontoparietal pattern of functional connectivity underlying saccade circuitry is preserved across Old World (macaques and humans) and New World (marmosets) species

5.1.1 Summary of the main findings

In the first part of my PhD I investigated the functional organization of the oculomotor network in common marmosets using ultra-high field resting-state fMRI. The goal was to investigate whether the frontoparietal pattern of functional connectivity underlying the saccade circuitry is preserved across Old World (macaques and humans) and New World (marmosets) species, thereby identifying putative saccade-related areas in the marmoset for future invasive investigations of this circuitry. We initially applied independent component analysis on marmoset resting-state fMRI data and identified eight resting-state networks (RSNs) that greatly overlapped with corresponding networks in macaques and humans. A distributed frontoparietal network was among those identified RSNs that potentially incorporated the cortical oculomotor circuitry. Next, we applied seed-region analyses on the marmoset superior colliculus (SC) and found functional connectivity patterns across homologous areas to macaques. The marmoset SC had the strongest frontal functional connectivity with area 8aD bordering area 6DR. We then applied seed-region analysis to this frontal region and found similar functional connectivity patterns as the frontal eye fields (FEF) in macaques and humans. Across the posterior parietal cortex, the strongest functional connectivity with both areas SC and 8aD was located around the lateral intraparietal sulcus in marmosets, potentially representing the putative area LIP that is known to be involved in saccadic eye movements in macaques. Our results supported an evolutionarily preserved frontoparietal system and

identified potential homologues of the well-established macaque oculomotor hubs in marmosets (Ghahremani et al., 2017). Establishing such homologies is an essential step towards utilizing common marmosets as alternative primate models of the oculomotor system and considering invasive electrophysiological studies of these areas.

5.1.2 Caveats and future directions

One of the main findings of my first PhD project was the identification of area 8aD bordering 6DR in common marmosets as the potential homologue of area FEF in macaques. This finding was in line with earlier microstimulation studies on marmosets that found areas 8aD, 6DC, 6DR and 46 of marmoset frontal cortex evoking ipsilateral and contralateral saccades (Blum et al., 1982). However, more recent anatomical studies suggested that it may be located within areas 8aV and 45 (Reser et al., 2013) and task-fMRI studies reported BOLD activation in these areas in response to visual stimuli (Hung et al., 2015). In my study, we proposed that area 8aD may correspond to putative marmoset area FEF encoding large amplitude saccades, while area 8aV might encode smaller amplitude saccades. It is clear that further clarification of these findings requires electrophysiological recordings or systemic electrical microstimulation to identify the precise location of the largest population of saccade-related neurons within marmoset frontal cortex. Such investigations were not defined within the boundaries of my project and as a matter of fact, a recent study from our group has provided further details in this regard using intracortical electrical microstimulation on marmoset frontal cortical areas. Based on this study, it appears that areas 45 and lateral 8av encode small contraversive saccades that correspond to properties of ventrolateral FEF in macaques (Bruce and Goldberg, 1985), while medial 8aV,

8C, 6DR and 6DC encode larger saccades and contralateral neck and shoulder movements which correspond to dorsomedial FEF in macaques (Elsley et al., 2007; Selvanayagam et al., 2019).

Another recent study by our group looked at the preparatory activity in marmosets performing a pro/anti-saccade task, using laminar electrodes that were inserted approximately at the border of areas 8aD and 6DR (Johnston et al., 2019). They found prominent task-related activity in area 8aD during the preparatory period where the animal was given the instruction about which of the pro/anti tasks he has to perform. Similar to macaque studies (Everling and Munoz, 2000), they found that marmoset area 8aD was also less active for antisaccade than for prosaccade trials during the preparatory period, providing evidence of area 8aD being putative marmoset FEF.

It is important to point out here that in spite of the benefits that marmoset lissencephalic cortex provides for electrophysiological recordings, its lack of sulci and gyri limits the ability to localize cortical areas such as the FEF on the basis of sulcal landmarks. There are high quality histology-based brain atlases that exist for marmosets which I mainly relied on throughout my first project (Hikishima et al., 2011). However, recent studies have shown that the cytoarchitectonic boundaries of marmoset frontal cortex as defined by these atlases, did not map directly to the observed functional boundaries (Schaeffer et al., 2019a) indicating the inaccuracy in identifying these regions based on histology alone. Over the last few years, considerable amount of effort has been put into creating marmoset brain atlases that are more compatible to 3D MRI data and can be accessed in digital format. Liu and colleagues (2018) have come up with a new MRI-based 3D digital atlas of the marmoset brain based on high-resolution ex-vivo MRI images of marmosets. Known as the NIH marmoset brain atlas, this

atlas is designed and optimized for MRI studies of marmoset brain and can map brain regions directly onto MRI images, avoiding the inaccuracy of histology to MRI registrations. Additionally, the multi-level parcellation schemes used to create this atlas allow for more precise localization of brain areas with hierarchical labelling (Liu et al., 2018). The NIH marmoset brain atlas is a great aid for fMRI studies on marmosets, as an initial non-invasive approach towards conducting cross-species comparisons and identifying potential homologies. A recent task-based fMRI study by our group in awake marmosets that used the NIH atlas for registration, reported that the SC had peak functional connectivity in both lateral 8aV and 8aD/6DR. Compared to the study by Schaeffer et al (2019), my findings may not have illustrated the full picture of functional connectivity pattern due to the light anesthesia applied using isoflurane that might have limited the full extent of resting-state connectivity profiles (Hutchison et al., 2014). More importantly, since my initial resting-state fMRI investigation in 2015-2016, the MRI setup and custom-made head coils used for marmoset fMRI at Robarts Research Institute have had dramatic improvements in terms of signal to noise ratio (SNR), providing higher resolution images with more well-defined functional boundaries (Schaeffer et al., 2019b). Moreover, at the time of my fMRI investigation, we only had 4 common marmosets to scan. Currently, we have access to a larger number of animals in our NHP unit. Replication of my first PhD project under the current fMRI related improvements with higher number of animals can yield a more complete picture of resting-state connectivity patterns in common marmosets. In any case though, only further electrophysiological studies can more precisely characterize properties of the proposed putative oculomotor areas in marmosets to confirm their role in saccade control.

5.2 Microstimulation of the LIP in marmosets evokes both fixed-vector and convergent saccades, supporting its homologous role to the macaque LIP.

5.2.1 Summary of the main findings

Despite considerable advantages of fMRI techniques in understanding the functional organization of the oculomotor system in common marmoset monkeys, microstimulation and electrophysiological recording techniques are still necessary to characterize the underlying properties of cortical oculomotor areas in marmosets. From my resting-state fMRI investigations, I identified a region at the putative location of area LIP in marmosets that exhibited strong functional connectivity with both areas SC and 8aD. Up until recently, no studies had investigated the oculomotor properties of the cytoarchitectonically defined region LIP in the common marmoset. Accordingly, in my second research project we applied for the first time electrical microstimulation to the posterior parietal cortex (PPC) of awake behaving marmosets and monitored eye position while the animals made unrestricted eye movements. We implanted a 32 channel Utah array in putative area LIP of marmosets and applied stimulation trains of varying current amplitudes while observing potential oculomotor effects. After the experiment, the location of the implanted array was confirmed using ex-vivo MRI in one animal and Micro-CT scan in the other. We observed that the array location mostly fell within the boundaries of area LIP, while covering parts of areas MIP and VIP in both animals. Microstimulation could elicit saccades in about 70 percent of the array sites in both animals, with the majority of saccades directed towards the hemifield contralateral to the site of stimulation, and predominantly toward the upper visual field. At some of these sites, we found

trials in which prolonged stimulation was able to evoke staircase saccades. The rest of the sites mostly elicited eye blinks. Most of the saccade-eliciting sites exhibited fixed-vector saccades that maintained similar amplitudes and directions irrespective of the starting position of the eye at the onset of microstimulation. In a subset of sites however, microstimulation evoked goal-directed saccade with varying amplitude and direction depending on the starting position of the eye, with the preferred “goal zone” generally in the contralateral upper visual field. These findings were consistent with previous microstimulation studies of PPC in macaques (Shibutani et al., 1984; Kurylo and Skavenski, 1991; Thier and Andersen, 1996, 1998) and supported the homologous role of marmoset LIP to that of the macaque in modulating eye movements (Gharemani et al., 2019).

5.2.2 Caveats and future directions

As mentioned in the previous section, intracortical microstimulation in the majority of sites within the implanted Utah array evoked saccadic eye movements. However, in a few sites in Marmoset B, there were sites that had no response following microstimulation. Since we did not record any spiking activity for the purpose of this project, we were not certain about the reason for the lack of response and proposed that maybe those electrodes were not in the grey matter. Utah arrays used in my study were fixed length and did not allow us to optimize the cortical depths at which stimulation was applied by moving individual electrodes. To clarify this issue in future, it would be necessary to collect spike activity data from individual array channels within a separate session from the same marmosets. As a matter a fact, in a later study published by Ma et al (2020), we used the same animals to study neuronal activity in marmoset

area LIP while the animals performed the gap task and were able to acquire spike activity from a subset of sites in Marmoset B that had exhibited no response to microstimulation before (Ma et al., 2020, See Fig. 4 and 6). This finding confirms that the electrodes at these few sites were indeed located in the grey matter. The lack of response to microstimulation in these sites from my study may then be related to the current amplitudes applied. It is possible that these sites had even a higher current threshold to respond to microstimulation, than what we applied (40 to 250 μ A). As observed in our study, there were differences in the threshold to elicit saccade across array sites, potentially related to the fixed length of Utah electrode array not allowing optimal targeting of layer V output neurons.

Compared to macaque studies, in my study it was generally more rare to elicit goal-directed saccades and there was no clear topographical organization of such sites. In macaques, sites at which goal-directed saccades are elicited, are confined to a small rostral region in the floor of the of the intraparietal sulcus and extending into the medial bank, termed the “intercalated zone” (Thier and Andersen, 1996, 1998). We explained the relative lack of goal-directed saccades in our study in terms of the oculomotor range of the marmoset being more limited than the macaque. Goal-directed saccades evoked from macaque intraparietal sulcus can sometimes drive the eyes to a goal zone that is beyond the range of ocular motility (Kurylo and Skavenski, 1991; Thier and Andersen, 1996). Compared to macaques, marmosets have a more limited oculomotor range (Mitchell et al., 2014; Mitchell and Leopold, 2015) and rely more on head movements to shift gaze (Mitchell et al., 2014). Since the marmosets in my study were head-fixed, it is possible that we could only observe the initial few degrees of the eye trajectories of gaze shifts, some of which might have converged well outside the oculomotor range. This is a limitation inherent to head-fixating the animals that is required for reliable microstimulation

and monitoring of eye movement in awake animals. An experimental design that would allow reliable microstimulation and monitoring of eye movement while the animal is head-free, can clarify the actual proportion of elicited goal-directed saccades. Alternatively, it might also be the case that such saccades are simply more rare and widely distributed in marmoset PPC.

In my study, in addition to area LIP, the implanted array also covered parts of area MIP according to Paxinos et al. (2012). In macaques, area MIP is known to mainly hold a representation of hand or reaching movements towards a visual target, with a small percentage of neurons also responsive to saccadic eye movements (Snyder et al., 1997, 2000). In spite of that, we did not observe any movements other than those of the eyes in marmosets, even after microstimulating sites corresponding to area MIP. This discrepancy may result from the amount of cortical coverage that our implanted array had. We may have only covered sites within the PPC that elicited saccades and blinks and did not reach areas from which non-eye movements could be evoked. Future work using larger arrays that cover a greater extent of PPC, can enhance the mapping of cortical areas related to non-eye movements. Another explanation for the observed discrepancy may have to do with the definition of areas LIP and MIP in the marmoset atlas (Paxinos, 2012). It may be the case that area MIP in marmosets is actually an extension of area LIP, since based on our findings it serves a similar function to area LIP. Future improvements in the definition of the cytoarchitectural boundaries of marmoset cortical areas and the underlying cellular structures can help clarify potential differences. Additionally, electrophysiological recordings of the neuronal activity within the marmoset PPC in marmosets performing motor tasks (saccade tasks and reaching movement tasks) can more definitively establish correspondence in neuronal response properties in PPC subdivisions with regards to motor control.

5.3 Marmoset oculomotor areas LIP and 8aD contain neurons with significant stimulus-related and saccade related activity after the onset of peripheral stimulus in the pro/antisaccade task

5.3.1 Summary of the main findings

The results of my second project on microstimulation of area LIP, provided evidence for the involvement of area LIP in saccadic eye movements in marmoset. All microstimulation sessions of this project were carried out in the absence of any explicit saccade task. As a follow-up to the findings of this study, we decided to investigate the role of neurons within marmoset area LIP in more details, by recording their activity while animals were engaged in an adapted version of the pro/antisaccade task. So far, there is only one study by our group that looked at neuronal activity in marmoset areas 8aD and LIP during the instruction period of the pro/antisaccade task using laminar electrodes (Johnston et al., 2019). Their findings demonstrated prominent task-dependent activity in alpha/gamma bands and single neuron activity during the preparatory period in area 8aD in specific (Johnston et al., 2019). They only analyzed the data during the preparatory period from 500 to 0 ms before the peripheral stimulus onset. My last PhD project was in fact based on the same dataset from Johnston et al. (2019), but aimed to investigate neuronal activity of marmoset areas LIP and 8aD in the pro/antisaccade task, with a focus on the activity from the peripheral stimulus onset until the end of the perisaccadic period. The antisaccade task is a popular paradigm to probe executive control via exploring the voluntary control of eye movement. In this task, participants are instructed to suppress a prepotent stimulus-driven response in favor of a less potent saccadic response away

from the stimulus. Electrophysiological evidence in macaque monkeys has revealed differences in neuronal activity in oculomotor areas between pro- and antisaccades, enhancing our understanding of mechanisms underlying the voluntary suppression of activity during the antisaccade task (Munoz and Everling, 2004). We trained two common marmosets on an adapted version of this task that involved alternating blocks of trials that required a saccade either toward a large bright stimulus (prosaccade) or the inhibition of this reflexive response in favor of a saccade toward a small, dim stimulus (antisaccade). We found that area 8aD neurons in marmoset were significantly more active for correct antisaccades in contralateral direction compared to erroneous antisaccades. We found neurons with significant stimulus-related activity in area LIP with preference for contralateral stimulus locations. Both areas 8aD and LIP contained neurons with significant saccade-related activity with preference for contralateral saccade direction. This study provided further evidence for the potential oculomotor role of neurons in areas 8aD and LIP of common marmosets during stimulus and perisaccadic periods of the pro/antisaccade task, enhancing our knowledge of the existing homologies to the macaques.

5.3.2 Caveats and future directions

The behavioral findings of this study were in line with previous literature on human and macaque performing a similar task (Everling and Fischer, 1998; Everling et al., 1999) and indicated the shared difficulty in performing the antisaccade task. However, compared to macaques, marmosets were generally harder to be trained on the antisaccade task. The conventional interleaved prosaccade/antisaccade task that is commonly used for macaques

(Munoz and Everling, 2004), had to be adjusted for marmoset performance level by resorting the task into blocks of prosaccade and antisaccade trials. It was also difficult for marmosets to make an antisaccade to a blank location in the display and thus, we had to include a small dim stimulus in that blank location as the target for an antisaccade (Johnston and Everling, 2011). This form of antisaccade trials is used in the final stage antisaccade training in macaque. In this case, the antisaccade task still examines the cognitive aspect of inhibition of the automatic saccade response and generation of a voluntary saccade in the opposite direction but may not involve the vector inversion process necessary for generating saccades to an empty location. Consequently, it may not demonstrate the full picture of the underlying processes in the antisaccade task in marmosets, as revealed in macaque monkeys. However, the adjustments we made to the task, made it possible to train common marmosets on performing the antisaccade task in a few months. In the future, longer periods of training may help to achieve performance levels comparable to macaque monkeys. A recent observation we have had with our marmoset training is that they tend to perform better if their food is taken away on the afternoon of the day before the experiment and then run the experiment the morning after. Moreover, we recently changed their reward from sweetened condensed milk that was used in my study to Acacia gum, which seems to work better in keeping them motivated throughout the task. Previously, we restricted them from food in the morning of the experiment day and then recorded in the afternoon. We might have a better chance at training marmosets to the final level of difficulty in the antisaccade task with the new food restriction routines.

The biggest caveat of this study was the small number of cells that were active especially around saccade onset time. The small number of cells per area further limited this study from investigating any layer related differences, even though the recording probe was in fact a

laminar electrode. The use of laminar electrodes as our recording technique may itself be a potential cause for the small number of cells. We waited about 20 minutes to allow the electrodes to settle in the brain before starting the data collection. However, 20 minutes may not be sufficient and longer amount of time is needed to properly allow the electrodes to settle in the brain, which was not practically possible with marmosets. They perform well within a limited amount of time and past that time, they start becoming restless and uncooperative to perform the task properly. In future, it may be better to use a different recording technique or implanted electrodes such as Utah arrays that do not require settling time and may be able to capture larger population of neurons.

Another issue with this study especially around saccade onset time was the lack of sufficiently high number of trials. The antisaccade task is hard to learn for marmosets compared to macaques, and therefore there wasn't a sufficiently high number of correct responses, especially correct antisaccade trials to properly detect task related differences in neuronal activity. This was again due to the fact that marmosets cannot perform well past a certain amount of time. Using a different recording technique can save time from waiting for the electrodes to settle, toward acquiring higher number of trials. Consequently, the results can improve in future by having higher number of sessions and trials per session to have a larger sample per trials type to average from. Another caveat of the use of laminar electrodes as our recording technique was the limited possibility of optimizing neuronal recordings based on the response field of individual neurons, which can heavily impact neuronal responses, especially stimulus-related visual responses. Future recording technique should consider such optimizations on the basis of neuronal response fields to be able to have a more comprehensive realization of neuronal characteristics.

All is all, the findings of this project, along with the results of resting-state fMRI and intracortical microstimulation, further emphasized the great potential of common marmoset monkeys as an additional primate model of the oculomotor system and laid a foundation for the application of advanced higher density recording techniques in future on marmoset oculomotor areas performing a variety of saccade tasks.

5.4 References

- Blum B, Kulikowski JJ, Carden D, Harwood D (1982) Eye movements induced by electrical stimulation of the frontal eye fields of marmosets and squirrel monkeys. *Brain Behav Evol* 21:34–41.
- Bruce CJ, Goldberg ME (1985) Primate frontal eye fields. I. Single neurons discharging before saccades. *J Neurophysiol* 53:603–635.
- Elsley JK, Nagy B, Cushing SL, Corneil BD (2007) Widespread presaccadic recruitment of neck muscles by stimulation of the primate frontal eye fields. *J Neurophysiol* 98:1333–1354.
- Everling S, Dorris MC, Klein RM, Munoz DP (1999) Role of primate superior colliculus in preparation and execution of anti-saccades and pro-saccades. *J Neurosci Off J Soc Neurosci* 19:2740–2754.
- Everling S, Fischer B (1998) The antisaccade: a review of basic research and clinical studies. *Neuropsychologia* 36:885–899.
- Everling S, Munoz DP (2000) Neuronal correlates for preparatory set associated with pro-saccades and anti-saccades in the primate frontal eye field. *J Neurosci Off J Soc Neurosci* 20:387–400.
- French JA (2019) The Marmoset as a Model in Behavioral Neuroscience and Psychiatric Research. In: *The Common Marmoset in Captivity and Biomedical Research*, pp 477–491. Elsevier. Available at: <https://linkinghub.elsevier.com/retrieve/pii/B9780128118290000261> [Accessed January 9, 2020].
- Ghahremani M, Hutchison RM, Menon RS, Everling S (2017) Frontoparietal Functional Connectivity in the Common Marmoset. *Cereb Cortex N Y N 1991* 27:3890–3905.

- Ghahremani M, Johnston KD, Ma L, Hayrynen LK, Everling S (2019) Electrical microstimulation evokes saccades in posterior parietal cortex of common marmosets. *J Neurophysiol* 122:1765–1776.
- Hikishima K, Quallo MM, Komaki Y, Yamada M, Kawai K, Momoshima S, Okano HJ, Sasaki E, Tamaoki N, Lemon RN, Iriki A, Okano H (2011) Population-averaged standard template brain atlas for the common marmoset (*Callithrix jacchus*). *NeuroImage* 54:2741–2749.
- Hung C-C, Yen CC, Ciuchta JL, Papoti D, Bock NA, Leopold DA, Silva AC (2015) Functional Mapping of Face-Selective Regions in the Extrastriate Visual Cortex of the Marmoset. *J Neurosci* 35:1160–1172.
- Hutchison RM, Hutchison M, Manning KY, Menon RS, Everling S (2014) Isoflurane induces dose-dependent alterations in the cortical connectivity profiles and dynamic properties of the brain's functional architecture. *Hum Brain Mapp* 35:5754–5775.
- Izpisua Belmonte JC et al. (2015) Brains, genes, and primates. *Neuron* 86:617–631.
- Johnston K, Everling S (2011) An Approach to Understanding the Neural Circuitry of Saccade Control in the Cerebral Cortex Using Antidromic Identification in the Awake Behaving Macaque Monkey Model. In: *Animal Models of Movement Disorders: Volume II* (Lane EL, Dunnett SB, eds), pp 161–181 *NeuroMethods*. Totowa, NJ: Humana Press. Available at: https://doi.org/10.1007/978-1-61779-301-1_9 [Accessed February 13, 2020].
- Johnston K, Ma L, Schaeffer L, Everling S (2019) Alpha Oscillations Modulate Preparatory Activity in Marmoset Area 8Ad. *J Neurosci Off J Soc Neurosci* 39:1855–1866.
- Kurylo DD, Skavenski AA (1991) Eye movements elicited by electrical stimulation of area PG in the monkey. *J Neurophysiol* 65:1243–1253.
- Liu C, Ye FQ, Yen CC-C, Newman JD, Glen D, Leopold DA, Silva AC (2018) A digital 3D atlas of the marmoset brain based on multi-modal MRI. *NeuroImage* 169:106–116.
- Ma L, Selvanayagam J, Ghahremani M, Hayrynen LK, Johnston KD, Everling S (2020) Single unit activity in marmoset posterior parietal cortex in a gap saccade task. *J Neurophysiol* Available at: <https://journals.physiology.org/doi/abs/10.1152/jn.00614.2019> [Accessed February 14, 2020].
- Miller CT, Freiwald WA, Leopold DA, Mitchell JF, Silva AC, Wang X (2016) Marmosets: A Neuroscientific Model of Human Social Behavior. *Neuron* 90:219–233.
- Mitchell JF, Leopold DA (2015) The marmoset monkey as a model for visual neuroscience. *Neurosci Res* 93:20–46.

- Mitchell JF, Reynolds JH, Miller CT (2014) Active vision in marmosets: a model system for visual neuroscience. *J Neurosci Off J Soc Neurosci* 34:1183–1194.
- Munoz DP, Dorris MC, Paré M, Everling S (2000) On your mark, get set: brainstem circuitry underlying saccadic initiation. *Can J Physiol Pharmacol* 78:934–944.
- Munoz DP, Everling S (2004) Look away: the anti-saccade task and the voluntary control of eye movement. *Nat Rev Neurosci* 5:218–228.
- Reser DH, Burman KJ, Yu H-H, Chaplin TA, Richardson KE, Worthy KH, Rosa MGP (2013) Contrasting patterns of cortical input to architectural subdivisions of the area 8 complex: a retrograde tracing study in marmoset monkeys. *Cereb Cortex N Y N* 1991 23:1901–1922.
- Schaeffer DJ, Gilbert KM, Gati JS, Menon RS, Everling S (2019a) Intrinsic Functional Boundaries of Lateral Frontal Cortex in the Common Marmoset Monkey. *J Neurosci* 39:1020–1029.
- Schaeffer DJ, Gilbert KM, Ghahremani M, Gati JS, Menon RS, Everling S (2019b) Intrinsic functional clustering of anterior cingulate cortex in the common marmoset. *NeuroImage* 186:301–307.
- Schaeffer DJ, Gilbert KM, Hori Y, Gati JS, Menon RS, Everling S (2019c) Integrated radiofrequency array and animal holder design for minimizing head motion during awake marmoset functional magnetic resonance imaging. *NeuroImage* 193:126–138.
- Schaeffer DJ, Gilbert KM, Hori Y, Hayrynen LK, Johnston KD, Gati JS, Menon RS, Everling S (2019d) Task-based fMRI of a free-viewing visuo-saccadic network in the marmoset monkey. *NeuroImage* 202:116147.
- Schiller PH, Tehovnik EJ (2001) Look and see: how the brain moves your eyes about. *Prog Brain Res* 134:127–142.
- Selvanayagam J, Johnston KD, Schaeffer DJ, Hayrynen LK, Everling S (2019) Functional Localization of the Frontal Eye Fields in the Common Marmoset Using Microstimulation. *J Neurosci Off J Soc Neurosci* 39:9197–9206.
- Shibutani H, Sakata H, Hyvärinen J (1984) Saccade and blinking evoked by microstimulation of the posterior parietal association cortex of the monkey. *Exp Brain Res* 55:1–8.
- Snyder LH, Batista AP, Andersen RA (1997) Coding of intention in the posterior parietal cortex. *Nature* 386:167–170.
- Snyder LH, Batista AP, Andersen RA (2000) Saccade-related activity in the parietal reach region. *J Neurophysiol* 83:1099–1102.

Thier P, Andersen RA (1996) Electrical microstimulation suggests two different forms of representation of head-centered space in the intraparietal sulcus of rhesus monkeys. *Proc Natl Acad Sci U S A* 93:4962–4967.

Thier P, Andersen RA (1998) Electrical microstimulation distinguishes distinct saccade-related areas in the posterior parietal cortex. *J Neurophysiol* 80:1713–1735.

Appendix: Documentation of Ethics Approval



2017-114:13

AUP Number: 2017-114

AUP Title: Role of Frontal Cortex in Cognitive Control in the Common Marmoset

Yearly Renewal Date: 12/01/2020

The YEARLY RENEWAL to Animal Use Protocol (AUP) 2017-114 has been approved by the Animal Care Committee (ACC), and will be approved through to the above review date.

Please at this time review your AUP with your research team to ensure full understanding by everyone listed within this AUP.

As per your declaration within this approved AUP, you are obligated to ensure that:

- 1) Animals used in this research project will be cared for in alignment with:
 - a) Western's Senate MAPPs 7.12, 7.10, and 7.15
http://www.uwo.ca/univsec/policies_procedures/research.html
 - b) University Council on Animal Care Policies and related Animal Care Committee procedures
http://uwo.ca/research/services/animalethics/animal_care_and_use_policies.html
- 2) As per UCAC's Animal Use Protocols Policy,
 - a) this AUP accurately represents intended animal use;
 - b) external approvals associated with this AUP, including permits and scientific/departmental peer approvals, are complete and accurate;
 - c) any divergence from this AUP will not be undertaken until the related Protocol Modification is approved by the ACC; and
 - d) AUP form submissions - Annual Protocol Renewals and Full AUP Renewals - will be submitted and attended to within timeframes outlined by the ACC. http://uwo.ca/research/services/animalethics/animal_use_protocols.html
- 3) As per MAPP 7.10 all individuals listed within this AUP as having any hands-on animal contact will
 - a) be made familiar with and have direct access to this AUP;
 - b) complete all required CCAC mandatory training (training@uwo.ca); and
 - c) be overseen by me to ensure appropriate care and use of animals.
- 4) As per MAPP 7.15,
 - a) Practice will align with approved AUP elements;
 - b) Unrestricted access to all animal areas will be given to ACVS Veterinarians and ACC Leaders;
 - c) UCAC policies and related ACC procedures will be followed, including but not limited to:
 - i) Research Animal Procurement
 - ii) Animal Care and Use Records
 - iii) Sick Animal Response
 - iv) Continuing Care Visits
- 5) As per institutional OH&S policies, all individuals listed within this AUP who will be using or potentially exposed to hazardous materials will have completed in advance the appropriate institutional OH&S training, facility-level training, and reviewed related (M)SDS Sheets, <http://www.uwo.ca/hr/learning/required/index.html>

Submitted by: Copeman, Laura
on behalf of the Animal Care Committee
University Council on Animal Care

The University of Western Ontario
Animal Care Committee / University Council on Animal Care
London, Ontario Canada N6A 5C1

Maryam Ghahremani

Robarts Research Institute, Western University, 1151 Richmond St. N., London, Ontario, Canada - N6A 5B7

Education

Western University

PH.D. IN NEUROSCIENCE

Thesis: Frontoparietal networks underlying saccadic eye movements in the common marmoset.

London, Canada

2015 - 2020

Korea Advanced Institute of Science and Technology (KAIST)

MSC. IN BRAIN AND BIO ENGINEERING

Thesis: Functional connectivity studies of Parkinson's and Major Depressive Disorder patients using fMRI and EEG.

Daejeon, South Korea

2011 - 2013

University of Tehran

BSC. IN ELECTRICAL ENGINEERING

Specialized in Biomedical Engineering.

Tehran, Iran

2007 - 2011

Carleton University

BSC. IN ELECTRICAL ENGINEERING (TRANSFERRED)

Credits transferred to University of Tehran.

Ottawa, Canada

2005 - 2007

Research Experience

Laboratory for Neural Circuits and Cognitive Control

GRADUATE STUDENT RESEARCHER

- Cross-species comparison of the frontoparietal attention network in common marmosets (9.4T), macaques (7T) and humans (3T) using resting-state fMRI
- Functional connectivity of the saccadic eye movement circuitry in common marmoset monkeys using ultra high field fMRI (9.4T)
- Chemogenetic unilateral deactivation of the superior colliculus and changes in orienting behavior
- Oculomotor effects of microstimulating the lateral intraparietal area (LIP) in common marmosets using Utah electrode arrays
- Mapping spike related activities in marmoset lateral intraparietal area (LIP) and frontal eye field (FEF) using laminar electrodes

Western University

Jan. 2015 - May 2020

Biomedical Image and Signal Processing Laboratory

RESEARCH SCIENTIST

- Investigation of resting-state networks in major depression disorder (MDD) patients using fMRI and EEG recording techniques
- Application of Persistent Homology analysis on brain networks in MDD patients

KAIST

Sep. 2013 - Sep. 2014

Clinical Neuroscience and Development Laboratory

RESEARCH INTERN

- Investigation of emotional disorders using task-based and resting-state fMRI
- Application of Persistent Homology analysis to this dataset

KAIST

Jun. 2014 - Aug. 2014

Biomedical Image and Signal Processing Laboratory

GRADUATE STUDENT RESEARCHER

- Resting-state functional connectivity in Parkinson's disease using fMRI (3T)
- Functional connectivity changes in Parkinson's disease patients with and without cognitive impairments
- Persistent Homology analysis of resting-state networks in Parkinson's disease patients

KAIST

Sep. 2011 - Aug. 2013

Laboratory for Cognitive Neuroscience and Neuroimaging

COLLABORATING RESEARCHER

- Preprocessing of Parkinson's disease resting-state fMRI datasets
- Grouping subjects based on Unified Parkinson's disease Rating Scale (UPDRS) demographics

KAIST

Feb. 2012 - Aug. 2013

School of Electrical and Computer Engineering

UNDERGRADUATE RESEARCHER

- Analysis of Arterial Spin Labeled (ASL) perfusion imaging datasets

University of Tehran

Dec. 2010 - Jul. 2011

Publications

F. Haddad*, M. Ghahremani*, C. De Oliveira, K. Johnston, S. Everling, S. Schmid (2020), A novel 3-choice touchscreen task to examine spatial attention and orienting responses in rodents, *eNeuro*, Currently under revision. *Co-first authorship.

L. Ma, J. Selvanayagam, M. Ghahremani, L. Hayrynen, K. Johnston, S. Everling (2020), Single unit activity in marmoset posterior parietal cortex in a gap saccade task, *J Neurophysiol.* 123(3):896-911.

M. Ghahremani, K. Johnston, L. Ma, L. Hayrynen, S. Everling (2019), Electrical microstimulation evokes saccades in posterior parietal cortex of common marmosets, *J Neurophysiol.* 122(4): 1765-1776.

D. Schaeffer, K. Gilbert, M. Ghahremani, J. Gati, R. Menon, S. Everling (2019), Intrinsic functional clustering of anterior cingulate cortex in the common marmoset, *Neuroimage* 186:301-307.

M. Ghahremani, J. Yoo, S. Chung, K. Yoo, J. Ye, Yong Jeong (2018), Alteration in the local and global functional connectivity of resting state networks in Parkinson's Disease, *J of Mov. Disord.* 11(1):13-23.

M. Ghahremani, R. Hutchison, R. Menon, S. Everling (2017), Frontoparietal functional connectivity in the common marmoset, *Cerebral Cortex.* 1-17.

Conference Presentations

Canadian Association for Neuroscience (CAN)

Toronto, Canada

POSTER PRESENTATION

May 2019

- M. Ghahremani, K. Johnston, L. Schaeffer, S. Everling, "Characterizing the role of the marmoset posterior parietal cortex in saccade generation".

London Health Research Day (LHRD)

London, Canada

POSTER PRESENTATION

April 2019

- M. Ghahremani, K. Johnston, L. Schaeffer, S. Everling, "Characterizing the role of the marmoset posterior parietal cortex in saccade generation".

Society for Neuroscience (SfN)

San Diego, USA

POSTER CO-AUTHORSHIP

Nov. 2018

- K. Johnston, M. Ghahremani, L. Schaeffer, S. Everling, "Oculomotor effects evoked by microstimulation of posterior parietal cortex in the common marmoset".

Federation of European Neuroscience Societies (FENS)

Berlin, Germany

POSTER PRESENTATION

Jul. 2018

- M. Ghahremani, R. Menon, S. Everling, "Functional connectivity patterns of the caudate and putamen in common marmoset and macaque monkeys".

Society for Neuroscience (SfN)

San Diego, USA

POSTER PRESENTATION

Nov. 2016

- M. Ghahremani, R. Hutchison, J. Gati, K. Gilbert, R. Menon, S. Everling, "Frontoparietal functional connectivity in the common marmoset".

Robarts Research Retreat

Western University, Canada

POSTER PRESENTATION

Jun. 2016

- M. Ghahremani, R. Hutchison, R. Menon, J. Gati, S. Everling, "Functional connectivity of the superior colliculus in macaques and marmosets investigated with resting-state ultrahigh-field fMRI".

Canadian Association for Neuroscience (CAN)

Toronto, Canada

INVITED TALK AND POSTER PRESENTATION

May 2016

- M. Ghahremani, R. Menon, S. Everling, "Resting-state functional connectivity studies in common marmoset monkeys at 9.4T".

Society for the Neural Control of Movement (NCM)

Montego Bay, Jamaica

POSTER CO-AUTHORSHIP

Apr. 2016

- S. Everling, M. Ghahremani, R. Hutchison, R. Menon, J. Gati, “Functional connectivity of the superior colliculus in macaques and marmosets investigated with resting-state ultrahigh-field fMRI”.

London Health Research Day (LHRD)

London, Canada

INVITED TALK

Mar. 2016

- M. Ghahremani, R. Menon, S. Everling, “Identification of a frontoparietal network in common marmoset monkeys at 9.4T”.

Organization for Human Brain Mapping (OHBM)

Hamburg, Germany

POSTER PRESENTATION

Jun. 2014

- M. Ghahremani, Y. Jong, J. Ye, “Functional connectivity of default mode network in Parkinson’s disease with cognitive impairment”.

International Congress on MRI (ICMRI)

Seoul, South Korea

POSTER PRESENTATION

Mar. 2013

- M. Ghahremani, Y. Jong, J. Ye, “Default mode network in patients with Parkinson’s disease and cognitive impairment”.

Korean Society of Human Brain Mapping (KHBM)

Seoul, South Korea

POSTER PRESENTATION

Nov. 2012

- M. Ghahremani, Y. Jong, J. Ye, “Brain resting state connectivity in patients with Parkinson’s disease and cognitive impairment”.

Relevant Courses & Skills

Winter 2020 **Introduction to Neural Networks**, Neural computations, Mathematical models of neural systems, Machine learning techniques Western University

Fall 2016 **Neuroimaging of Cognition**, Current brain imaging techniques for experimental design and analysis, Neuroimaging as a tool for cognitive neuroscientists Western University

Winter 2015 **Introduction to Statistics Using R**, Standard statistical data analysis techniques, Using R language for statistical computing and graphical displays of data Western University

Winter 2012 **Clinical Functional Neuroimaging**, fMRI experimental design and data analysis, Clinical applications of fMRI techniques KAIST

Programming and imaging tools, MATLAB, R, FSL, MELODIC, SPM, CONN, Caret, AFNI, MRICron, BCT

Teaching & Supervisory Experience

Principles of Neuroscience

COURSE COORDINATOR: DR. ARTHUR BROWN

- First year graduate course

Western University

Sept. 2018 - Apr. 2020

Motor Neurophysiology

COURSE COORDINATOR: DR. STEFAN EVERLING

- Fourth year undergraduate course

Western University

Jan. 2015 - Apr. 2017

Introduction to Biomedical Engineering

COURSE COORDINATOR: DR. KAMAL SETAREGAN

- Third year undergraduate course

University of Tehran

Sep. 2010 - Jan. 2011

Physiology Undergraduate Thesis

SUPERVISOR: DR. STEFAN EVERLING

- Data collection and analysis, thesis editing

Western University

Jan. 2016 - Apr. 2016

Honors & Awards

May 2019, Second prize on Canadian Open Neuroscience Platform (CONP) Photo Contest	McGill, Canada
May 2017, Ontario Graduate Scholarship (OGS)	London, Canada
Sep. 2016, Western University's International Graduate Student Scholarships in Cognitive Neuroscience	London, Canada
Sep. 2011, KAIST Entrance Scholarship	Daejeon, S.Korea
Sep. 2006, George Fierheller Scholarship	Ottawa, Canada
Sep. 2006, Carleton University's Deans Honor List of students with average A or higher	Ottawa, Canada
Sep. 2005, Carleton University Entrance Scholarship	Ottawa, Canada
Jun. 2005, Glebe Collegiate Institute's Honor List of students with high academic standing	Ottawa, Canada

Workshops & Certificates

2019	Touchscreen Cognition Training , by BrainsCAN Rodent Cognition Core at Western University	London, ON
2019	Neural Signal and Image Processing: Quantitative Analysis of Neural Activity , by Canadian Association for Neuroscience as a satellite workshop	Toronto, ON
2019	Teaching Mentor Program , by Western University on teaching and classroom management	London, ON
2019	safeTALK , by Western University on Suicide Alterness For Everyone	London, ON
2019	Future Professor Workshop Series , by Western University on teaching strategies across disciplines	London, ON
2019	Cross Cultural Team Communications , by Mitacs as on how to communicate in cross cultural teams	London, ON
2017	FSL Course Workshop , by Oxford University on fMRI Software Library tools	Vancouver, BC
2016	EEG/ERP Workshop , by Brain and Mind Institute on EEG/ERP data analysis	London, ON
2015	TATP , by Western University on Teaching Assistant Training Program	London, ON
2015	Basic Animal Care and Use , by Western University as a requirement for Animal Research Protocol	London, ON

Extracurricular Activity

International Graduate Students' Issues Committee (IGSIC)

[London, Canada](#)

SENIOR MEMBER

Sep. 2016 - PRESENT

- Advocating for international graduate students issues
- Organizing orientation and social events to balance graduate students lives

Society of Neuroscience Graduate Students (SONGS)

[London, Canada](#)

MEMBER

Jan. 2019 - Oct. 2019

- Organizing panel discussion series for new students take insight from experiences of senior program members
- Organizing the Women in Neuroscience panel to address gender-related challenges within the neuroscience community

International & Exchange Students Centre (IESC)

[London, Canada](#)

PEER GUIDE/MENTOR

Aug. 2019 - present

- Participating in a 2-day training provided by IESC about leadership, communication, cultural awareness and social integration
- Leading a team of international newcomer students, preparing them for their transition to Western University

Science Rendezvous

[London, Canada](#)

VOLUNTEER

May 2019

- Helping in setting up the neuroscience booth
- Leading groups of visitors at the booth and preparing them to take part in the demonstrated neuroscientific activities

BrainBee Competition

[London, Canada](#)

VOLUNTEER

April 2019

- Creating questions and Powerpoint slides on selected study materials
- Acting as a team leader and marker for groups of participating students

KAIST International Office

[Daejeon, S.Korea](#)

INTERNATIONAL ADVISOR

Jan. 2013 - Dec. 2013

- Team leader for international students orientation
- Providing advice and support for international students on their issues

Biomedical Engineering Society of University of Tehran

[Tehran, Iran](#)

MEMBER

Jan. 2011 - Jun. 2011

- Organizing talks and panel discussions in Biomedical Engineering program on future career and research possibilities for students